

Graz University of Technology

Institute of Biomechanics
Stremayrgasse 16-II
8010 Graz, Austria

Master Thesis

Construction of a phono-mimetic bioreactor for culturing vocal fold cells

to achieve the degree of
Master of Science

Author: Theresia Stachl
Registration number: 01231493

Supervisors: Gerhard Sommer, Markus Gugatschka

Head of Institute: Professor Gerhard A. Holzapfel, PhD

October 31, 2017

Contents

Abstract **V**

Zusammenfassung **VII**

Acknowledgment **IX**

Nomenclature **XI**

1 Introduction **1**
1.1 Vocal folds - anatomy and physiology 1
1.2 Biomechanics of vocal folds 4
1.3 Thesis objective 5

2 Methods **7**
2.1 Development of a bioreactor 7
2.2 Laser vibrometry 9
2.2.1 Measurements with the laser vibrometer 10
2.2.2 Data analysis 12
2.3 Cell culture techniques 13
2.3.1 Change of medium 14
2.3.2 Passaging of the cells 15
2.3.3 Freezing of cells 15
2.3.4 Thawing of cells 15
2.3.5 Seeding of cells 15
2.4 Testing of two different coatings 16
2.5 Viability testing 16
2.5.1 Preparation 17
2.5.2 Data analysis 21

3 Results **23**
3.1 The bioreactor 23
3.2 Laser vibrometer measurements 23
3.2.1 Measurements of the prototype with the structure-borne driver . . 24
3.2.2 Measurements of the prototype with the loudspeaker 24
3.3 Testing of two different coatings 51
3.4 Viability testing 51

4 Discussion **55**
4.1 Discussion of the laser vibrometry results 55
4.2 Discussion of the flow cytometry results 58
4.3 General Discussion 59

5 Appendix A **61**

6 Appendix B **149**

7 Appendix C **153**

8 Appendix D **165**

Bibliography **217**

Abstract

It is believed that vocal fold fibroblasts behave differentially under vibrational stimulation than in static culture. To verify this behaviour the aim of this thesis was to develop a phono-mimetic bioreactor, which can generate a environment *in vitro*, which resembles the vibration of vocal folds *in vivo*.
For the bioreactor a loudspeaker and a carrier with six wells with flexible silicone membranes as bottoms for cell seeding were used. The setting was milled with a CNC milling machine out of polyoxymethylene. With the method of vibrometry the similarity in oscillation of the silicone membranes was investigated. Furthermore, the "eigenfrequencies" of the materials, where the amplitude of the vibration increases manyfold due to resonance were determined. Based on that a sinusoidal signal with 55 Hz was used as stimulation pattern.
To investigate the magnitude of deflection the cells can endure, static and stimulated cells were stained with propidium iodide and investigated with flow cytometry. This allowed to differentiate between living and dead cells. It as observed that the cells survive deflections at about 33 and at about 147 μm in good shape.
Overall this first prototype of a phono-mimetic bioreactor provides an appropriate tool for further investigations regarding for example differences in gene expression.

Zusammenfassung

Man geht davon aus, dass Stimmlippen-Fibroblasten sich unter Vibrationsstimulation anders verhalten als in statischer Kultur. Um dieses Verhalten zu untersuchen wurde als Ziel dieser Arbeit festgelegt einen phono-mimetischen Bioreaktor zu entwickeln, der eine *in vitro* - Umwelt generiert, die die Vibration der Stimmlippen *in vivo* wiederspiegelt.
Für den Bioreaktor wurden ein Lautsprecher sowie ein Träger mit sechs Wells mit flexiblen Silikonmembranen als Boden verwendet. Der Prototyp wurde mit einer CNC Fräse aus Polyoxymethylen gefräst. Mit der Methode der Vibrometry wurde die Ähnlichkeit der Schwingungen der Silikonmembranen untersucht. Weiters wurden die Eigenfrequenzen der Materialien, wo die Amplitude der Vibration wegen der Resonanz um ein vielfaches ansteigt, bestimmt. Darauf basierend wurde ein Sinussignal mit 55 Hz als Stimulationspattern ausgewählt.
Um die Amplitude der Auslenkung zu ermitteln, die die Zellen ertragen können, wurden statischer und stimulierte Zellen mit Propidiumiodid gefärbt und mit Durchflusszytometrie untersucht. Dadurch konnte zwischen lebenden und toten Zellen unterschieden werden. Es wurde beobachtet, dass die Zellen Auslenkungen von ca. 33 and 147 μm in guter Verfassung überleben.
Im Großen und Ganzen bietet dieser erste Protoyp eines phono-mimetischen Bioreaktors ein passendes Werkzeug für weitere Untersuchungen bezüglich beispielsweise Unterschieden in der Genexpression.

Acknowledgment

Firstly, I would like to thank my Supervisors from the research group LTTEG for their encouragement and support. Secondly, I want to thank my Supervisor Gerhard Sommer for his quick responses, answering all my questions and improvement suggestions. It was a pleasure to work with you.

I would also like to thank Jakob Woisetschläger and his colleagues for their time and their suggestions and especially for the opportunity to use the laser vibrometer of the institute. My great thanks also go to the company NBN Electronics for the help in milling the bioreactor.

Further, I would like to thank the whole Institute of Biomechanics, for giving me a good foundation through providing fundamental knowledge about mechanics and especially biomechanics in their lectures.

I would also like to thank the Technical University of Graz, for bombarding me with knowledge from various fields, to help me get a basis for research, studying and engineering.

Also, thank you to all my study colleagues, for coping with my challenging questions and for all the fun we had together.

Last but not the least, I want to mention how grateful I am for my whole family, who supports me no matter what happens. Especially, I want to thank my grandmother, as she is always there for me and pushes me when I hesitate.
Thank you mum for listening, thank you dad for the good discussions and thank you Matthias for the help with the milling. Thank you all. I love you.

Nomenclature

a	maximal radius (17.5 mm)
A	parameter used for fitting (for simplification)
CO_2	carbon dioxide
DMEM	Dulbecco's Modified Eagle Medium
DMSO	$(CH_3)_2SO$ or dimethyl sulfoxide
DNA	deoxyribonucleic acid
DSR	Dynamic Spring Rate
ϵ	strain at r = 0
ϵ_r	radial strain
ϵ_t	tangential strain
E	Young's modulus
EDTA	ethylenediaminetetraacetic acid
f	frequency
$f(r)$	function of r
FBS	fetal bovine serum
FFT	fast Fourier transform
h	thickness of the membrane
Hz	Hertz
g	gram-force, 1 g $\approx$ 0.01 N;
ν	Poisson's ratio
π	pi (ratio of circumference to diameter of a circle)
p	pressure
PBS	phosphate-buffered saline
PI	propidium iodide
POM	polyoxymethylene
r	radius
σ	stress at r = 0
σ_r	radial stress
σ_t	tangential stress
TA	thyroarytenoid
x	deflection
U_{eff}	root mean square value of the voltage
w	bending curve

1 Introduction

In this thesis a bioreactor for stimulating vocal fold fibroblasts was developed. Therefore in this section an overview of anatomy, physiology and biomechanics of vocal folds is provided.

1.1 Vocal folds - anatomy and physiology

In Fig. 1.1 a scheme of the larynx is provided, where the vocal folds can be found. The larynx can be divided into three parts:

- Glottis: level, where the vocal folds are located
- Supraglottis: level above the vocal folds, including the epiglottis
- Subglottis: level from 1 cm below the vocal folds until the beginning of the trachea (Sasaki and Kim (2003), Piazza et al. (2008), Friedrich (2013), Eichel (2014)).

In the respiratory configuration the glottis looks V-shaped. The peak of the V, where the vocal folds contact, is called the anterior commissure. The other part is the so-called vocal process (Lalwani (2012), Eichel (2014))

The larynx is build up by three main structures: cartilages, muscles and mucosa.
The main cartilages are: the thyroid, circoid and arytenoid cartilages. The thyroid cartilage forms the so-called Adam's apple in the adult male. The circoid cartilage is circular-shaped and situated below the thyroid cartilage. The arytenoid cartilages are shaped like pyramides and include the vocal and muscular process (Sasaki and Kim (2003), Iro and Waldfahrer (2005), Piazza et al. (2008), Faller and Schünke (2012), Eichel (2014)).

Various muscles are involved in voice production. For opening of the glottis the posterior cricoarytenoid muscle is responsible. The lateral cricoarytenoid muscle, also called muscle lateralis, the intraarytenoid muscle (transverse and oblique arytenoid muscles) and the lateral part of the thyroarytenoid muscle are responsible for the closing of the glottis. Further, the cricothyroid muscle and the medial part of the thyroarytenoid muscle, also referred to as vocalis muscle, are responsible for the tensioning of the vocal folds. (Sasaki and Kim (2003), Iro and Waldfahrer (2005), Boenninghaus and Lenarz (2007), Lalwani (2012), Faller and Schünke (2012), Eichel (2014)).

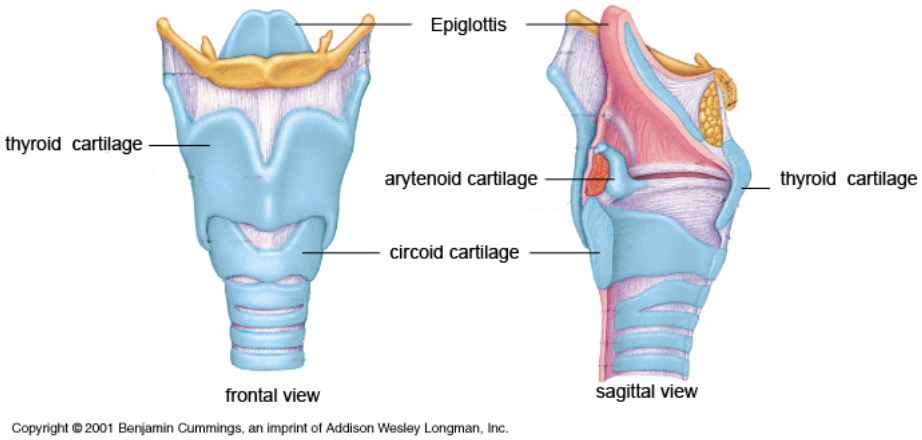


Figure 1.1 Scheme of a larynx. Adopted from Copyright 2001 Benjamin Cummings, an imprint of Addison Wesley Longman, Inc. (12/06/2017).

Vocal folds are important regarding the ability of humans to communicate. The airflow from the lungs passes the larynx, where the vocal folds are stimulated to vibrate. Then the sound wave propagates through the so-called vocal tract, which consists of the supraglottis, the pharynx and the oral and nasal cavity. These parts act as resonators (Arnold and Ganzer (2011), Lalwani (2012), Faller and Schünke (2012), Friedrich (2013), Sweet (2013), Eichel (2014)). Vowels can be generated in the larynx through changes of the vocal tract. Consonants are generated through articulation in the mouth (Faller and Schünke (2012)).
To describe the vibration of vocal folds often the aerodynamical - myoelastical theory of voice production is used. The myoelastic aspect is related to the stored elastic energy of the muscles and the connective tissue in the larynx. The vocal folds change from the respiratory configuration to the phonatory configuration - from an open to a closed state - through muscle contraction. Then during expiration the subglottic pressure rises, which leads to an opening of the vocal folds. Thereafter, through the rising streaming velocity an under-pressure develops, which leads to closing of the vocal folds again. This process is also often referred to as the law of Bernoulli. Through the frequent opening and closing of the vocal folds the air is compacted and diluted, which leads to the generation of a sound wave (Van den Berg (1958), Titze (1980), Scherer (2003), Piazza et al. (2008), Friedrich (2013), Speckmann et al. (2013), Eichel (2014)). The vibration movement represents the frequency (vibrations per second) of the primary voice signal in the larynx. This voice signal is not sinusoidal. It consists of one main frequency and many overtones (Rosanowski and Eysholt (2005), Friedrich (2013), Eichel (2014)). After the flow through the resonators, the articulation happens in the mouth and a complex voice sound is produced. Adult females have an average fundamental frequency of 200 Hz, adult male 120

Hz and children about 250 Hz (Lalwani (2012)). During puberty the vocal folds elongate and therefore the fundamental frequency decreases (Hartnick et al. (2005), Boenninghaus and Lenarz (2007), Speckmann et al. (2013)). When a low-pitched tone is generated, the vocal folds are short, flaccid and under little tension. When a high-pitched tone is generated, the vocal folds are elongated, narrow and under high tension (Boenninghaus and Lenarz (2007), Friedrich (2013)), Eichel (2014)). The volume of the voice depends on the amplitude of the vibration.

The vocal folds consist of different layers. The top layer is the epithelium, consisting of squamous cells, followed by the basal membran between the epithelial cells and the lamina propria, which is build up of extracellular matrix of collagen type IV and VII (Kiminori (2003), Gray and Titze (2000), Jetté and Thibeault (2012)). The lamina propria consists of superior (Reinke space), intermediate and deep layer. In the lamina propria there are various fibroblasts, which generate a great network of fibres in the extracellular matrix. Important extracellular matrix proteins regarding the biomechanics are collagen (type I, II and III identified), elastin and hyaluronic acid. Further there is also decorin, fibronectin and fibromodulin. The innermost layer is the thyroarytenoid muscle (Gray (2000), Chan et al. (2001), Kiminori (2003), Piazza et al. (2008), Lalwani (2012), Rohlfs et al. (2013), Eichel (2014)), which contains stratified muscle cells (Gray and Titze (2000), Piazza et al. (2008), Jetté and Thibeault (2012)). The so-called vocal ligament belongs to the intermediate and deep layers of the lamina propria (Piazza et al. (2008), Lalwani (2012), Rohlfs et al. (2013)). A scheme of the different layers is provided in Fig. 1.2.

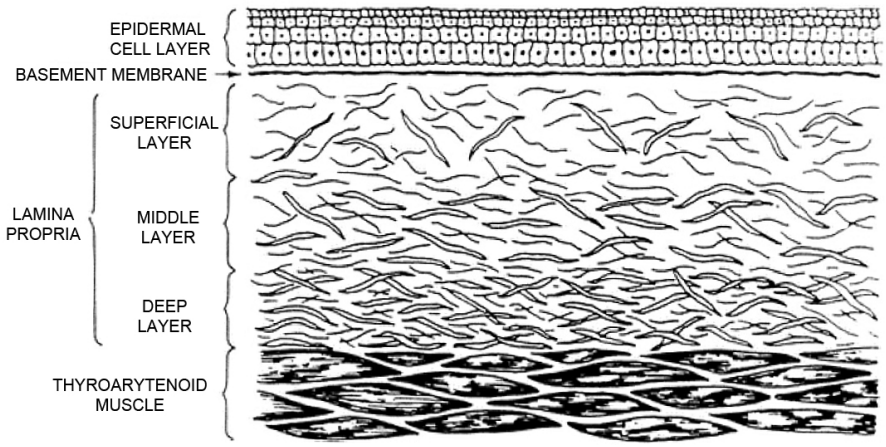


Figure 1.2 Scheme of the layers of the vocal folds. Adopted from Gray and Titze (2000).

Vocal folds are often divided into two parts: the body and the cover. It was observed, that the cover can move more freely and during phonation it glides in an ellipsoid form over

the body (Gray and Titze (2000), Lalwani (2012), Friedrich (2013), Chhetri et al. (2011), Eichel (2014)). The body is defined as the thyroarytenoid(TA) muscle and the deep layer of the lamina propria. The intermediate layer of the lamina propria is often called the transitional layer. The upper two parts build the cover (Gray and Titze (2000), Piazza et al. (2008), Lalwani (2012)).

1.2 Biomechanics of vocal folds

The structure of a tissue is crucial for its macroscopical behaviour. This connection can be described and examined through biomechanics. Therefore, a lot of studies have been conducted to study the biomechanics of the vocal folds. A lot of different examination methods have been used, e.g. indentation was performed by Goodyer et al. (2007), Chhetri et al. (2011), Kelleher et al. (2013) and Oren et al. (2014). Chhetri et al. (2011) also made a great effort in studying the effect of the different parameters of indentation - like indenter diameter, indentation depth and thickness of the sample - and also examined the relation between them. However, he used a cylindrical indenter with sharp edges. This might have lead to some boundary disturbances. Furthermore, not all studies met the criteria, Chhetri et al. (2011) estimated.

Goodyer et al. (2007), Dailey et al. (2009) Goodyer et al. (2009) and Rohlfs et al. (2013) used a modified Linear Shear Rheometer to study shear stress. Dailey et al. (2009) made matrices with measurements points to generate DSR (dynamic spring rate) maps, which revealed the great anisotropy of the vocal folds, as the DSR depended highly on the location. Rohlfs et al. (2013) tested different angles and different layers and revealed also some location-dependent variability. Further, Rohlfs et al. (2013) also carried out histological analysis, which revealed a quite parallel alignment of collagen in some layers, which fits well to the differences observed for the different measurement angles. Also Chan et al. (2007), Chhetri et al. (2011) and Kelleher et al. (2013) revealed differences for different layers. Overall, the results fit very well, with the assumption of anisotropy. Gray and Titze (2000) made histological analyses, which fit well with this assumption. The extracellular matrix of the vocal folds contains a lot of elastin and collagen. This fits well with the obtained stress-strain curves (Chan et al. (2007), Alipour et al. (2011), Kelleher et al. (2011), Alipour and Vigmostad (2012), Oren et al. (2014)), which all showed a linear behaviour in the beginning at small strains and changed to a non-linear behaviour at large strains. This can be explained by the recruitment of the collagen fibres.
Furthermore, also a time-dependent response was observed (Alipour et al. (2011), Kelleher et al. (2011), Kelleher et al. (2013)). Sometimes cyclic preconditioning was applied(Chan et al. (2007), Alipour et al. (2011), Kelleher et al. (2011), Alipour and Vigmostad (2012), Kelleher et al. (2013)). This is a result, which is often observed for biological materials containing collagen. In most cases a hysteresis was observable, which further suggests a viscoelastic behaviour. Apart from collagen and elastin, the extracellular matrix of vocal

folds also contains hyaluronic acid, which attracts water and is known for its importance in tissue viscosity (Chan et al. (2001), Jetté and Thibeault (2012)).

Interestingly, nearly all studies used a linear approach for data fitting. The hybrid linear-exponential model used by Chan et al. (2007) was better, but no ideal choice for a non-linear material. Oren et al. (2014) only used an exponential model. Linear measures such as the Young's or shear modulus, are not the ideal parameters to describe the biomechanics of the vocal folds.

1.3 Thesis objective

In general cells can behave differently, when cultured under different conditions. As this is also believed for human vocal fold fibroblasts, the aim of this study was to develop and evaluate a phono-mimetic bioreactor, which can generate an environment *in vitro*, which resembles the vibration of vocal folds *in vivo*. For evaluation of the developed bioreactor, laser vibrometry and flow cytometry were used. The thesis was conducted in coorperation with the research group LTTEG (Laryngo Tracheal Tissue Engineering Graz) leaded by Prof. Markus Gugatschka.

2 Methods

2.1 Development of a bioreactor

The first task was to find a flexible carrier for seeding the cells. The best carrier solution were the BioFlex culture plates(Flexcell International Corporation, Burlington, NC, USA), which are 6-well-plates with a flexible bottom made of silicone (shown in Fig. 2.1). This plate is intended to be used in the FlexCell System. A scheme of the mode of operation of the system is shown in Fig. 2.2.

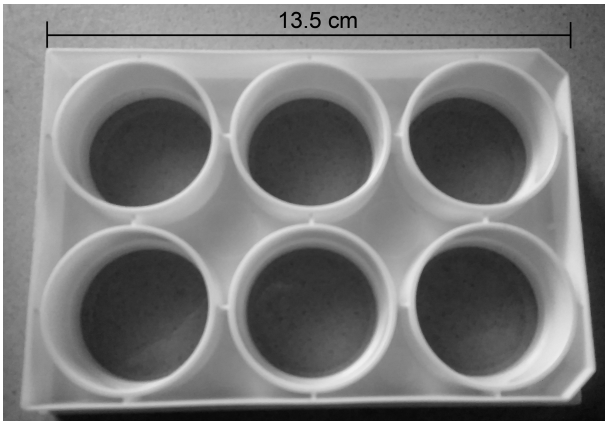


Figure 2.1 The BioFlex 6-well plate.

The system applies a shear force on the membrane by using a vacuum pressure to suck the membrane against the loading post, which can be conducted in a cyclic manner. However, the normal working frequencies are too low. Therefore a custom-built stimulation system was designed and built using different loudspeakers (AL 170 and TIW 300 from Visaton).
In a first approach different setups were tested using various pots and tubes to transport the soundwave. It was tested manually, if some vibration of the membranes was noticeable. As this was not the case, we tried a new approach, where the plates were mounted near the loudspeakers. First a plastic plate was used, in which a rectangular hole was cut, over which the plate was mounted with tape. As the plastic plate was not a ideal material, we switched to a tube, in which the plate was put, for first testings. As a vibration was noticeable, this approach was further investigated. Therefore a wooden plate was gathered and a rectangular hole was milled. Further a ledge was made, where the plate could be

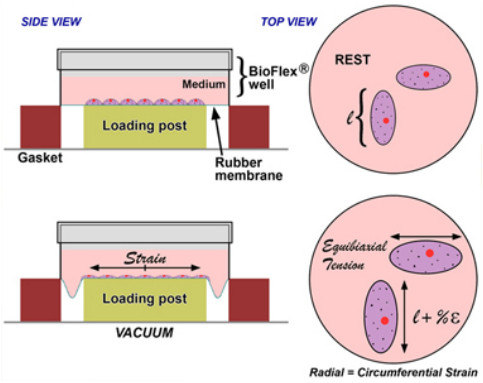


Figure 2.2 Scheme of the mode of operation of the FlexCell system. Adopted from Flex Cell International Corporation (01/08/2017).

placed. On the back of the plate two circles were milled, so that the tube, which was a little conic-shaped, could be mounted in both directions. In Fig. 2.3 the tube and the wooden plate are shown.

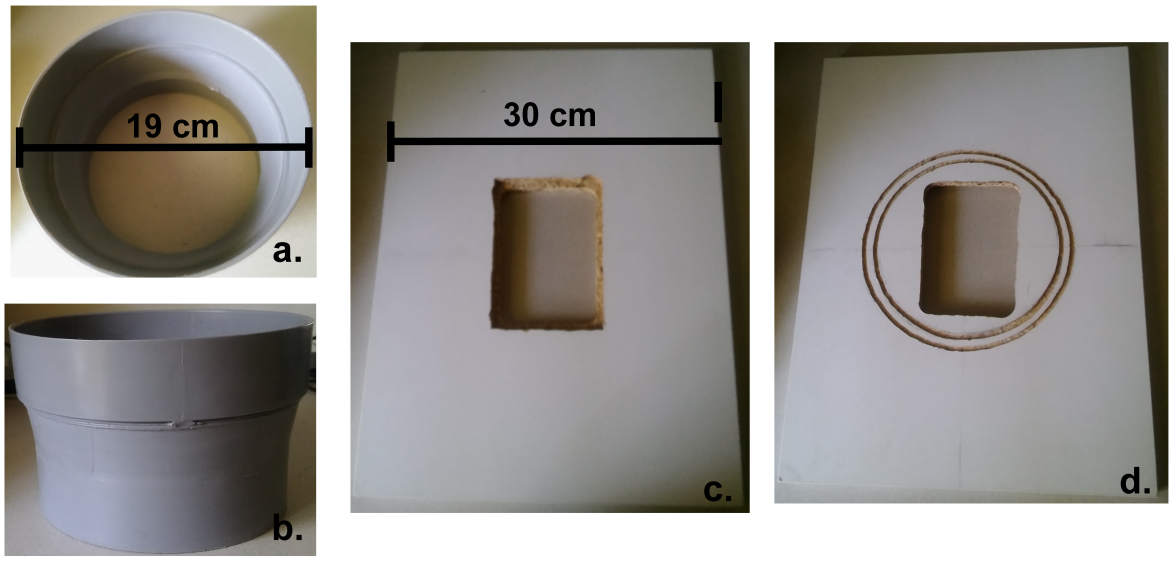


Figure 2.3 **a.** top view of the tube, **b.** side view of the tube, **c.** top view of the wooden plate, **d.** bottom view of the wooden plate.

This first prototype was taken to the Institute for Thermal Turbomachinery and Machine Dynamics of the Graz University of Technology, where some recommendations were received for the further development. Also a structure-borne driver (BSX 130 WP from

Visaton) was examined during this session and it was decided to develop a second prototype with this structure-borne driver. Further the first prototype was fine-tuned. As also a loudspeaker box was needed and as the upper part with the tube and the plate needed upgrading (was not perfectly leakproof and wood is not a perfect material for an incubator), it was decided to produce a new prototype made of polyoxymethylene(POM). As only a milling machine for wood was available, the company NBN Electronics in Graz was asked for assistance, as they had a CNC milling machine and POM plates available. A CAD scheme of the new protoype, which was created by the company NBN, is shown in in Fig. 2.4.

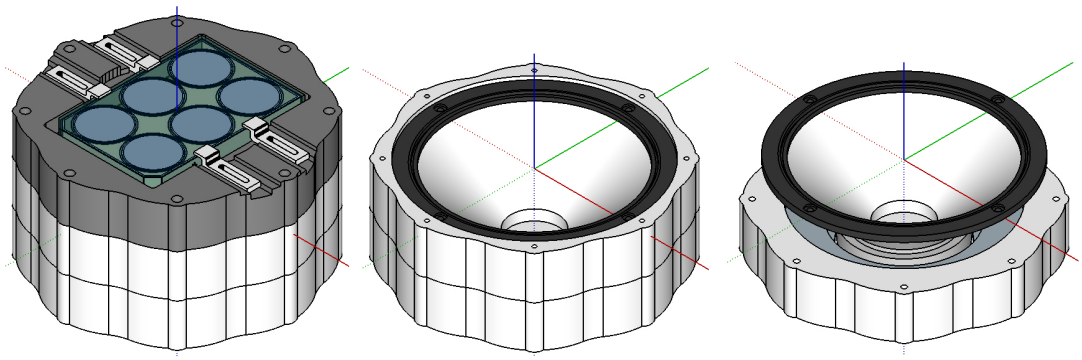


Figure 2.4 Scheme of the new protoype designed with SketchUp software.

The distance between plate and loudspeaker should be as small as possible, as we wanted the total height to be small enough to put the bioreactor into a standard incubator. A straight approach was preferred to a conic one, to get a more homogeneous distribution of the sound waves. Edges were avoided as far as possible to prevent possible deflections of the sound waves.

A hole was milled in the prototype, where a XLR connector was placed. Then a XLR cable and a adapter from XLR to SpeakOn were used to connect the loudspeaker to a power amplifier.

2.2 Laser vibrometry

The vibration behaviour of the membranes of the plates under stimulation with the prototypes was examined with the method of laser vibrometry.
A scheme of the working principle of a laser doppler vibrometer is shown in Fig. 2.5.

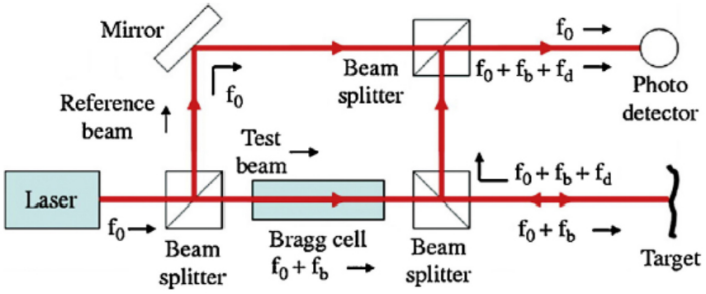


Figure 2.5 Scheme of the operation principle of a laser doppler vibrometer. Adopted from Sitnik et al. (2015).

In the system of a laser vibrometer a reference laser beam is compared to a testing beam, which is reflected from the target, on which the testing beam is applied. The difference between these two laser beams represents the vibration of the target. If the signal is obtained at different measurement points, the movement of the surface of a target can be investigated. Further noise or another signal containing many frequencies with the same amplitude are applied to investigate the ”eigenfrequencies” of a target. These frequencies are visible through a higher peak than peaks at other frequencies.

2.2.1 Measurements with the laser vibrometer

For this measurement the surface of a target can not be transparent, as the beam needs to be reflected. Therefore, the membranes were sprinkled with baby powder.
First the prototype with the structure-borne driver was examined. For that a white noise signal was applied and the instrument parameter was set to 25 mm/s/V.
For the first measurement with the loudspeaker prototype a signal was generated with the software Audacity. This chirp signal consisted of successive chirps from 1 to 2500 HZ over a time period of 0.25 seconds. The signal was magnified using a power amplifier (crown XLS 1502). One output of the amplifier was used to measure the voltage U_V during the measurements. For the later measurements the instrument parameter was set to 125 mm/s/V. Different measurement points were measured for each well (a scheme is available in Fig. 2.6). Therefore a stencil made out of paper was prepared and taped on the well position on the cover of the plate. Then the laser doppler vibrometer was placed manually, so that the laser pointed at the measurement point. When measuring the next well position, the stencil was re-taped on the new position on the cover.

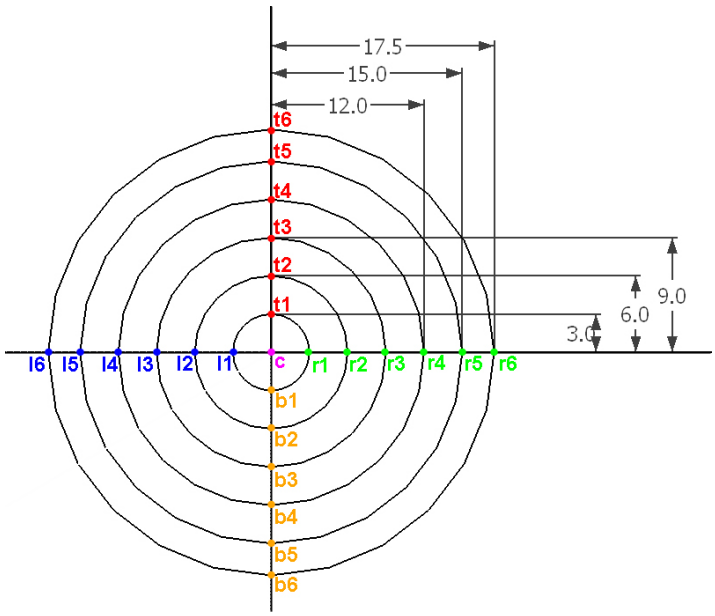


Figure 2.6 Scheme of the measurement points of each well. The numerical values are in mm.

The wells were numbered, as shown in Fig. 2.7, where also the measurement points of the support are provided.

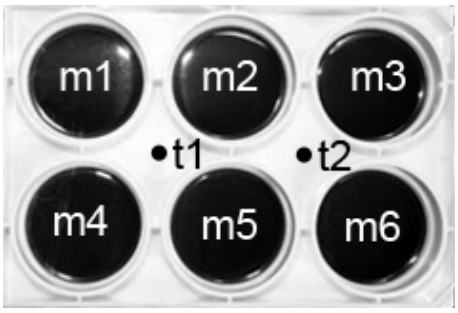


Figure 2.7 Scheme of the numbering of the wells and measurement points of the support.

All wells from two plates were measured to compare between wells and between the plates. To mimic the cell suspension, which is present during cell cultivation, the well of interest was filled with 2.5 ml of water and further measurements were conducted. As it would not work with baby powder any more, a cross was drawn on the back of the membrane with a pen. After the chirp signal, also sinus signals with different frequencies were applied. The group under Michael Döllinger investigated the larynx signal *in vitro* by blowing air through the glottis. From this data an artificial primary larynx signal was created and also used for measurements with the laser vibrometer. Frequencies from 100

Hz to 1000 Hz in 100 Hz steps with a decrease of - 3dB per step were overlapped and were measured.
For a 55 Hz sinus signal the center point of the membrane was measured with different volume settings. Therefore the voltage parameter from the multimeter was used.

2.2.2 Data analysis

The raw data was fourier transformed using a Matlab program, provided by the institute for Thermal Turbomachinery and Machine Dynamics. A sample size of 5000 and a number for the grid points of 2048 was chosen. Plots with different data points were created and interesting frequencies were estimated manually. For them the deflection x over the membrane was calculated.

$$x = \frac{U_{eff} \cdot \sqrt{2} \cdot 0.125}{2 \cdot \pi \cdot f}, \tag{2.1}$$

with U_{eff} as the root mean square value of the voltage. The resolution factor set at the laser vibrometer was m/s/V. f denotes the frequency. The radial σ_r and tangential stresses σ_t and corresponding strains in the membranes were approximates using the equations for bending of a circular plate:

$$\sigma_r = \frac{6p}{16h^2} \cdot \left[(1+\nu)\, a^2 - (3+\nu)\, r^2\right], \tag{2.2}$$

$$\sigma_t = \frac{6p}{16h^2} \cdot \left[(1+\nu)\, a^2 - (1+3\nu)\, r^2\right], \tag{2.3}$$

$$\epsilon_r = \frac{1}{E} \cdot \left[\sigma_r - \nu\sigma_t\right], \tag{2.4}$$

$$\epsilon_t = \frac{1}{E} \cdot \left[\sigma_t - \nu\sigma_r\right], \tag{2.5}$$

where p is the pressure, h denotes the thickness of the circular plate (in this case the thickness of the membrane is 1 mm), r denotes the radius and a is the maximum radius (in our case 17.5 mm). For the Poisson's ratio ν a value of 0.47 was assumed and for the Young's modulus E a value of 0.93 kPa was used (value provided from FlexCell) was used.
The strain at the center (r = 0) was wanted, as it was assumed that the strain is maximal there and the maximal strain might be a good parameter for further measurements. First the data for one frequency was fitted to the equation of the bending curve $w(r)$:

$$w(r) = p \cdot \frac{3(1-\nu^2)}{16Eh^3} \cdot (r^2 - a^2). \tag{2.6}$$

Below the function for the fitting is shown:

$$f(r) = A \cdot (r^2 - 17.5^2)^2, \tag{2.7}$$

where $A = p \cdot \frac{3(1-\nu^2)}{16Eh^3}$, which was calculated with the fitting function. For r the measurement points along the membrane surface were inserted and for y the calculated deflection

was provided. From that p could be calculated. At r = 0 the stresses and strains are the same:

$$\sigma_r = \sigma_t = \sigma = \frac{6p}{16h^2} \cdot \left[(1+\nu)a^2\right] \tag{2.8}$$

$$\epsilon_r = \epsilon_t = \epsilon = \frac{1}{E} \cdot [\sigma - \nu\sigma] = (1-\nu) \cdot \frac{\sigma}{E} \tag{2.9}$$

By insertion of p into Eq. 2.8 and then insertion of the result into Eq. 2.9, the strain in the center of the bending curve, corresponding to the center of the membrane, was calculated. For the fitting measurement points over the membrane surface were needed. As the fitting was not totally perfect and as not always measurement points over the membrane surface were gathered, this calculations were only used for some data.

The data gathered with the chirp signal from all six membranes of 2 plates was further examined with the Pearson correlation coefficient, which is provided in Eq. 2.10.

$$r = \frac{\sum_{i=1}^{n}(x_i - \bar{x}) \cdot (y_i - \bar{y})}{\sqrt{\sum_{i=1}^{n}(x_i - \bar{x})^2 \sum_{i=1}^{n}(y_i - \bar{y})^2}}, \tag{2.10}$$

where $\bar{x}$ and $\bar{y}$ denote the mean values of the data x and y with n datapoints. The FFT of the signals at the center of the membranes was used as x and y.

2.3 Cell culture techniques

For my studies I used human vocal fold fibroblasts (hVFFA8), which were harvested from a 21-year-old male donor and immortalized. Our research group received the cells from the Thibeault Lab at the University of Wisconsin-Madison. A representative photograph of the cells with passage number P146 with high confluence is shown in Fig. 2.8.

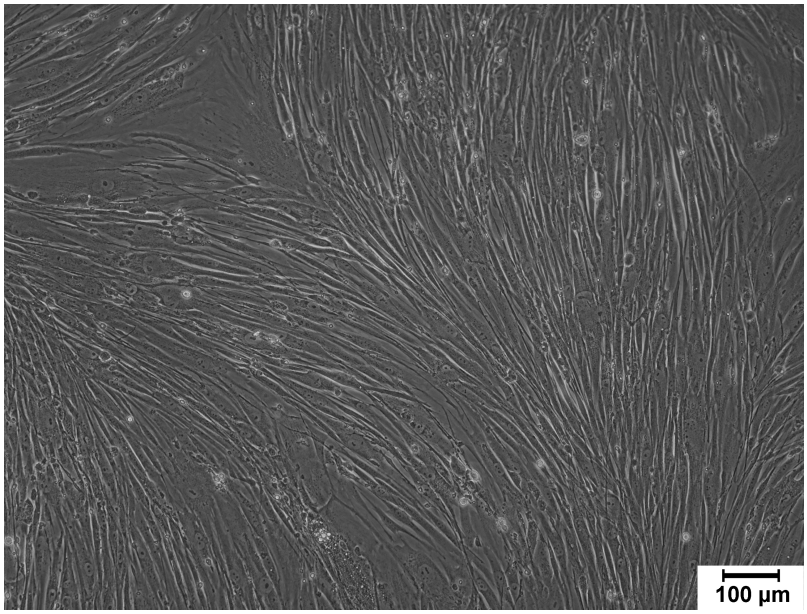


Figure 2.8 Human vocal fold fibroblasts in culture. Passage Number P146. 10× magnification.

The cells were cultured in DMEM medium with 10 % FBS and 1 % penicillin/streptomycin and kept at 5 % CO_2 at 37 °C under humidified conditions in an incubator. In Table 2.1 an overview of the volumina of the solutions used in the different cell culture flasks is available. The area of culture surface in cm^2 is represented by the number by the flask name, e.g. T25-flask corresponds to a surface of 25 cm^2.

Table 2.1 Voluminas of the solutions used in the different cell culture flasks.

Solution	T25-flask	T75-flask	T175-flask
DMEM medium	5 ml	15 ml	30 ml
PBS (for washing)	5 ml	10 ml	20 ml
Trypsin/EDTA 0.25 %	0,5 ml	1 ml	2 ml

2.3.1 Change of medium

The culture medium was changed every two to three days. The old medium was removed. Then the cells were washed with PBS and after removal of the PBS new prewarmed culture medium was added.

2.3.2 Passaging of the cells

When a sufficient confluence of the cells was reached the cells were passaged with a ratio of 1:2 most of the time. After washing Trypsin/EDTA 0.25 % was added and the flasks were incubated for 3 minutes. After confirming the trypsinization under the microscope (mostly slight beating at the bottom of the flask was needed), the medium was added and used for washing of the bottom of the flask. Thereafter, the cell suspension was split up and placed into the flasks and the amount of cell medium, which was needed for each flask (subtracting the cell suspension in it) was added.

2.3.3 Freezing of cells

If cells were very confluent and not required for experiments, they were frozen and stored in liquid nitrogen. For that the working steps until the cell suspension after trypsinization were performed. Thereafter the cell suspension was placed in a tube and centrifuged (centrifuge: Multifuge 1 L-R , setting: 170 g, 7 min, 22–23 °C). In the meanwhile 100 μl DMSO were placed in each cryotube. The supernatant fluid was removed and the pellet was re-suspended in FBS (0.9 ml per cryotube). The vials were placed on ice and stored in a freezer at -80 °C overnight. Then the tubes were placed in liquid nitrogen at -190 °C.

2.3.4 Thawing of cells

If cells were needed for experiments or culturing, frozen cells were thawed. For that one tube with 10 ml medium and one tube with 5 ml medium were prepared. The second tube was warmed. With tweezers the cryotube was gathered from the liquid nitrogen and thawed manually or in a water bath. After that the solution was added to the first tube and centrifuged (same settings as for freezing). The supernatant was removed and the pellet was resolved through gentle beating of the tube. Then it was added to the second warmed tube. After several up and down pipetting the cell suspension was placed in a T25 flask. The next morning the medium was changed, because the freezing and thawing process often leads to a lot of dead cells swimming in the solution.

2.3.5 Seeding of cells

Seeding in the BioFlex plates was carried out. Out of simplification a surface of 9.6 cm^2 (as known for normal six well plates) was assumed. Cells were seeded with a density of 6000 cells / cm^2. In each well 2.5 ml of solution were placed in total. The working steps until trypsinization and followed re-suspending were carried out. Then the solution was placed in a tube. In an Eppendorf tube 10 μl of trypan blue were prepared and 50 μl of the cell suspension were added. It was pipetted up and down eight times and afterwards four times and then the solution was placed in the top part of the counting chamber. After that followed up and down pipetting for four times, the remaining solution was placed in the bottom part of the counting chamber.

Thereafter the cells were counted under the microscope. The number of viable cells in the counted large squares in both parts was noted. Thereafter the cells per large square were calculated and multiplied by 12,000 to gather the cells per ml. The needed number of cells were divided by this figure to gather the amount of ml needed of the cell suspension. The corresponding amount of medium was calculated by subtracting the amount of cell suspension from the total amount of needed solution. The voluminas of cell suspension and medium were prepared in a tube. After several up and down pipetting the right amount of solution was placed in each well. The rest of the cell suspension was either discarded, kept in culture or frozen.

2.4 Testing of two different coatings

The BioFlex plates from FlexCell are available in a wide range of different coatings of the silicone membrane. To test which coating might work for the human vocal fold fibroblasts, seeding in plates with two different coatings (Pronectin and Collagen Type I) was carried out. Pronectin is a fibronectin-like engineered protein polymer and collagen type I is a extracellular protein, which appears naturally in human bodies. For comparison, pictures of the cells were made using a microscope with $10\times$ magnification for 5 days every 24 hours.

2.5 Viability testing

It was completely unclear which deflection the cells might withstand. Therefore, the viability of the cells was estimated for static and for stimulated cells, to investigate, how much deflection the cells survive.
To test the viability of the cells at two different conditions the BD LSR II (in connection with the BD FACSDiva software) at the center of medical research was used. The BD LSR II is based on the technique of flow cytometry, which is a popular technique for cell counting and cell sorting (Brown and Wittwer et al. (2000),Jahan-Tigh et al. (2012)). A lot of different stainings can be used with this system. As the parameter of interest was the viability, the dye propidium iodide (PI) was used. PI is a DNA dye used to differentiate between dead and viable cells. The dye should only be able to reach the nucleus of damaged cells and generate a signal there.
The cells flow through the flow cytometer, where a laser beam is applied. With different detectors (shown in the scheme in Fig. 2.9) the information is gathered.

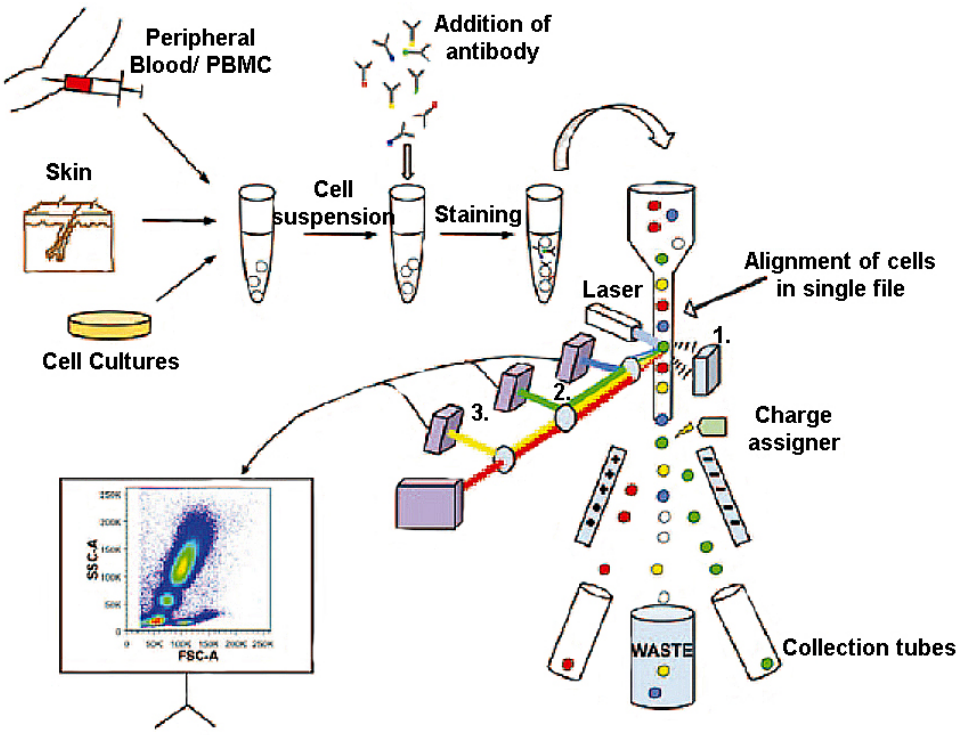


Figure 2.9 Scheme of the flow cytometer technique with the detectors **1.** forward-scatter, **2.** side-scatter and **3.** fluorescence detector. Adopted from Jahan-Tigh et al. (2012)

The forward-scatter (FSC) detector detects light, which was scattered at an small angle and gives information corresponding to the cell size. The side-scatter (SSC) detector detects light, which was scattered at an angle of 90° and gives information corresponding the granularity of a cell (Jahan-Tigh et al. (2012)). The fluorescence detector detects the fluorescent light - in our case of the PI dye.

2.5.1 Preparation

For these experiments seeding into two plates with pronectin coating was performed. Then the plates were incubated for 24 hours. Thereafter one plate was placed on the bioreactor and the loudspeaker was started. A mechanical sinusoidal simulation signal with 55 Hz was applied for 12 hours with a 1h on, 1h off pattern. Different amplitudes were used, corresponding to the maximal deflections measured with the laser vibrometer. After another 4 hours the cells were harvested. The harvesting process was refined in-between the experiments. The working steps and investigation methods are listed below for each experiment. In blue the refinements are highlighted.

experiment #1: $\approx$ 33 μm deflection (U_V = 0.08 V) applied

- working steps in the cell culture:
  - preparing of two 15 ml tubes
  - removal of the cell medium
  - washing with 2 ml PBS per well
  - adding 24 μl of trypsin and incubating for 3 minutes
  - adding of 2 ml medium and placing it in the tubes
  - centrifugation (170 g, 7 min, 22–23 °C)
  - removal of the supernatant & resuspending in PBS
  - centrifugation (170 g, 7 min, 22–23 °C)
  - removal of the supernatant & resuspending in PBS
- investigation methods:
  - viability testing via flow cytometry with PI

experiment #2: $\approx$ 33 μm deflection (U_V = 0.08 V) applied

- working steps in the cell culture:
  - preparing of two 15 ml tubes
  - removal of the cell medium
  - washing with 2 ml PBS per well
  - adding 250 ml of trypsin and incubating for 3 minutes
  - adding of 2 ml medium and placing it in the tubes
  - centrifugation (170 g, 7 min, 22–23 °C)
  - removal of the supernatant & resuspending in PBS
  - centrifugation (170 g, 7 min, 22–23 °C)
  - removal of the supernatant & resuspending in PBS
- investigation methods:
  - pictures (10$\times$ magnification) after the vibration before the harvesting for optical comparisons
  - viability testing via flow cytometry with PI

experiment #3: $\approx$ 298 μm deflection (U_V = 0.77 V) applied

- working steps in the cell culture:
  - preparing of two 15 ml tubes

  - removal of the cell medium
  - washing with 2 ml PBS per well
  - adding 250 ml of trypsin and incubating for 3 minutes
  - adding of 2 ml medium and placing it in the tubes
  - centrifugation (170 g, 7 min, 22–23 °C)
  - removal of the supernatant & resuspending in PBS
  - centrifugation (170 g, 7 min, 22–23 °C)
  - removal of the supernatant & resuspending in PBS
- investigation methods:
  - pictures (10× magnification) after the vibration before the harvesting for optical comparisons
  - viability testing via flow cytometry with PI

experiment #4: $\approx$ 147 μm deflection (U_V = 0.35 V) applied

- working steps in the cell culture:
  - preparing of two 50 ml tubes
  - removal of the cell mediumand placing it in the tubes
  - washing with 2 ml PBS per well and placing it in the tubes
  - adding 500 ml of trypsin and incubating for 5 minutes
  - adding of 2 ml medium and placing it in the tubes
  - centrifugation (170 g, 7 min, 22–23 °C)
  - removal of the supernatant & resuspending in PBS
  - centrifugation (170 g, 7 min, 22–23 °C)
  - removal of the supernatant & resuspending in PBS
- investigation methods:
  - pictures (10× magnification) before the vibration before the harvesting for optical comparisons
  - pictures (10× magnification) after the vibration before the harvesting for optical comparisons
  - viability testing via flow cytometry with PI

experiment #5: $\approx$ 147 μm deflection (U_V = 0.35 V) applied

- working steps in the cell culture:

  - preparing of two 50 ml tubes
  - removal of the cell medium and placing it in the tubes
  - washing with 2 ml PBS per well and placing it in the tubes
  - adding 500 ml of trypsin and incubating for 5 minutes
  - adding of 2 ml medium and placing it in the tubes
  - centrifugation (170 g, 7 min, 22–23 °C)
  - removal of the supernatant & resuspending in PBS
  - centrifugation (170 g, 7 min, 22–23 °C)
  - removal of the supernatant & resuspending in PBS

- investigation methods:
  - pictures (10× magnification) before the vibration before the harvesting for optical comparisons
  - pictures (10× magnification) after the vibration before the harvesting for optical comparisons
  - viability testing via flow cytometry with PI

experiment #6: $\approx$ 147 μm deflection (U_V = 0.35 V) applied

- working steps in the cell culture:
  - preparing of two 50 ml tubes
  - removal of the cell medium and placing it in the tubes
  - washing with 2 ml PBS per well and placing it in the tubes
  - adding 500 ml of trypsin and incubating for 5 minutes
  - adding of 2 ml medium and placing it in the tubes
  - centrifugation (170 g, 7 min, 22–23 °C)
  - removal of the supernatant & resuspending in PBS
  - centrifugation (170 g, 7 min, 22–23 °C)
  - removal of the supernatant & resuspending in PBS

- investigation methods:
  - pictures (10× magnification) before the vibration before the harvesting for optical comparisons
  - pictures (10× magnification) after the vibration before the harvesting for optical comparisons
  - viability testing via flow cytometry with PI

During experiment #4 some of the solution was heated to 65 °C for 20 minutes and measured as well.
Between experiment #4 and #5 normal cells were compared with cells, which where heated for 50 minutes to 100 °C. The cells of one T75 flask were harvested. The normal procedure of cell passaging was performed until re-suspending after trypsinization. Then the cells were placed in a tube and centrifuged. Thereafter the supernatant was removed and PBS was added, in which the pellet was resolved. Centrifugation was carried out again, followed by removal of the supernatant again. Finally, resolving of the pellet in PBS was carried out and the tubes were transferred to the flow cytometer for testing and heating.

For each condition 500 μl of cell suspension were placed in the testing tubes, used for the flow cytometry, and 3 μl of PI were added for staining. The settings of the voltage for FSC, SSC and PI for the experiments channel in the BD FACSDiva software are provided in the Table 2.2.

Table 2.2 The settings of the channels in the BD FACSDIVA software for the different experiments.

Experiment	FSC	SSC	PI
#1	139	193	496
#2 - #6	190	221	496
heating experiment	190	221	496

2.5.2 Data analysis

For data analysis plots were generated and ”gates” were applied. Through gating a sub-population of the data is selected for further analysis(Jahan-Tigh et al. (2012)). First a plot with FSC-A on the x-axis and SSC-A on the y-axis was generated. There a gate was applied to distinguish between cells and other parts in the solution (e.g. DNA parts). Thereafter two plots were generated with FSC-A on the x-axis and FSC-H on the y-axis and FSC-W on the x-axis and FSC-A on the y-axis. In these plots two gates were generated to distinguish between single cells and duplets, as sometimes the cells stick together leading to a wrong signal, therefore this data is excluded. Finally, a plot was generated with PI-A on the x-axis and SSC-A on the y-axis. Here two gates were generated to distinguish PI-positive (dead) and PI-negative (living) cells. This gate should be set with the help of the measurement of unstained cells. During the heating experiment and the experiments #5 and #6 an signal of unstained was recorded. For this signal all data points should be PI-negative, as there was no PI in the probe. Further, for all data recordings the same gates were applied to allow better comparability.

3 Results

3.1 The bioreactor

The firstprototype was made using the structure-borne driver. A picture is shown in Fig. 3.1b.. The bioreactor was secured using screws on a fixation milled out of POM.

For the second prototype with the loudspeaker it was possible with the CNC milling machine to built a bioreactor made of POM. A picture of the bioreactor during the laser vibrometry measurments is provided in Fig. 3.1a. The bioreactor was made of several plates of POM, which were put together. On top a support was made to secure the well plate. The support works with or without the top of the well plate.

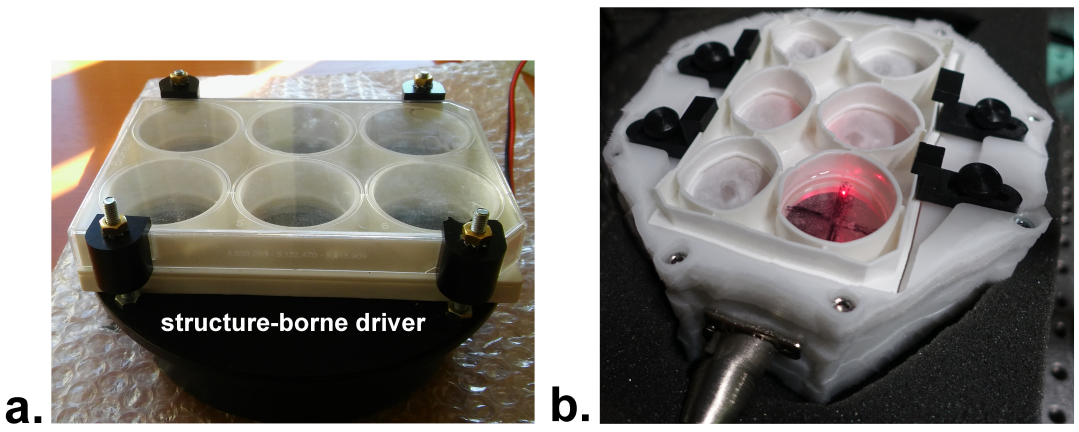


Figure 3.1 **a.**The Prototype with the structure-borne driver. **b.** The Prototype with the loudspeaker during the laser vibrometry measurements.

3.2 Laser vibrometer measurements

The developed prototypes were investigated with a laser vibrometer to examine the vibration behaviour of the silicone membranes.

3.2.1 Measurements of the prototype with the structure-borne driver

For the measurement a white noise signal was used. In Fig. 3.2 the diagram for the center of membrane m5, the support and solely the structure-borne driver is provided.

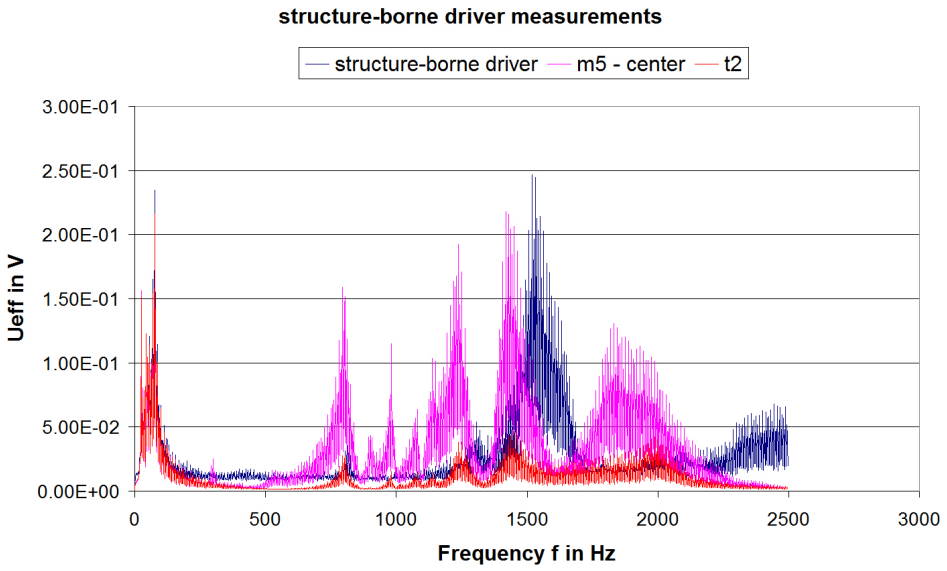


Figure 3.2 The FFT of the laser vibrometry signal U_{eff} against the frequency; a white noise signal was applied.

It was observed, that although a white noise signal was inserted (with the same amplitude over all frequencies) the structure-borne driver excerted different amplitudes at different frequencies. This might come from the main purpose of the structure-borne driver, as it is normally fixed to a plate, which is then vibrating. The frequency response depends then on the plate. The behaviour for different signals was not predictable and this prototype was not further investigated.

3.2.2 Measurements of the prototype with the loudspeaker

Thereafter the behaviour of the prototype with the loudspeaker was investigated.

Dry measurements

Following measurements were made using the chirp signal with repeating chirps from 1 to 2500 Hz for 0.25 seconds. The measured voltage was 0.92 V. In Fig. 3.3 the fast Fourier transform of the laser vibrometer signal of the measurement points on the left side of membrane 1 of plate 1 are provided.

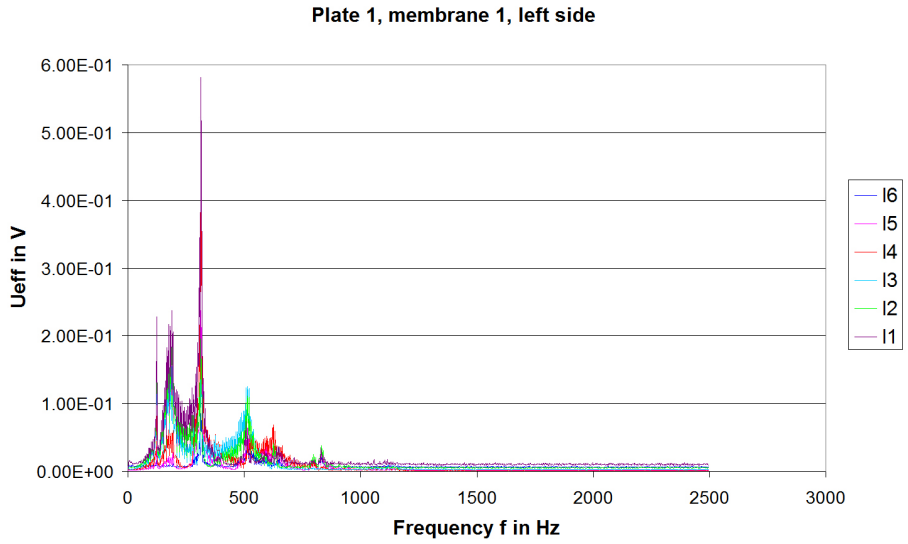


Figure 3.3 All data points (1024) from the left side of membrane m1 of plate 1; the FFT of the laser vibrometer signal U_{eff} against the frequency; a chirp signal was applied.

For magnification only the first 250 data points (until a frequency of 607.91) were plotted in Fig. 3.4.

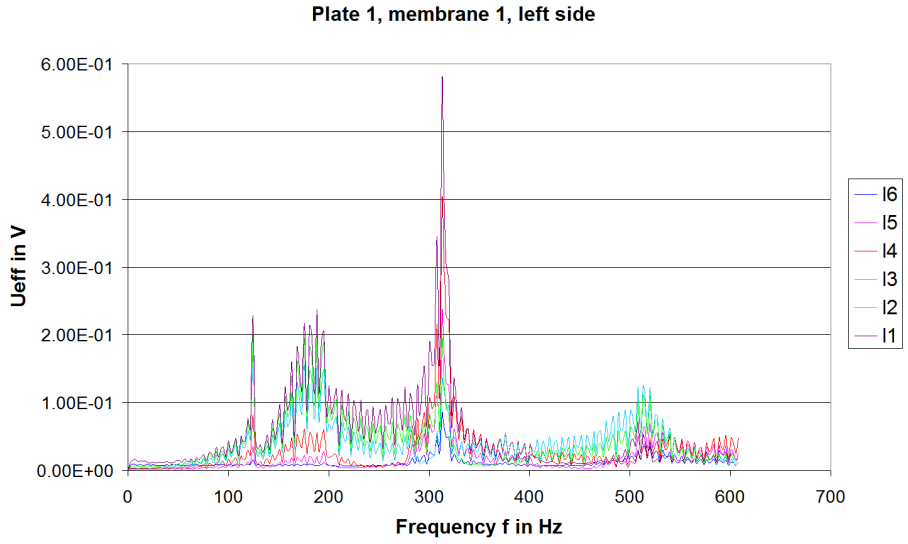


Figure 3.4 First 250 data points from the left side of membrane m1 of plate 1; the FFT of the laser vibrometer signal U_{eff} against the frequency; a chirp signal was applied.

In Appendix A the diagrams of all other directions and membranes of plate 1 and 2 are provided.

In Fig. 3.5 and 3.6 the fast Fourier transform of the laser vibrometer signal of the measurement points in the center of the membranes of plate 1 are provided.

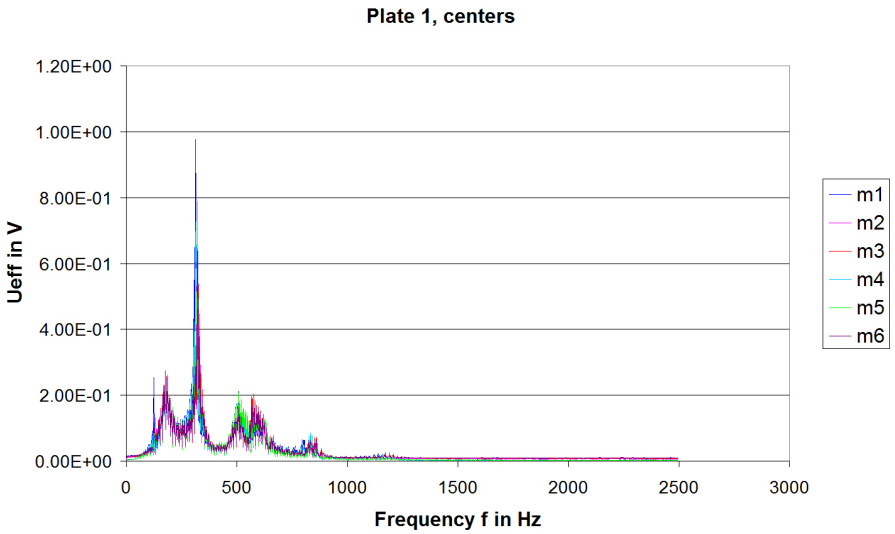


Figure 3.5 All data points (1024) from the center of the membranes of plate 1; the FFT of the laser vibrometer signal U_{eff} against the frequency; a chirp signal was applied.

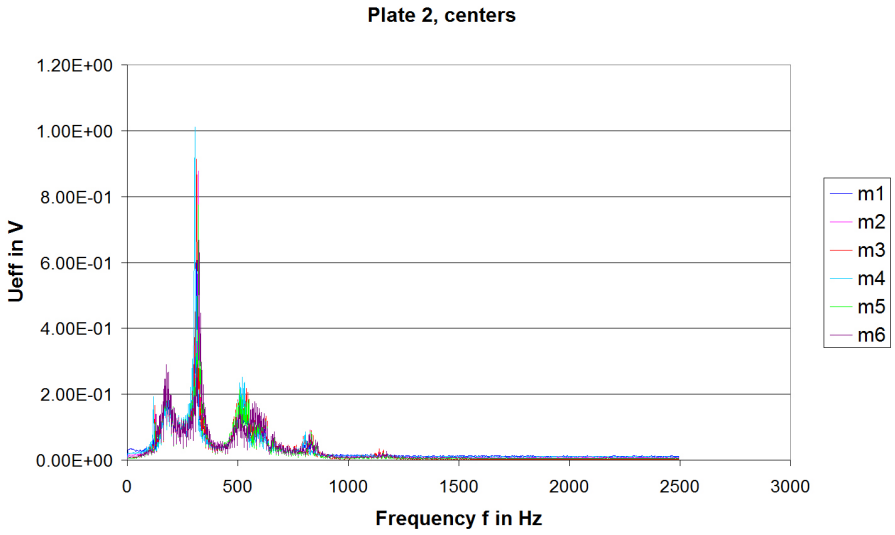


Figure 3.6 All data points (1024) from the center of the membranes of plate 2; the FFT of the laser vibrometer signal U_{eff} against the frequency; a chirp signal was applied.

For magnification only the first 250 data points (until a frequency of 607.91) were plotted in Fig. 3.7 and 3.8.

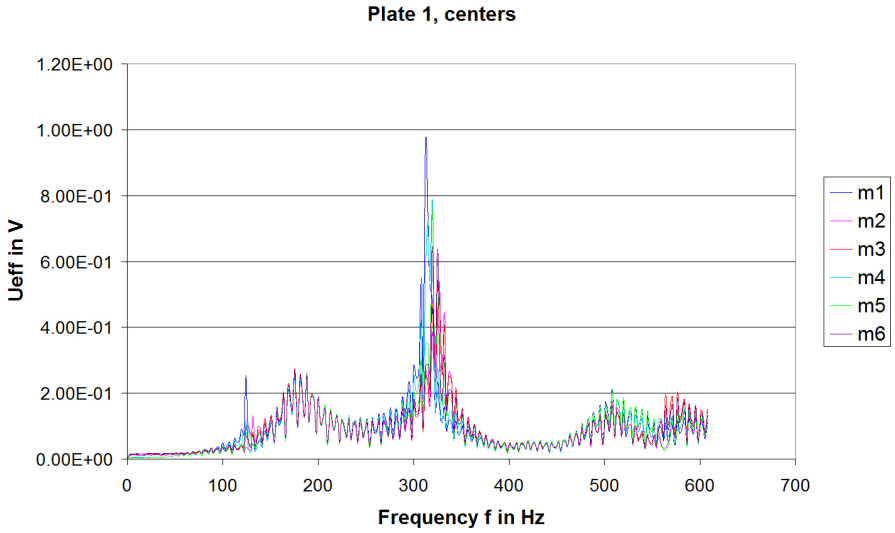


Figure 3.7 First 250 data points from the center of the membranes of plate 1; the FFT of the laser vibrometer signal U_{eff} against the frequency; a chirp signal was applied.

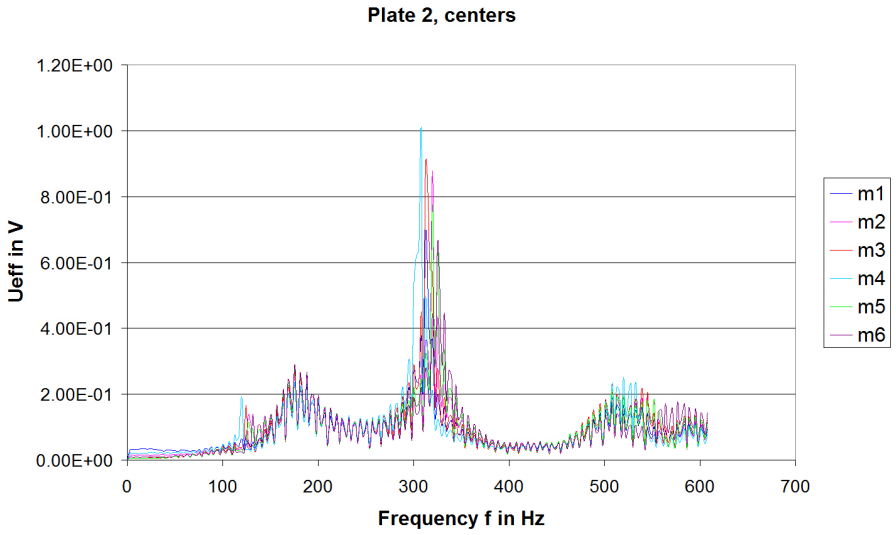


Figure 3.8 First 250 data points from the center of the membranes of plate 2; the FFT of the laser vibrometer signal U_{eff} against the frequency; a chirp signal was applied.

The signals form the measurement points of the support of plate 1 and 2 are shown in Fig. 3.9 and 3.10.

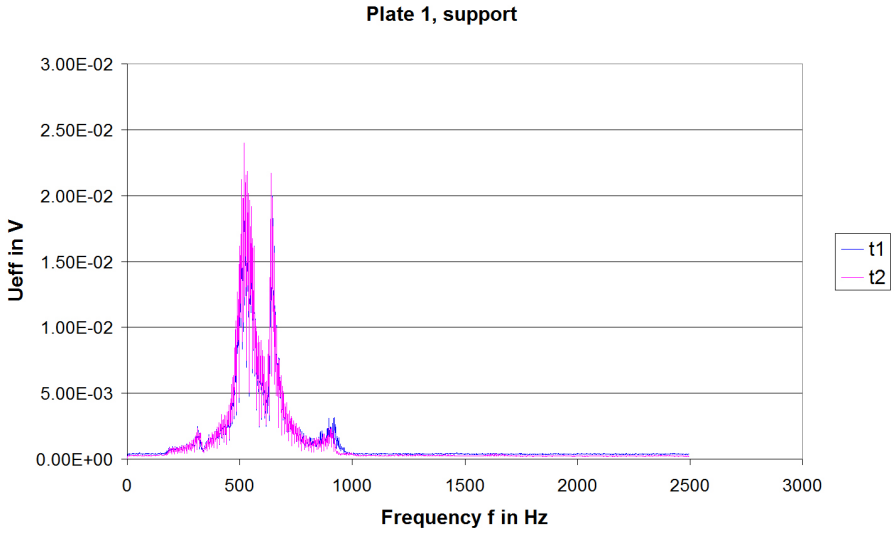


Figure 3.9 All data points (1024) from the support measurement points of plate 1; the FFT of the laser vibrometer signal U_{eff} against the frequency; a chirp signal was applied.

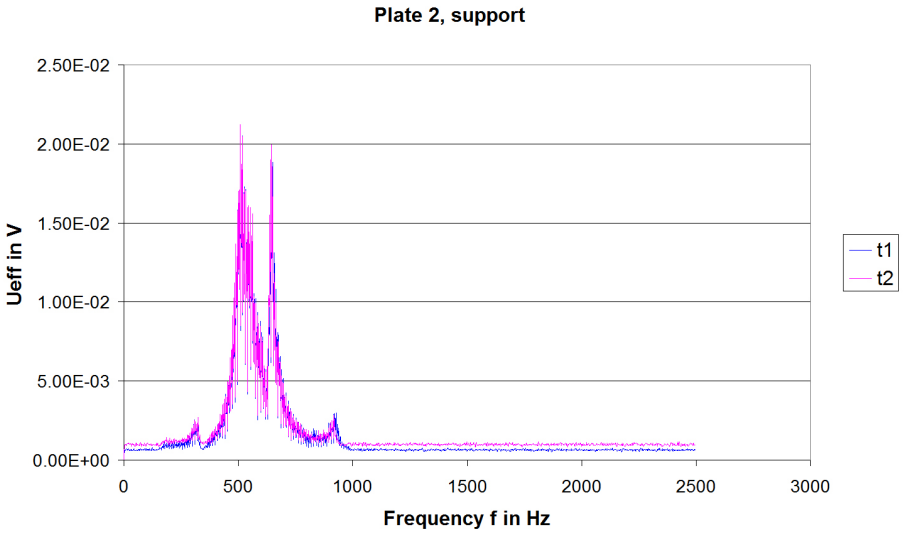


Figure 3.10 All data points (1024) from the support measurement points of plate 2; the FFT of the laser vibrometer signal U_{eff} against the frequency; a chirp signal was applied.

As can be seen, the amplitude of the support is lower than the amplitude of the membrane. Therefore, the influences of the support on the oscillation behaviour of the membrane can be neglected.

For all membranes a peak at about 180 and 310 Hz was observed. To find the grid point with the maximum peak, the curves from various frequencies around this values were plotted. There was a little variation between the membranes. Therefore for the frequencies, which were quite high, the deflection was calculated and plotted. The deflection for the horizontal measurement points of membrane 1 of plate 1 around 180 Hz and around 310 Hz is shown in Fig. 3.11 and 3.12.

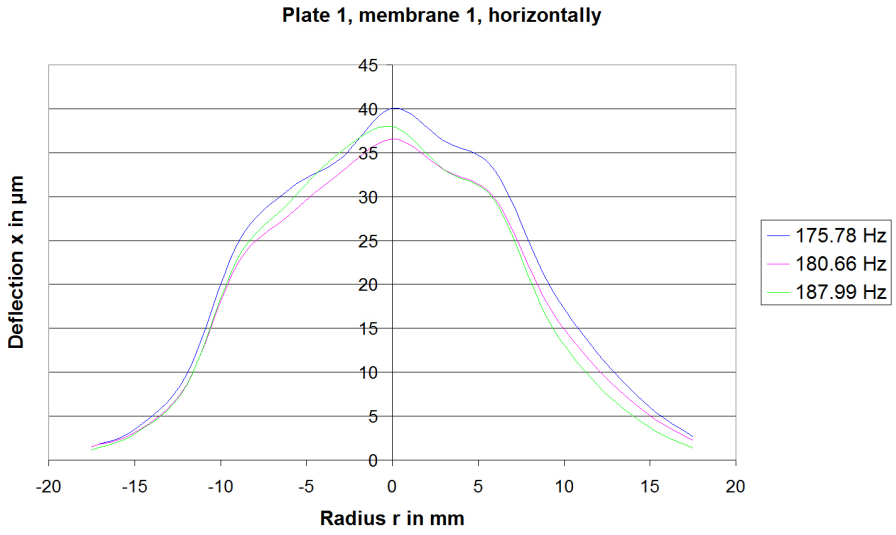


Figure 3.11 Horizontal measurement points of membrane m1 of plate 1; the deflection x against the radius r around 180 Hz

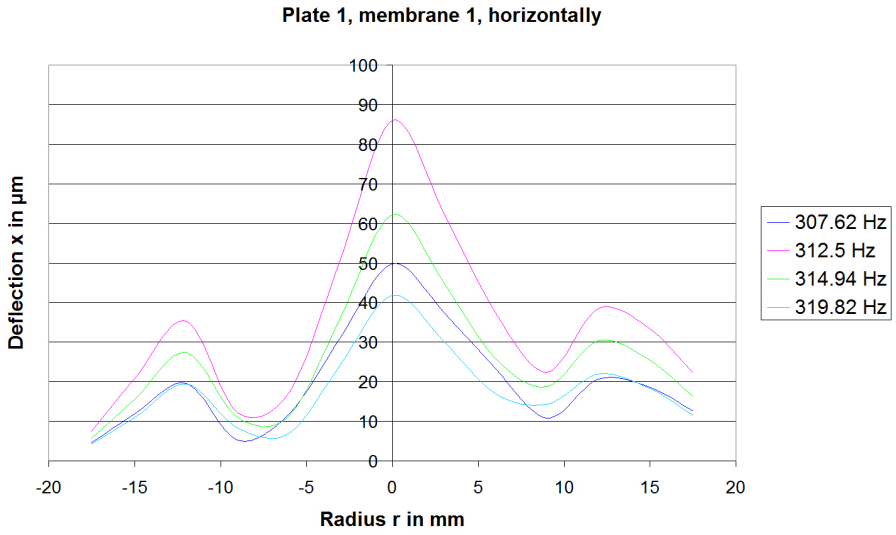


Figure 3.12 Horizontal measurement points of membrane m1 of plate 1; the deflection x against the radius r around 310 Hz

In Appendix A the diagrams of all other directions and membranes of plate 1 and 2 are provided.

For comparison the Pearson correlation coefficient was calculated to examine the correlation between the membranes of each plate and between the membranes of the two plates.

In Table 3.1 the minimal, maximal and mean values of the correlation coefficients are provided. The detailed correlation coefficients are provided in Appendix B.

Table 3.1 Minimal, maximal and mean values of the pearson coefficients.

correlation calculated between	mean r	SD of r	minimal r	maximal r
m1 - m6 of plate 1	0.901	0.072	0.779	0.982
m1 - m6 of plate 2	0.841	0.097	0.652	0.986
m1 - m6 of plate 1 and m1 - m6 of plate 2	0.880	0.096	0.65	0.992

Measurements taken with water in the well

Thereafter for the next measurements the well of interest was filled with 2.5 ml of water to resemble the cell suspension, which is normally present during cell cultivation. First, measurements with the chirp were taken. The measured voltage was again 0.92 V.

In Fig. 3.3 the fast Fourier transform of the laser vibrometer signal of the measurement points on the left side of membrane 3 of plate 1 are provided.

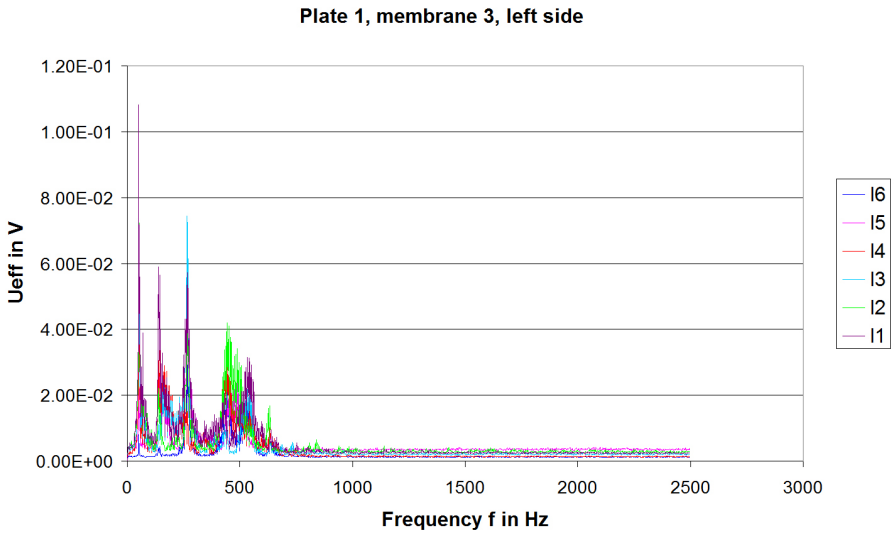


Figure 3.13 All data points (1024) from the left side of membrane m3 of plate 1; the FFT of the laser vibrometer signal U_{eff} against the frequency; the well was filled with 2.5 ml of water; a chirp signal was applied.

For magnification only the first 250 data points (until a frequency of 607.91) were plotted in Fig. 3.4.

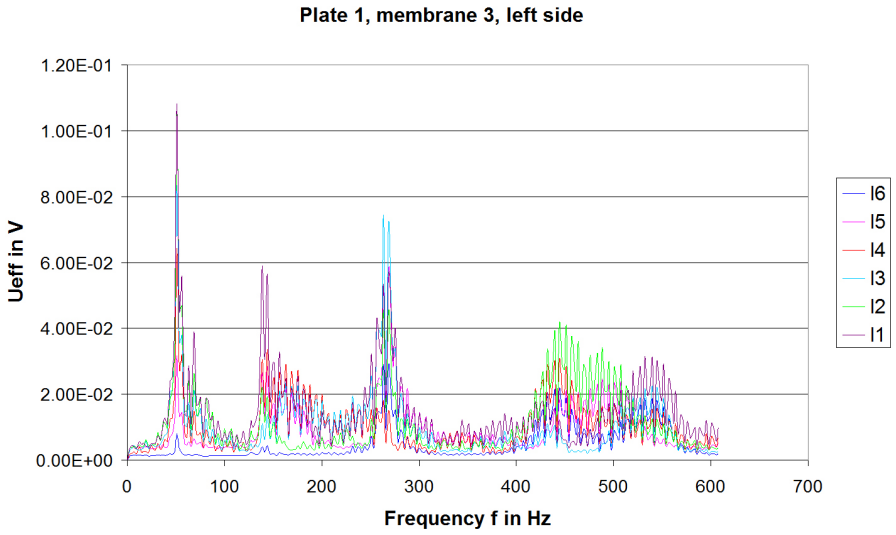


Figure 3.14 First 250 data points from the left side of membrane m3 of plate 1; the FFT of the laser vibrometer signal U_{eff} against the frequency; the well was filled with 2.5 ml of water; a chirp signal was applied.

The FFT of the laser vibrometer signal of the measurement point in the center of membrane 3 in total and in detail is shown in Fig. 3.15 and 3.16.

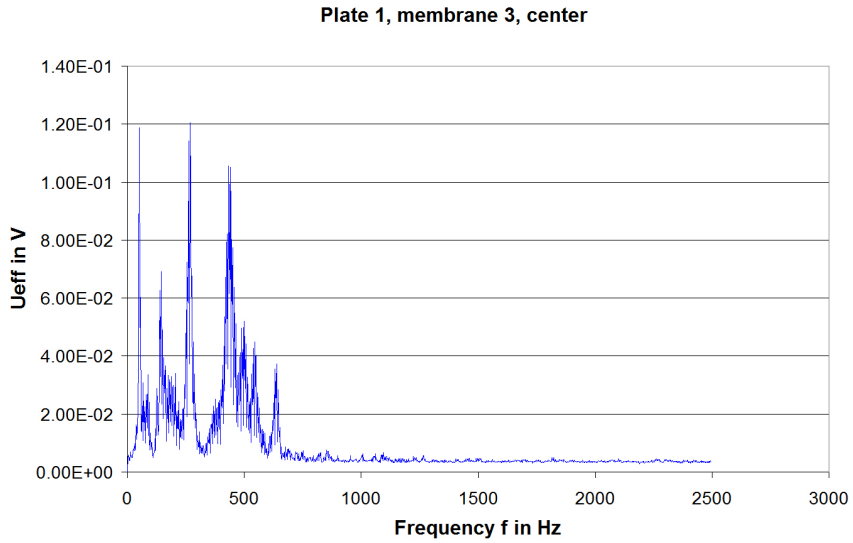


Figure 3.15 All data points (1024) from the center of membrane m3 of plate 1; the FFT of the laser vibrometer signal U_{eff} against the frequency; the well was filled with 2.5 ml of water; a chirp signal was applied.

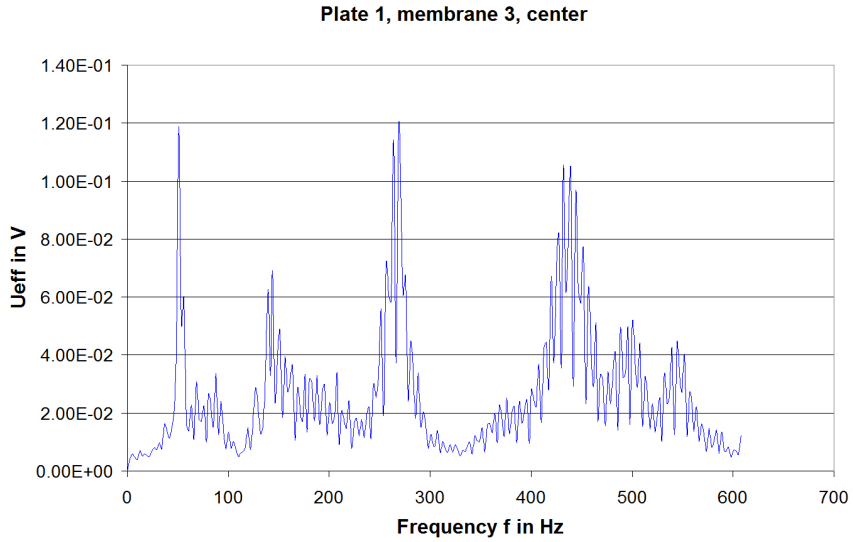


Figure 3.16 First 250 data points from the center of membrane m3 of plate 1; the FFT of the laser vibrometer signal U_{eff} against the frequency; the well was filled with 2.5 ml of water; a chirp signal was applied.

In Appendix A the diagrams of all other directions of membrane 3 of plate 1 are shown.

For the frequencies, which were quite high, the deflection was calculated and plotted. The deflection for the horizontal measurement points of membrane 3 of plate 1 around 55, 140, 270 and 440 Hz is provided from Fig. 3.17 to Fig. 3.20.

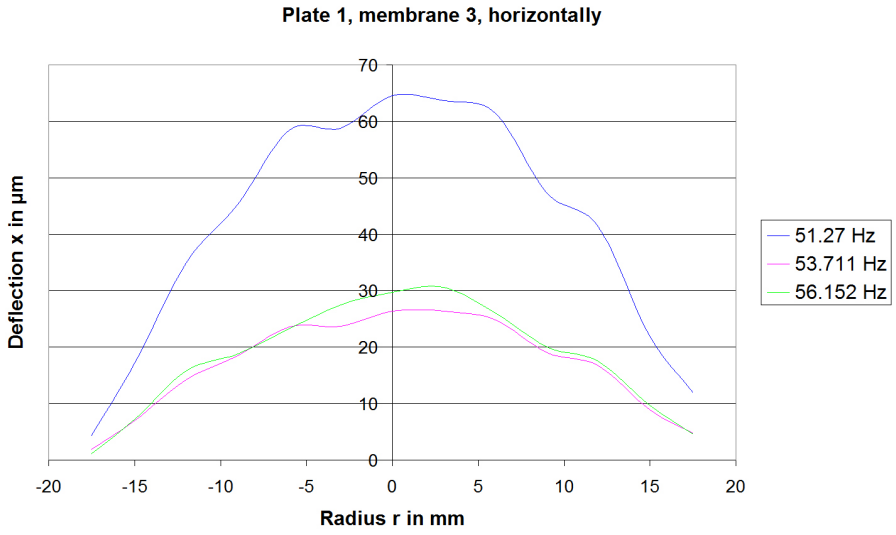


Figure 3.17 Horizontal measurement points of membrane m1 of plate 1; the deflection x against the radius r around 55 Hz; the well was filled with 2.5 ml of water

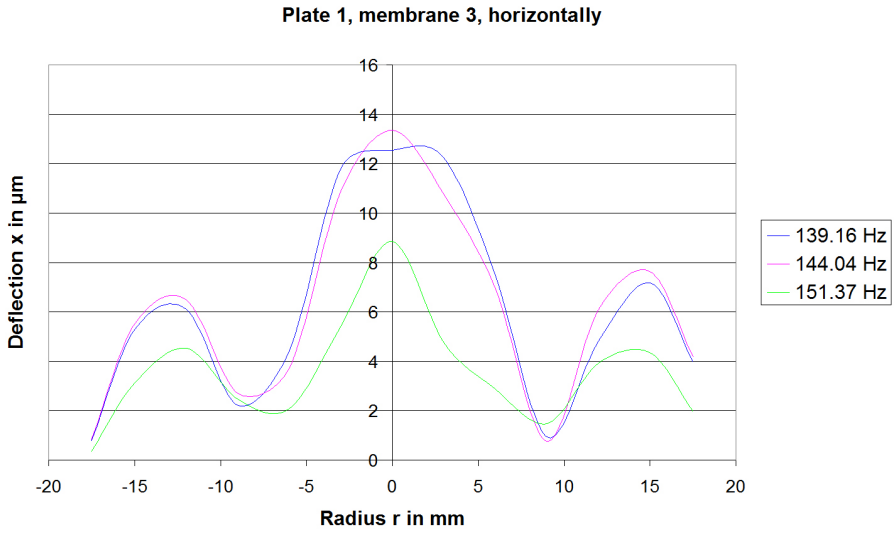


Figure 3.18 Horizontal measurement points of membrane m1 of plate 1; the deflection x against the radius r around 140 Hz; the well was filled with 2.5 ml of water;

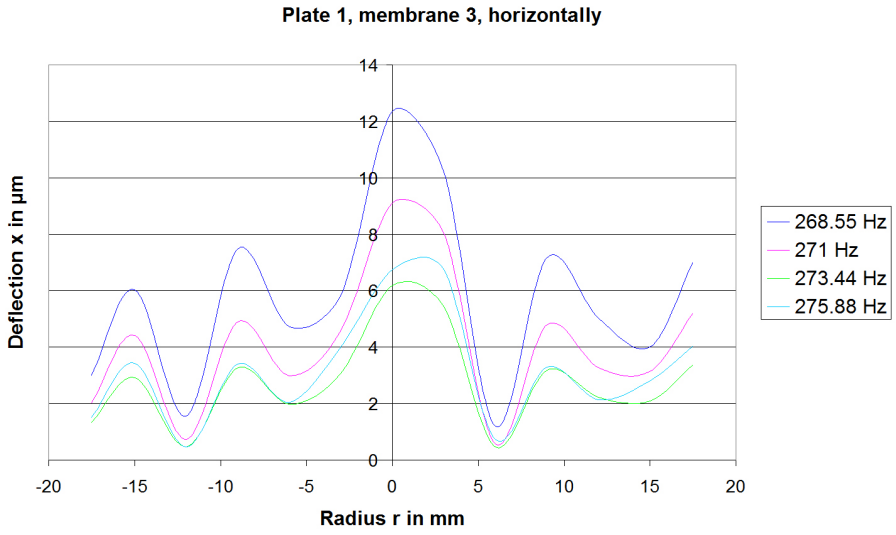


Figure 3.19 Horizontal measurement points of membrane m1 of plate 1; the deflection x against the radius r around 270 Hz; the well was filled with 2.5 ml of water

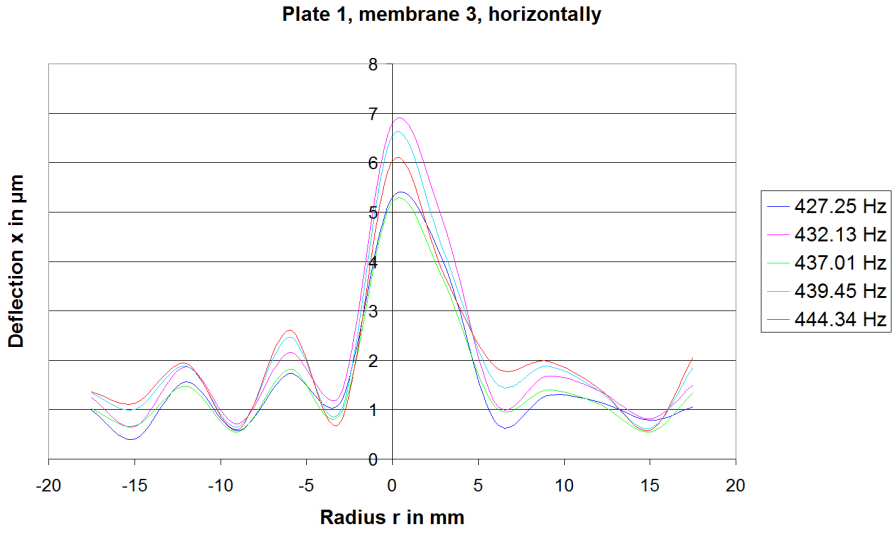


Figure 3.20 Horizontal measurement points of membrane m1 of plate 1; the deflection x against the radius r around 440 Hz; the well was filled with 2.5 ml of water

In Appendix A the deflections for the vertical measurement are shown.

Thereafter sinusoidal signals with 55, 140, 180, 200 and 300 Hz were applied and the horizontal measurement points were recorded. For the 55 Hz signal the voltage was 0.95

V, for the 140 and 180 Hz signal it was 0.97 V and for the 200 and 300 Hz signal it was 0.98 V. This measurements were taken at membrane m3 of plate 2. The resulting zoomed signals for the left side and the center are shown from Fig. 3.21 to Fig.

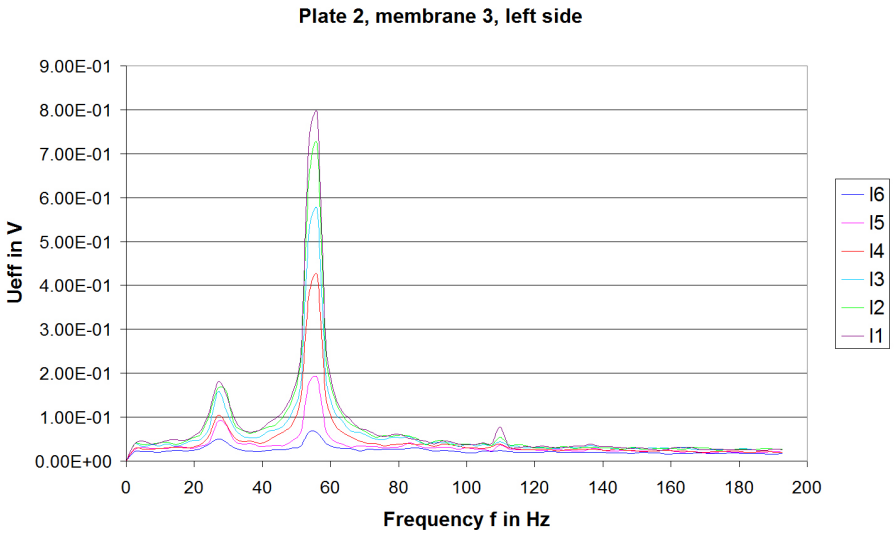


Figure 3.21 First 80 data points (until a frequency of 192.87 Hz) from the left side of membrane m3 of plate 2; the FFT of the laser vibrometer signal U_{eff} against the frequency; the well was filled with 2.5 ml of water; a sinusoidal signal with 55 Hz was applied

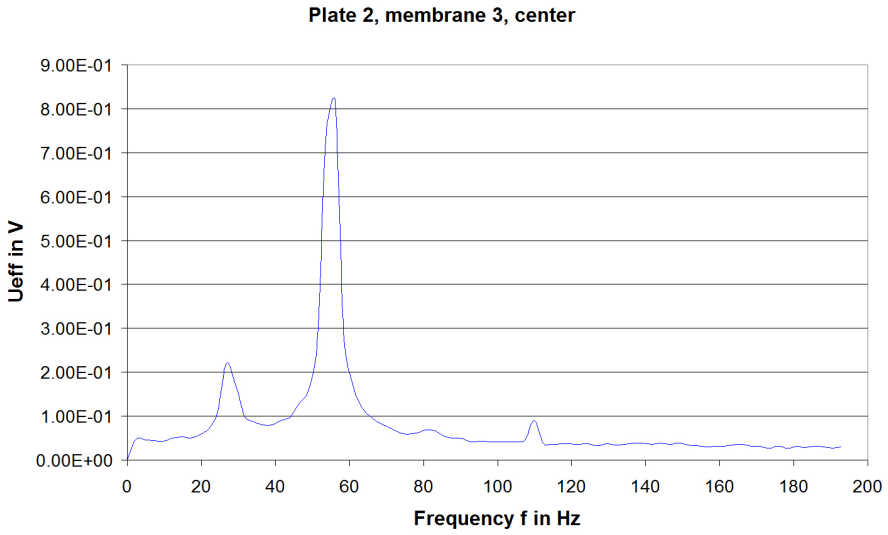


Figure 3.22 First 80 data points (until a frequency of 192.87 Hz) from the center of membrane m3 of plate 2; the FFT of the laser vibrometer signal U_{eff} against the frequency; the well was filled with 2.5 ml of water; a sinusoidal signal with 55 Hz was applied

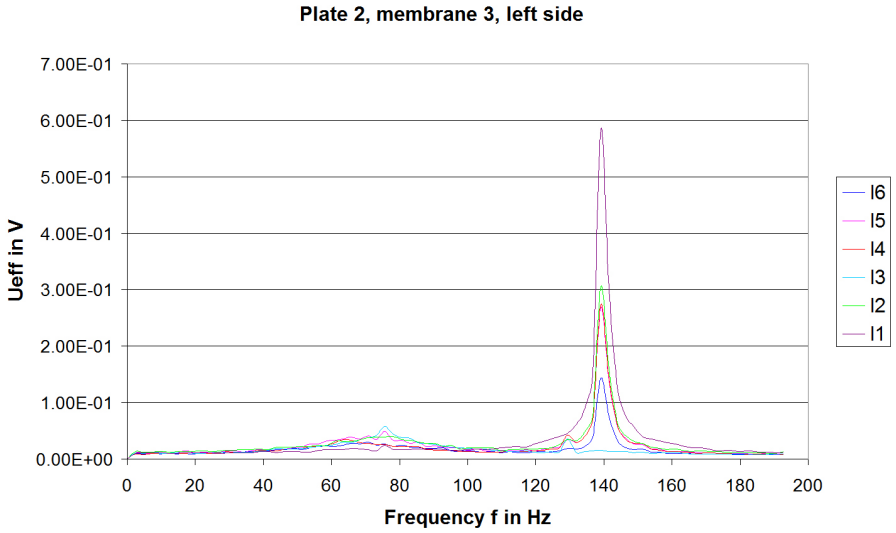


Figure 3.23 First 80 data points (until a frequency of 192.87 Hz) from the left side of membrane m3 of plate 2; the FFT of the laser vibrometer signal U_{eff} against the frequency; the well was filled with 2.5 ml of water; a sinusoidal signal with 140 Hz was applied

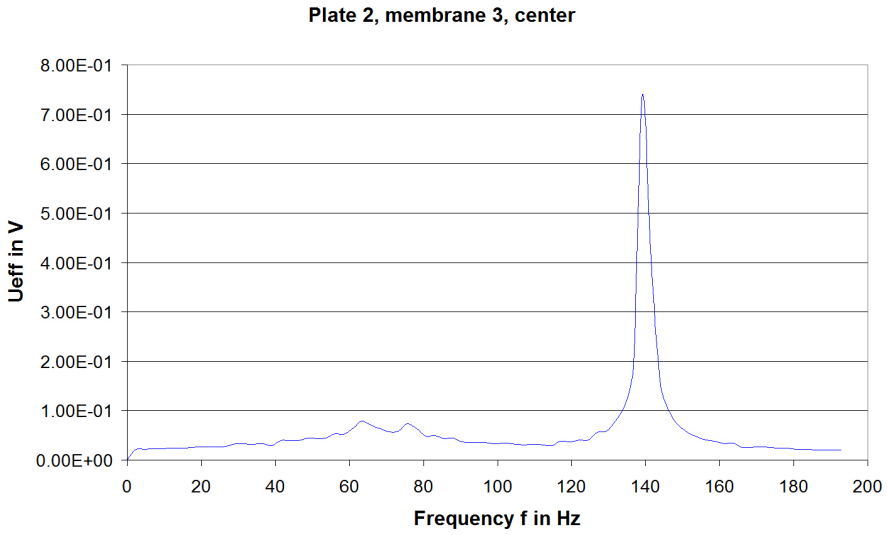


Figure 3.24 First 80 data points (until a frequency of 192.87 Hz) from the center of membrane m3 of plate 2; the FFT of the laser vibrometer signal U_{eff} against the frequency; the well was filled with 2.5 ml of water; a sinusoidal signal with 140 Hz was applied

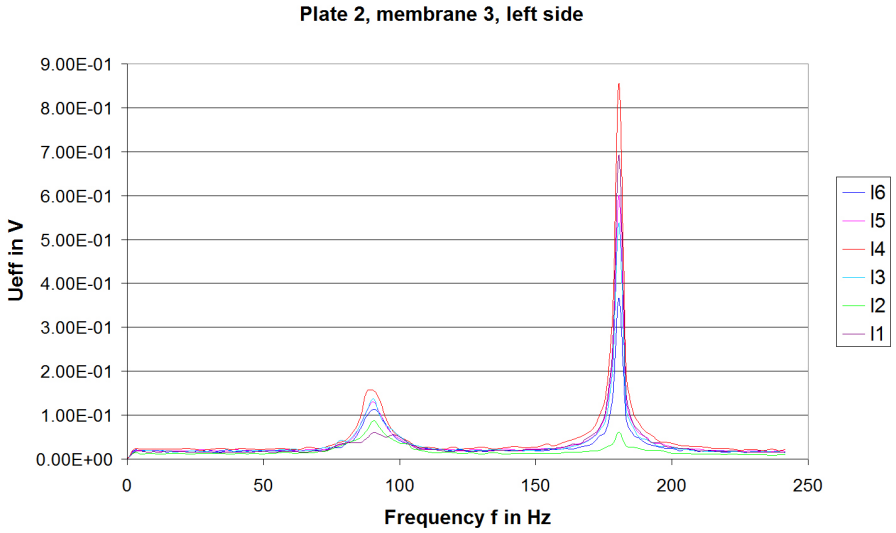


Figure 3.25 First 100 data points (until a frequency of 241.7 Hz) from the left side of membrane m3 of plate 2; the FFT of the laser vibrometer signal U_{eff} against the frequency; the well was filled with 2.5 ml of water; a sinusoidal signal with 180 Hz was applied

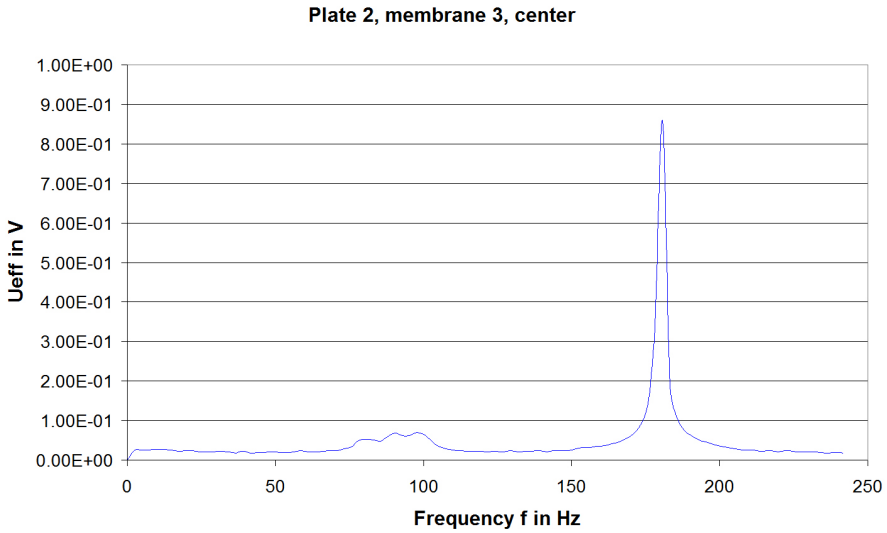


Figure 3.26 First 100 data points (until a frequency of 241.7 Hz) from the center of membrane m3 of plate 2; the FFT of the laser vibrometer signal U_{eff} against the frequency; the well was filled with 2.5 ml of water; a sinusoidal signal with 180 Hz was applied

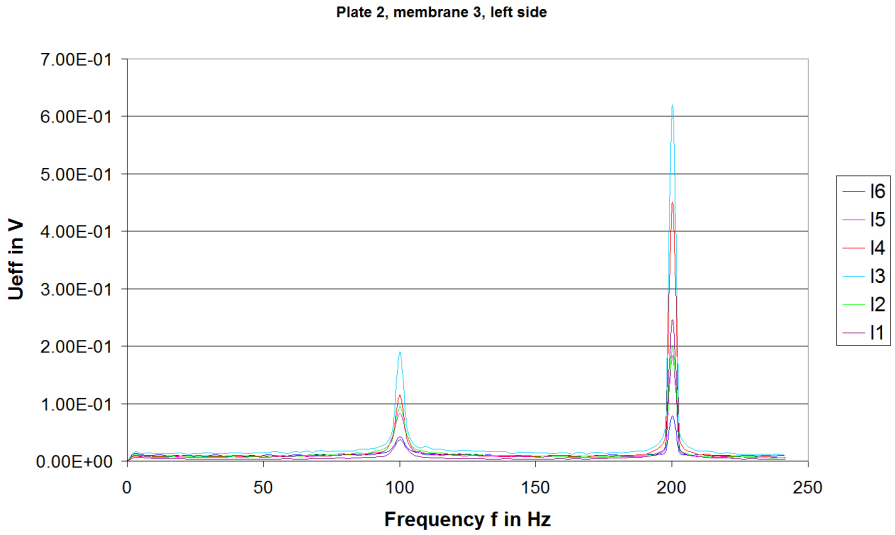


Figure 3.27 First 100 data points (until a frequency of 241.7 Hz) from the left side of membrane m3 of plate 2; the FFT of the laser vibrometer signal U_{eff} against the frequency; the well was filled with 2.5 ml of water; a sinusoidal signal with 200 Hz was applied

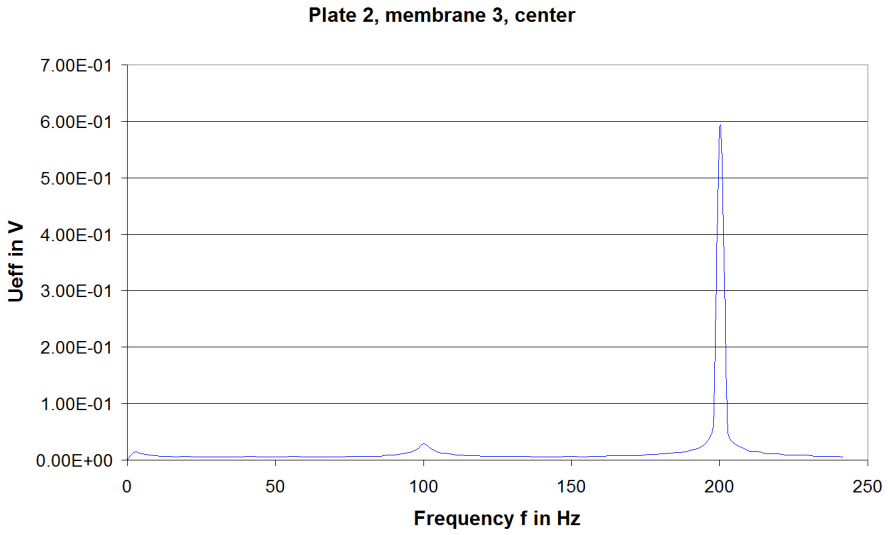


Figure 3.28 First 100 data points (until a frequency of 241.7 Hz) from the center of membrane m3 of plate 2; the FFT of the laser vibrometer signal U_{eff} against the frequency; the well was filled with 2.5 ml of water; a sinusoidal signal with 200 Hz was applied

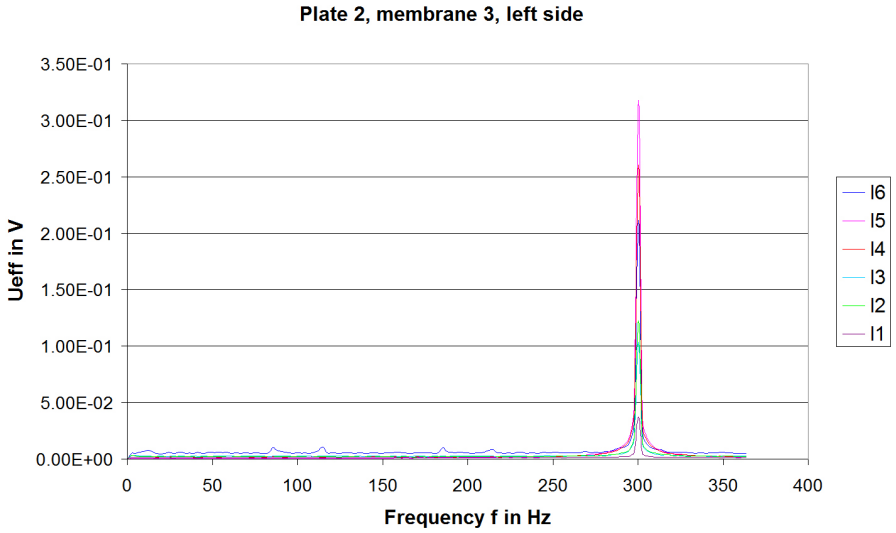


Figure 3.29 First 150 data points (until a frequency of 363.77 Hz) from the left side of membrane m3 of plate 2; the FFT of the laser vibrometer signal U_{eff} against the frequency; the well was filled with 2.5 ml of water; a sinusoidal signal with 300 Hz was applied

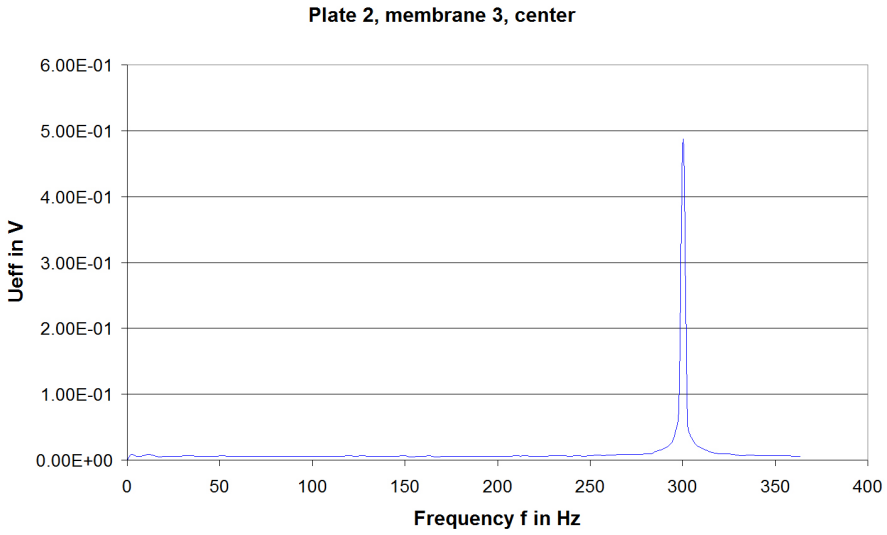


Figure 3.30 First 150 data points (until a frequency of 363.77 Hz) from the center of membrane m3 of plate 2; the FFT of the laser vibrometer signal U_{eff} against the frequency; the well was filled with 2.5 ml of water; a sinusoidal signal with 300 Hz was applied

The signals with all data points for this measurement points and the signals from the ride side are provided in Appendix A.

For the 55 Hz signal, apart from the expected peak, another smaller peak around 27 Hz appeared. This was also observed for the 200 Hz signal, where another smaller peak appeared around 100 Hz. The deflections for the mono-frequent measurements for the observed peaks are shown from Fig. 3.31 to Fig. 3.37.

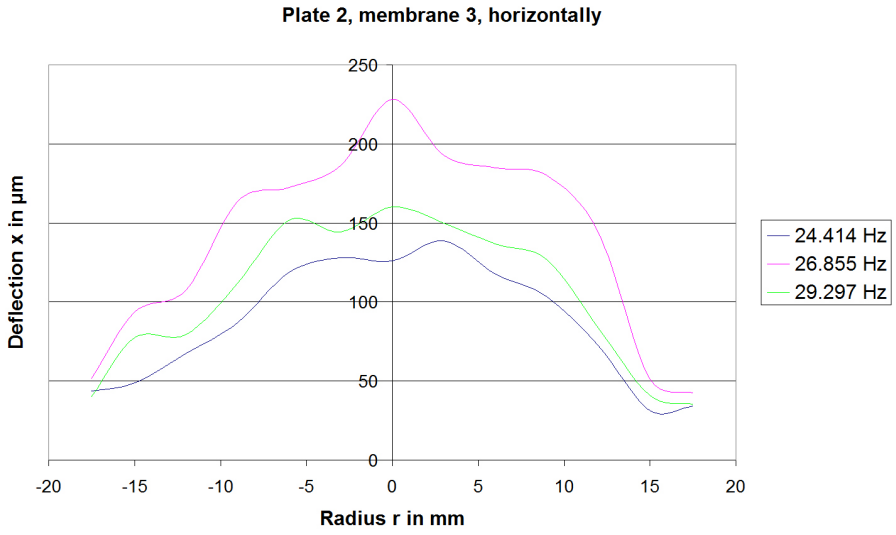


Figure 3.31 Horizontal measurement points of membrane m3 of plate 2; the deflection x against the radius r around 27 Hz; the well was filled with 2.5 ml of water; a sinusoidal signal with 55 Hz was applied

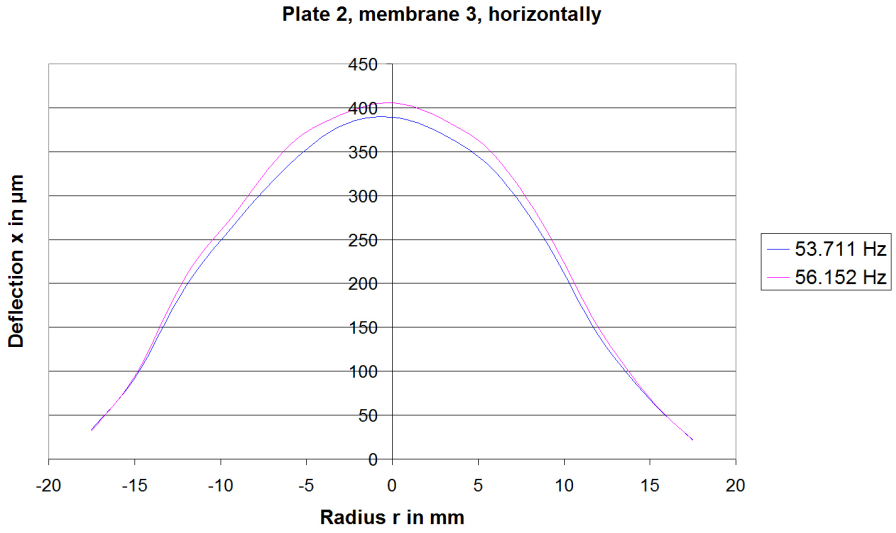


Figure 3.32 Horizontal measurement points of membrane m3 of plate 2; the deflection x against the radius r around 55 Hz; the well was filled with 2.5 ml of water; a sinusoidal signal with 55 Hz was applied

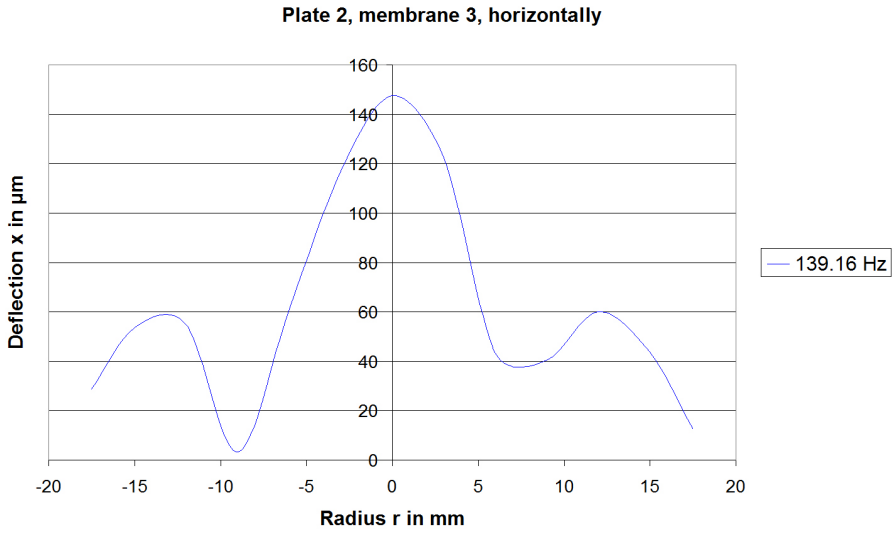


Figure 3.33 Horizontal measurement points of membrane m3 of plate 2; the deflection x against the radius r around 140 Hz; the well was filled with 2.5 ml of water; a sinusoidal signal with 140 Hz was applied

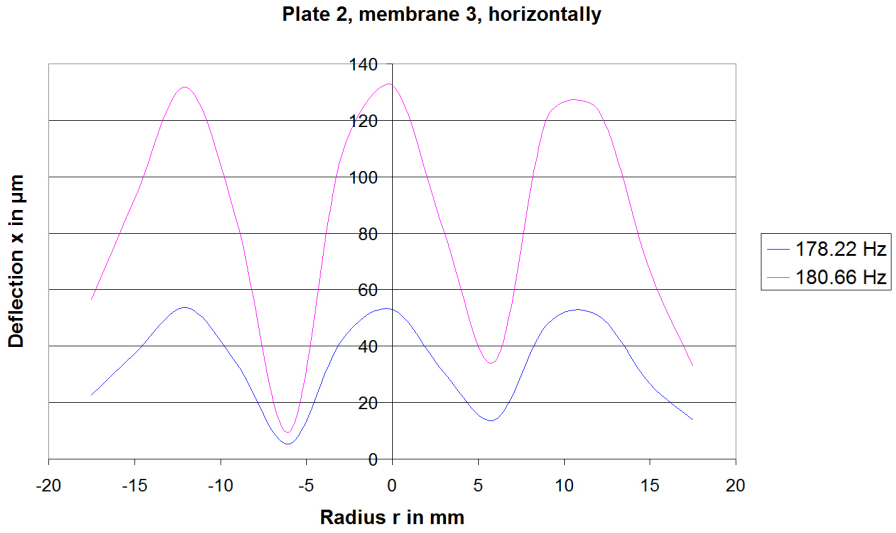


Figure 3.34 Horizontal measurement points of membrane m3 of plate 2; the deflection x against the radius r around 180 Hz; the well was filled with 2.5 ml of water; a sinusoidal signal with 180 Hz was applied

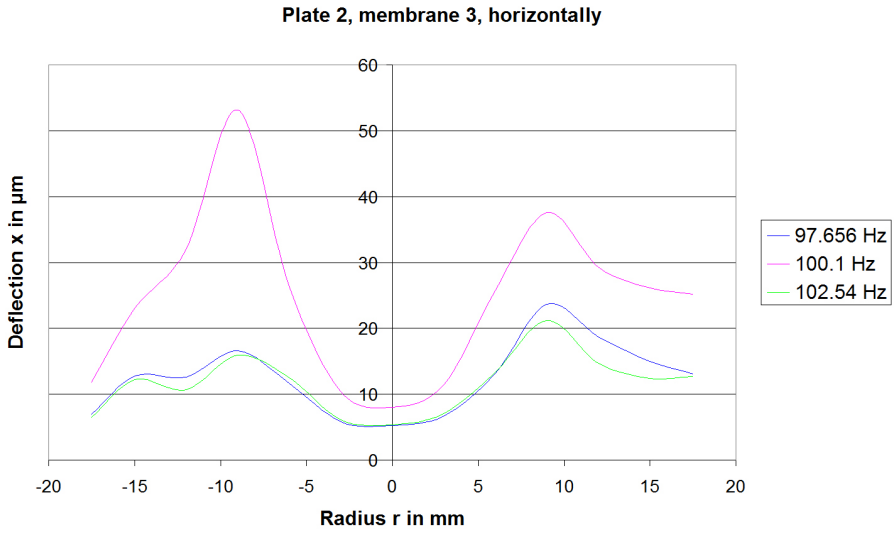


Figure 3.35 Horizontal measurement points of membrane m3 of plate 2; the deflection x against the radius r around 100 Hz; the well was filled with 2.5 ml of water; a sinusoidal signal with 200 Hz was applied

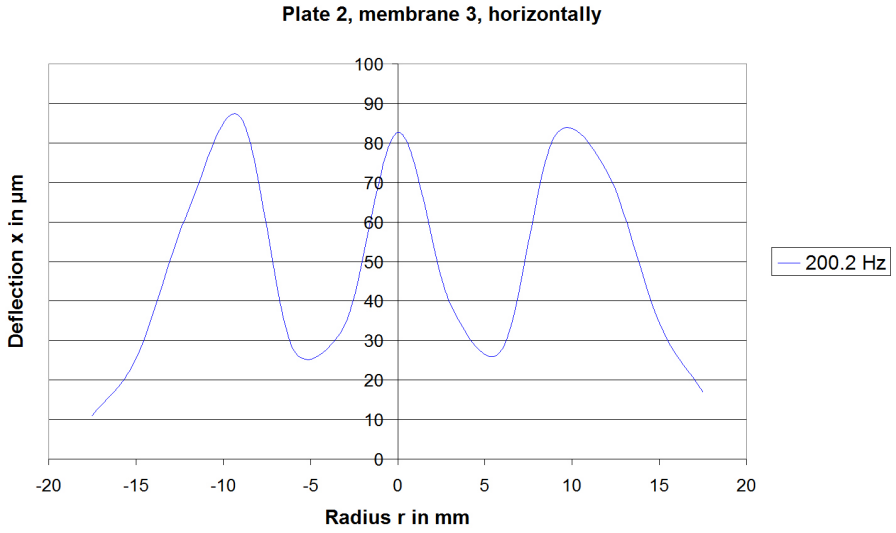


Figure 3.36 Horizontal measurement points of membrane m3 of plate 2; the deflection x against the radius r around 200 Hz; the well was filled with 2.5 ml of water; a sinusoidal signal with 200 Hz was applied

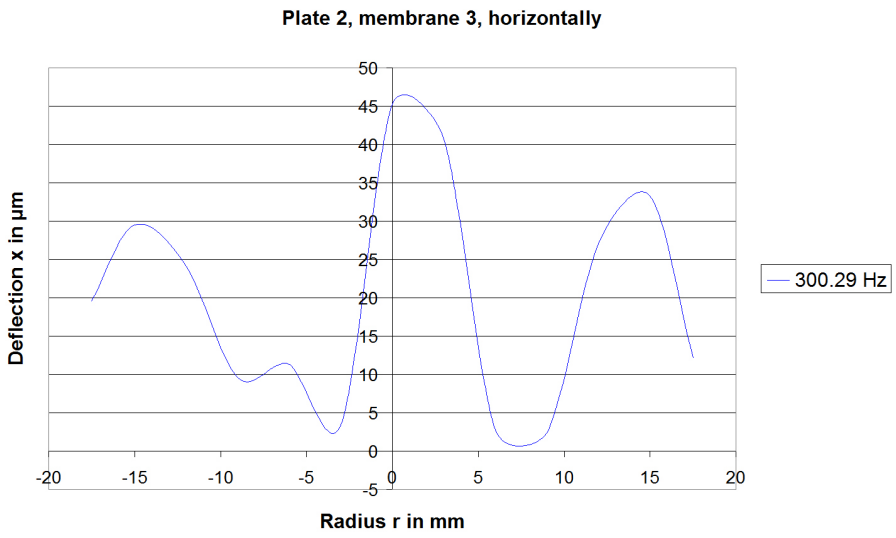


Figure 3.37 Horizontal measurement points of membrane m3 of plate 2; the deflection x against the radius r around 300 Hz; the well was filled with 2.5 ml of water; a sinusoidal signal with 300 Hz was applied

Thereafter a artifical signal, resembling the measurements taken from the larynx from the Group around Micheal D¨linger. The measured voltage was 0.98 V.

The total and zoomed signals for the left side and the center are shown from Fig. 3.38 to Fig. 3.41.

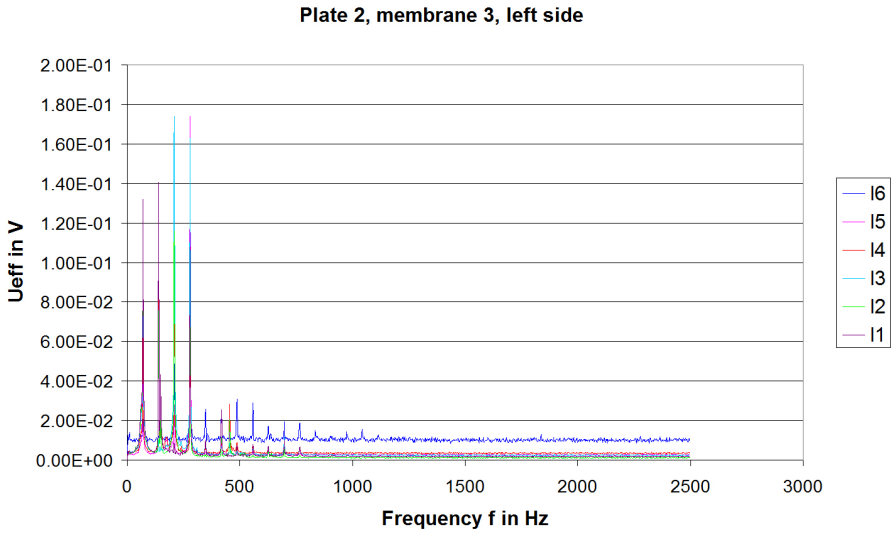


Figure 3.38 All data points (1024) from the left side of membrane m3 of plate 2; the FFT of the laser vibrometer signal U_{eff} against the frequency; the well was filled with 2.5 ml of water; a artificial larynx signal was applied.

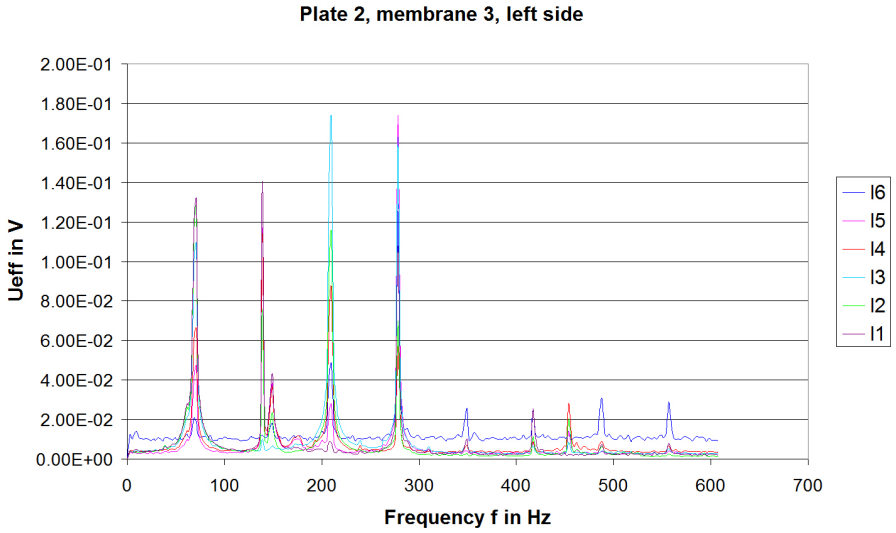


Figure 3.39 First 250 data points from the left side of membrane m3 of plate 2; the FFT of the laser vibrometer signal U_{eff} against the frequency; the well was filled with 2.5 ml of water; a artificial larynx signal was applied.

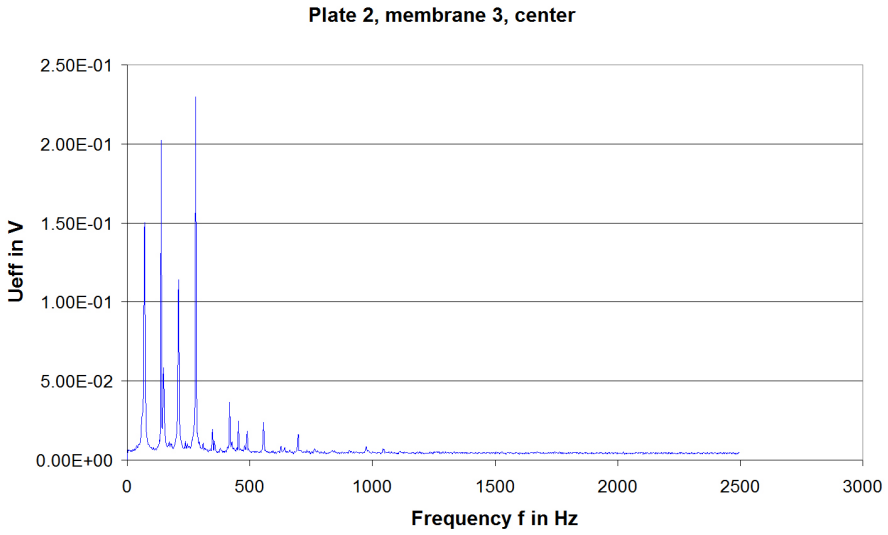


Figure 3.40 All data points (1024) from the center of membrane m3 of plate 2; the FFT of the laser vibrometer signal U_{eff} against the frequency; the well was filled with 2.5 ml of water; a artificial larynx signal was applied.

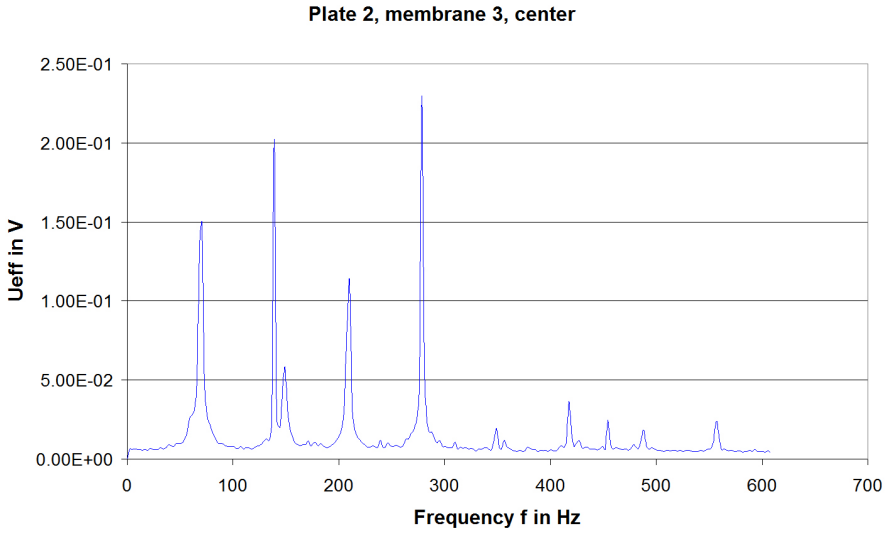


Figure 3.41 First 250 data points from the center of membrane m3 of plate 2; the FFT of the laser vibrometer signal U_{eff} against the frequency; the well was filled with 2.5 ml of water; a artificial larynx signal was applied.

In Fig. 3.42 the corresponding deflections for the frequency peaks for the horizontal

measurement points are provided.

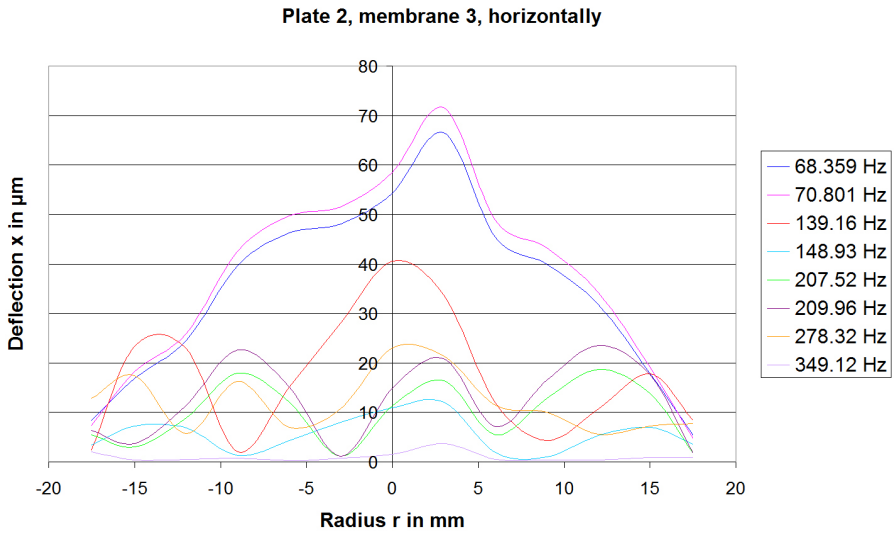


Figure 3.42 Horizontal measurement points of membrane m3 of plate 2; the deflection x against the radius r; the well was filled with 2.5 ml of water; a artificial larynx signal was applied.

Further also a measurement was taken with a signal with overlapped sinusoidal signals from 100 to 1000 Hz with decreasing volume. The measured voltage was 0.98 V. The total and zoomed signal is provided in Fig. 3.43 and 3.44.

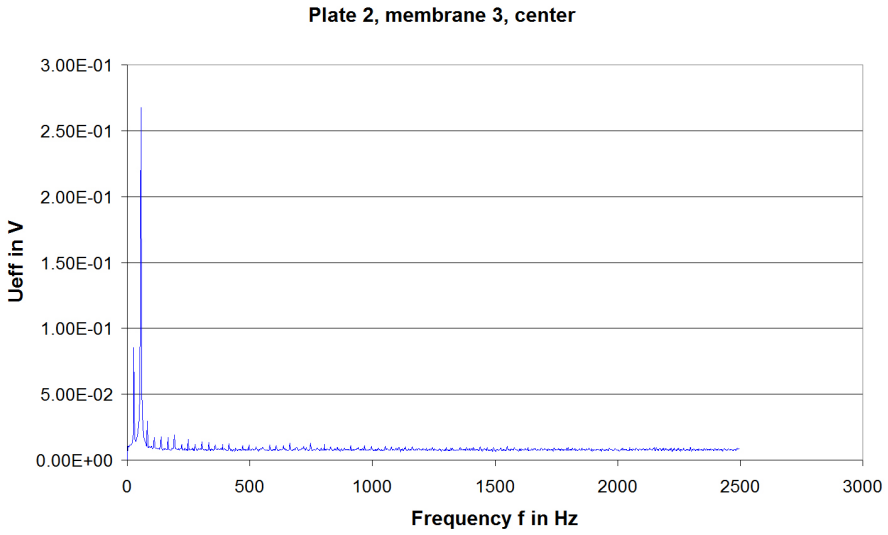


Figure 3.43 All data points (1024) from the center of membrane m3 of plate 2; the FFT of the laser vibrometer signal U_{eff} against the frequency; the well was filled with 2.5 ml of water; a signal with overlapped sinusoidal signals from 100 to 1000 Hz with decreasing volume was used.

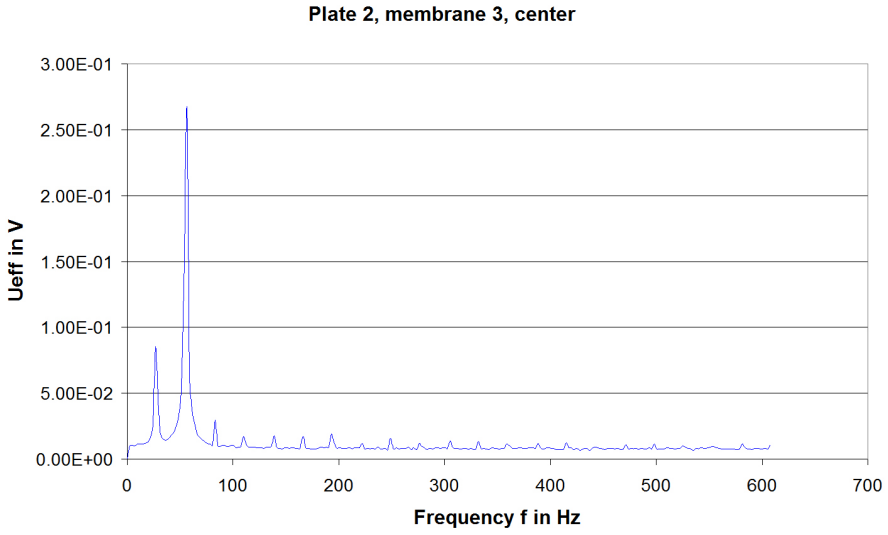


Figure 3.44 First 250 data points from the center of membrane m3 of plate 2; the FFT of the laser vibrometer signal U_{eff} against the frequency; the well was filled with 2.5 ml of water; a signal with overlapped sinusoidal signals from 100 to 1000 Hz with decreasing volume was used.

For the 55 Hz sinusoidal signal repeated measurements at different voltages were taken. The corresponding deflections at the peaks at 26.855 and 56.152 Hz are provided in Table 3.2.

Table 3.2 The deflection at 26.855 and 56.152 Hz using the sinusoidal signal with 55 Hz at different voltages.

voltage in V	deflection at 26.855 Hz in μm	deflection at 56.152 Hz in μm
0.08	2.32	33.33
0.12	3.06	48.35
0.18	4.22	71.99
0.25	98.4	147.43
0.51	191.23	239.47
0.77	206.09	298.58
1.05	246.29	381.51
1.23	233.56	416.1
1.54	227.19	468.33
1.73	233.06	524.19
2.05	217.54	572.4
2.31	232.34	584.6
2.59	236.81	629.09
2.75	190.02	673.68
3.09	190.88	685.14

In Fig. 3.45 the deflection values are shown against the voltage.

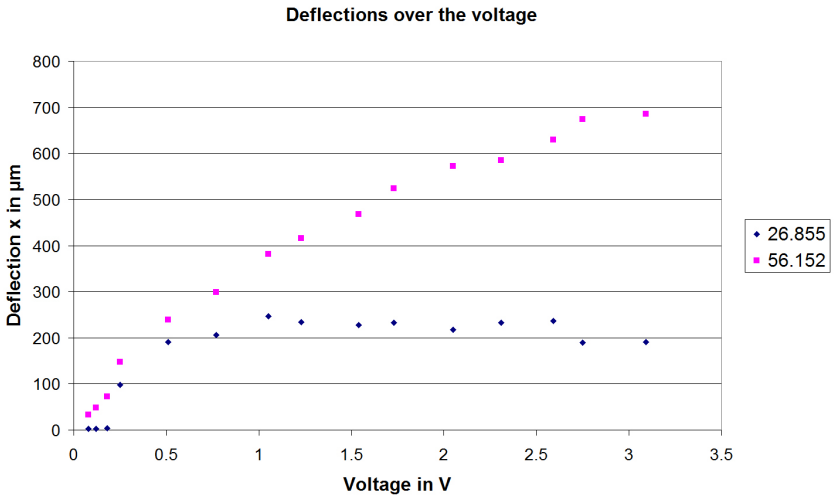


Figure 3.45 Deflection values over the voltage at 26.855 and 56.152 Hz.

For the sinusoidal signal with 55 Hz the data points measured at 56.152 Hz were fitted in Matlab to gather the strain value. The fitting is provided in Fig. 3.46. The corresponding strain at $r = 0$ was estimated to be 0.0029.

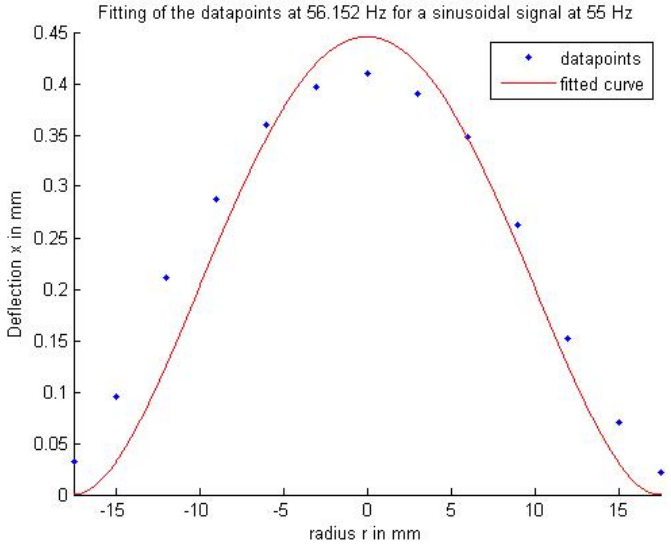


Figure 3.46 Fitting of the data points measured at 56.152 Hz for the sinusoidal signal with 55 Hz.

3.3 Testing of two different coatings

In Appendix C the pictures of the two plates with the two different coatings pronectin and collagen type I over 8 days is provided. As the cells in the wells with pronectin coating grew faster, it was decided to use pronectin-coated wells in the future.

3.4 Viability testing

In Appendix D the pictures taken by the microscope are provided. The raw data diagrams for all measurements are provided in Appendix D. Exemplary the diagrams of the static plate of experiment #2 are provided here. In Fig. 3.47 SSC-A over FSC-A with the gate for the differentiation between cells and other particles is shown. In Fig. 3.48 FSC-H over FSC-A and FSC-A over FSC-W and the gates for the differentiation between single cells and duplets is provided. The diagram with SSC-A over PI-A is shown in Fig. 3.49. In Fig. 3.50 two additional histograms showing the distribution of all events and the data points left by the gate singlets2 are shown.

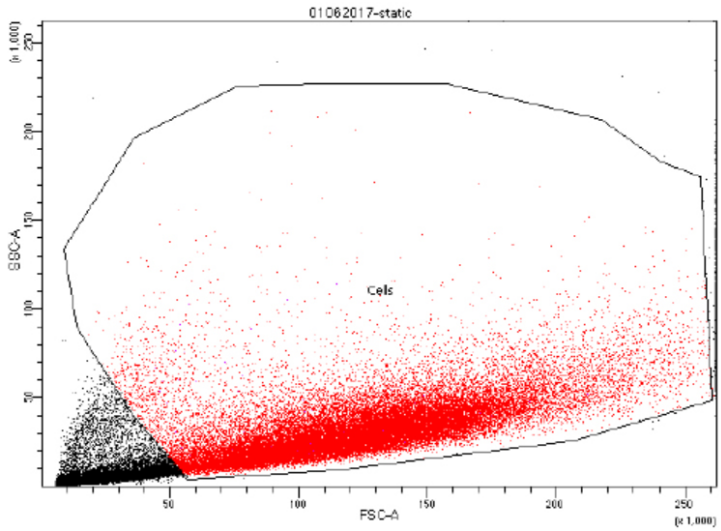


Figure 3.47 SSC-A over FSC-A with the gate to differentiate cells and other particles.

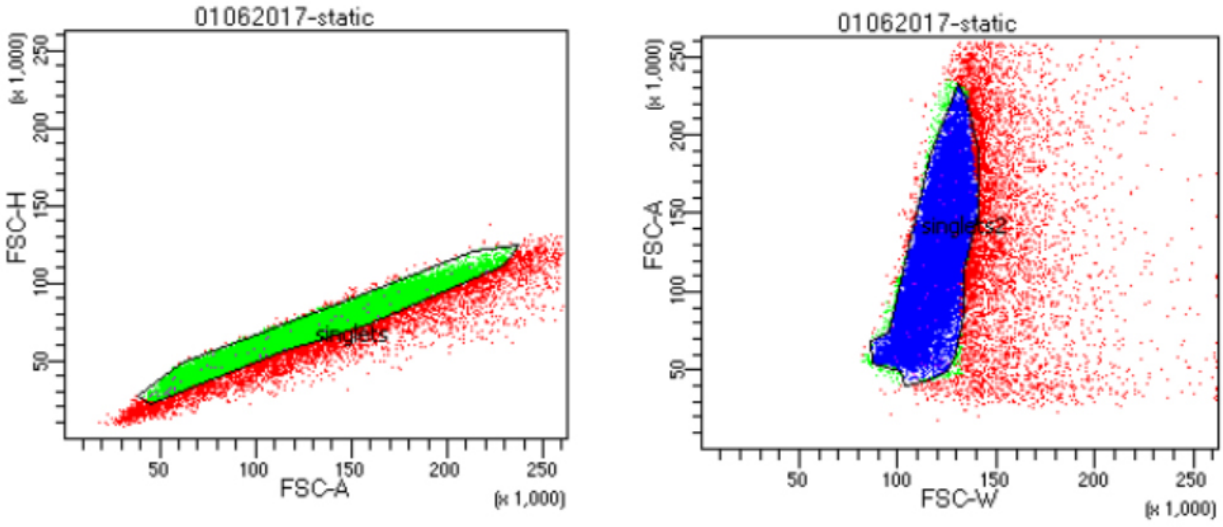


Figure 3.48 FSC-H over FSC-A and FSC-A over FSC-W with the gates for the differentiation between single cells and duplets.

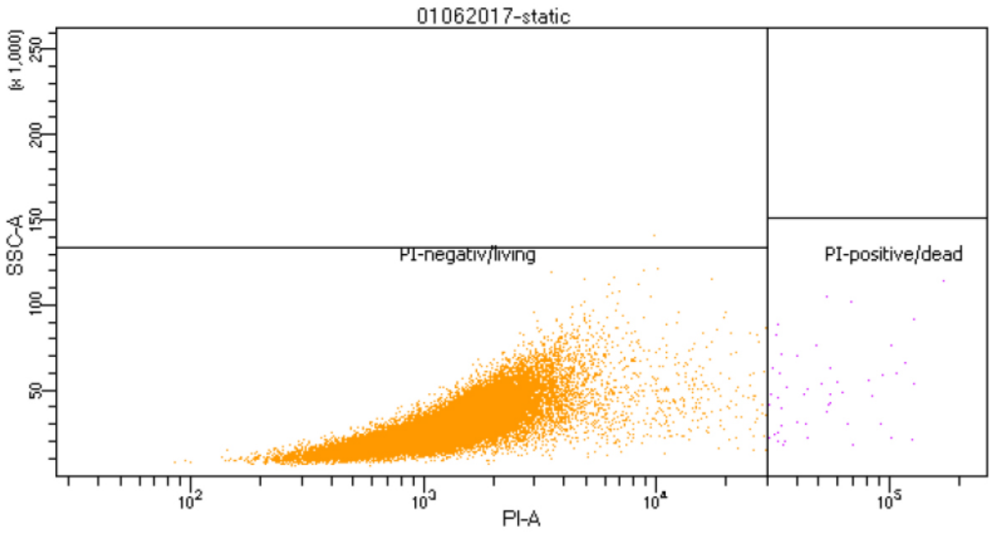


Figure 3.49 SCC-A over PI-A with the gates PI-positive and PI-negative to differentiate living and dead cells.

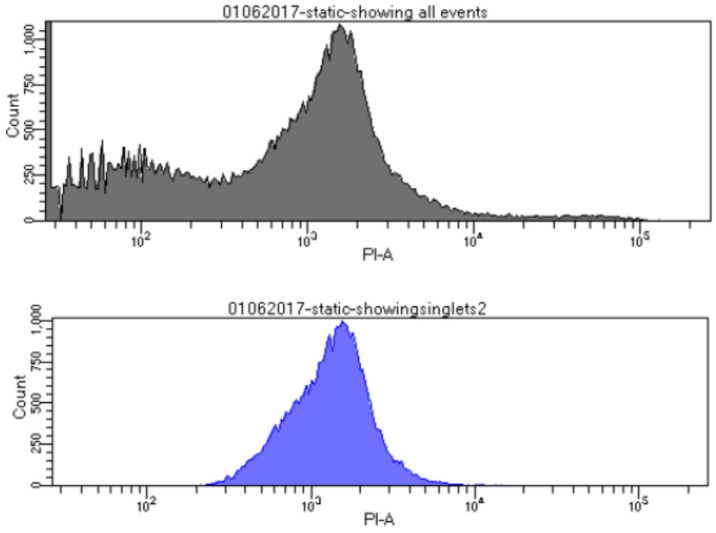


Figure 3.50 Histograms showing the distribution over PI-A for all events and the events of singlets2.

In Table 3.4 the number of events in total and for each gate are provided. For the PI-positive/dead and PI-negative/living gate the percentages regarding the events of gate ”singlets2” are provided.

Table 3.3 Number of events for the probes of the experiments and percentages regarding singlets2

Exp.	probe	Number of events in						Percentage of singlets2	
		total	cells	singlets	sing-lets2	PI-positive	PI-negative	PI-positive	PI-negative
#1	static	12538	3898	2898	2866	2864	2	99.9 %	0.1 %
#1	vibrated	8228	1671	1121	1102	1097	5	99.5 %	0.5 %
#2	static	70000	39252	34375	34031	33983	48	99.9 %	0.1 %
#2	vibrated	70000	41912	35226	34801	34762	39	99.9 %	0.1 %
#3	static	58358	30060	23721	23497	23447	50	99.8 %	0.2 %
#3	vibrated	40000	28150	22956	22736	22642	94	99.6 %	0.4 %
#4	static	17857	8577	5704	5577	5537	40	99.3 %	0.7 %
#4	vibrated	14999	9414	7617	7521	7442	79	98.9 %	1.1 %
#4	heated	17984	9343	6779	6689	6632	57	99.1 %	0.9 %
#5	static	16681	9900	6853	6642	6586	56	99.2 %	0.8 %
#5	vibrated	3646	898	522	495	482	13	97.4 %	2.6 %
#6	static	22332	11262	8043	7793	7661	132	98.3 %	1.7 %
#6	vibrated	17726	9887	7019	6778	6653	125	98.2 %	1.8 %
heating	normal	80000	27203	14935	14763	14696	67	99.5 %	0.5 %
heating	heated	80000	22514	12219	10807	8091	2716	74.9 %	25.1 %

4 Discussion

4.1 Discussion of the laser vibrometry results

Two prototypes were developed and examined with a laser vibrometer to investigate the vibration behaviour of the silicone membranes of the used 6-well plates placed on the prototypes.
First measurements were taken of the prototype with the structure-borne driver. The use of this device was recommended at the institute for Thermal Turbomachinery and Machine Dynamics. However, the measurements revealed, that this type of device was not suitable for our purpose. Although white noise was used as signal, the output of the structure-borne driver was not white noise. The amplitudes at different frequencies varied highly. This might come from the normal purpose of this device, e. g. it is attached to a panel of a car body, which than oscillates. The vibration behaviour depends highly on the material, to which the device is attached.
So this prototype was not further investigated and the measurements of the prototype with the loudspeaker were started with a chirp signal. The calculated mean Pearson correlation coefficients of all membranes of two plates indicate a good linear correlation between the membranes. Therefore, it is assumed, that the vibration is similar for all membranes and for different plates. The plates are fabricated industrially and therefore a very small variation in the fixation of the membranes, which might affect the behaviour, is expected.
In general it should be mentioned, that the laser vibrometer was placed on the measurement points manually. This might lead to some measurement error, as the placing was quite difficult, as the diameter of the laser was quite big compared to the distance between the measurement points.
Also measurements were taken at two places of the support to be sure that the influence of it on the vibration behaviour of the membranes is limited. As the peaks observed for the support were smaller and at other frequencies than the membranes, the influence is assumed neglectable.
It was expected, that if all frequencies are present with the same amplitude in the output signal (which is the case for the chirp signal), the ”eigenfrequencies” of the material will appear as peaks in the output of the laser vibrometer. For the chirp signal peaks at about 180 and 310 Hz appeared. The deflection values over the surface were plotted for several frequencies of around the peaks, as the resolution of the frequency axis was limited. At about 180 Hz a parabolic deflection was observed. At about 310 Hz a higher bending form with 3 peaks was observed.
For further measurements the wells were filled with 2.5 ml of water, which is a typical

volume which is also used in cell culture. Here peaks at smaller frequencies were observed. The behaviour before observed at about 180 Hz appeared now at about 55 Hz and the behaviour before observed at about 310 Hz appeared at about 140 Hz. The water in the well might work as a damping factor. As it was decided, that as a first approach a deflection behaviour with one peak is desired, also mono-frequent signals were tested. Only for the sinusoidal signal at 55 Hz this behaviour was observed. However, for this signal there also appeared a smaller peak at about 27 Hz. So in practice the sinusoidal oscillation at 27 Hz and the oscillation at 55 Hz overlap and the membrane oscillates with one peak in a kind of sinusoidal fashion. To get a better idea, the overlap of a peak deflection of 230 at 27 Hz and a peak deflection of 405 at 55 Hz is illustrated in Fig. 4.1.

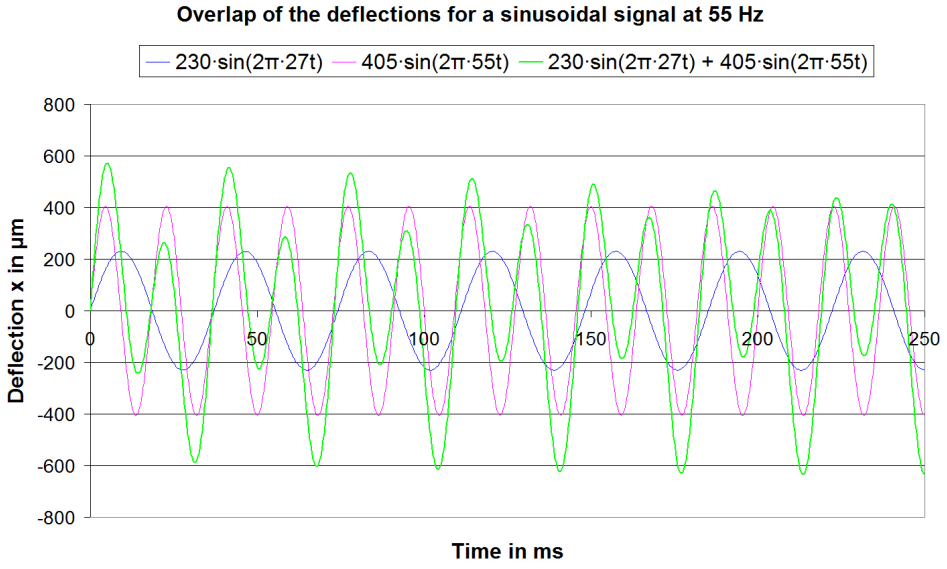


Figure 4.1 The behaviour of the silicone membrane over the time due to the overlap of the deflections at about 27 and about 55 Hz.

For the 55 Hz signal also the strain ϵ was estimated. For that a curve fitting tool or rather a fitting function was used. However, as the fitting did not look so well for the 55 Hz, this approach was not further used for other signals. Instead the parameter of deflection was used to describe the mechanical behaviour for different signals. Another disadvantage of the strain calculation would have been, that it only worked for the bending with one peak and new formulas would have been needed for higher modes. Further also always measurement points over the surface would be needed for the fitting.
As it was decided to use the 55 Hz signal as a first pattern in the cell culture, several measurements were taken with varying voltage to have some selection of the magnitude of the maximal deflection.

Further also a larynx signal was used for testing. A frequency spectrum of it is shown in Fig. 4.2. This spectrum was created with the software Audacity. The Hanning-window was used and the size was set to 32768, which resulted in a frequency resolution of about 1.35 Hz. The Audacity software uses the Fast Fourier Transform to create the Spectrum.

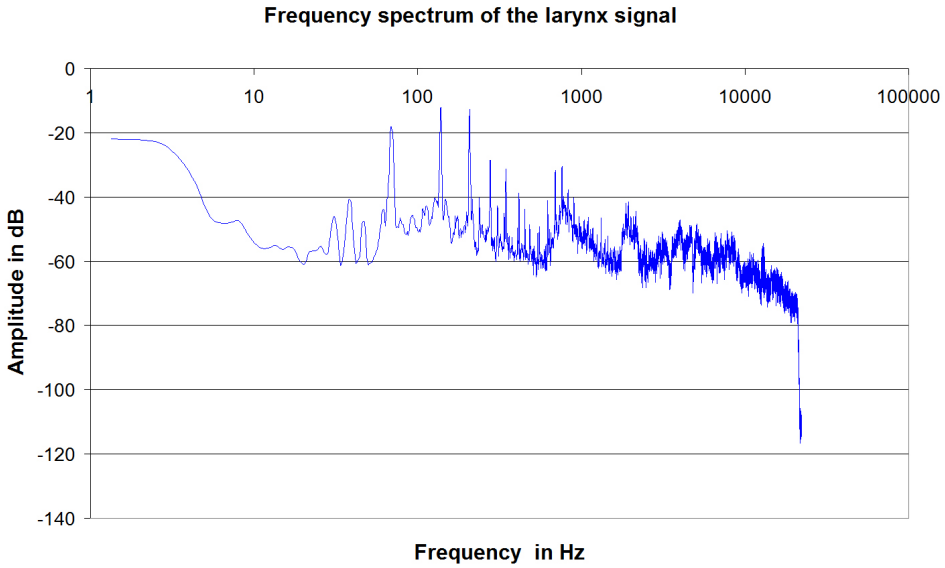


Figure 4.2 The frequency spectrum of the larynx signal, which was used for the measurements.

For the larynx signal a lot of different peaks were observed. Further various bending behaviours overlap for this signal.
Also a signal from overlapping sinus signals with frequencies from 100 to 1000 Hz was used for measurements in the center. Here also several peaks occurred. The frequency spectrum of it is provided in Fig. 4.3. It was created again with the Audacity software using the same settings. As can be seen, there is some resemblance between this two signals.

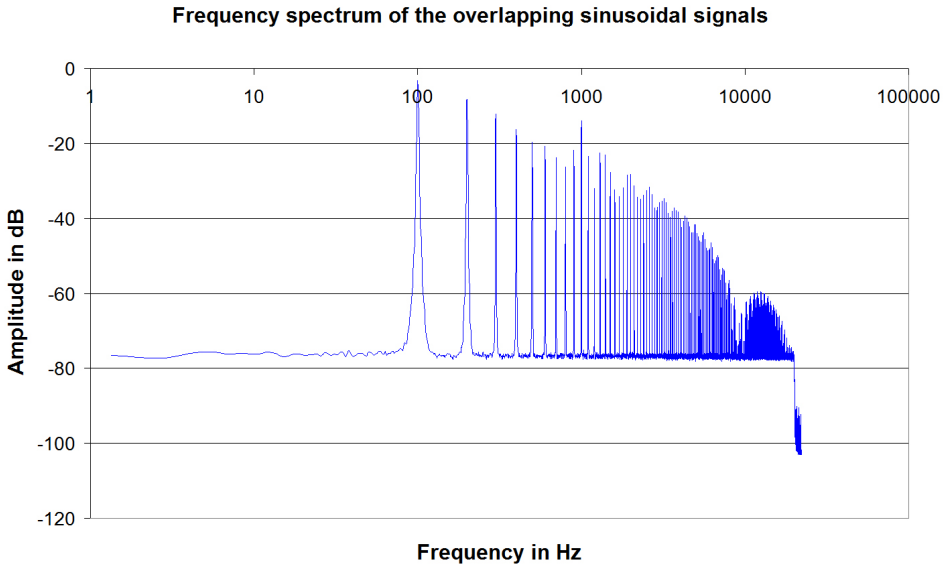


Figure 4.3 The frequency spectrum of the signal with the overlapping sinusoidal signals, which was used for the measurements.

4.2 Discussion of the flow cytometry results

Different deflections were tested to investigate, which magnitude the cells can endure. First a maximal deflection of about 33 μm was used. However, for experiment #1 the amount of trypsine was far to small and it was observed, that hardly any cells came off the membrane. Further also the settings of the flow cytometer were not right.
A second attempt was started. The amount of trypsine was increased and the settings were adjusted by a expert. It was again hard to get the cells off the membrane. A lot of washing was required. Further it was decided to take pictures of the cells after the vibration to investigate, if there is a optical difference visible between the static and vibrated cells. For the deflection of 33 μm used for experiment #2 there was no optical difference observed. Further also the percentages of the flow cytometer indicated no difference.
A much higher deflection of about 298 μm was used for experiment #3. Here a optical difference was observed. The vibrated cells looked rolled up and had hardly any extensions. However, the flow cytometer measurements were quite similar. All together it was decided, that this deflection might be too much for the cells. It looked like the cells survived, but were under great stress.
As next step a value between 33 and 298 μm was wanted. It was chosen to use a deflection of about 147 μm for experiment #4. For this and later experiments pictures were also taken before the vibration to guarantee that the cells in both plates look alike before the stimulation pattern. Further also again the amount of trypsine was increased, as it was still quite

hard to get the cells of the membranes during experiment #2 and #3. Unfortunately, there was a optical difference observed between the cells before the vibration. The difference was also visible afterwards. It was unclear, if the difference at the end was connected to the difference before or to the stimulation pattern. Some of the cells from the static plate were heated at 65 °C for 20 minutes. The difference between static and heated cells was not really big. To test, if the PI really worked properly some cells from a T75-flask were measured separately and also the gates regarding PI-positive and PI-negative cells were improved and checked by a expert. The improved gates were then used for all experiments. During the heating experiment the cells were heated at 100 °C for 50 minutes. There was a bigger difference observed here. So it was clarified, that the PI dye works properly. It might be a explanation for the results of experiment #4 that the cells are quite robust and really survived the condition. The higher heat and longer time period of the second attempt than killed of more cells.
As the output of experiment #4 was not really interpretable regarding the difference between static and vibrated cells, the experiment was repeated. During experiment #5 no optical difference between the plates was observed. However, there happened a mistake at the flow cytometer measurements. It was possible to measure the cells from the static plate properly, but it was not possible to gather a high enough number of cells of the plate, which was vibrated. Maybe the pellet after the centrifugation was not perfectly dissolved. It was decided to repeat the measurements. So experiment #6 was started with the same conditions. Here also no optical difference was observed and also the flow cytometer measurements revealed a similar viability for both conditions. So from the measurements it can be assumed that the cells survive deflections between about 33 and 147 μm.

4.3 General Discussion

For tissue engineering it is essential to choose the proper cells, scaffold and the proper bioreactor (Ringel et al. (2006)). Apart from the aim to use this technique to grow tissues for transplantation, this research is also relevant to gather a *in vitro* model of a *in vivo* tissue to conduct experiments investigating features of the tissue more easily. In the case of vocal folds it is believed that the vocal fold fibroblasts respond to vibratory forces, as they are genetically programmed to (Li et al. (2016)). Further it might also be interesting to have a *in vitro* model of fibrogenesis (Graupp et al. (2015)).
A lot of approaches have been made regarding the development of phono-mimetic bioreactors. Wolchok et al. (2009) used a voice coil actuator to insert a horizontal movement on a six-well plate and observed some difference regarding gene expression. Titze et al. (2004) developed a bioreactor which was able to put the elastometric substrate stripes under tension and also put a vibration on them with a actuator and observed a difference regarding the mRNA expression. Farran et al. (2013) used a loudspeaker for the stimulation. With a tubing system the excitation was passed on to a silicone membrane, which was fixed manually. A difference in gene expression was revealed. Zerdoum et al. (2014) developed another bioreactor using a loudspeaker. Some difference in the cell response was observed.

Tong et al. (2014) developed a bioreactor, where a silicone elastomer was placed on a mini-woofer and observed a increase of cell proliferation. Gaston et al. (2012) used synthetic ECM stripes, which were stimulated with strain and vibration. For vibration a actuator was used. Here also a difference was observed.

The aim of the study was to develop and evaluate a bioreactor which resembles *in vitro* the vibration of the vocal folds *in vivo*. A first generation bioreactor was generated with a loudspeaker used for stimulation. The loudspeaker membrane moves during sound production and thereby the air in the device is moved, which than moves the membranes. To investigate the oscillation behaviour of the membranes measurements with the laser vibrometer were taken. It was observed, that all membranes experience the same vibration and that there is hardly any difference between plates. As the plates are manufactured industrially the difference in general between plates should be very small. At least the difference should be smaller, as if a silicone membrane was fixed manually. Furthermore, the use of a industrially produced carrier has a lot of advantages. It is delivered sterile and can be put easily in the bioreactor. Through the six wells, it is possible to investigate several solution conditions simultaneously. For this bioreactor a big loudspeaker was used, which is able to generate signals with small frequencies in the range of the human voice properly. In the past, often small loudspeakers were used, which are perfect for high frequencies. Further through the big loudspeaker it is also possible to apply a greater deflection on the cells.
To investigate which deflection the cells are able to resist, measurements were taken with the flow cytometer using the PI dye to distinguish between living and dead cells and it was observed that the cells can tolerate stimulation with the sinusoidal signal at 55 Hz for deflections from about 33 to about 147 μm. A lot of the other studies tested much smaller deflections.

In the future further investigation of the cells, stimulated with the bioreactor, will be needed to investigate possible differences regarding for example the gene expression. This simple system provides a first approach to study cells under vibration conditions. Of course the bioreactor will need some refinements in the future to mimic the phonation even better.

5 Appendix A

From Fig. 5.1 to Fig. 5.94 the remaining FFT signals for all directions of all membranes of the two plates are provided. The signals are shown in total and also the part of the first 250 data points is shown enlarged.
From Fig. 5.95 to Fig. 5.140 the remaining deflection signals for the horizontal and vertical measurement points around 180 and 310 Hz of all membranes of the two plates are provided.
The signals for different directions measured for membrane m3 of plate 1, filled with 2.5 ml of water using the chirp signal are provided from Fig. 5.141 to Fig. 5.146. The signals are shown in total and also the part of the first 250 data points is shown enlarged.
The deflections for this signals are shown from Fig. 5.147 to Fig. 5.150.
The signal gathered with the application of the artificial larynx signal for the right side is shown in total in Fig. 5.171 and zoomed in Fig. 5.172.

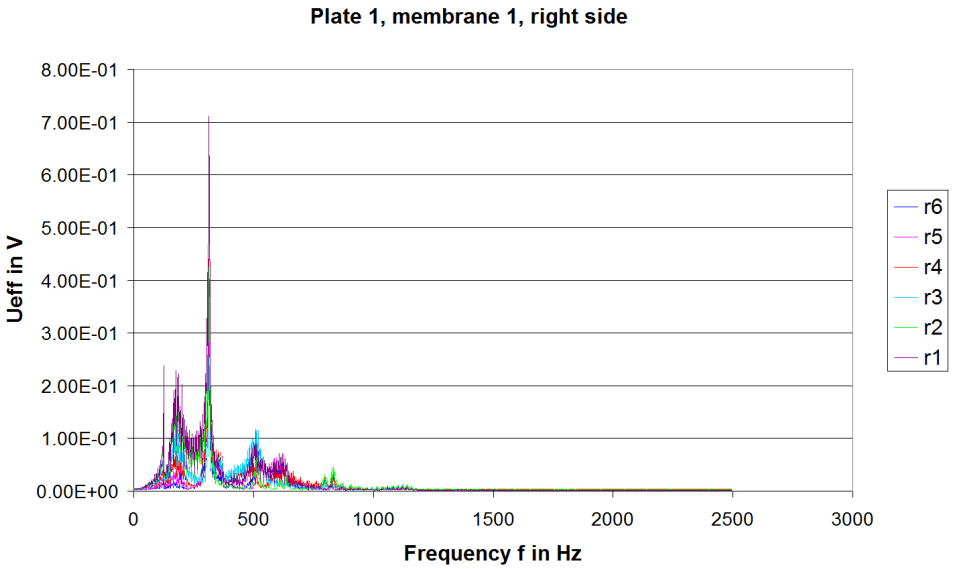


Figure 5.1 All data points (1024) from the right side of membrane m1 of plate 1; the FFT of the laser vibrometer signal U_{eff} against the frequency; a chirp signal was applied.

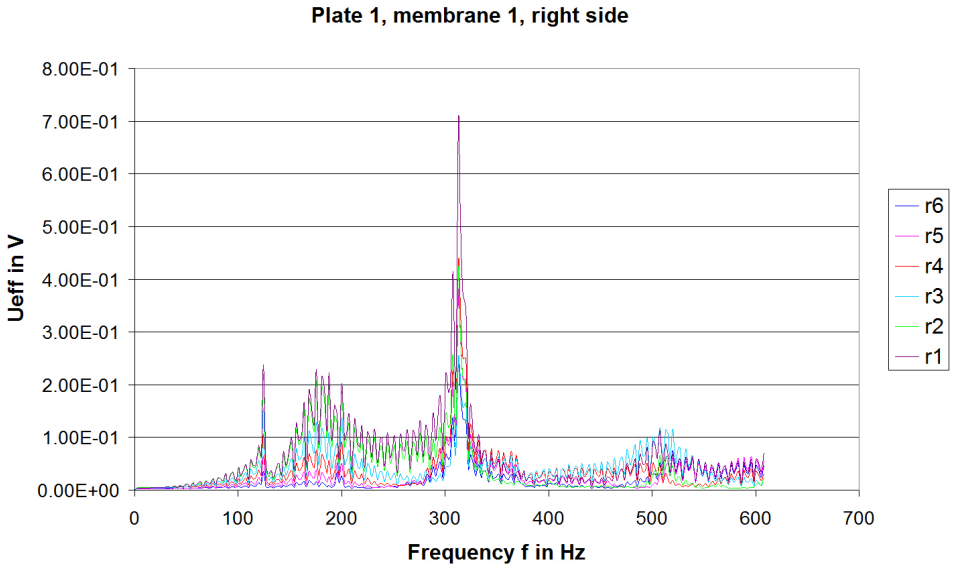


Figure 5.2 First 250 data points from the right side of membrane m1 of plate 1; the FFT of the laser vibrometer signal U_{eff} against the frequency; a chirp signal was applied.

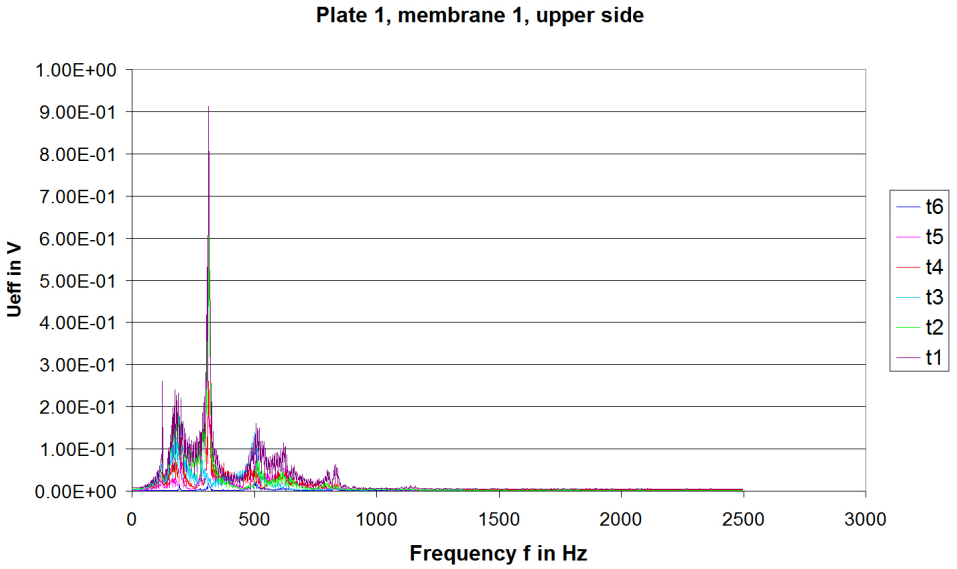


Figure 5.3 All data points (1024) from the upper side of membrane m1 of plate 1; the FFT of the laser vibrometer signal U_{eff} against the frequency; a chirp signal was applied.

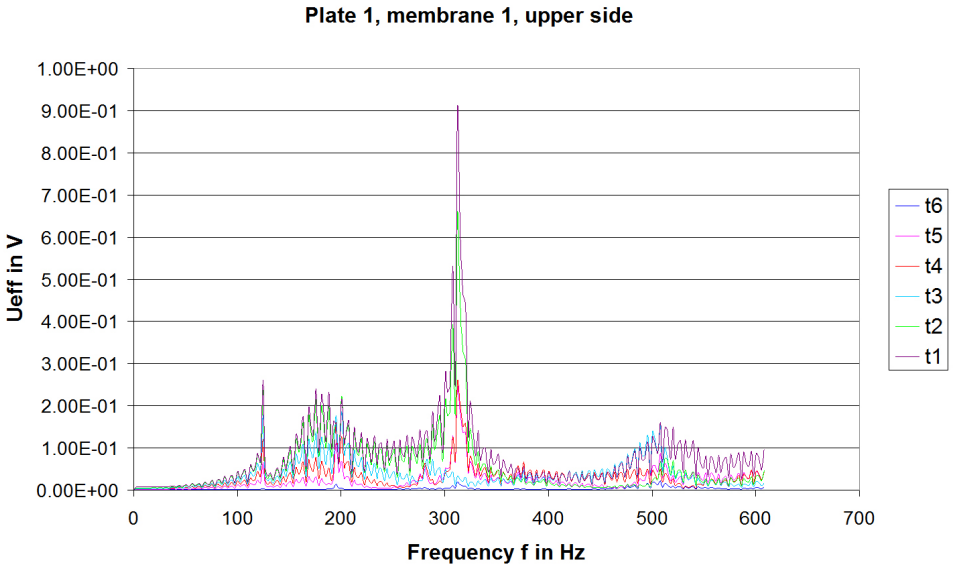


Figure 5.4 First 250 data points from the upper side of membrane m1 of plate 1; the FFT of the laser vibrometer signal U_{eff} against the frequency; a chirp signal was applied.

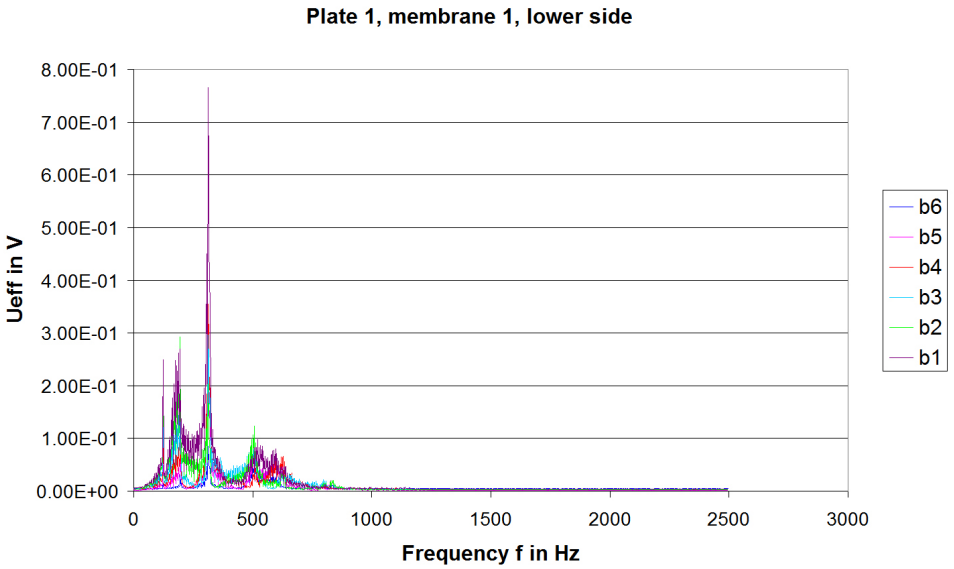


Figure 5.5 All data points (1024) from the lower side of membrane m1 of plate 1; the FFT of the laser vibrometer signal U_{eff} against the frequency; a chirp signal was applied.

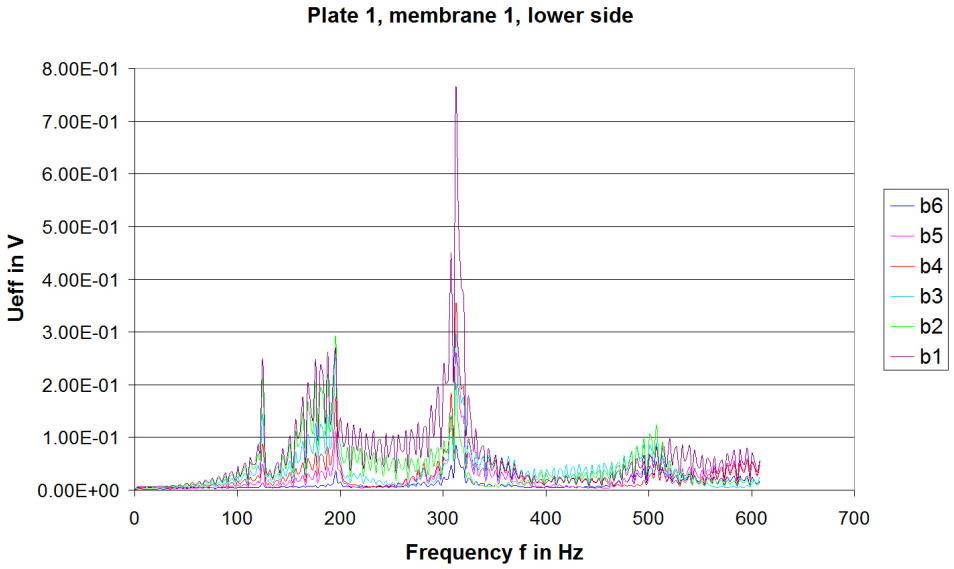


Figure 5.6 First 250 data points from the lower side of membrane m1 of plate 1; the FFT of the laser vibrometer signal U_{eff} against the frequency; a chirp signal was applied.

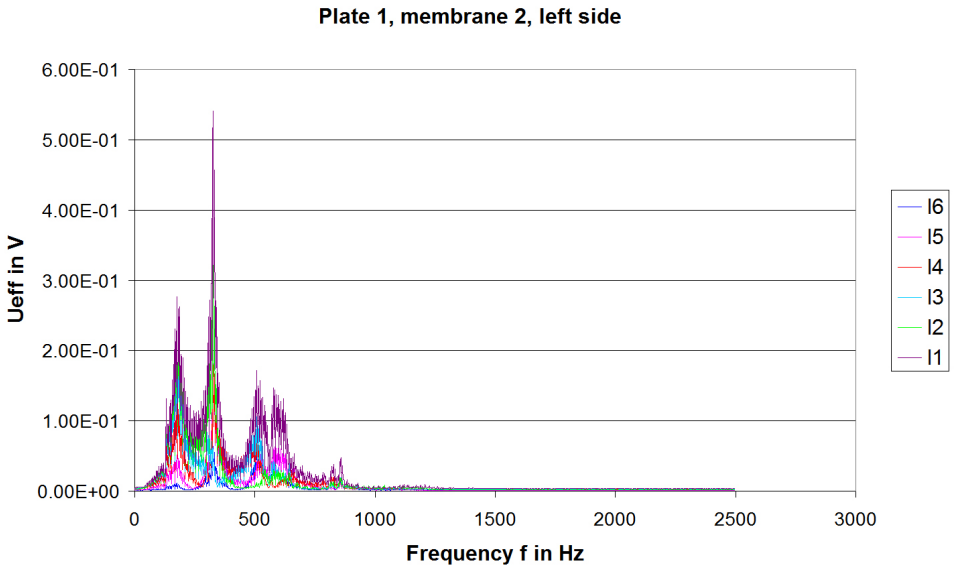


Figure 5.7 All data points (1024) from the left side of membrane m2 of plate 1; the FFT of the laser vibrometer signal U_{eff} against the frequency; a chirp signal was applied.

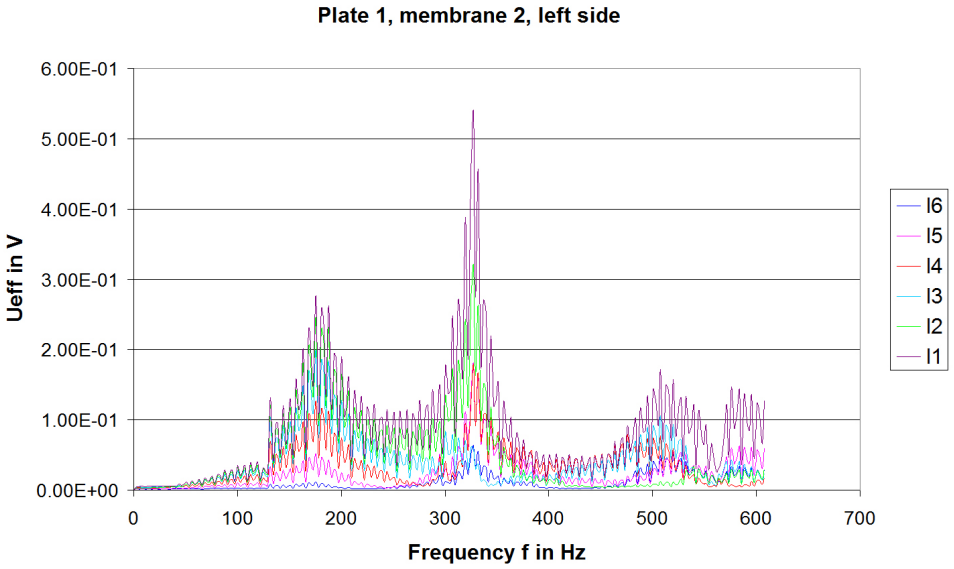


Figure 5.8 First 250 data points from the left side of membrane m2 of plate 1; the FFT of the laser vibrometer signal U_{eff} against the frequency; a chirp signal was applied.

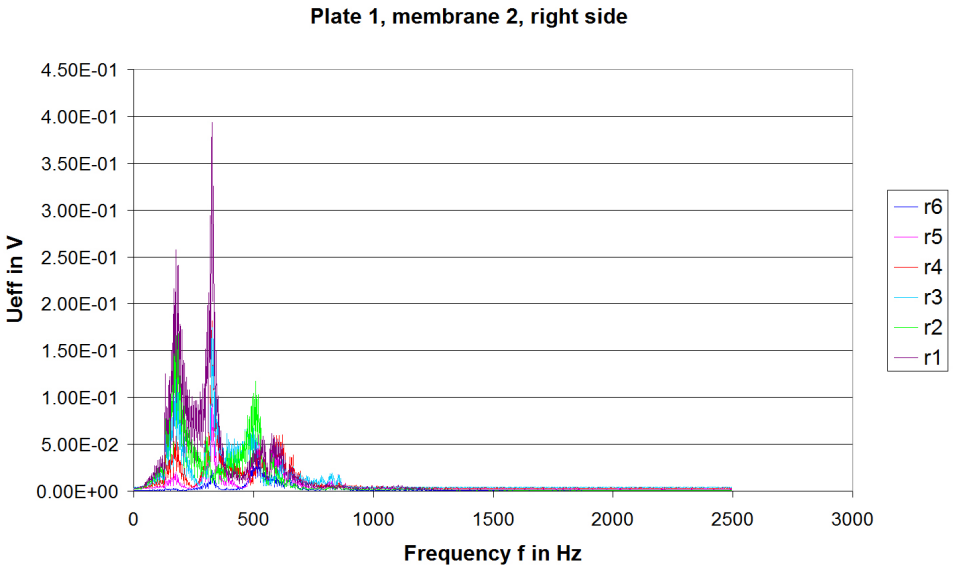


Figure 5.9 All data points (1024) from the right side of membrane m2 of plate 1; the FFT of the laser vibrometer signal U_{eff} against the frequency; a chirp signal was applied.

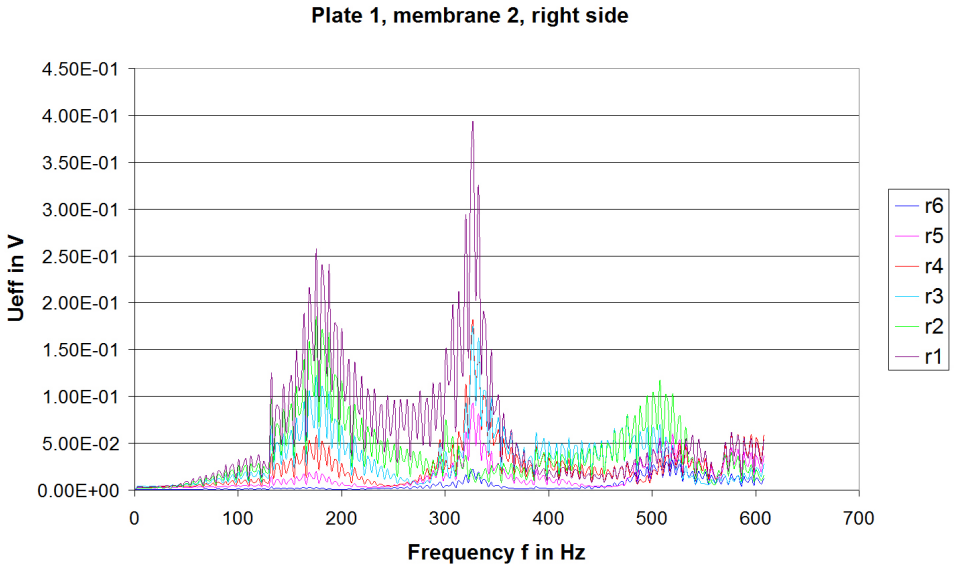


Figure 5.10 First 250 data points from the right side of membrane m2 of plate 1; the FFT of the laser vibrometer signal U_{eff} against the frequency; a chirp signal was applied.

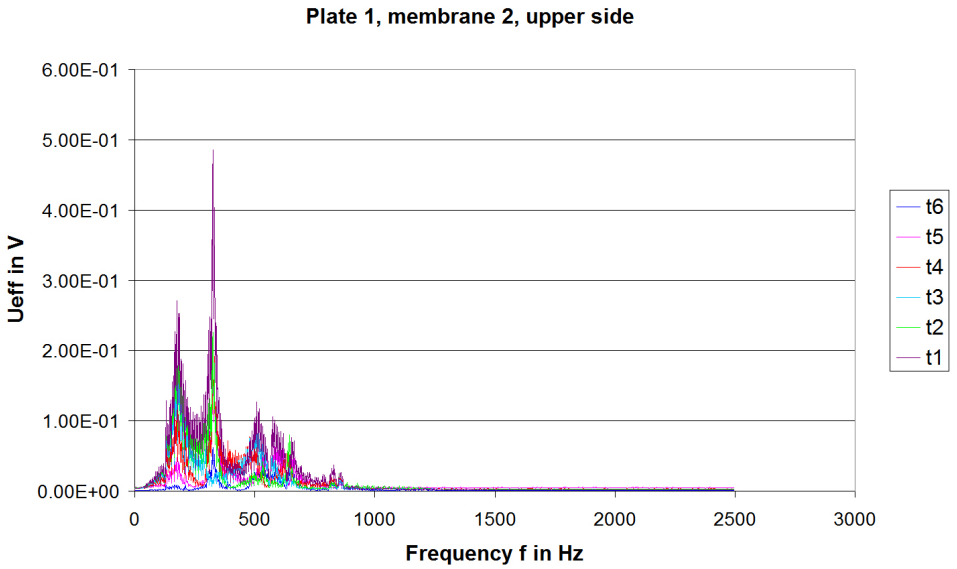


Figure 5.11 All data points (1024) from the upper side of membrane m2 of plate 1; the FFT of the laser vibrometer signal U_{eff} against the frequency; a chirp signal was applied.

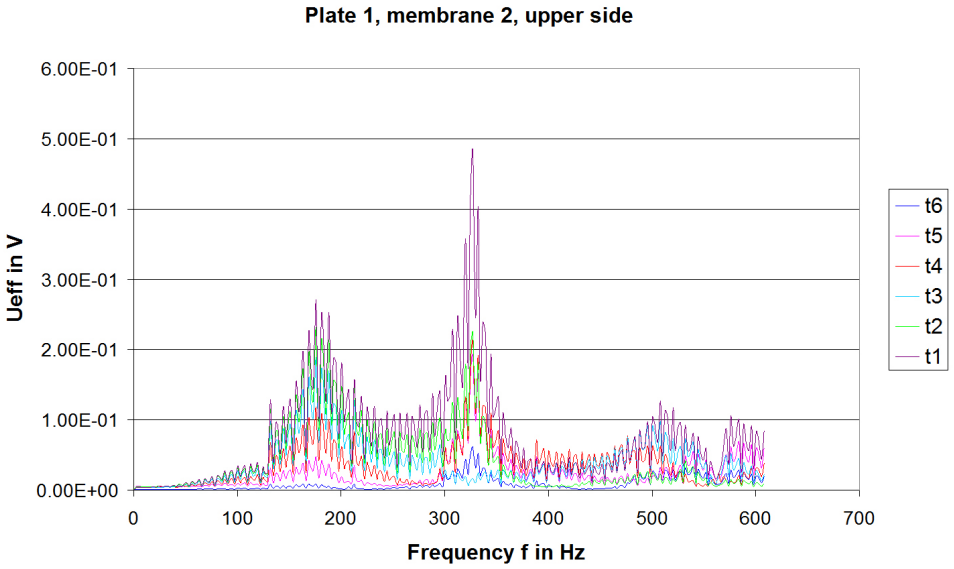


Figure 5.12 First 250 data points from the upper side of membrane m2 of plate 1; the FFT of the laser vibrometer signal U_{eff} against the frequency; a chirp signal was applied.

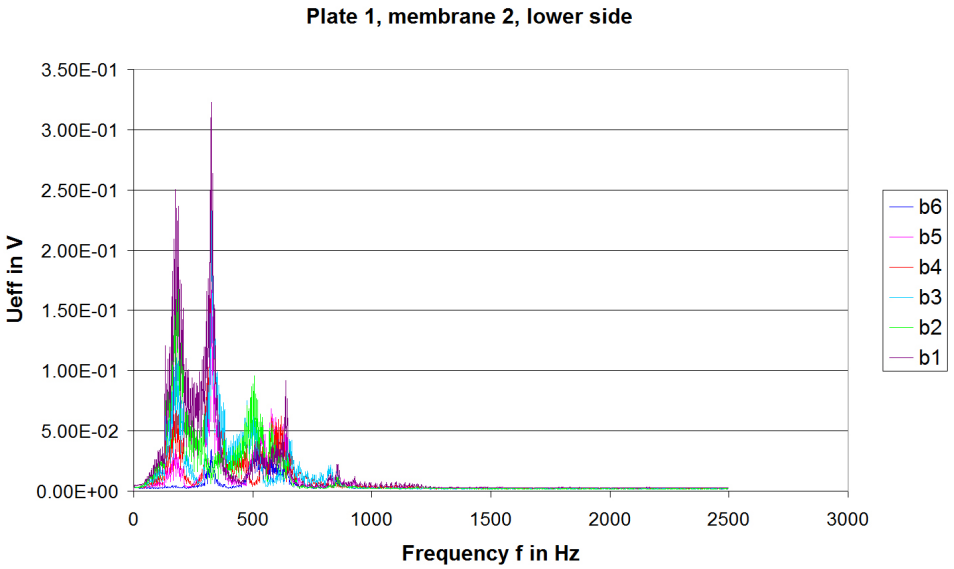


Figure 5.13 All data points (1024) from the lower side of membrane m2 of plate 1; the FFT of the laser vibrometer signal U_{eff} against the frequency; a chirp signal was applied.

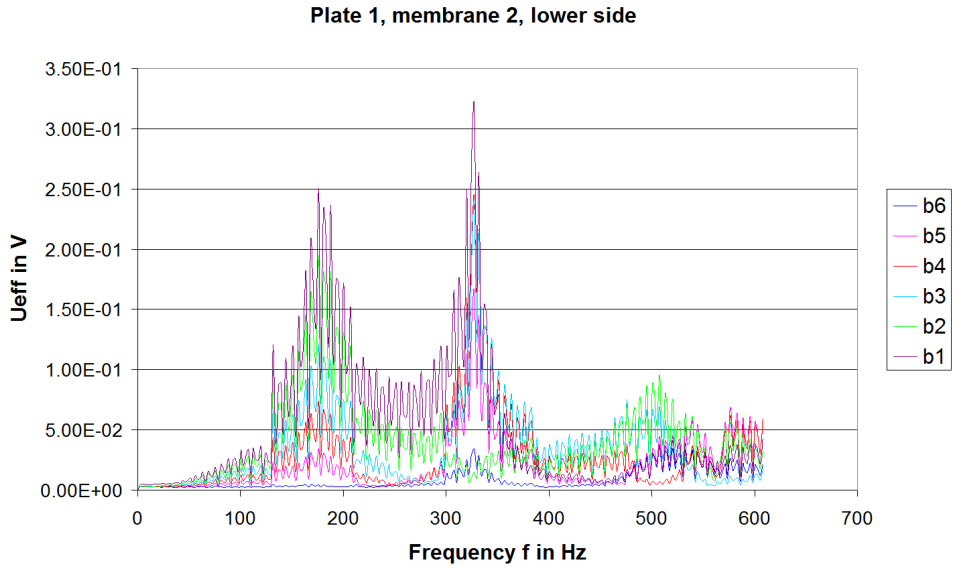


Figure 5.14 First 250 data points from the lower side of membrane m2 of plate 1; the FFT of the laser vibrometer signal U_{eff} against the frequency; a chirp signal was applied.

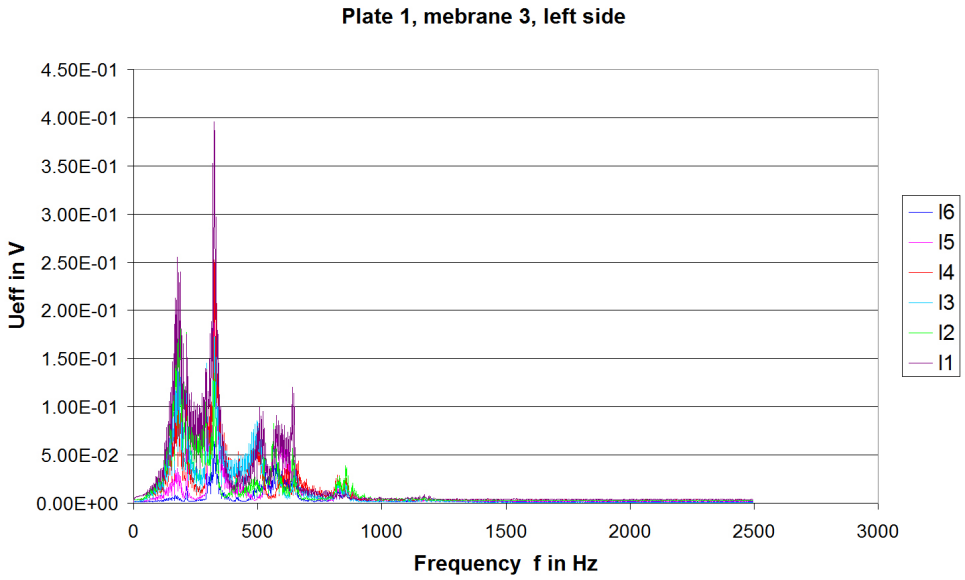


Figure 5.15 All data points (1024) from the left side of membrane m3 of plate 1; the FFT of the laser vibrometer signal U_{eff} against the frequency; a chirp signal was applied.

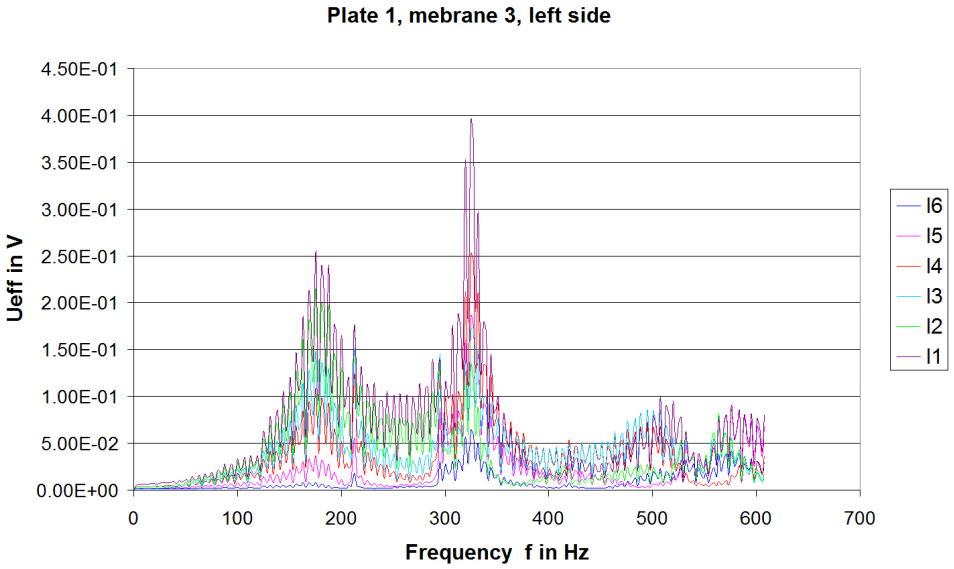


Figure 5.16 First 250 data points from the left side of membrane m3 of plate 1; the FFT of the laser vibrometer signal U_{eff} against the frequency; a chirp signal was applied.

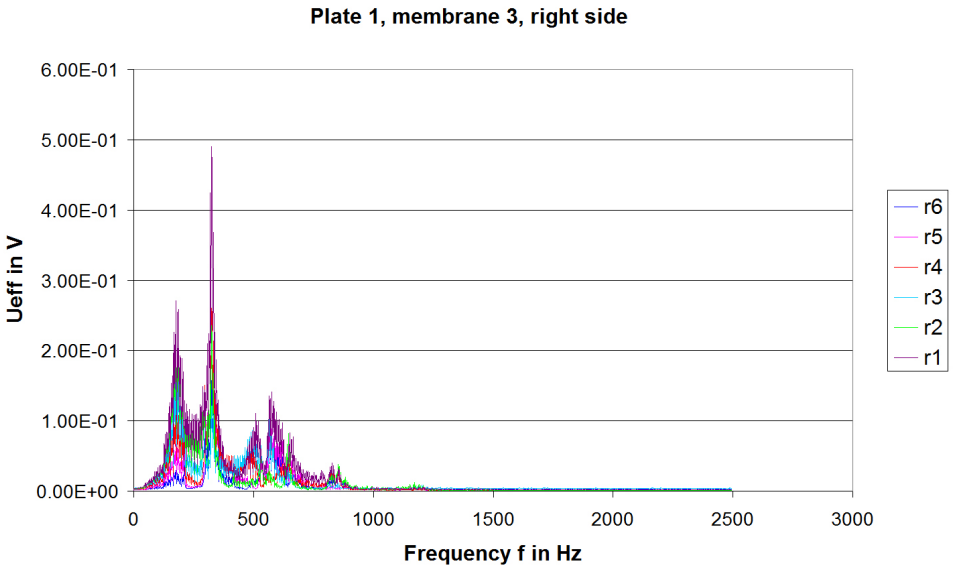


Figure 5.17 All data points (1024) from the right side of membrane m3 of plate 1; the FFT of the laser vibrometer signal U_{eff} against the frequency; a chirp signal was applied.

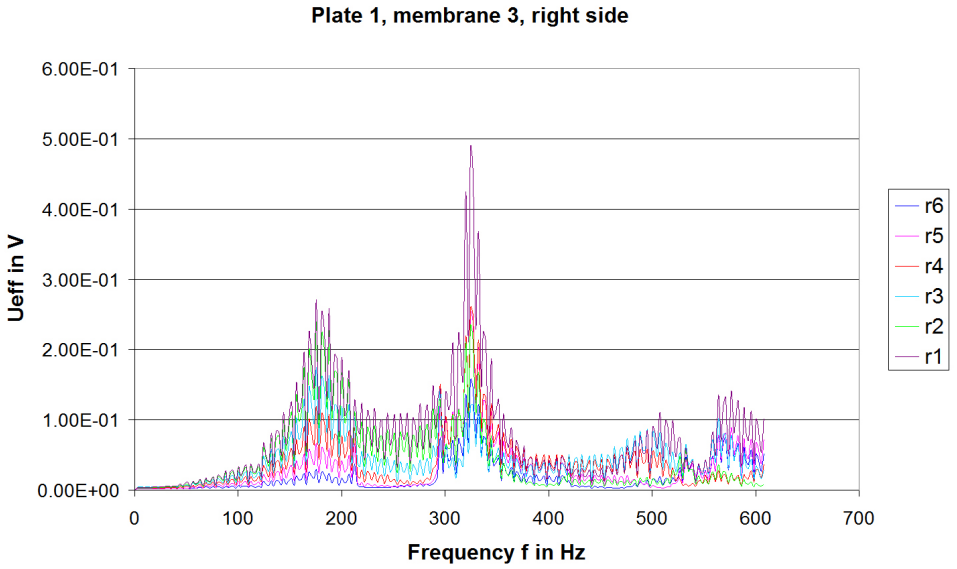


Figure 5.18 First 250 data points from the right side of membrane m3 of plate 1; the FFT of the laser vibrometer signal U_{eff} against the frequency; a chirp signal was applied.

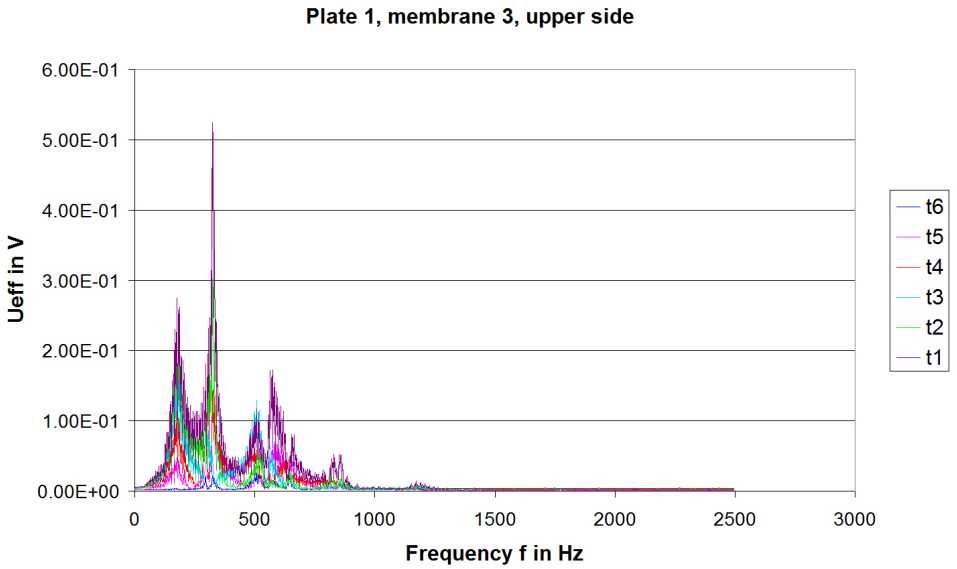


Figure 5.19 All data points (1024) from the upper side of membrane m3 of plate 1; the FFT of the laser vibrometer signal U_{eff} against the frequency; a chirp signal was applied.

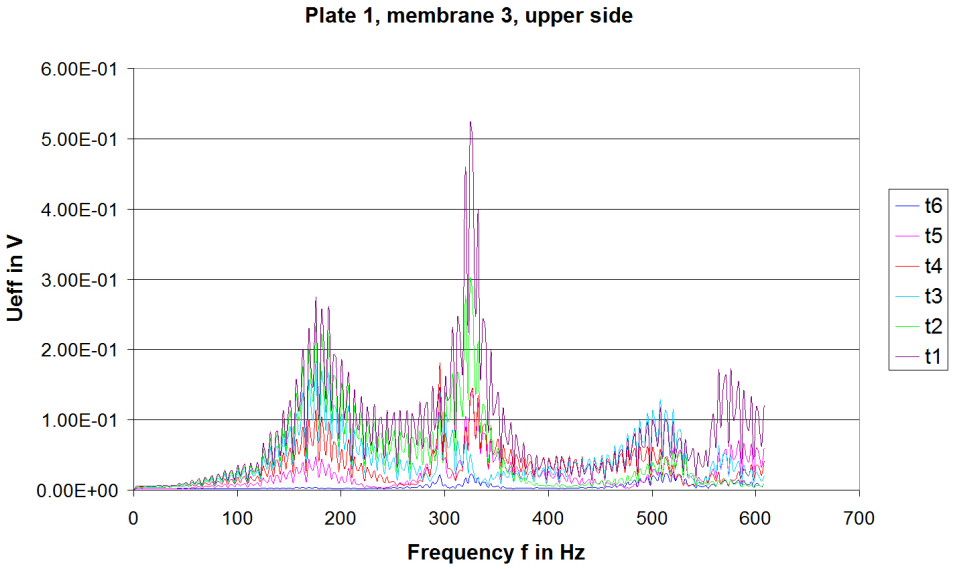


Figure 5.20 First 250 data points from the upper side of membrane m3 of plate 1; the FFT of the laser vibrometer signal U_{eff} against the frequency; a chirp signal was applied.

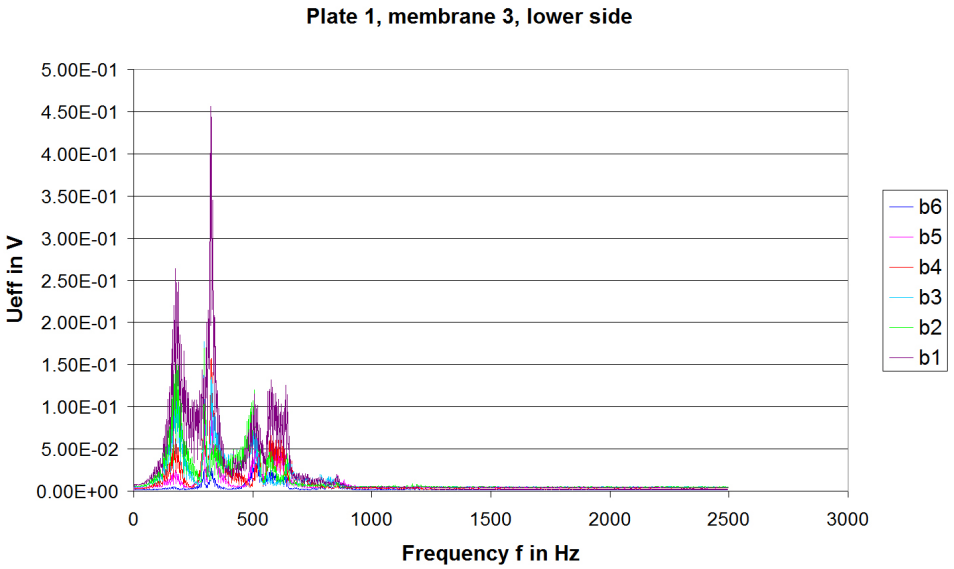


Figure 5.21 All data points (1024) from the lower side of membrane m3 of plate 1; the FFT of the laser vibrometer signal U_{eff} against the frequency; a chirp signal was applied.

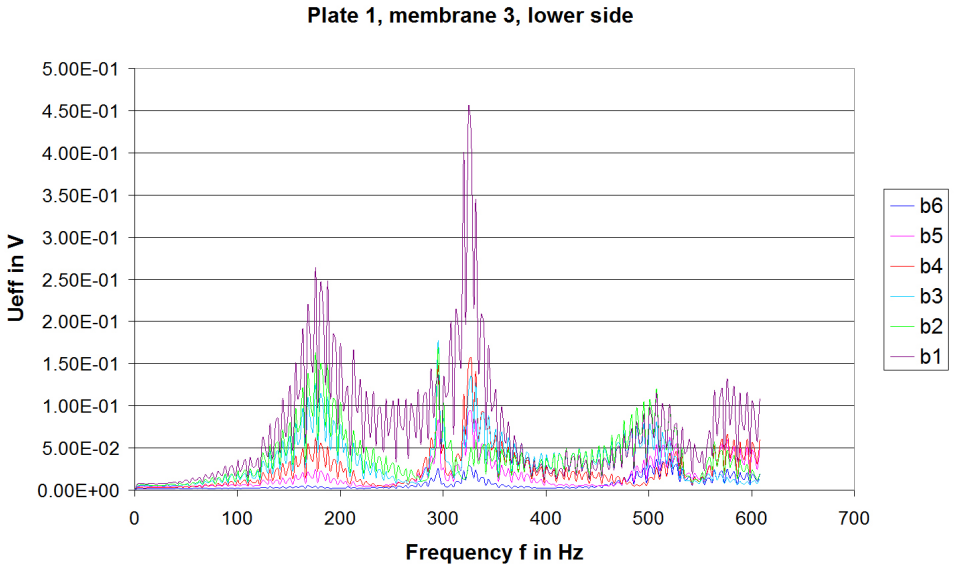


Figure 5.22 First 250 data points from the lower side of membrane m3 of plate 1; the FFT of the laser vibrometer signal U_{eff} against the frequency; a chirp signal was applied.

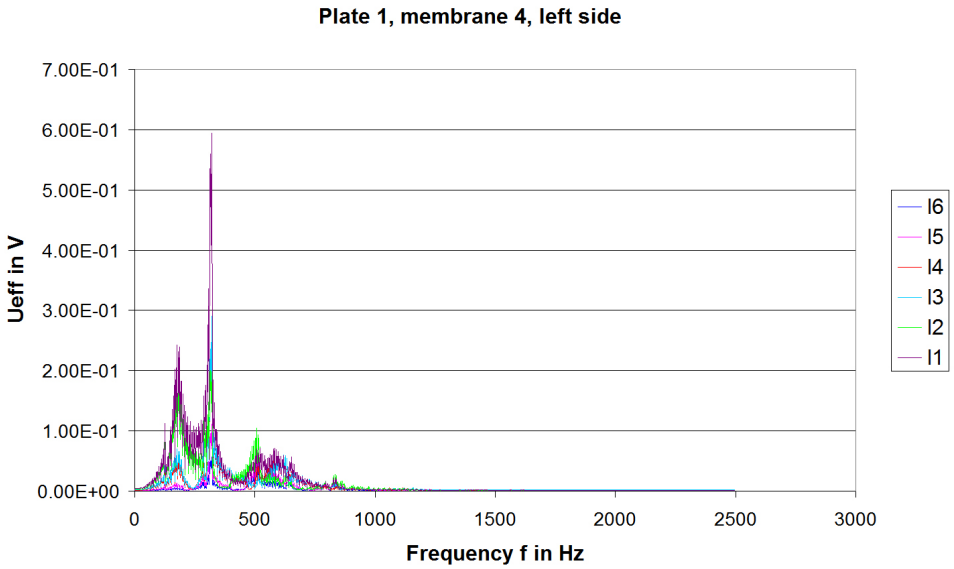


Figure 5.23 All data points (1024) from the left side of membrane m4 of plate 1; the FFT of the laser vibrometer signal U_{eff} against the frequency; a chirp signal was applied.

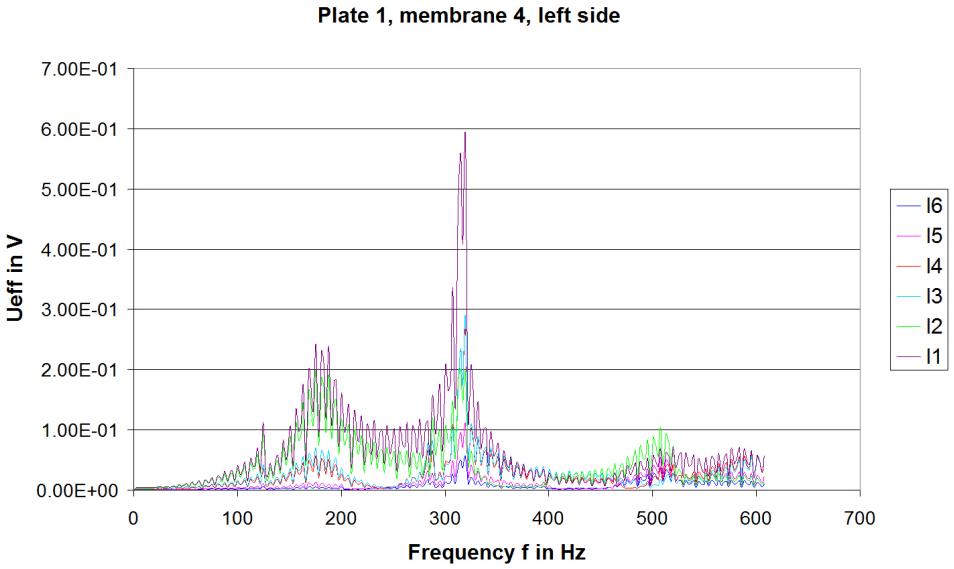


Figure 5.24 First 250 data points from the left side of membrane m4 of plate 1; the FFT of the laser vibrometer signal U_{eff} against the frequency; a chirp signal was applied.

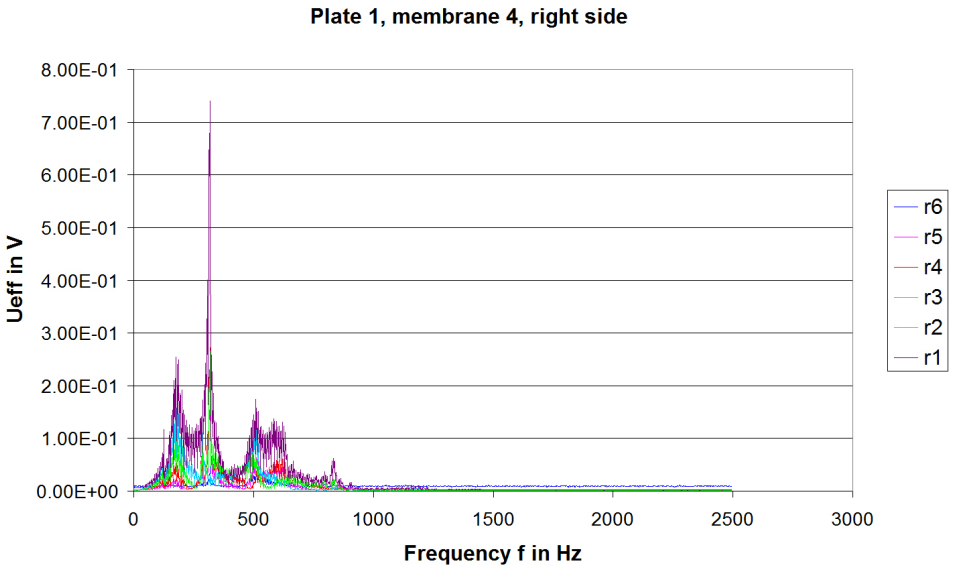


Figure 5.25 All data points (1024) from the right side of membrane m4 of plate 1; the FFT of the laser vibrometer signal U_{eff} against the frequency; a chirp signal was applied.

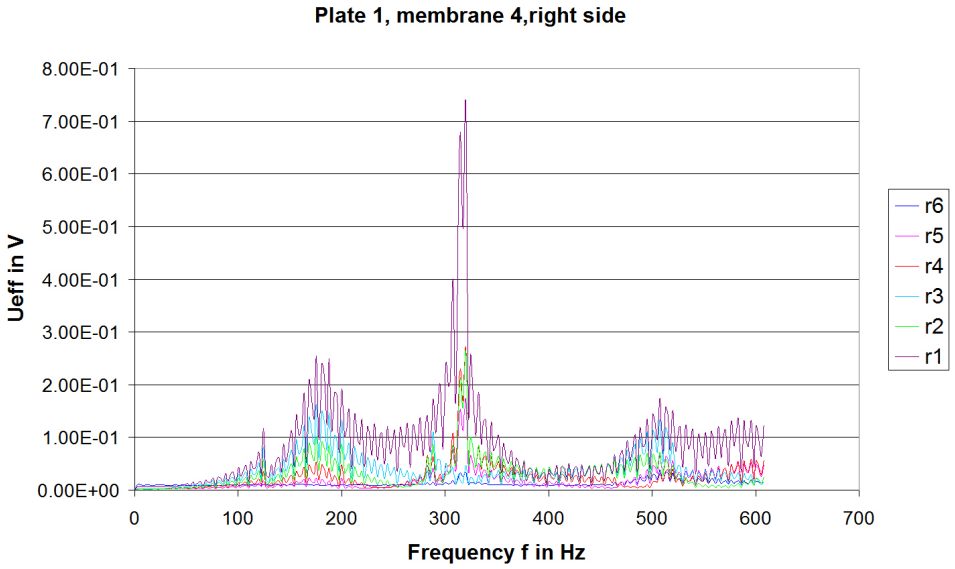


Figure 5.26 First 250 data points from the right side of membrane m4 of plate 1; the FFT of the laser vibrometer signal U_{eff} against the frequency; a chirp signal was applied.

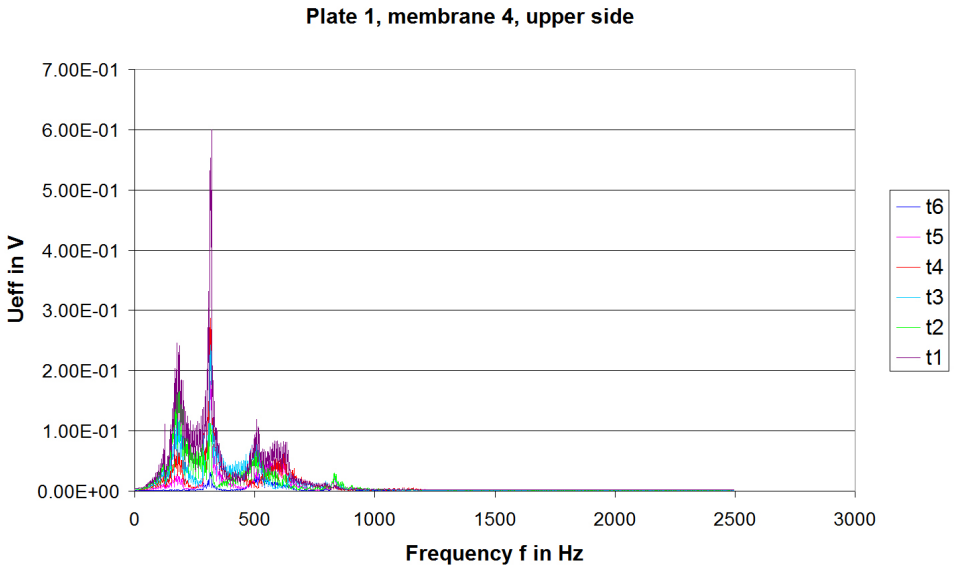


Figure 5.27 All data points (1024) from the upper side of membrane m4 of plate 1; the FFT of the laser vibrometer signal U_{eff} against the frequency; a chirp signal was applied.

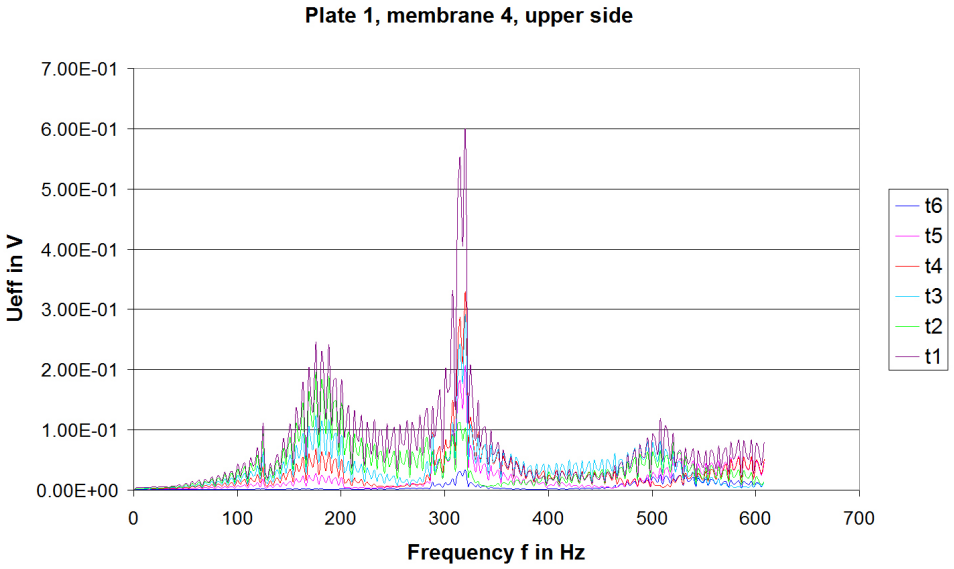


Figure 5.28 First 250 data points from the upper side of membrane m4 of plate 1; the FFT of the laser vibrometer signal U_{eff} against the frequency; a chirp signal was applied.

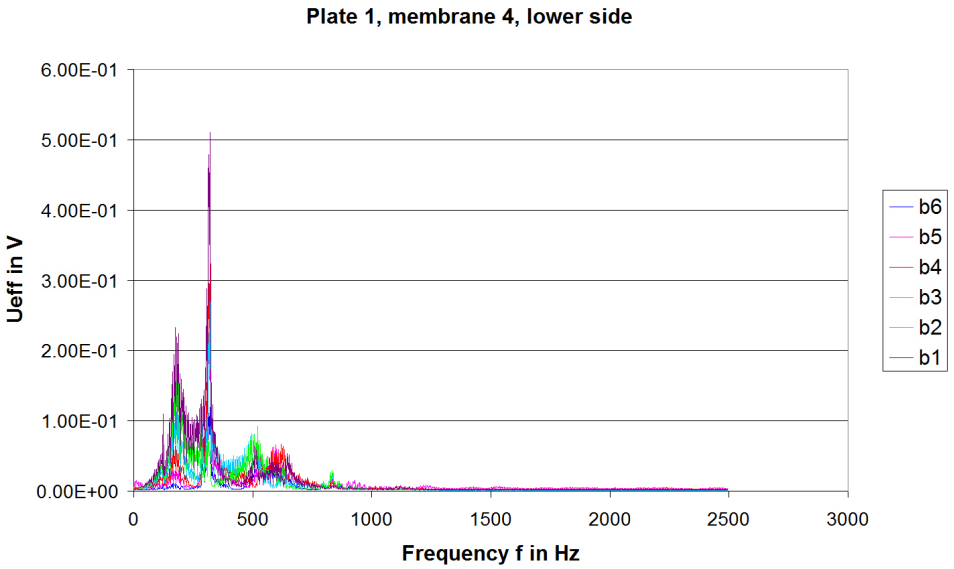


Figure 5.29 All data points (1024) from the upper side of membrane m4 of plate 1; the FFT of the laser vibrometer signal U_{eff} against the frequency; a chirp signal was applied.

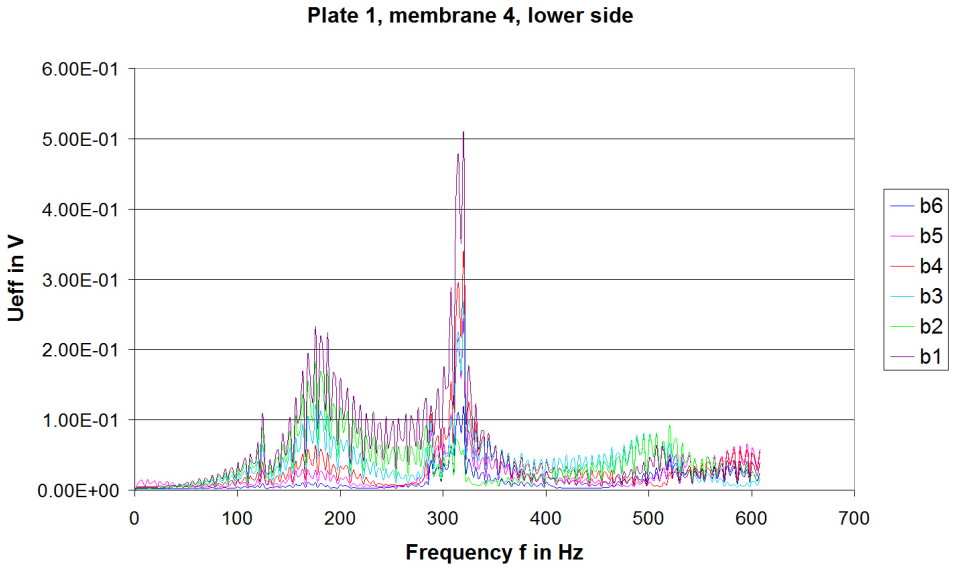


Figure 5.30 First 250 data points from the lower side of membrane m4 of plate 1; the FFT of the laser vibrometer signal U_{eff} against the frequency; a chirp signal was applied.

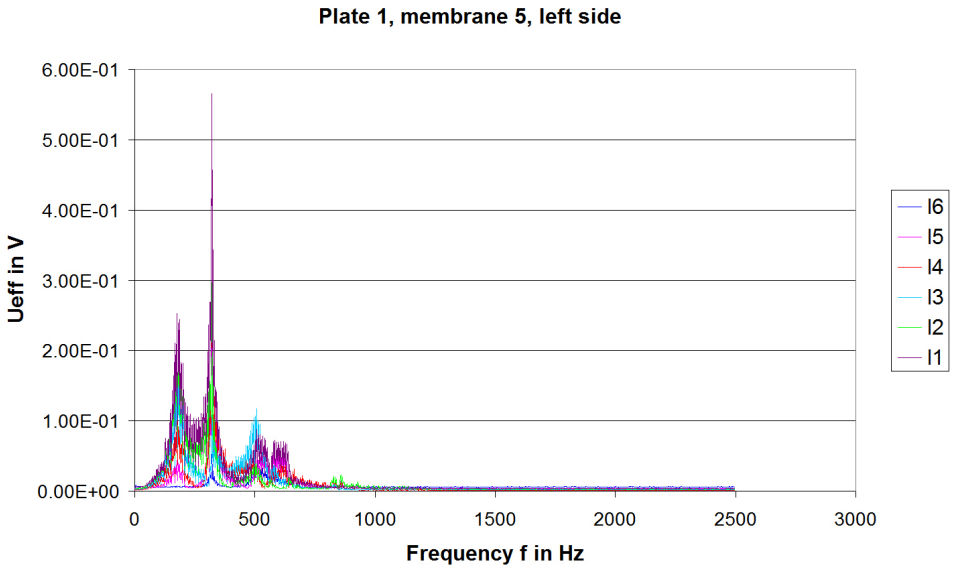


Figure 5.31 All data points (1024) from the left side of membrane m5 of plate 1; the FFT of the laser vibrometer signal U_{eff} against the frequency; a chirp signal was applied.

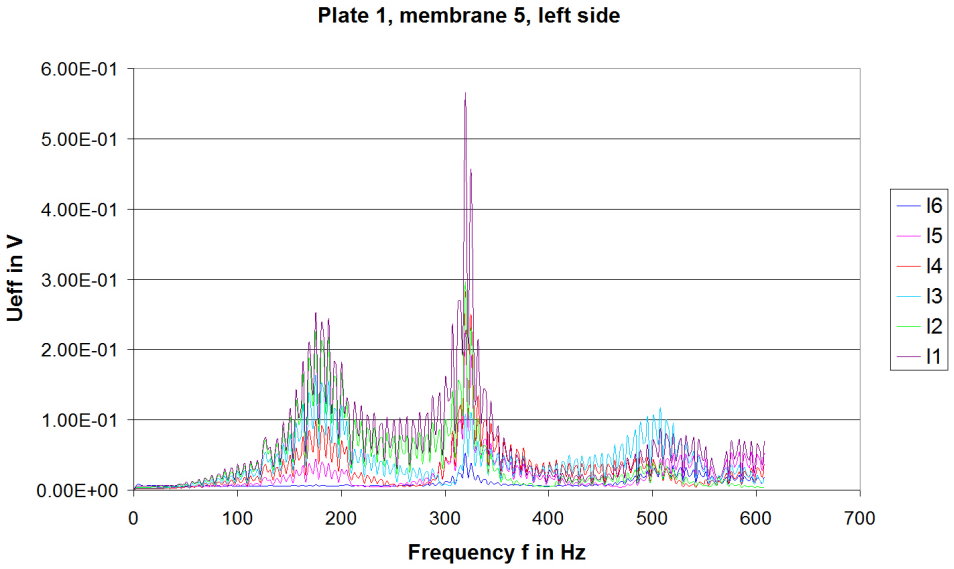


Figure 5.32 First 250 data points from the left side of membrane m5 of plate 1; the FFT of the laser vibrometer signal U_{eff} against the frequency; a chirp signal was applied.

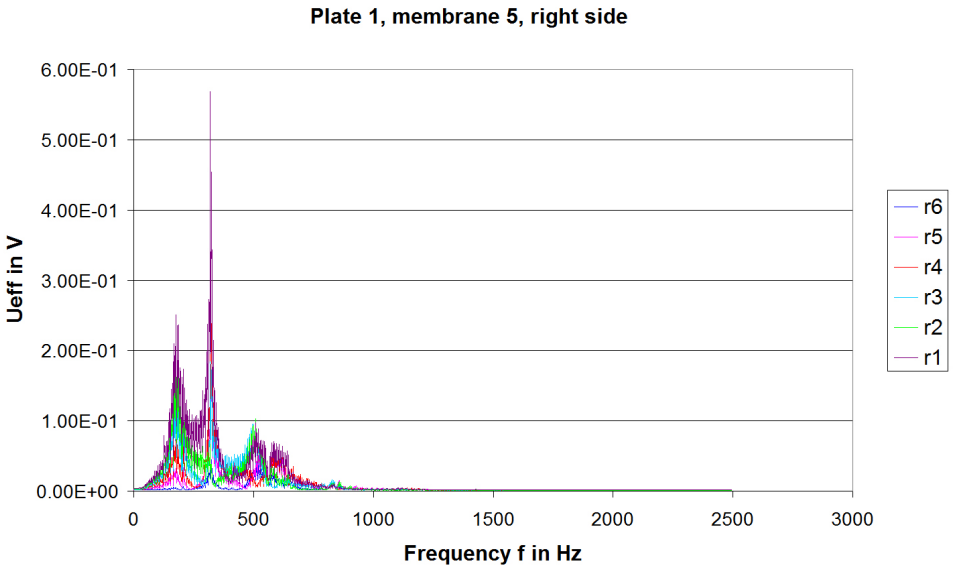


Figure 5.33 All data points (1024) from the right side of membrane m5 of plate 1; the FFT of the laser vibrometer signal U_{eff} against the frequency; a chirp signal was applied.

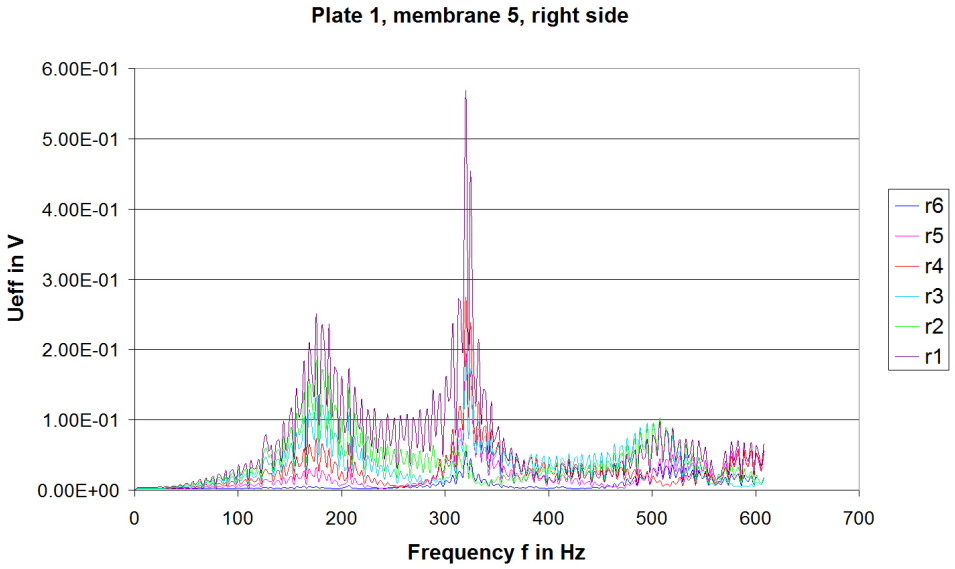


Figure 5.34 First 250 data points from the right side of membrane m5 of plate 1; the FFT of the laser vibrometer signal U_{eff} against the frequency; a chirp signal was applied.

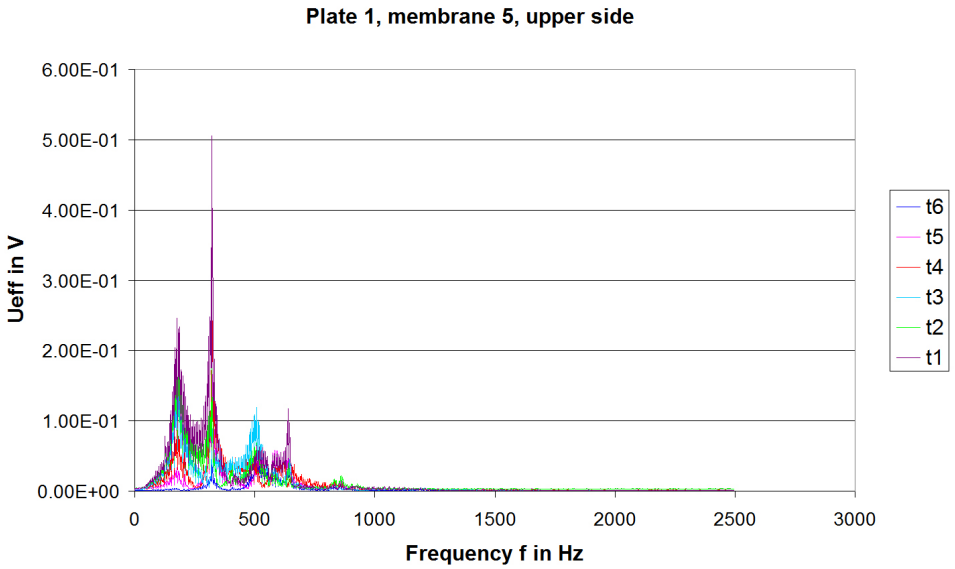


Figure 5.35 All data points (1024) from the upper side of membrane m5 of plate 1; the FFT of the laser vibrometer signal U_{eff} against the frequency; a chirp signal was applied.

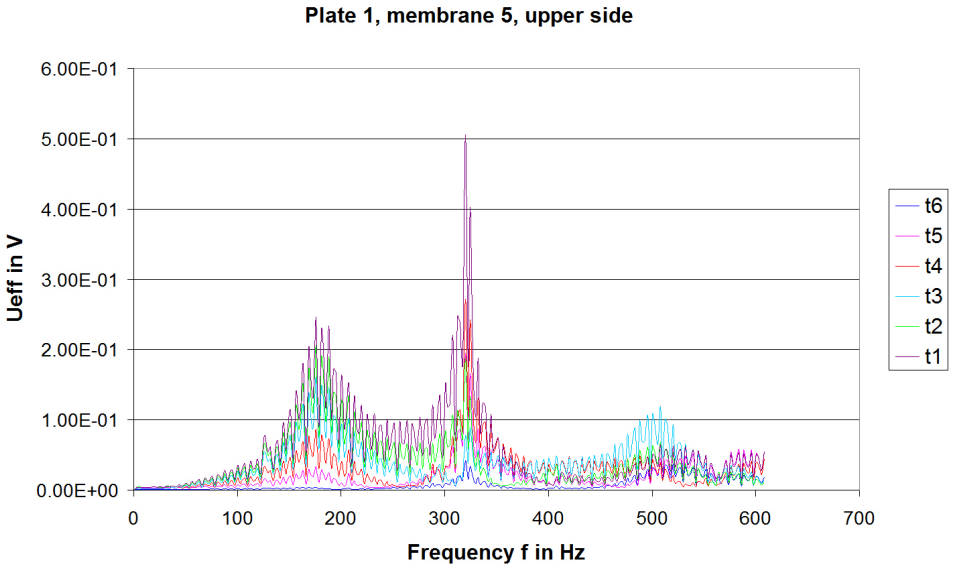


Figure 5.36 First 250 data points from the upper side of membrane m5 of plate 1; the FFT of the laser vibrometer signal U_{eff} against the frequency; a chirp signal was applied.

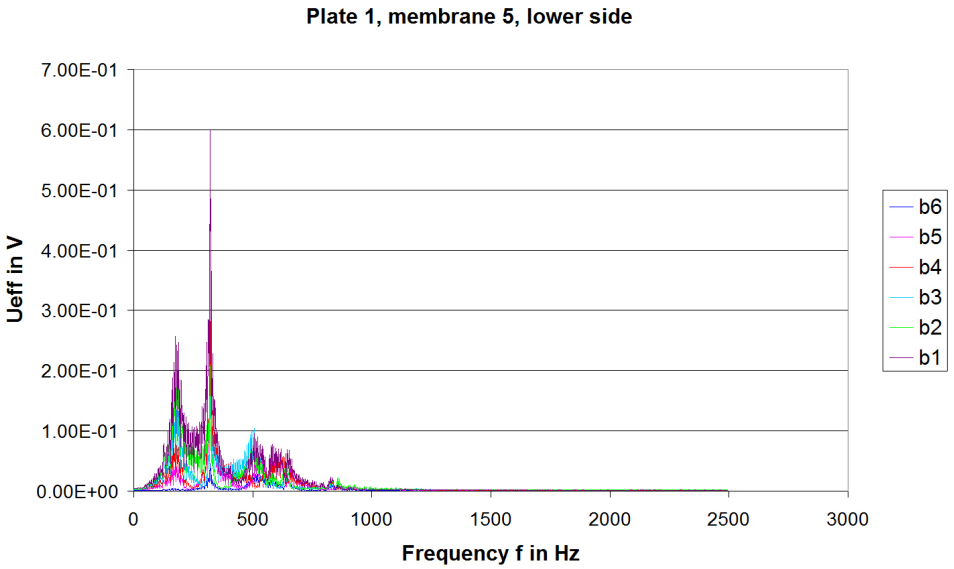


Figure 5.37 All data points (1024) from the lower side of membrane m5 of plate 1; the FFT of the laser vibrometer signal U_{eff} against the frequency; a chirp signal was applied.

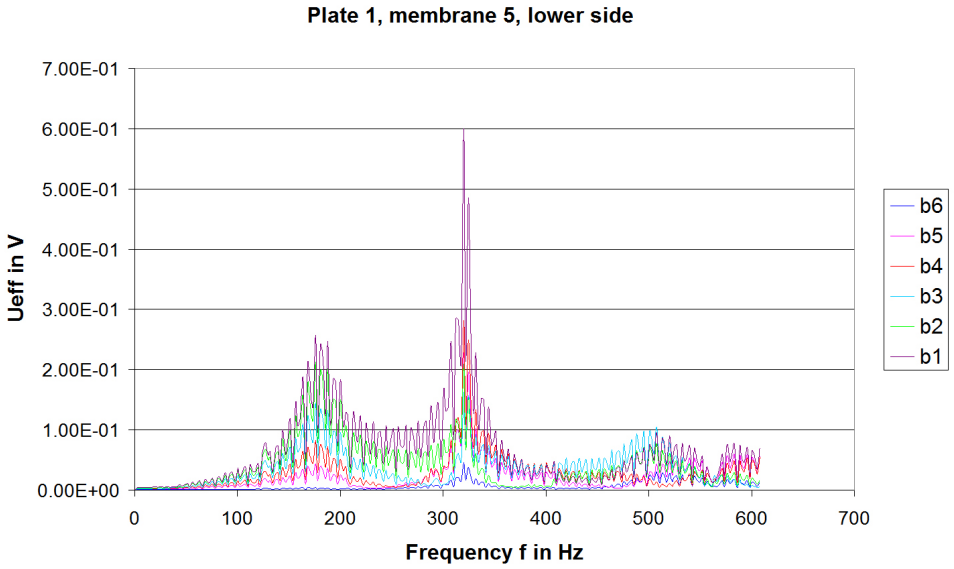


Figure 5.38 First 250 data points from the lower side of membrane m5 of plate 1; the FFT of the laser vibrometer signal U_{eff} against the frequency; a chirp signal was applied.

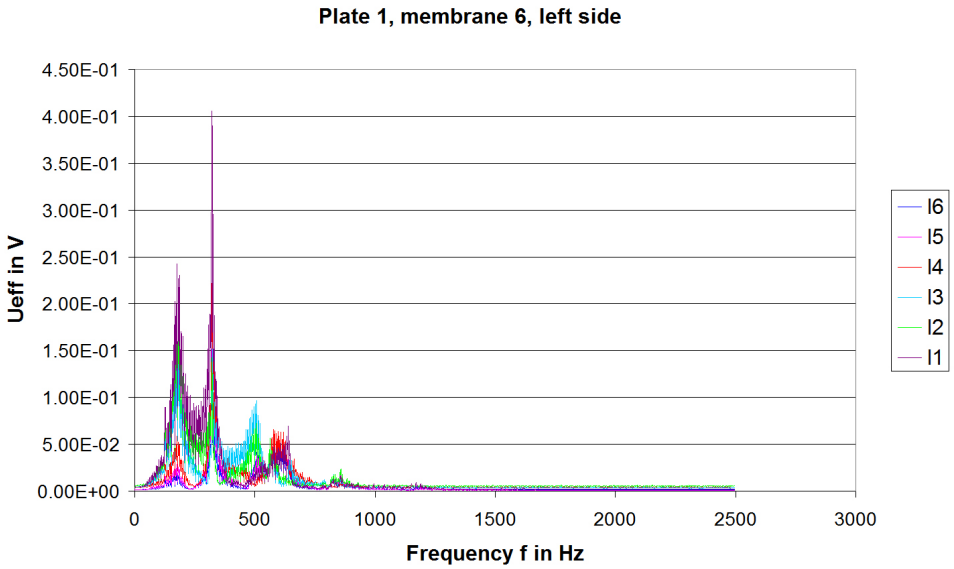


Figure 5.39 All data points (1024) from the left side of membrane m6 of plate 1; the FFT of the laser vibrometer signal U_{eff} against the frequency; a chirp signal was applied.

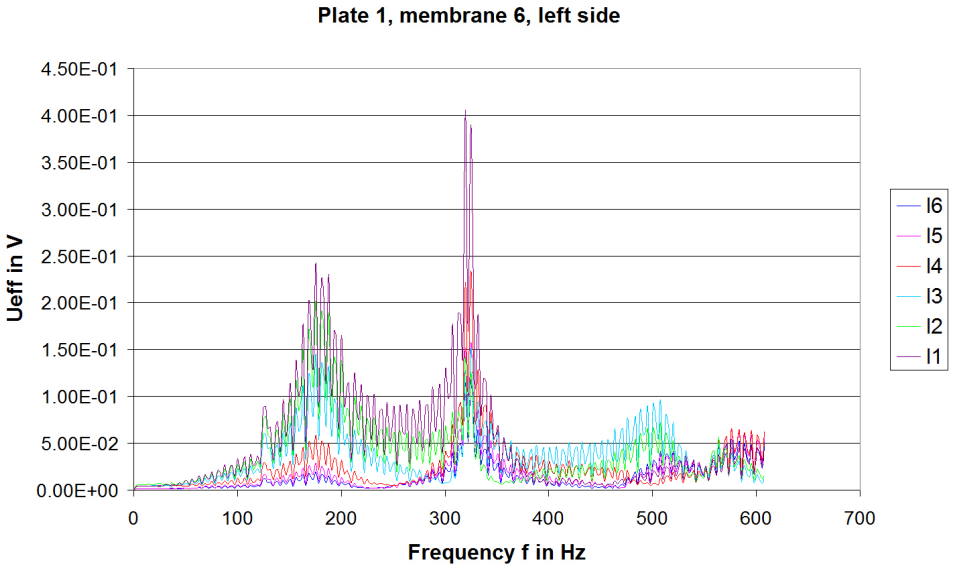


Figure 5.40 First 250 data points from the left side of membrane m6 of plate 1; the FFT of the laser vibrometer signal U_{eff} against the frequency; a chirp signal was applied.

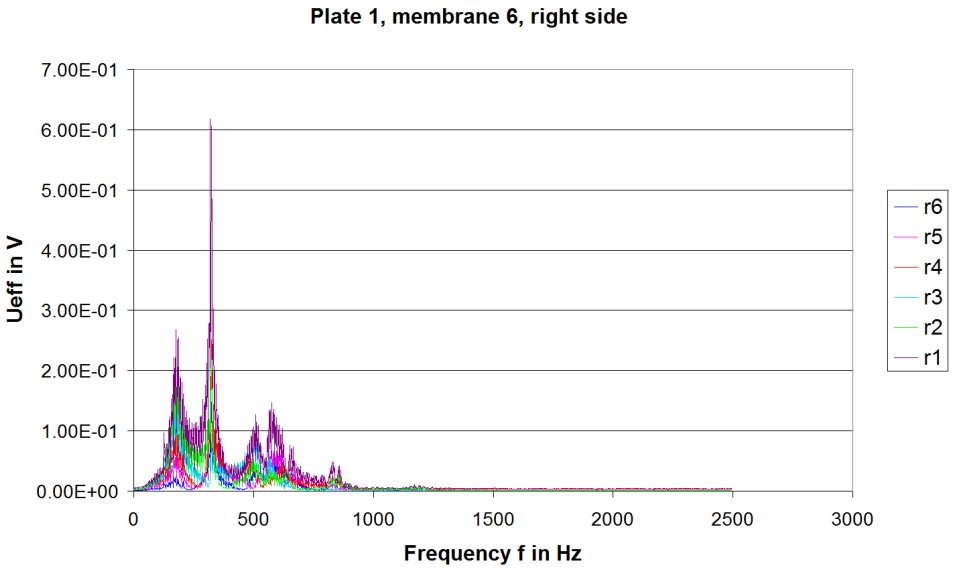


Figure 5.41 All data points (1024) from the right side of membrane m6 of plate 1; the FFT of the laser vibrometer signal U_{eff} against the frequency; a chirp signal was applied.

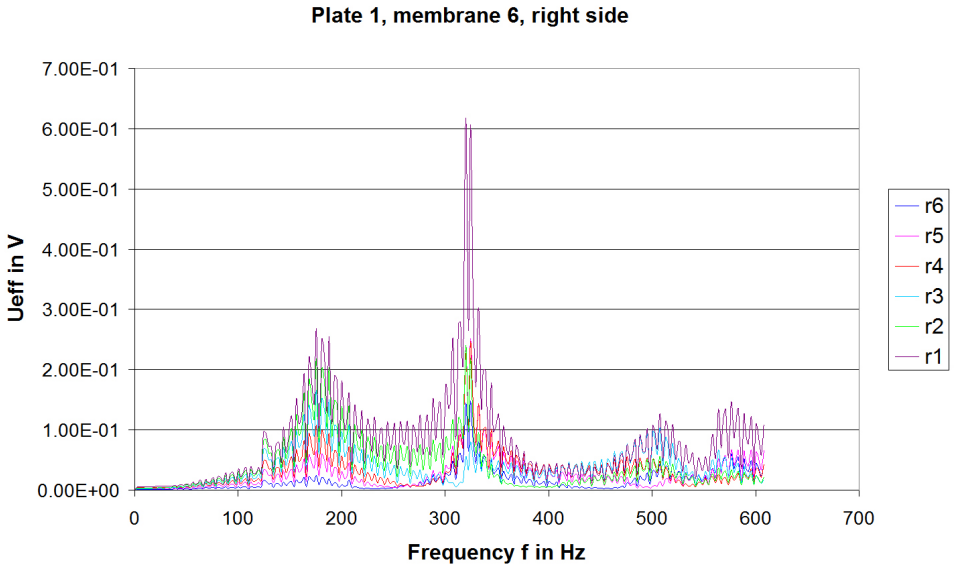


Figure 5.42 First 250 data points from the right side of membrane m6 of plate 1; the FFT of the laser vibrometer signal U_{eff} against the frequency; a chirp signal was applied.

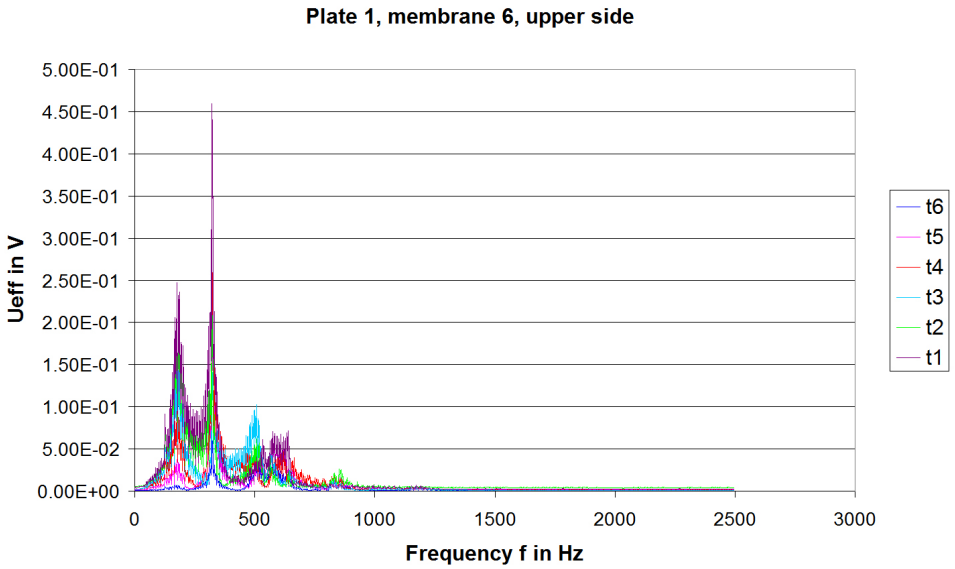


Figure 5.43 All data points (1024) from the upper side of membrane m6 of plate 1; the FFT of the laser vibrometer signal U_{eff} against the frequency; a chirp signal was applied.

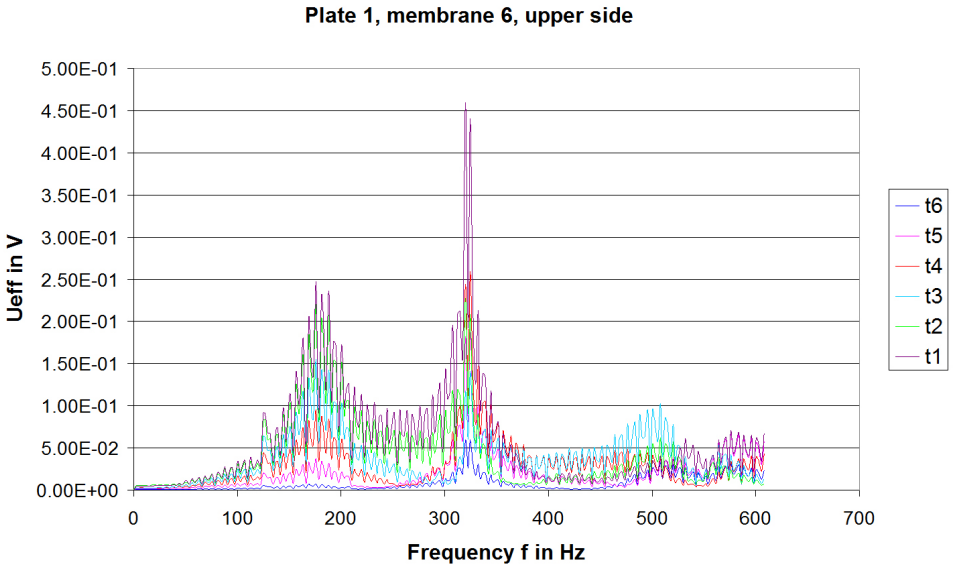


Figure 5.44 First 250 data points from the upper side of membrane m6 of plate 1; the FFT of the laser vibrometer signal U_{eff} against the frequency; a chirp signal was applied.

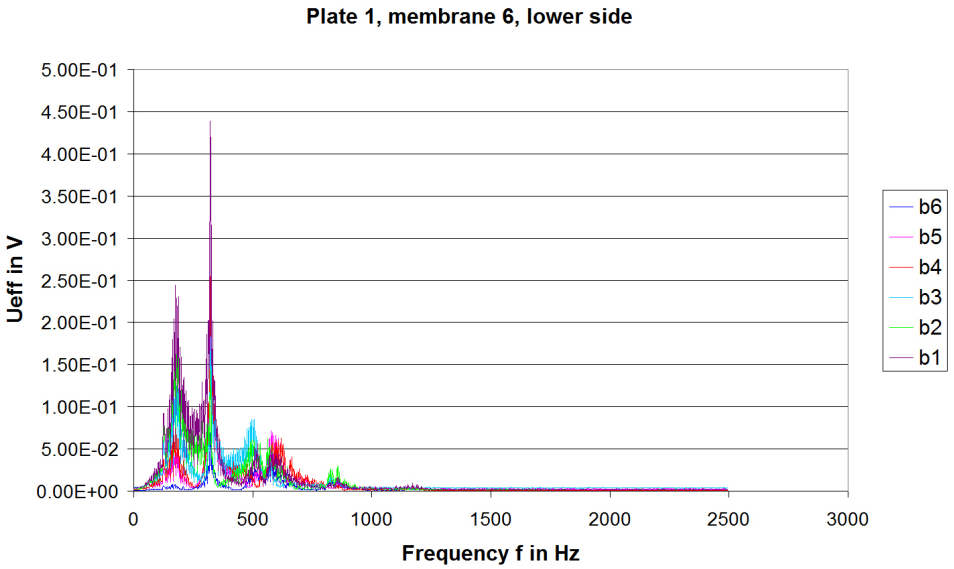


Figure 5.45 All data points (1024) from the lower side of membrane m6 of plate 1; the FFT of the laser vibrometer signal U_{eff} against the frequency; a chirp signal was applied.

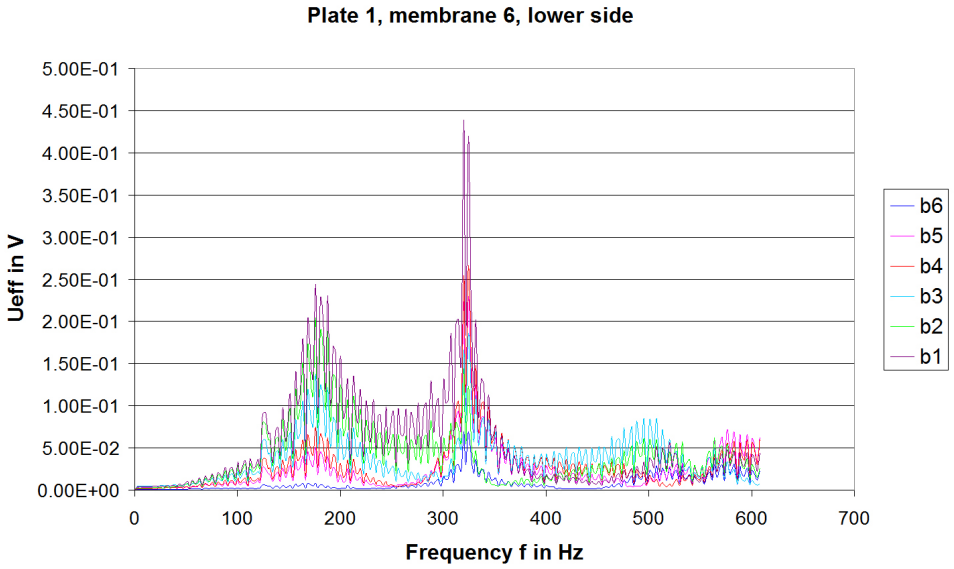


Figure 5.46 First 250 data points from the lower side of membrane m6 of plate 1; the FFT of the laser vibrometer signal U_{eff} against the frequency; a chirp signal was applied.

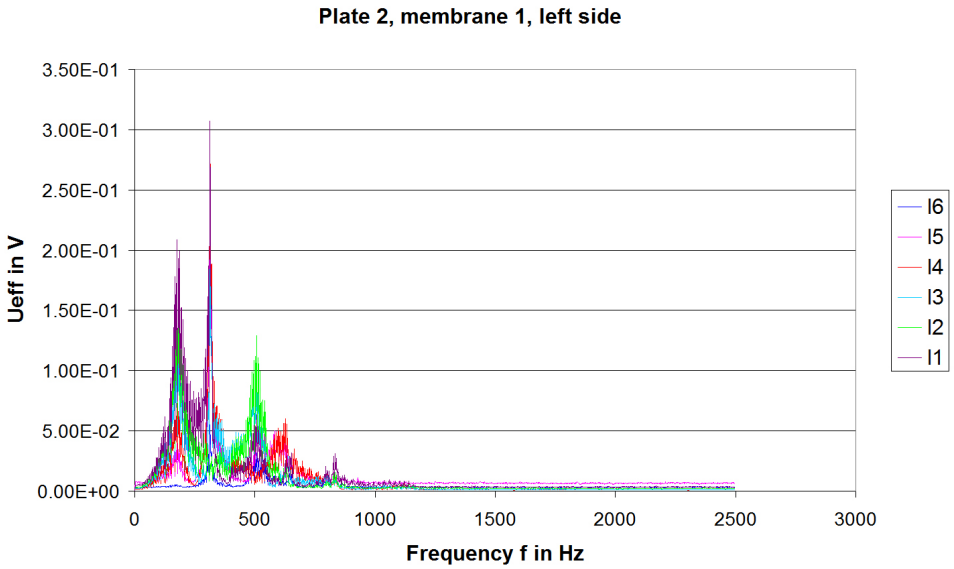


Figure 5.47 All data points (1024) from the left side of membrane m1 of plate 2; the FFT of the laser vibrometer signal U_{eff} against the frequency; a chirp signal was applied.

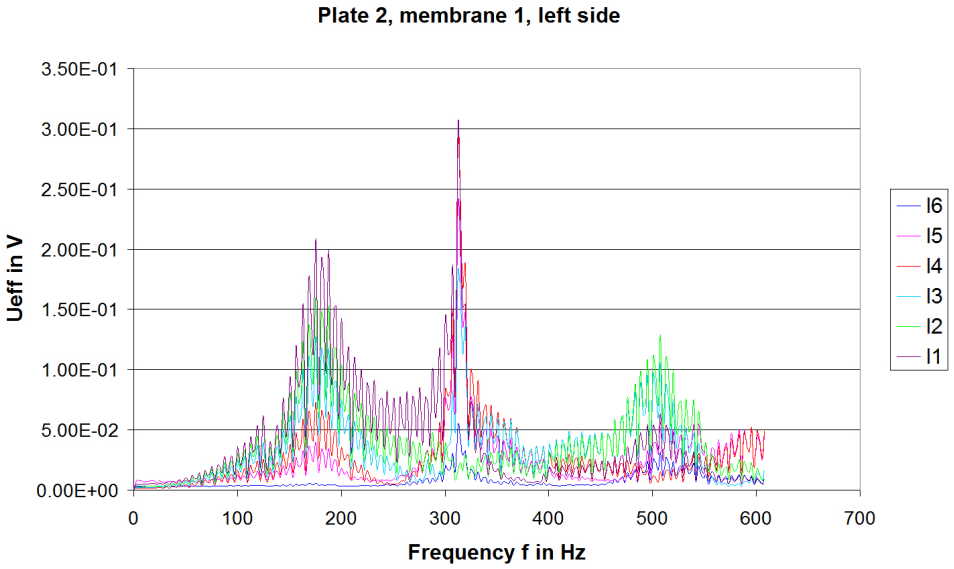


Figure 5.48 First 250 data points from the left side of membrane m1 of plate 2; the FFT of the laser vibrometer signal U_{eff} against the frequency; a chirp signal was applied.

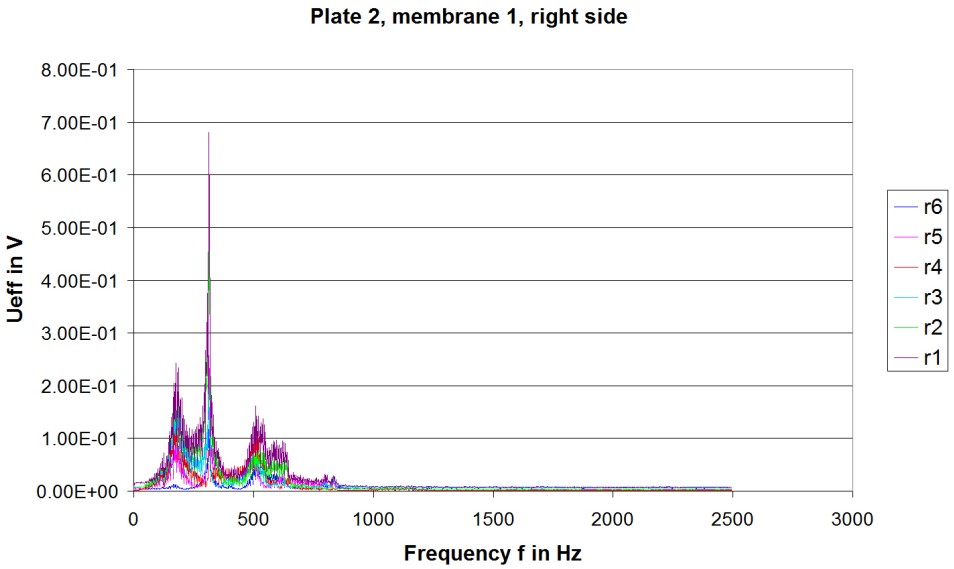


Figure 5.49 All data points (1024) from the right side of membrane m1 of plate 2; the FFT of the laser vibrometer signal U_{eff} against the frequency; a chirp signal was applied.

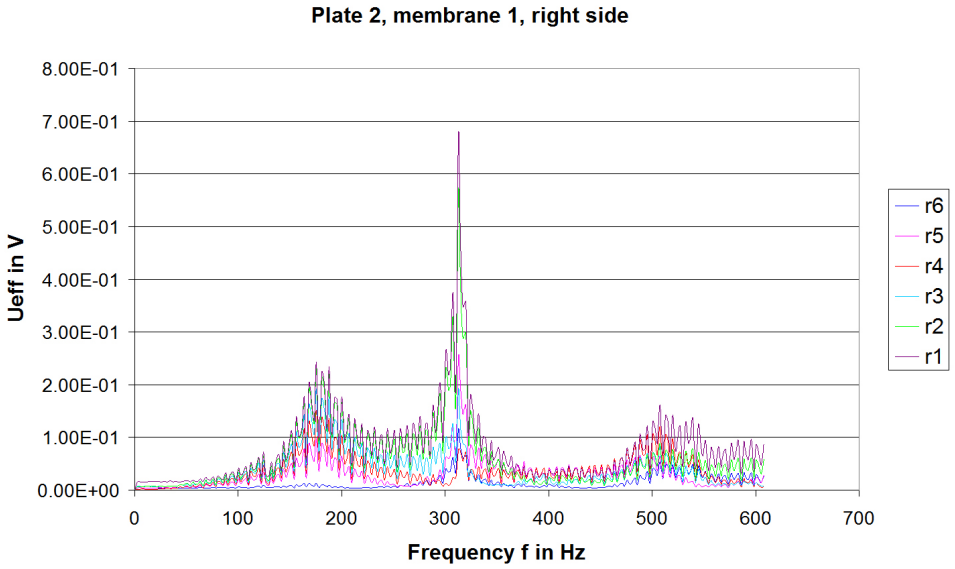


Figure 5.50 First 250 data points from the right side of membrane m1 of plate 2; the FFT of the laser vibrometer signal U_{eff} against the frequency; a chirp signal was applied.

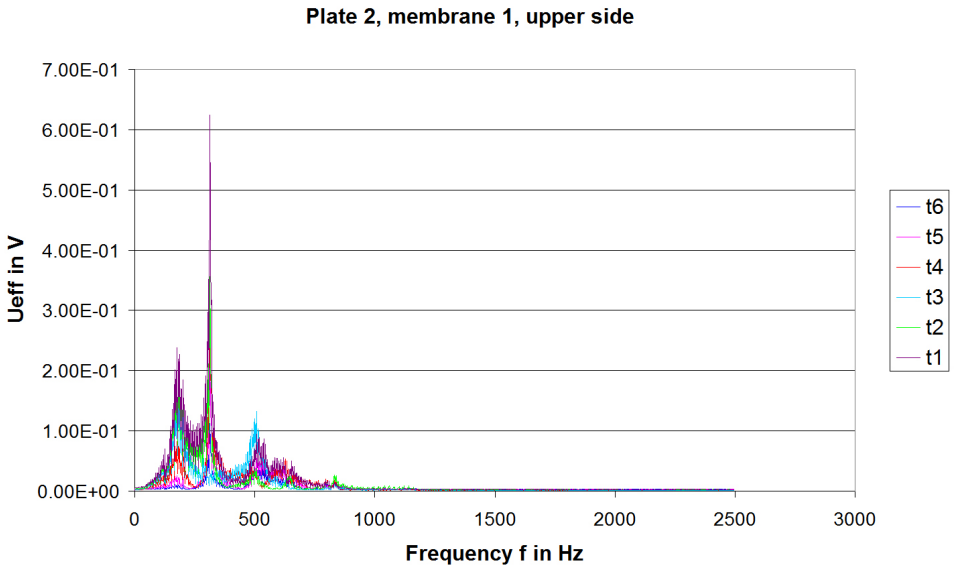


Figure 5.51 All data points (1024) from the upper side of membrane m1 of plate 2; the FFT of the laser vibrometer signal U_{eff} against the frequency; a chirp signal was applied.

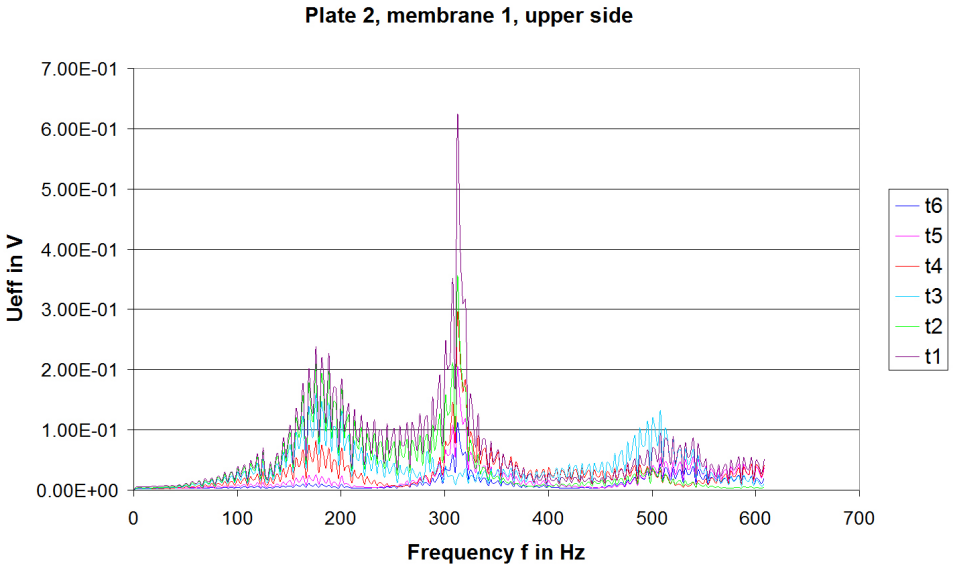


Figure 5.52 First 250 data points from the upper side of membrane m1 of plate 2; the FFT of the laser vibrometer signal U_{eff} against the frequency; a chirp signal was applied.

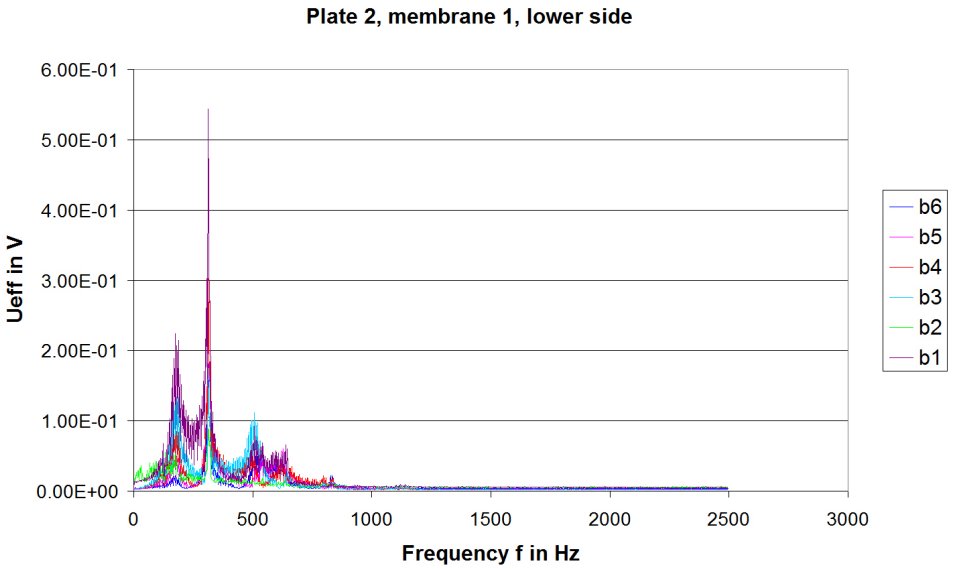


Figure 5.53 All data points (1024) from the lower side of membrane m1 of plate 2; the FFT of the laser vibrometer signal U_{eff} against the frequency; a chirp signal was applied.

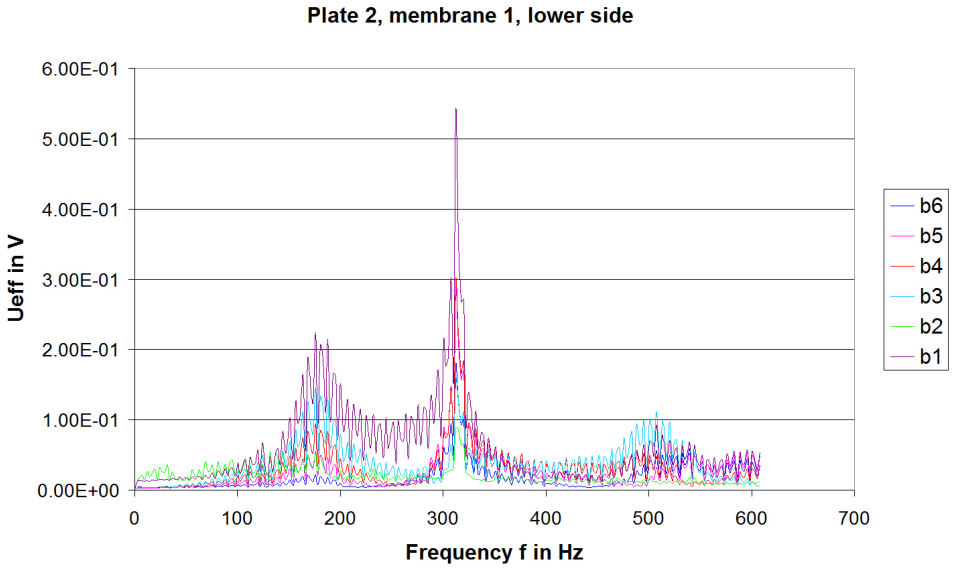


Figure 5.54 First 250 data points from the lower side of membrane m1 of plate 2; the FFT of the laser vibrometer signal U_{eff} against the frequency; a chirp signal was applied.

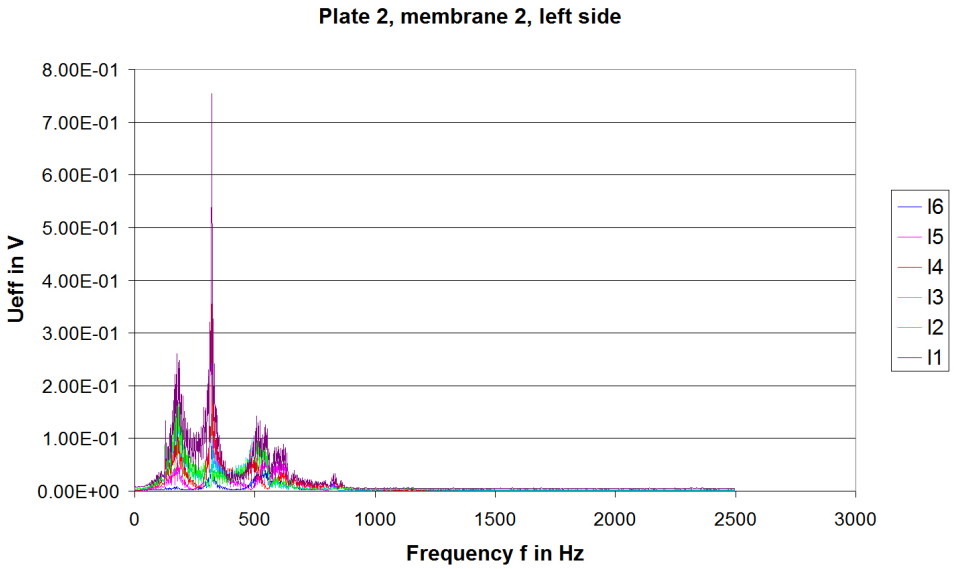


Figure 5.55 All data points (1024) from the left side of membrane m2 of plate 2; the FFT of the laser vibrometer signal U_{eff} against the frequency; a chirp signal was applied.

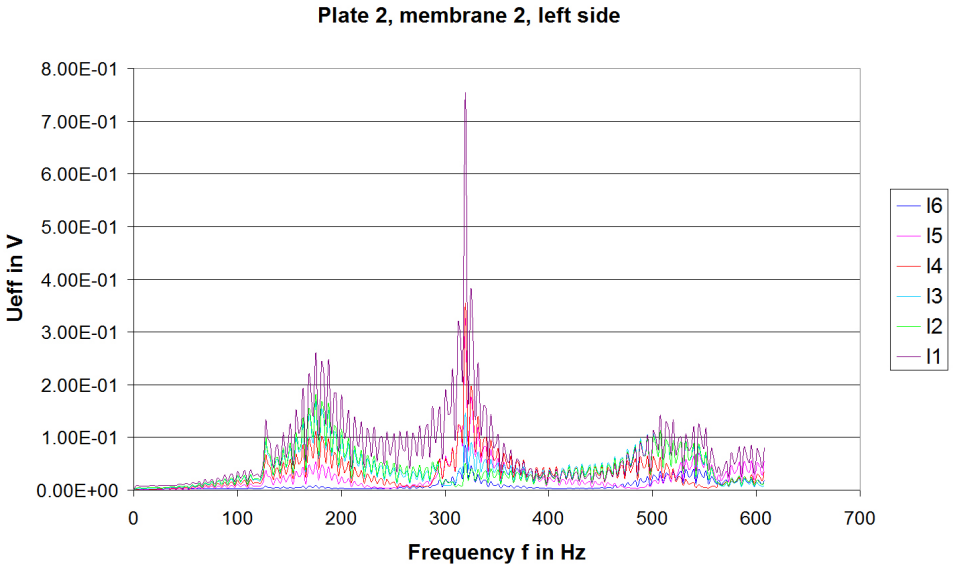


Figure 5.56 First 250 data points from the left side of membrane m2 of plate 2; the FFT of the laser vibrometer signal U_{eff} against the frequency; a chirp signal was applied.

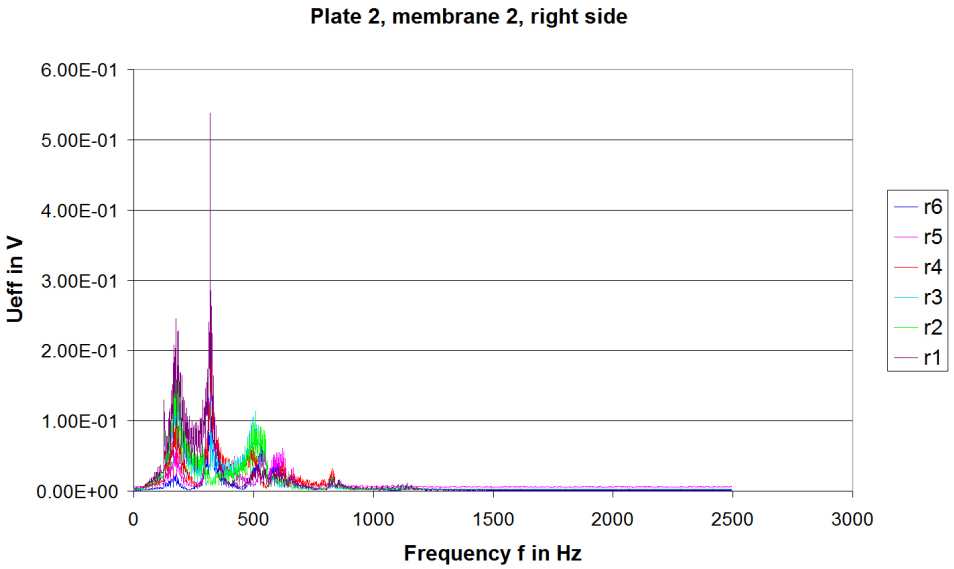


Figure 5.57 All data points (1024) from the right side of membrane m2 of plate 2; the FFT of the laser vibrometer signal U_{eff} against the frequency; a chirp signal was applied.

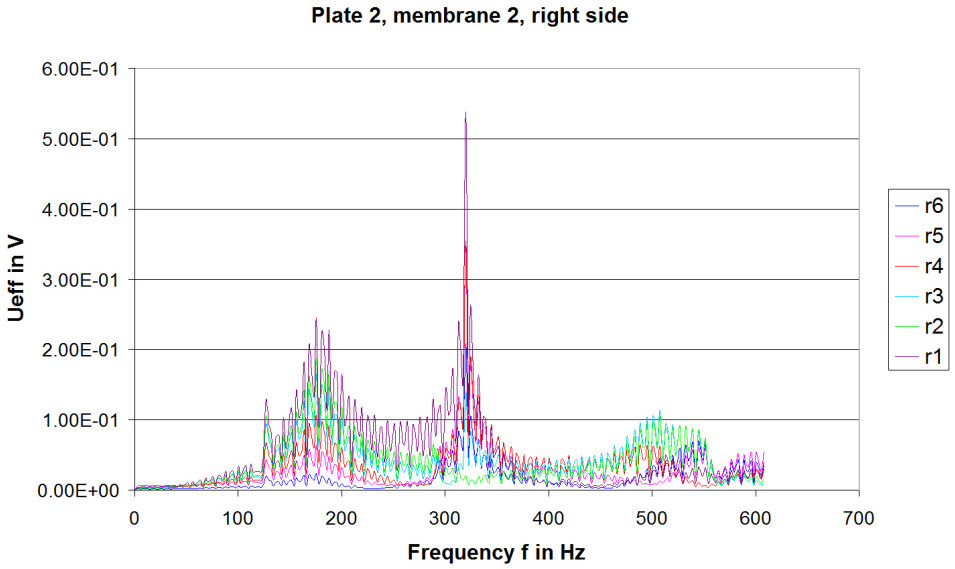


Figure 5.58 First 250 data points from the right side of membrane m2 of plate 2; the FFT of the laser vibrometer signal U_{eff} against the frequency; a chirp signal was applied.

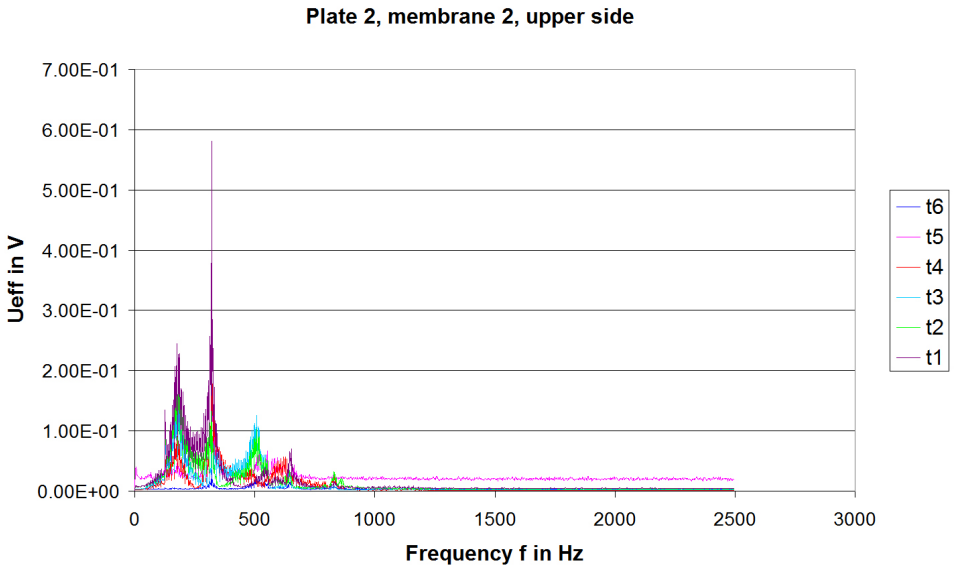


Figure 5.59 All data points (1024) from the upper side of membrane m2 of plate 2; the FFT of the laser vibrometer signal U_{eff} against the frequency; a chirp signal was applied.

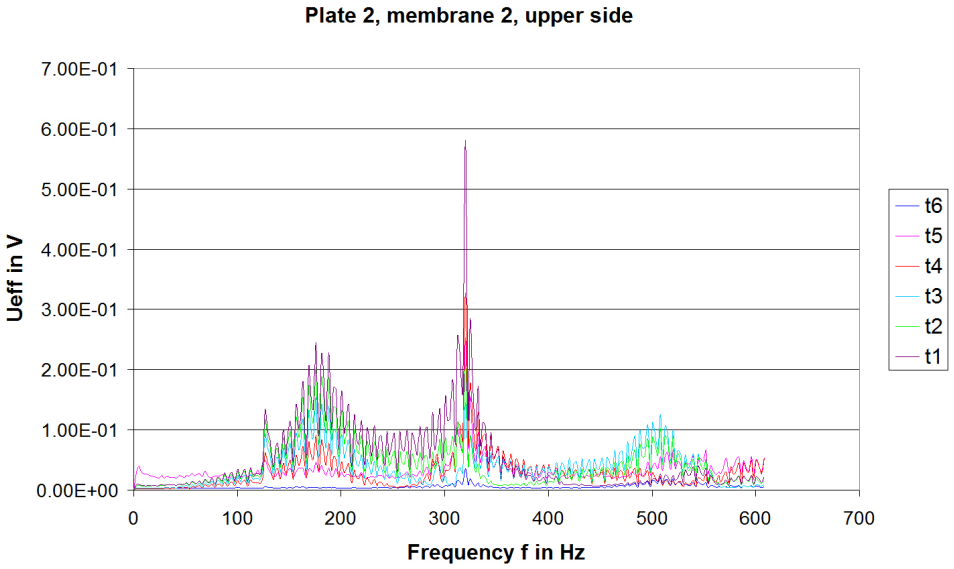


Figure 5.60 First 250 data points from the upper side of membrane m2 of plate 2; the FFT of the laser vibrometer signal U_{eff} against the frequency; a chirp signal was applied.

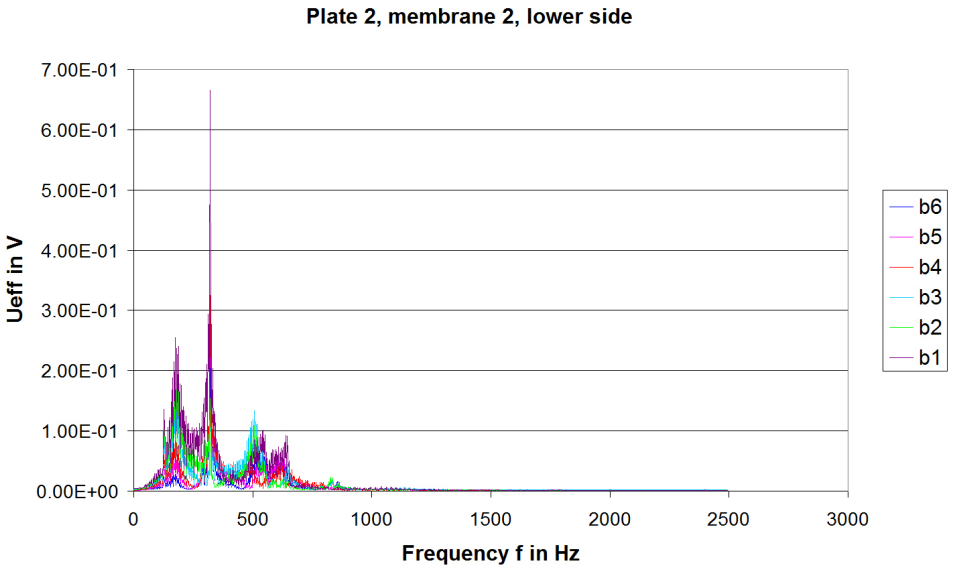


Figure 5.61 All data points (1024) from the lower side of membrane m2 of plate 2; the FFT of the laser vibrometer signal U_{eff} against the frequency; a chirp signal was applied.

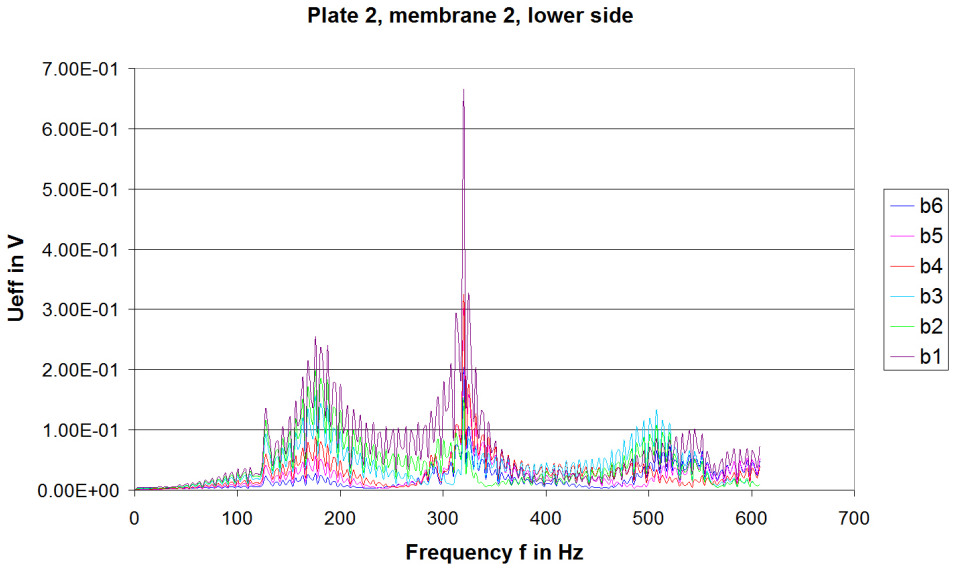


Figure 5.62 First 250 data points from the lower side of membrane m2 of plate 2; the FFT of the laser vibrometer signal U_{eff} against the frequency; a chirp signal was applied.

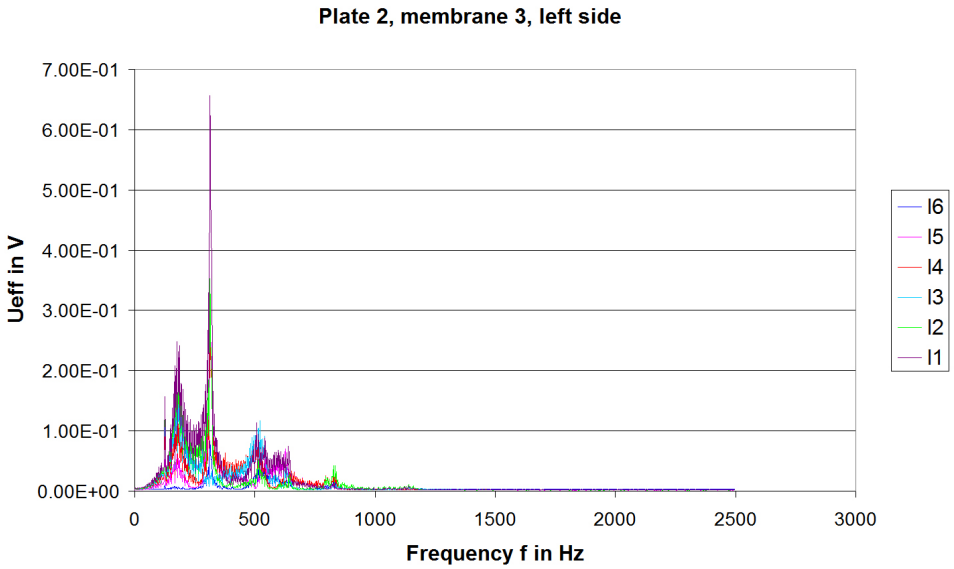


Figure 5.63 All data points (1024) from the left side of membrane m3 of plate 2; the FFT of the laser vibrometer signal U_{eff} against the frequency; a chirp signal was applied.

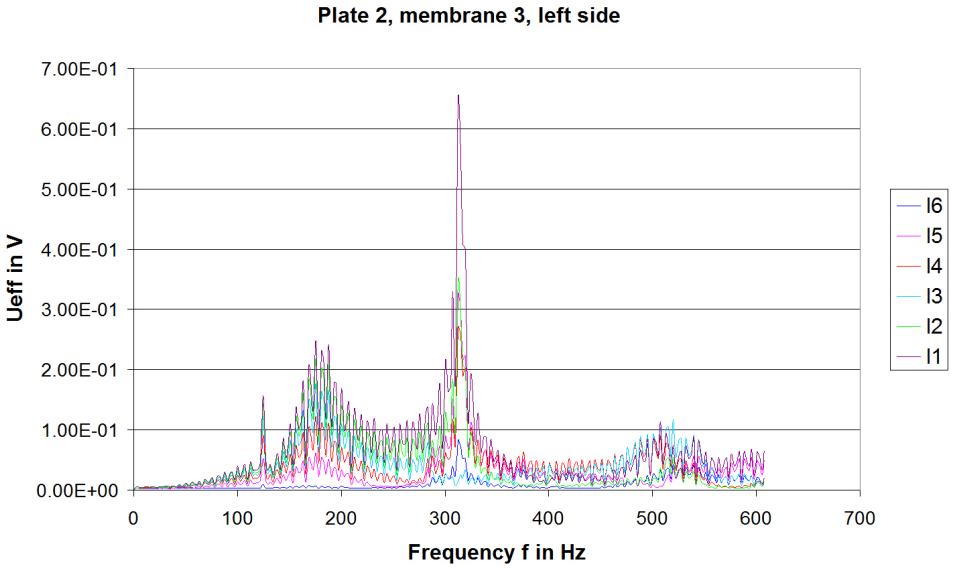


Figure 5.64 First 250 data points from the left side of membrane m3 of plate 2; the FFT of the laser vibrometer signal U_{eff} against the frequency; a chirp signal was applied.

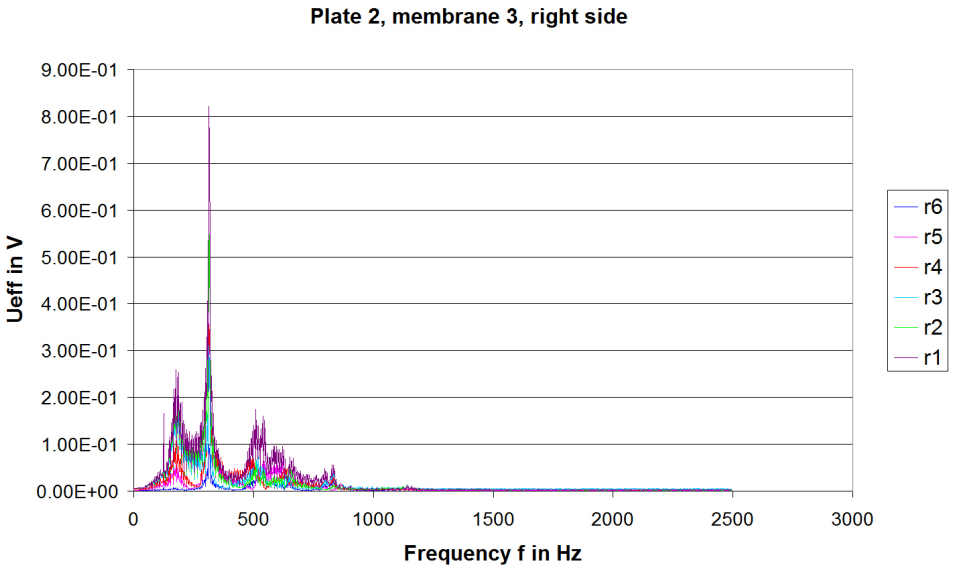


Figure 5.65 All data points (1024) from the right side of membrane m3 of plate 2; the FFT of the laser vibrometer signal U_{eff} against the frequency; a chirp signal was applied.

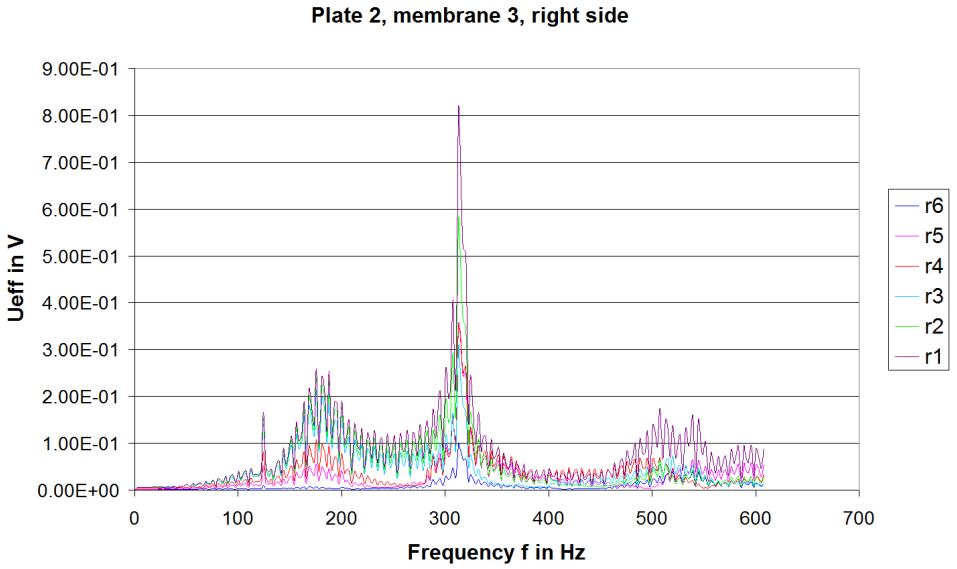


Figure 5.66 First 250 data points from the right side of membrane m3 of plate 2; the FFT of the laser vibrometer signal U_{eff} against the frequency; a chirp signal was applied.

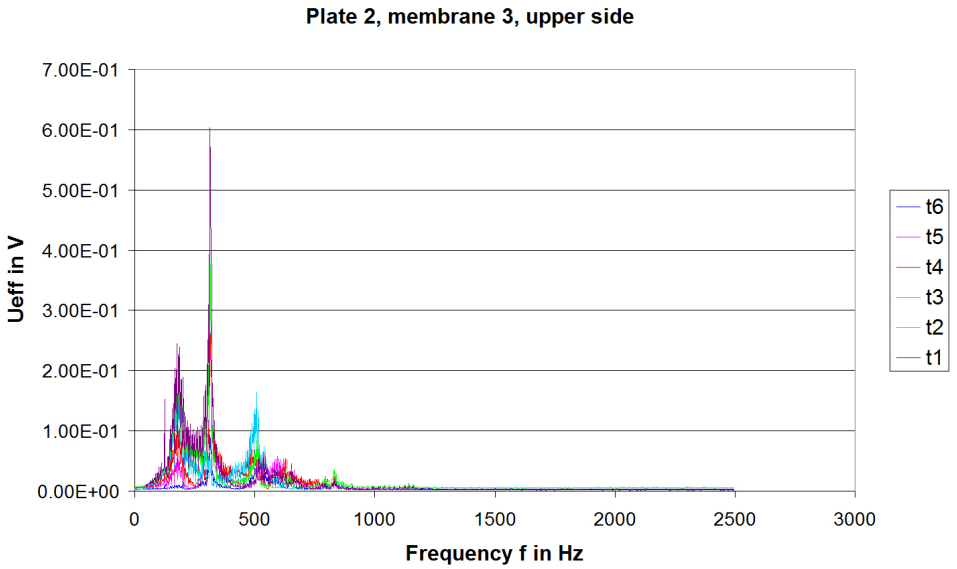


Figure 5.67 All data points (1024) from the upper side of membrane m3 of plate 2; the FFT of the laser vibrometer signal U_{eff} against the frequency; a chirp signal was applied.

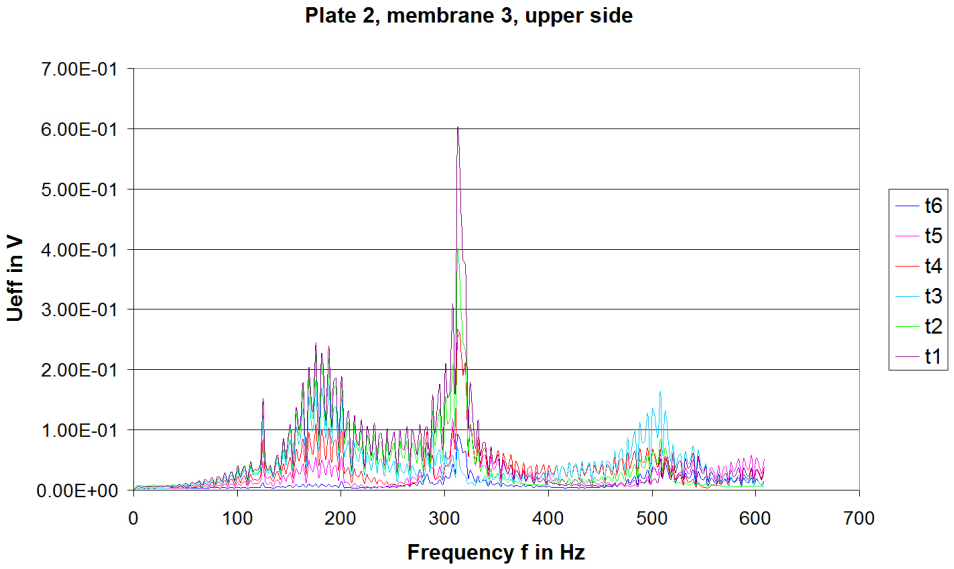


Figure 5.68 First 250 data points from the upper side of membrane m3 of plate 2; the FFT of the laser vibrometer signal U_{eff} against the frequency; a chirp signal was applied.

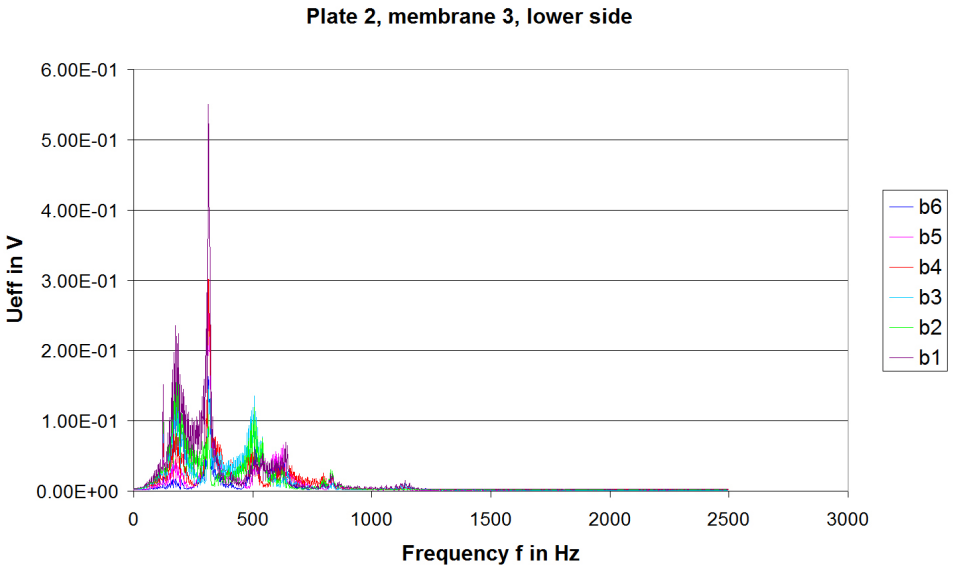


Figure 5.69 All data points (1024) from the lower side of membrane m3 of plate 2; the FFT of the laser vibrometer signal U_{eff} against the frequency; a chirp signal was applied.

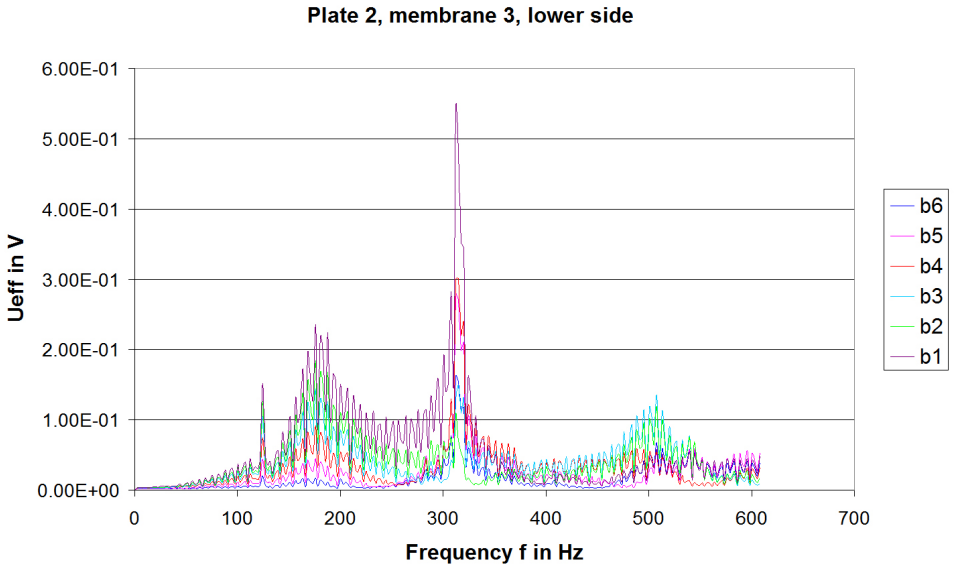


Figure 5.70 First 250 data points from the lower side of membrane m3 of plate 2; the FFT of the laser vibrometer signal U_{eff} against the frequency; a chirp signal was applied.

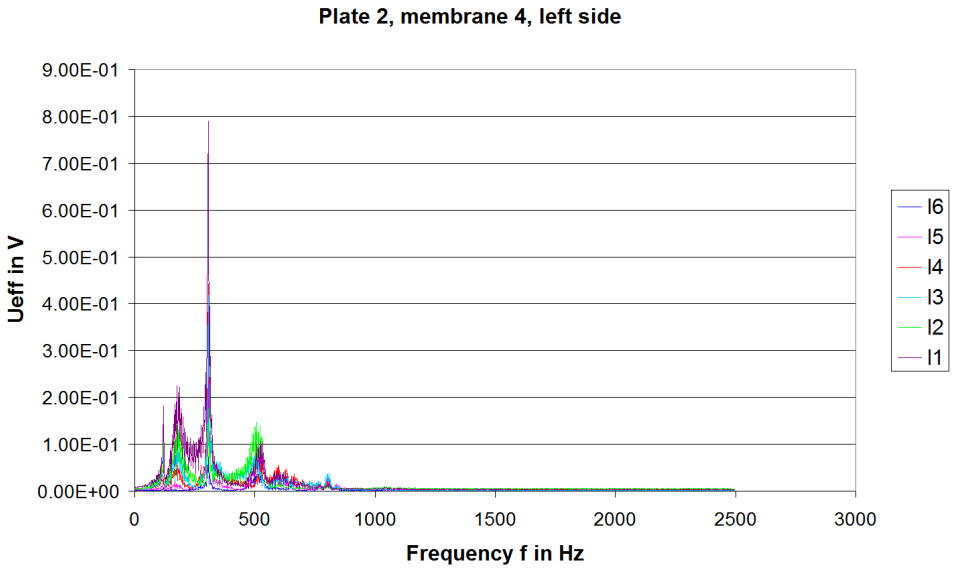


Figure 5.71 All data points (1024) from the left side of membrane m4 of plate 2; the FFT of the laser vibrometer signal U_{eff} against the frequency; a chirp signal was applied.

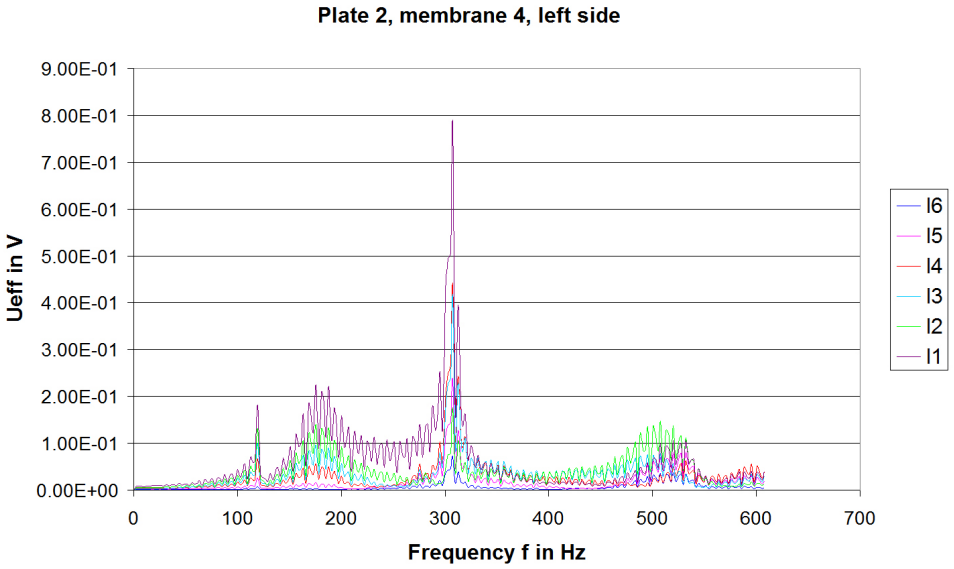


Figure 5.72 First 250 data points from the left side of membrane m4 of plate 2; the FFT of the laser vibrometer signal U_{eff} against the frequency; a chirp signal was applied.

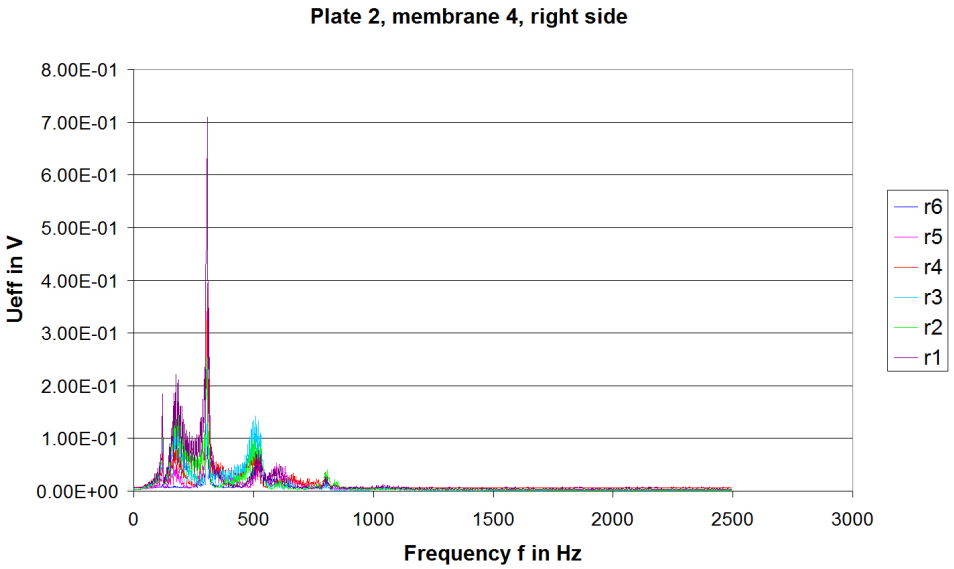


Figure 5.73 All data points (1024) from the right side of membrane m4 of plate 2; the FFT of the laser vibrometer signal U_{eff} against the frequency; a chirp signal was applied.

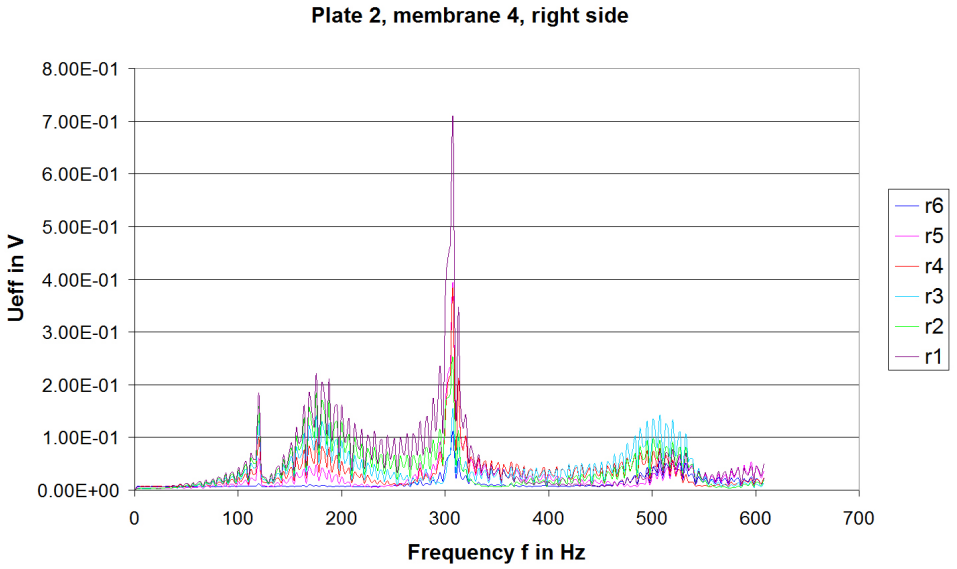


Figure 5.74 First 250 data points from the right side of membrane m4 of plate 2; the FFT of the laser vibrometer signal U_{eff} against the frequency; a chirp signal was applied.

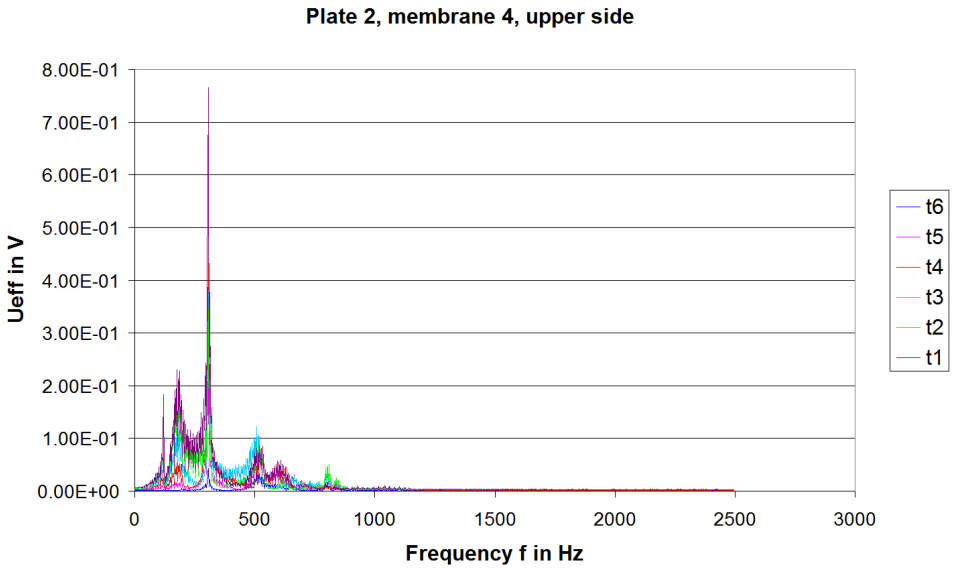


Figure 5.75 All data points (1024) from the upper side of membrane m4 of plate 2; the FFT of the laser vibrometer signal U_{eff} against the frequency; a chirp signal was applied.

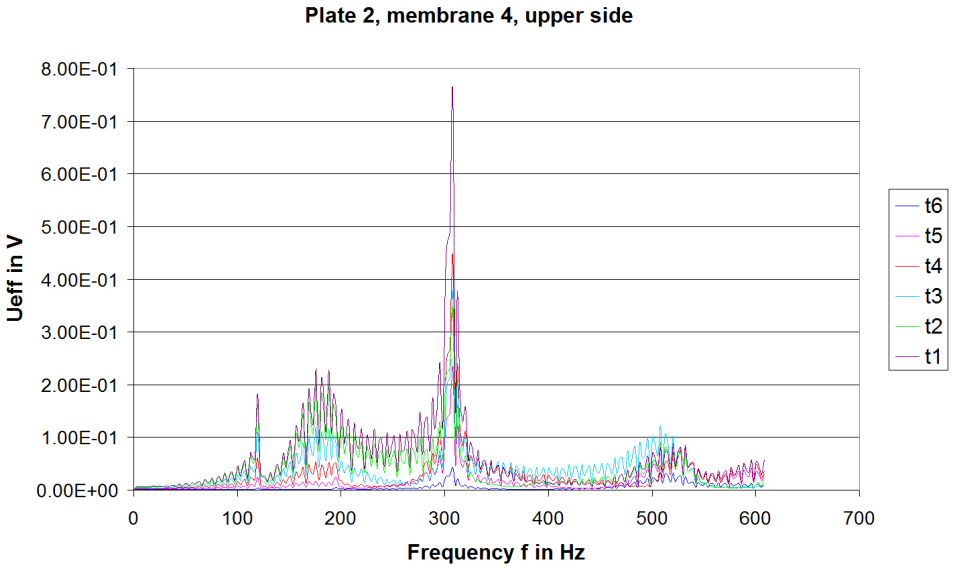


Figure 5.76 First 250 data points from the upper side of membrane m4 of plate 2; the FFT of the laser vibrometer signal U_{eff} against the frequency; a chirp signal was applied.

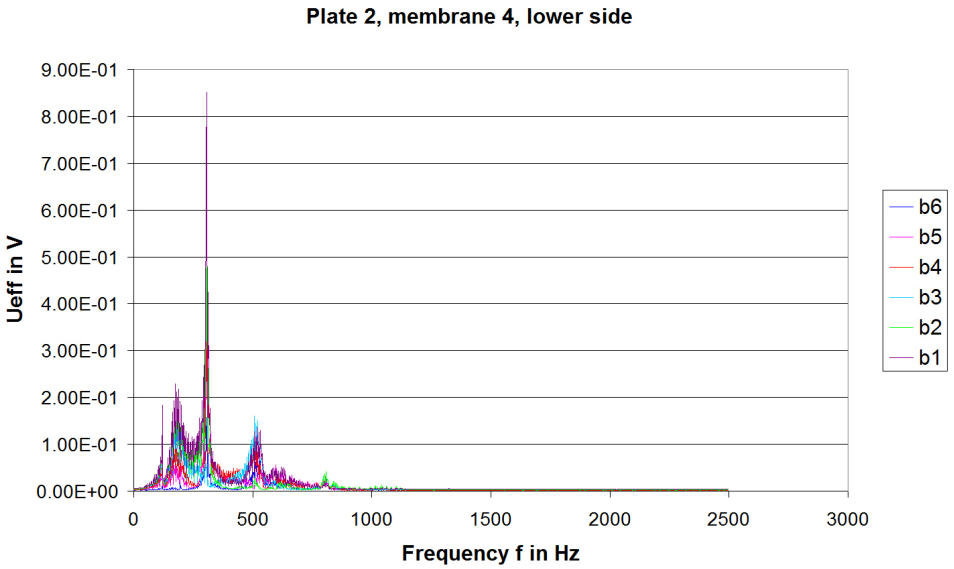


Figure 5.77 All data points (1024) from the upper side of membrane m4 of plate 2; the FFT of the laser vibrometer signal U_{eff} against the frequency; a chirp signal was applied.

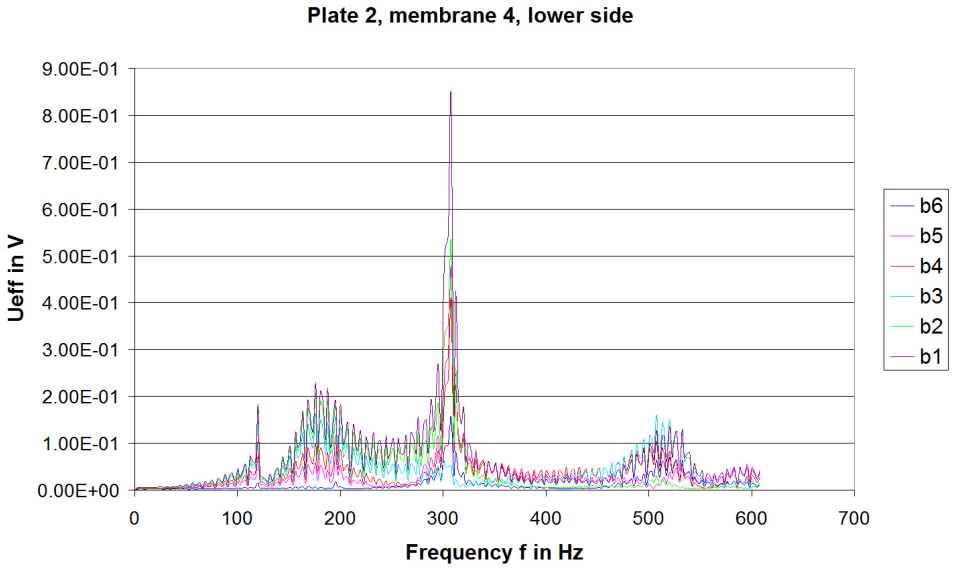


Figure 5.78 First 250 data points from the lower side of membrane m4 of plate 2; the FFT of the laser vibrometer signal U_{eff} against the frequency; a chirp signal was applied.

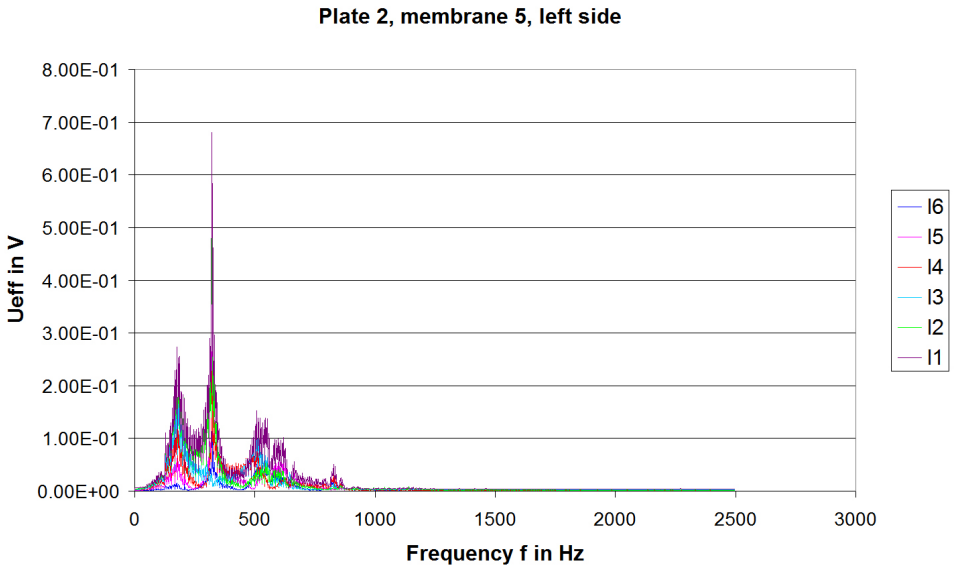


Figure 5.79 All data points (1024) from the left side of membrane m5 of plate 2; the FFT of the laser vibrometer signal U_{eff} against the frequency; a chirp signal was applied.

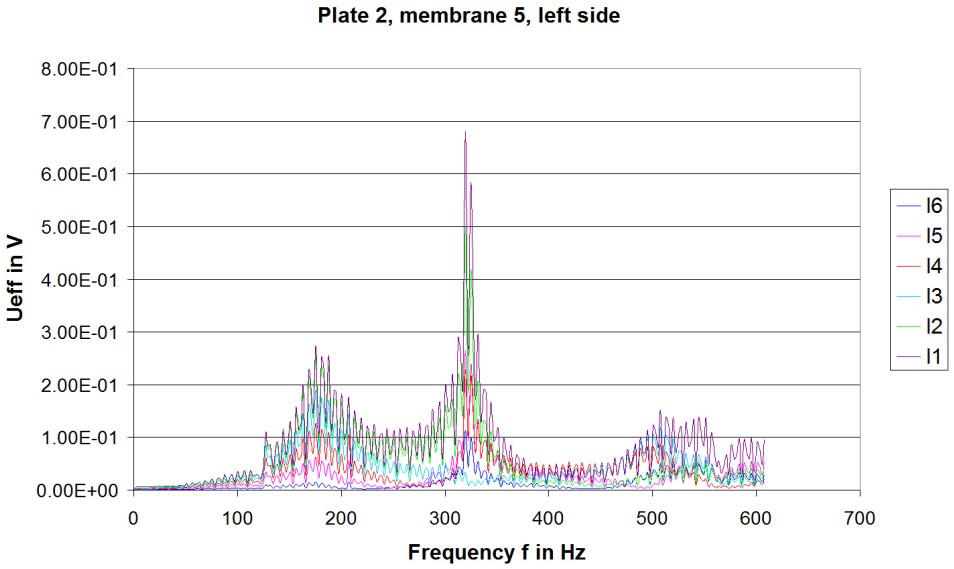


Figure 5.80 First 250 data points from the left side of membrane m5 of plate 2; the FFT of the laser vibrometer signal U_{eff} against the frequency; a chirp signal was applied.

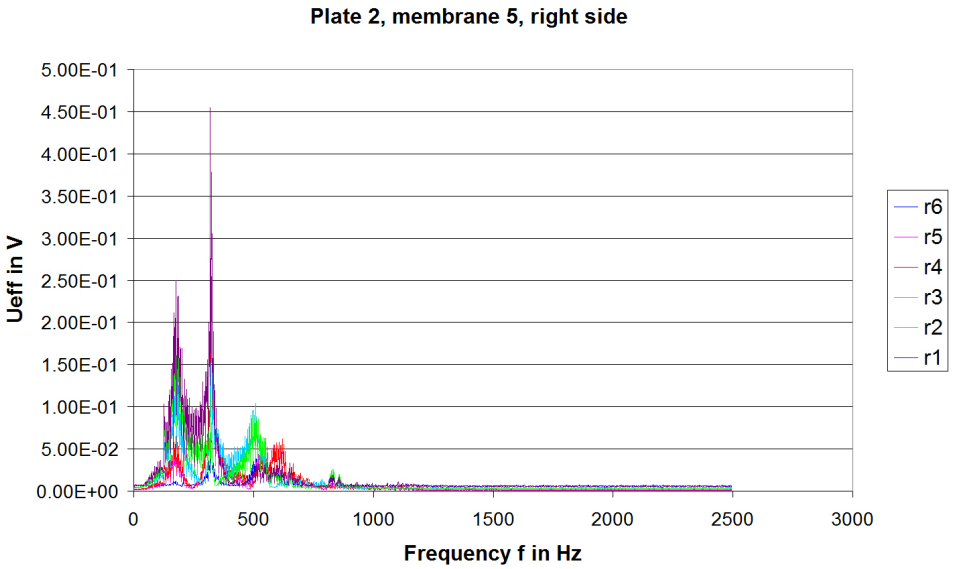


Figure 5.81 All data points (1024) from the right side of membrane m5 of plate 2; the FFT of the laser vibrometer signal U_{eff} against the frequency; a chirp signal was applied.

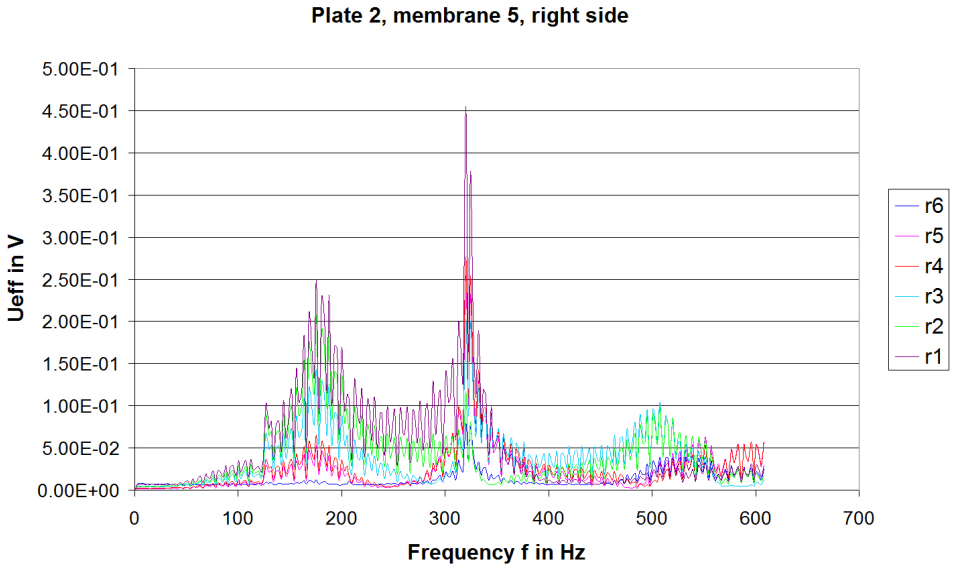


Figure 5.82 First 250 data points from the right side of membrane m5 of plate 2; the FFT of the laser vibrometer signal U_{eff} against the frequency; a chirp signal was applied.

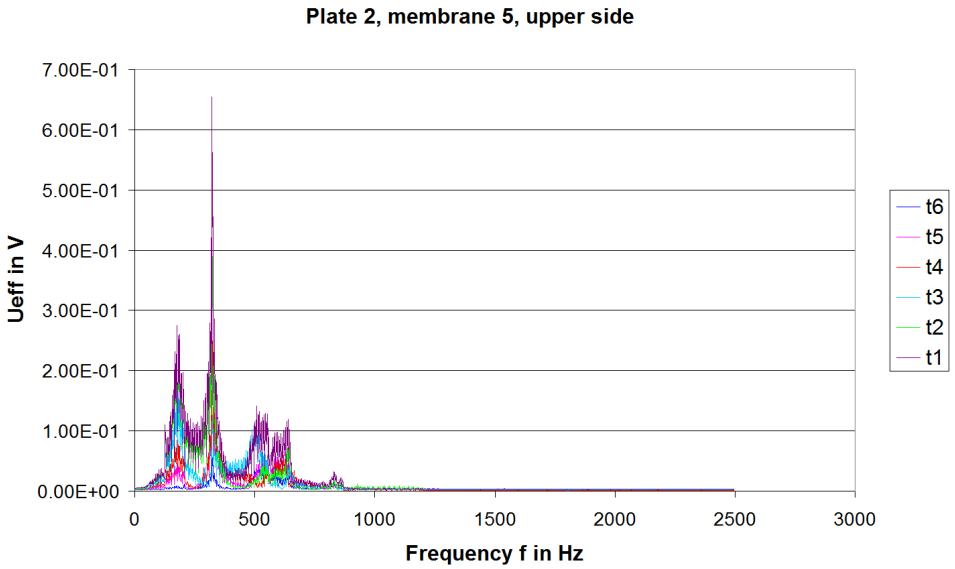


Figure 5.83 All data points (1024) from the upper side of membrane m5 of plate 2; the FFT of the laser vibrometer signal U_{eff} against the frequency; a chirp signal was applied.

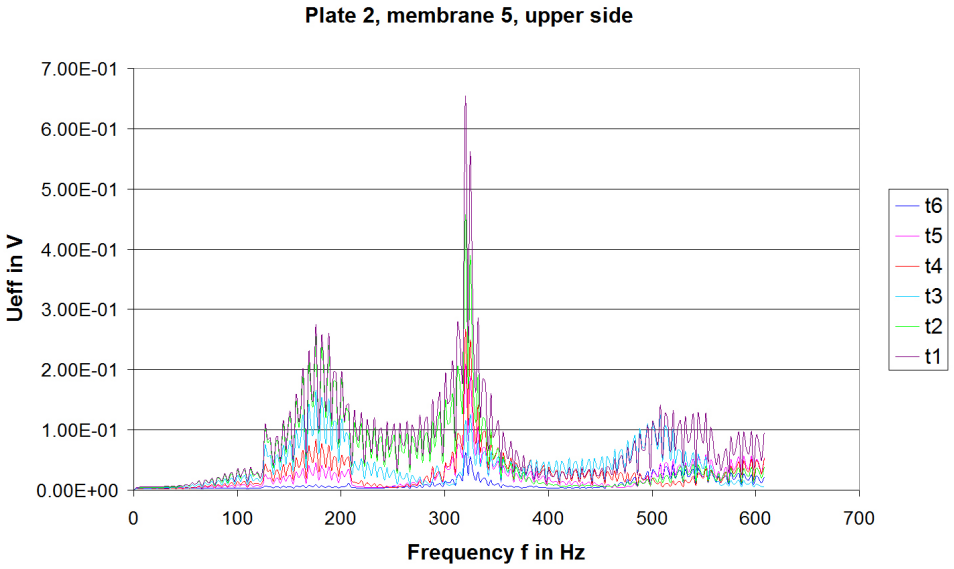


Figure 5.84 First 250 data points from the upper side of membrane m5 of plate 2; the FFT of the laser vibrometer signal U_{eff} against the frequency; a chirp signal was applied.

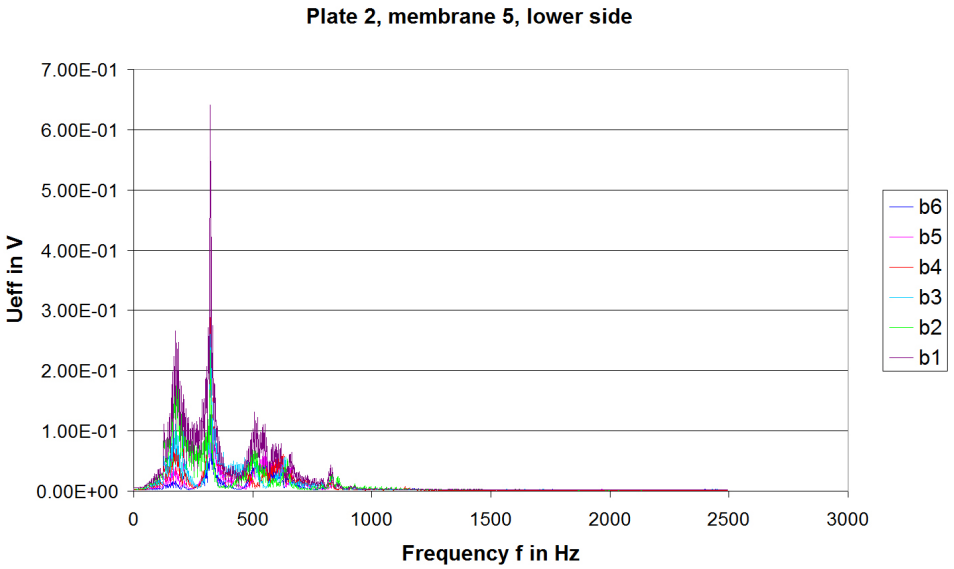


Figure 5.85 All data points (1024) from the lower side of membrane m5 of plate 2; the FFT of the laser vibrometer signal U_{eff} against the frequency; a chirp signal was applied.

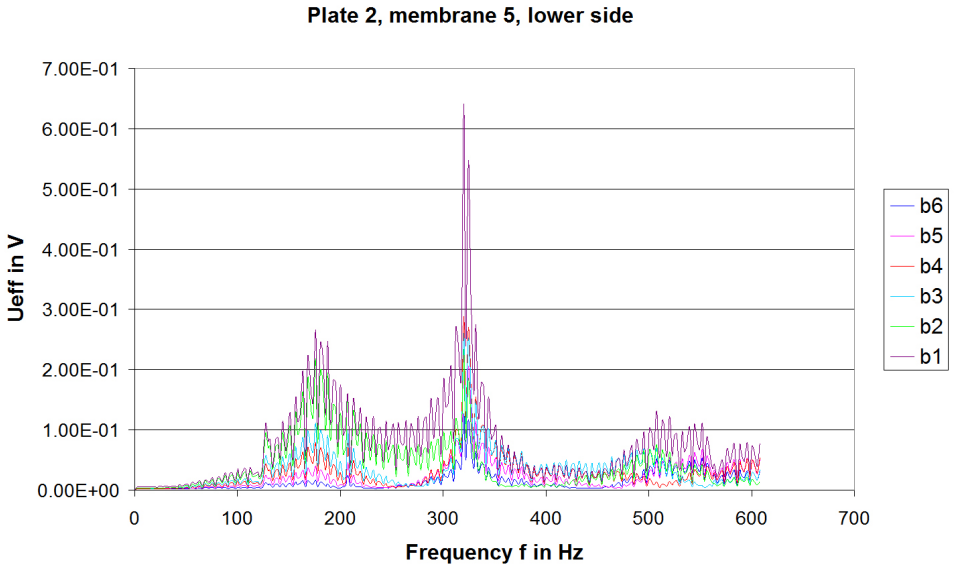


Figure 5.86 First 250 data points from the lower side of membrane m5 of plate 2; the FFT of the laser vibrometer signal U_{eff} against the frequency; a chirp signal was applied.

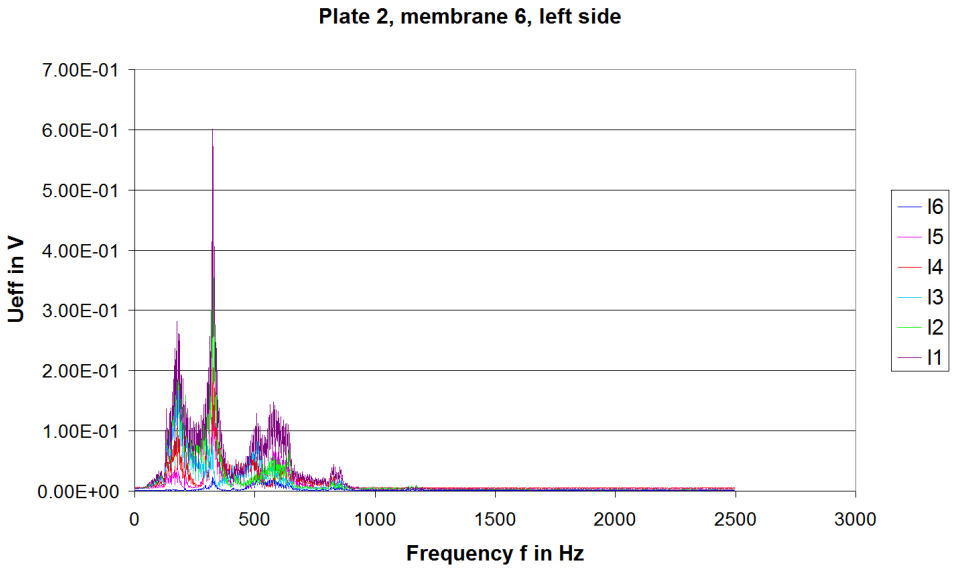


Figure 5.87 All data points (1024) from the left side of membrane m6 of plate 2; the FFT of the laser vibrometer signal U_{eff} against the frequency; a chirp signal was applied.

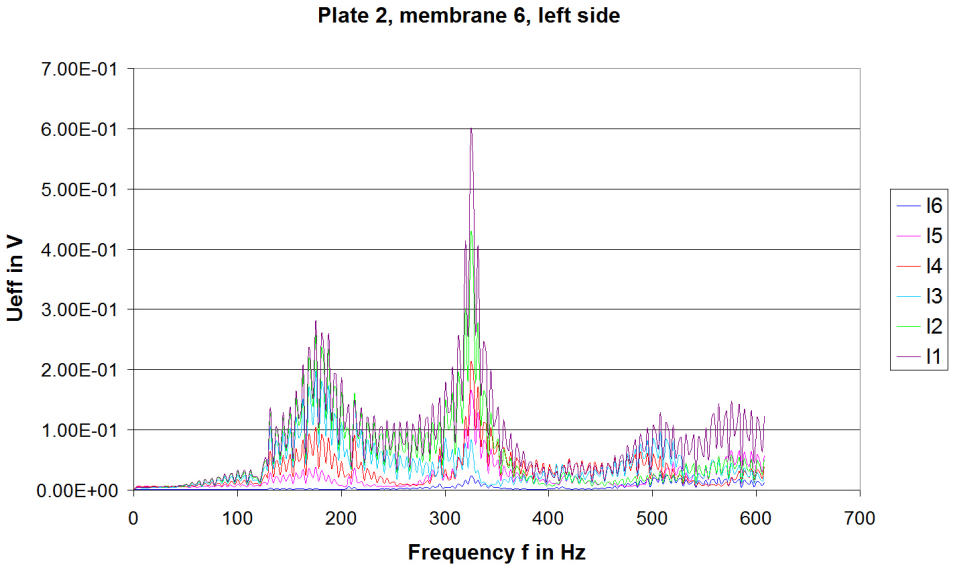


Figure 5.88 First 250 data points from the left side of membrane m6 of plate 2; the FFT of the laser vibrometer signal U_{eff} against the frequency; a chirp signal was applied.

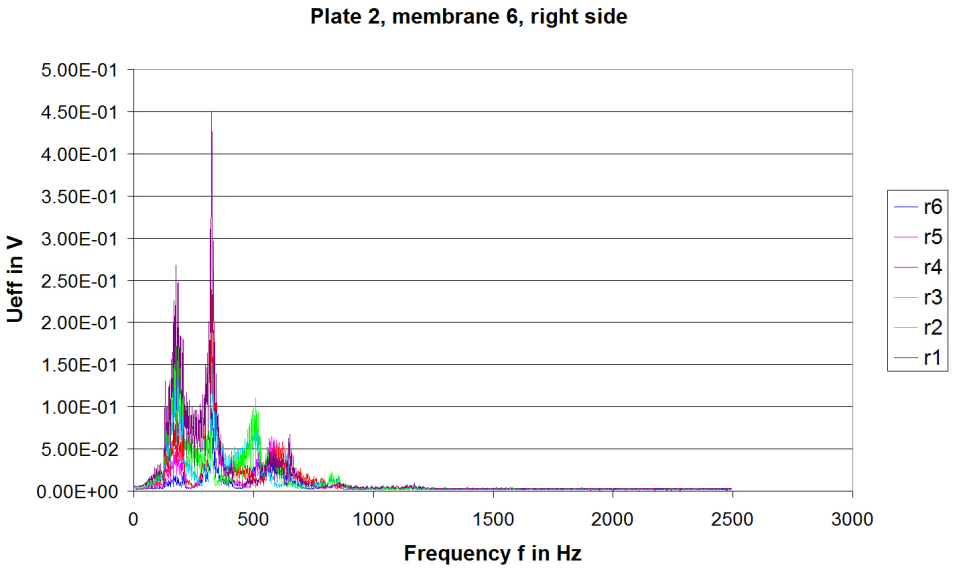


Figure 5.89 All data points (1024) from the right side of membrane m6 of plate 2; the FFT of the laser vibrometer signal U_{eff} against the frequency; a chirp signal was applied.

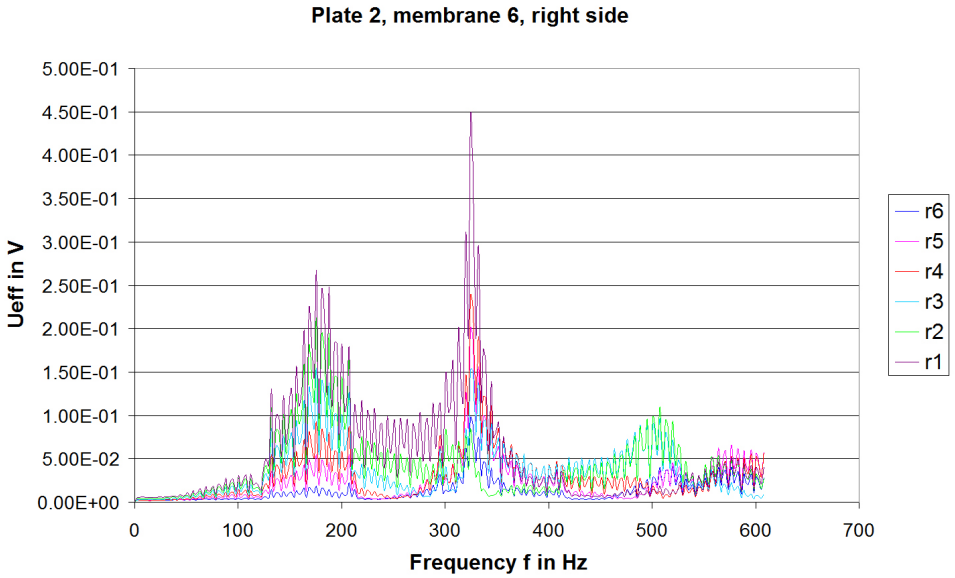


Figure 5.90 First 250 data points from the right side of membrane m6 of plate 2; the FFT of the laser vibrometer signal U_{eff} against the frequency; a chirp signal was applied.

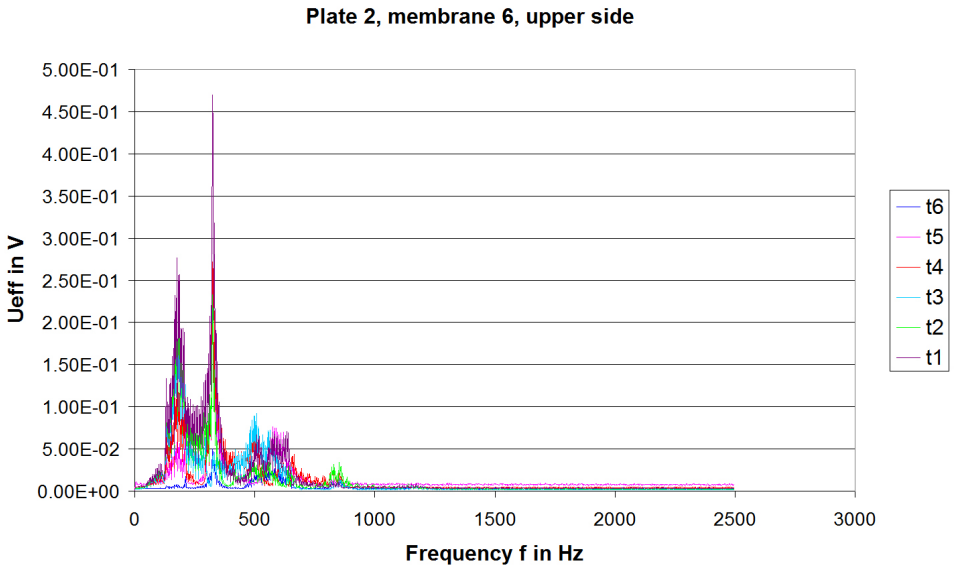


Figure 5.91 All data points (1024) from the upper side of membrane m6 of plate 2; the FFT of the laser vibrometer signal U_{eff} against the frequency; a chirp signal was applied.

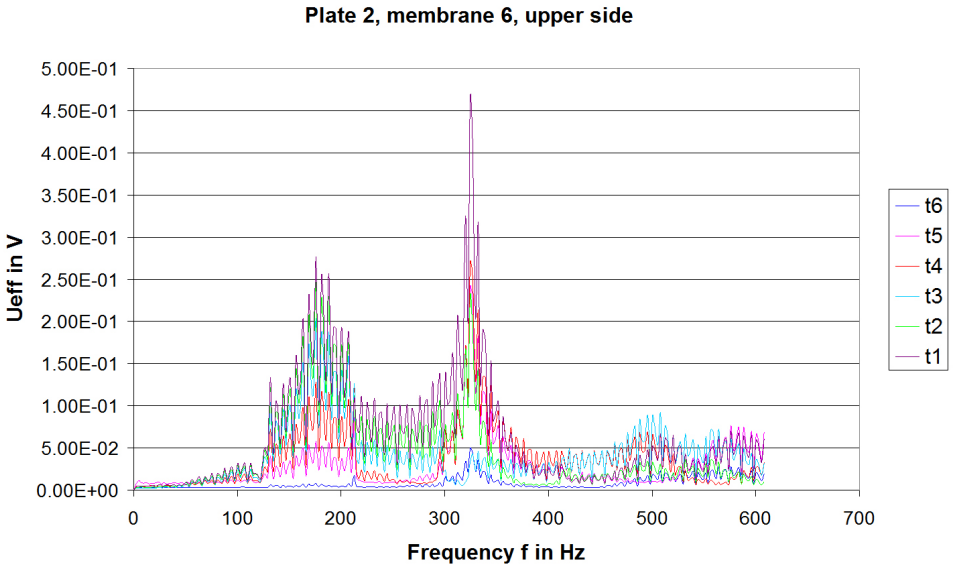


Figure 5.92 First 250 data points from the upper side of membrane m6 of plate 2; the FFT of the laser vibrometer signal U_{eff} against the frequency; a chirp signal was applied.

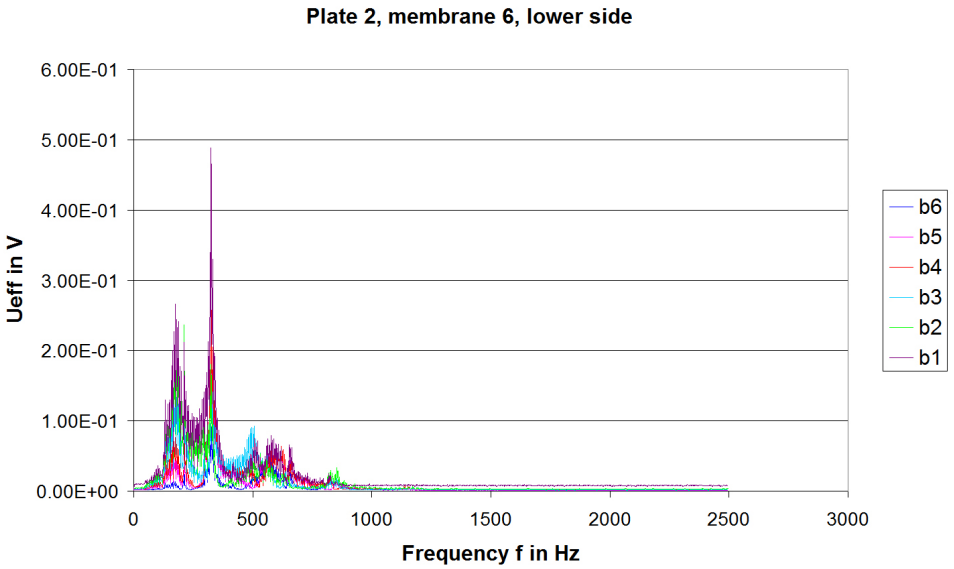


Figure 5.93 All data points (1024) from the lower side of membrane m6 of plate 2; the FFT of the laser vibrometer signal U_{eff} against the frequency; a chirp signal was applied.

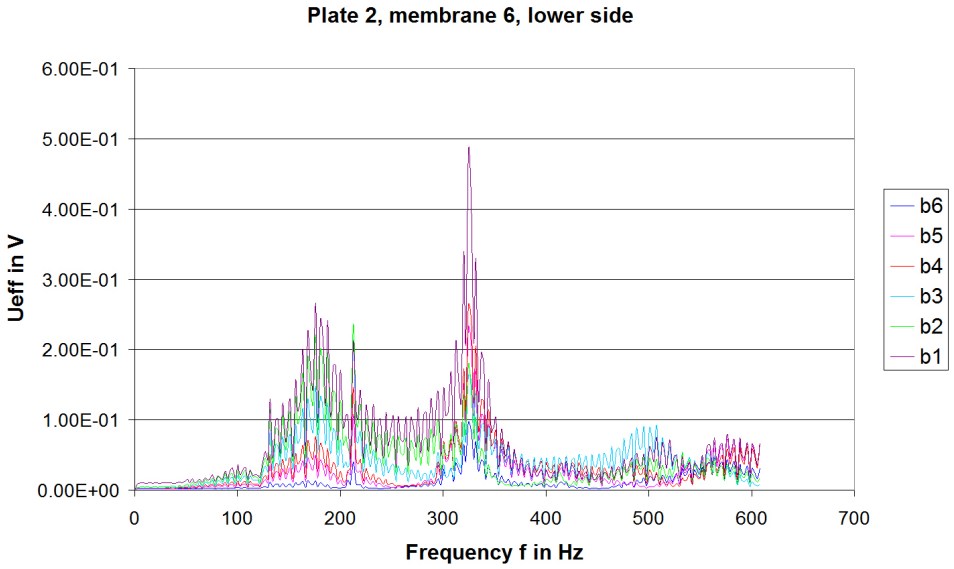


Figure 5.94 First 250 data points from the lower side of membrane m6 of plate 2; the FFT of the laser vibrometer signal U_{eff} against the frequency; a chirp signal was applied.

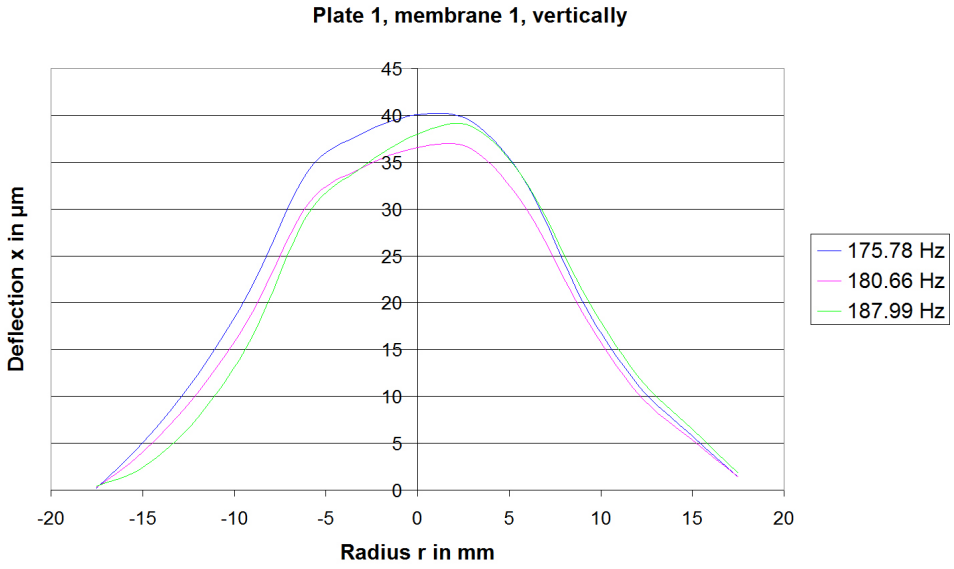


Figure 5.95 Vertical measurement points of membrane m1 of plate 1; the deflection x against the radius r around 180 Hz

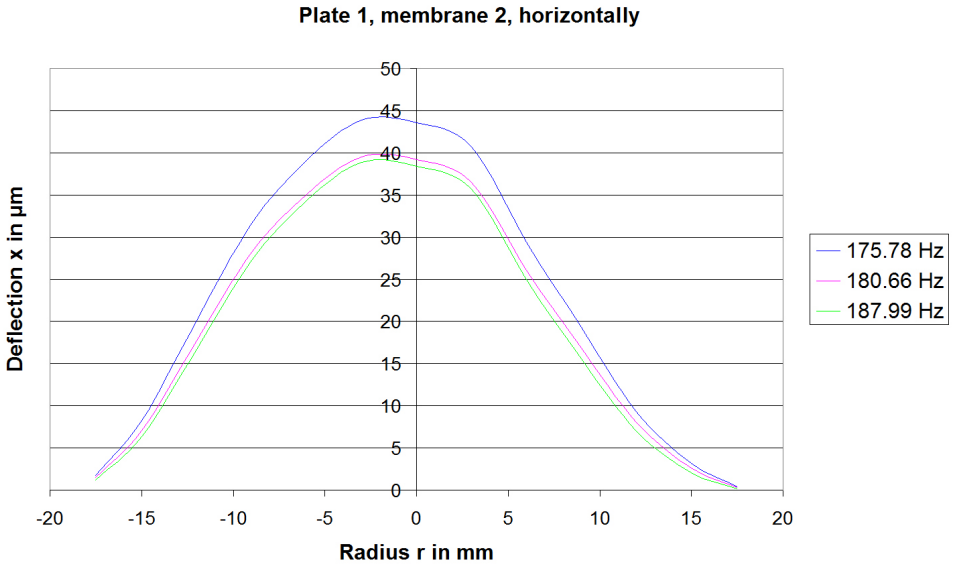


Figure 5.96 Horizontal measurement points of membrane m2 of plate 1; the deflection x against the radius r around 180 Hz

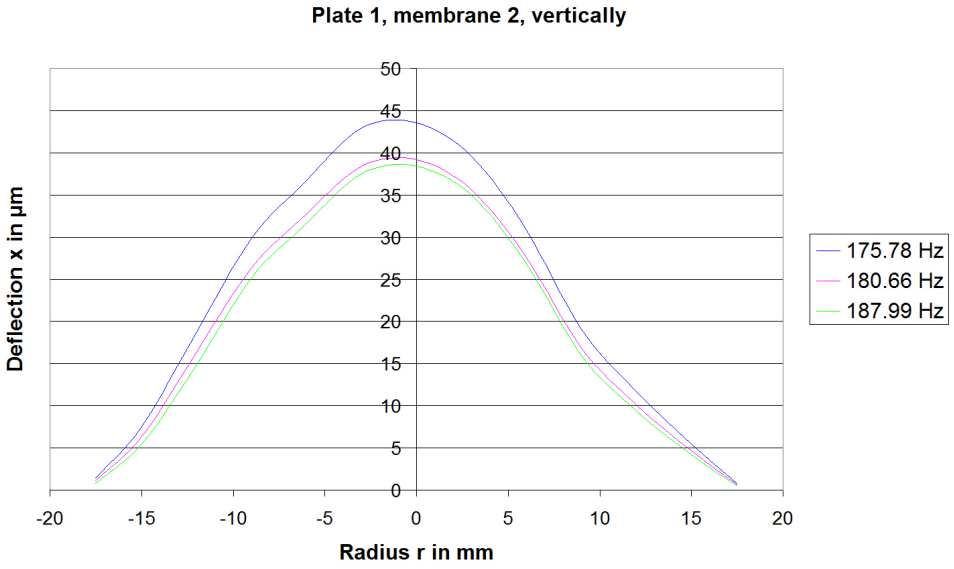


Figure 5.97 Vertical measurement points of membrane m2 of plate 1; the deflection x against the radius r around 180 Hz

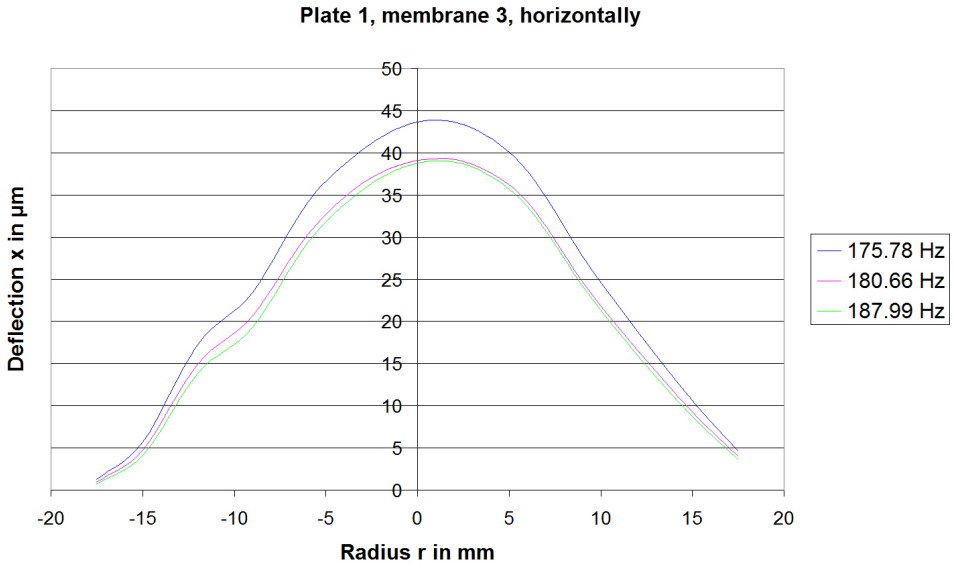


Figure 5.98 Horizontal measurement points of membrane m3 of plate 1; the deflection x against the radius r around 180 Hz

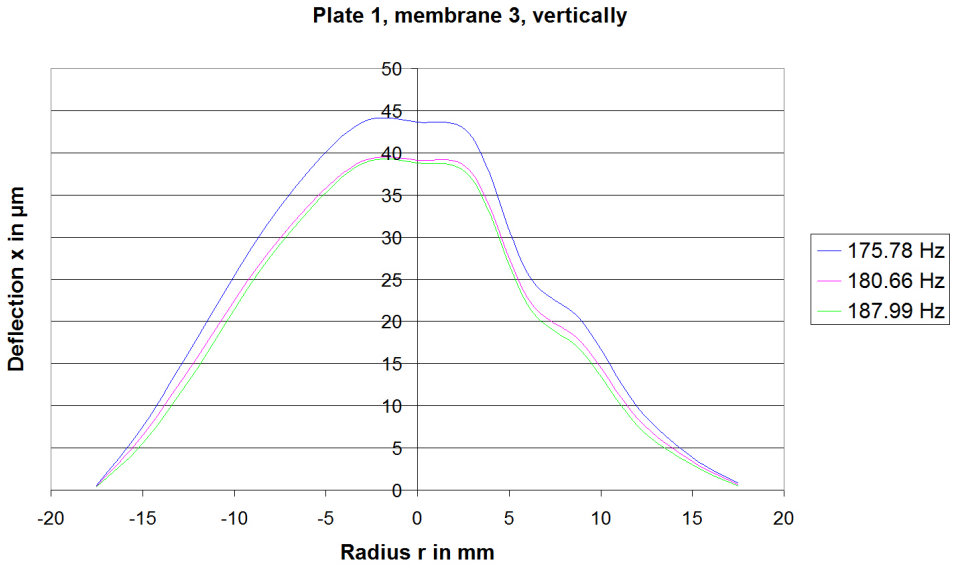


Figure 5.99 Vertical measurement points of membrane m3 of plate 1; the deflection x against the radius r around 180 Hz

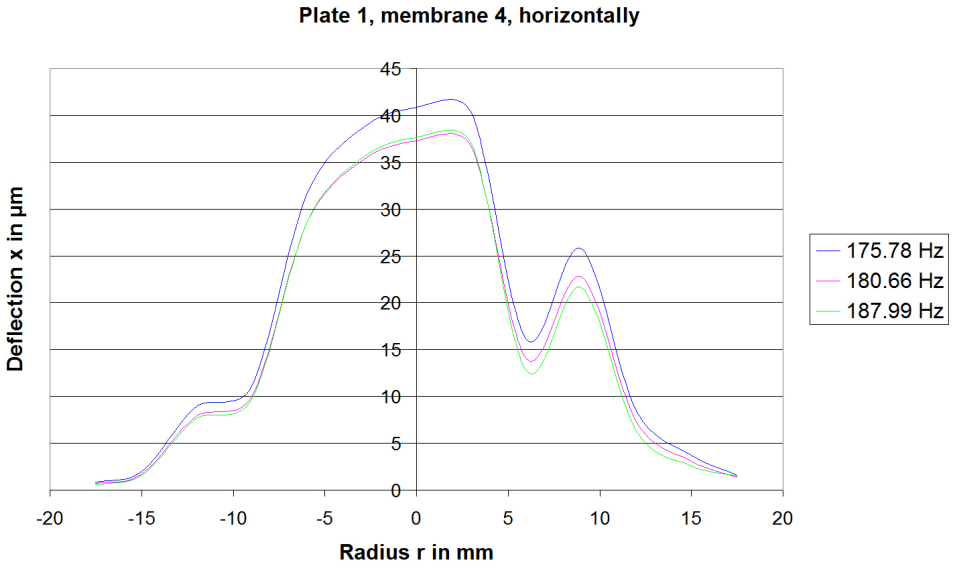


Figure 5.100 Horizontal measurement points of membrane m4 of plate 1; the deflection x against the radius r around 180 Hz

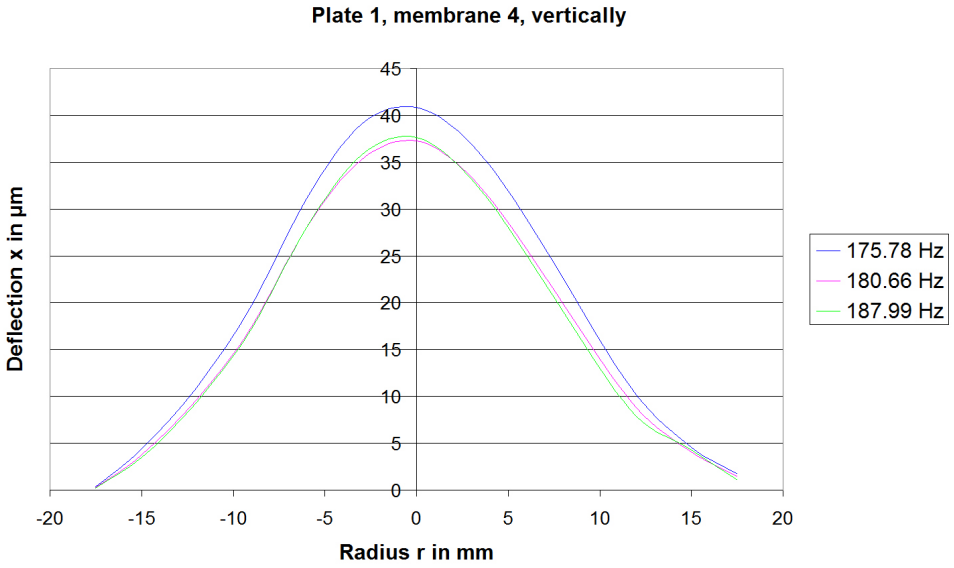


Figure 5.101 Vertical measurement points of membrane m4 of plate 1; the deflection x against the radius r around 180 Hz

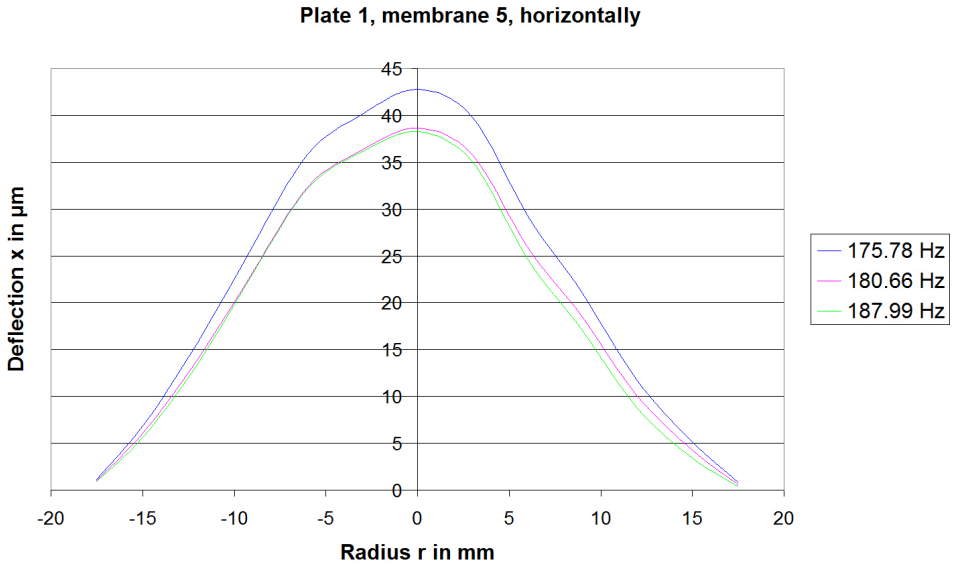


Figure 5.102 Horizontal measurement points of membrane m5 of plate 1; the deflection x against the radius r around 180 Hz

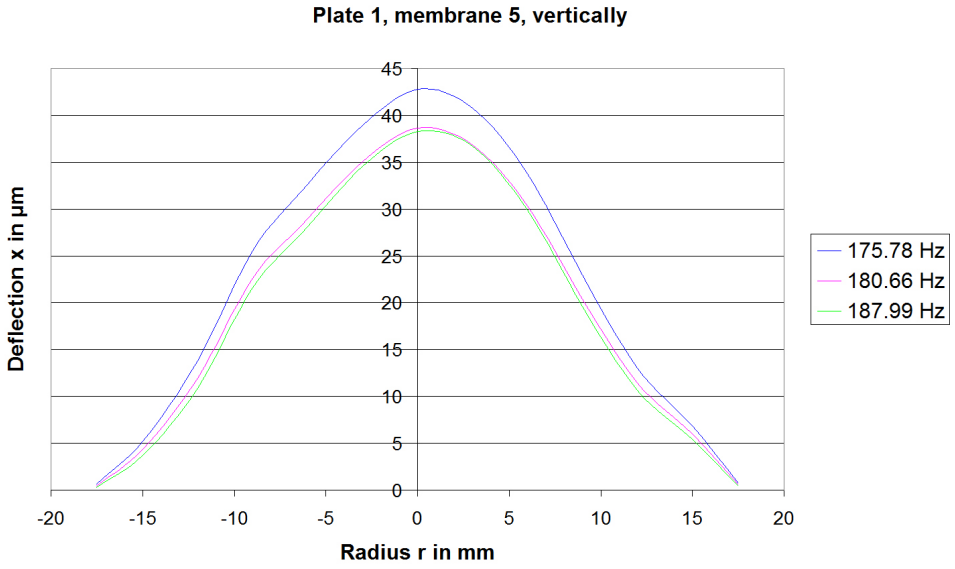


Figure 5.103 Vertical measurement points of membrane m5 of plate 1; the deflection x against the radius r around 180 Hz

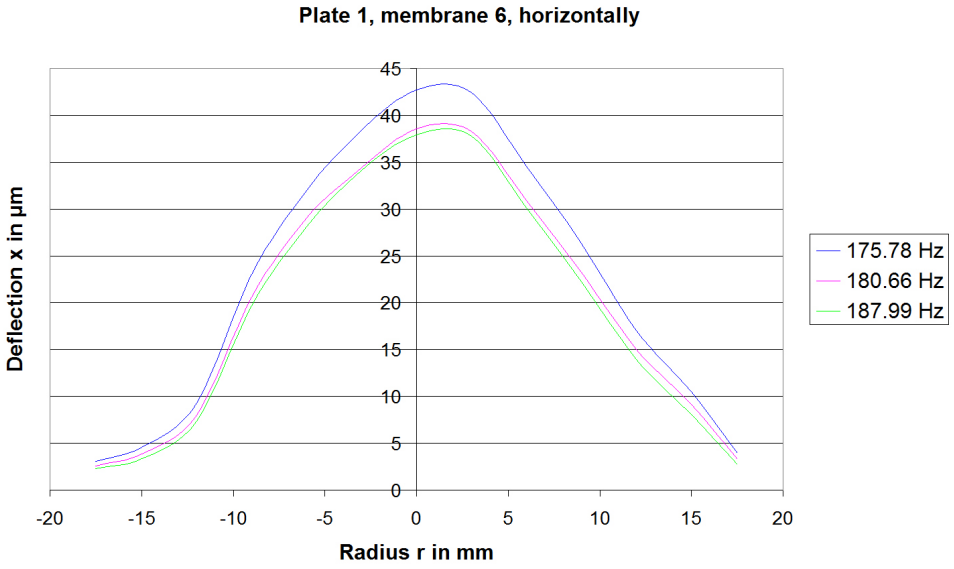


Figure 5.104 Horizontal measurement points of membrane m6 of plate 1; the deflection x against the radius r around 180 Hz

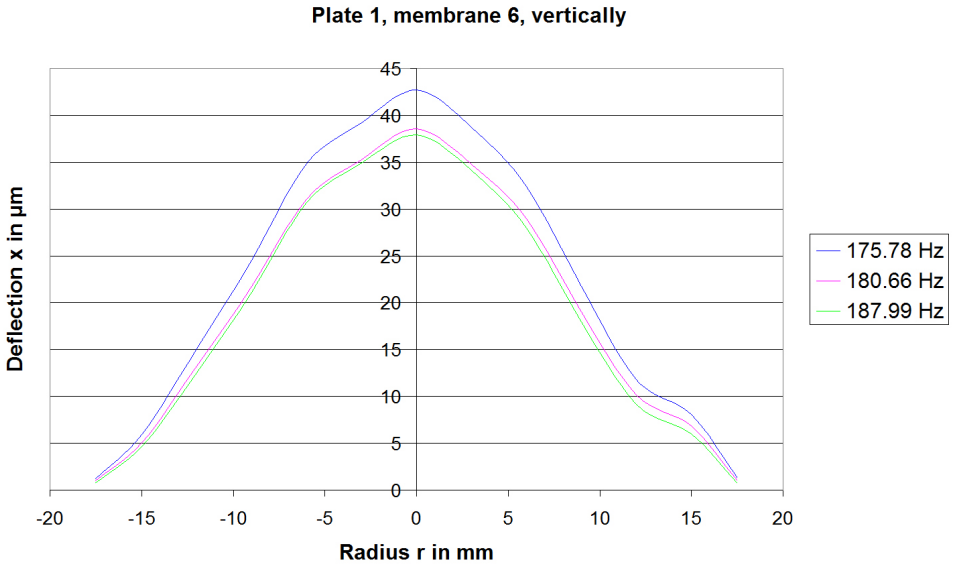


Figure 5.105 Vertical measurement points of membrane m6 of plate 1; the deflection x against the radius r around 180 Hz

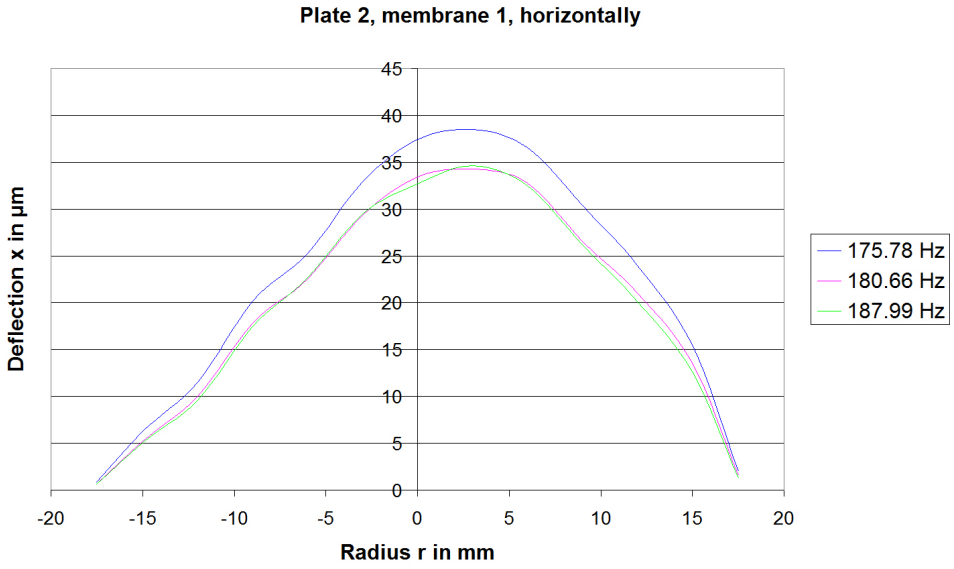


Figure 5.106 Horizontal measurement points of membrane m1 of plate 2; the deflection x against the radius r around 180 Hz

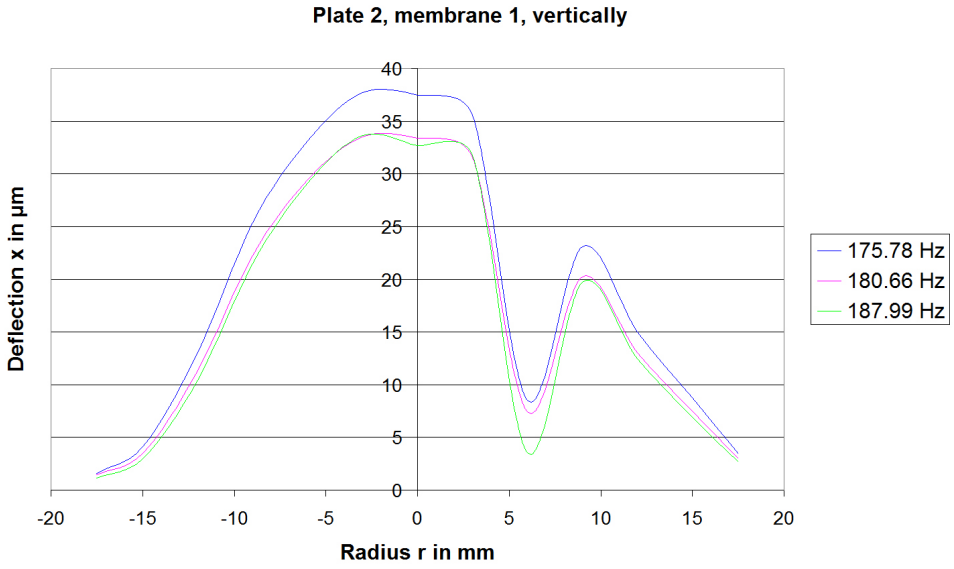


Figure 5.107 Vertical measurement points of membrane m1 of plate 2; the deflection x against the radius r around 180 Hz

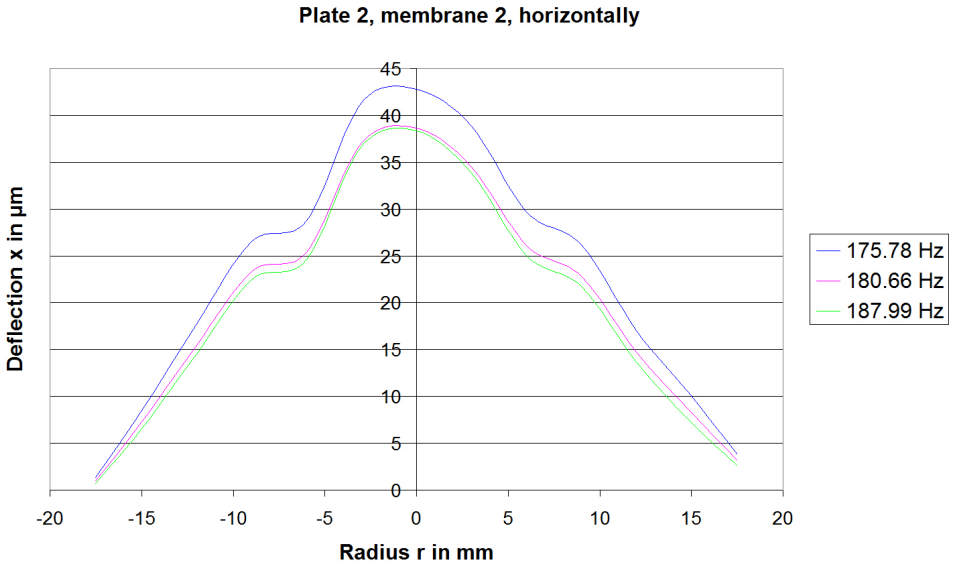


Figure 5.108 Horizontal measurement points of membrane m2 of plate 2; the deflection x against the radius r around 180 Hz

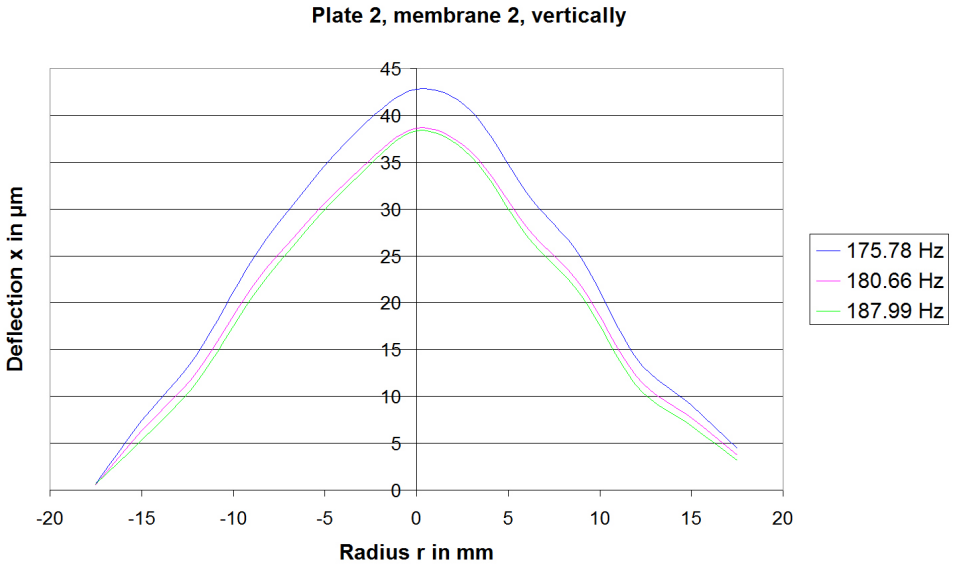


Figure 5.109 Vertical measurement points of membrane m2 of plate 2; the deflection x against the radius r around 180 Hz

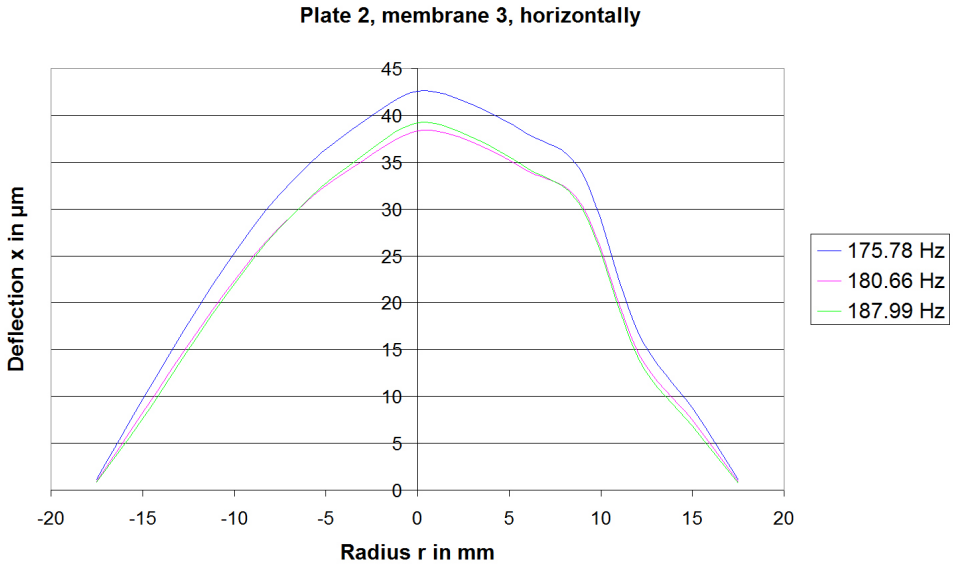


Figure 5.110 Horizontal measurement points of membrane m3 of plate 2; the deflection x against the radius r around 180 Hz

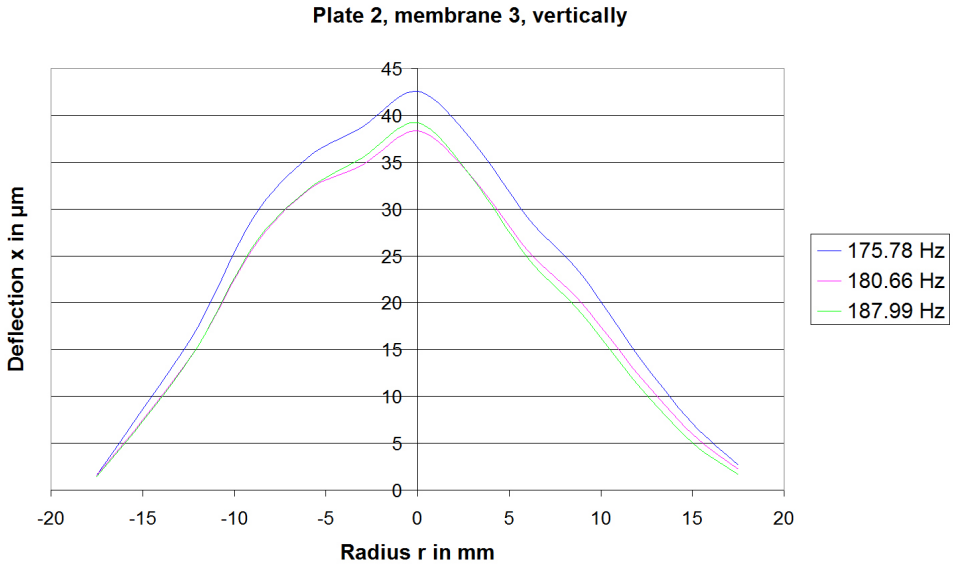


Figure 5.111 Vertical measurement points of membrane m3 of plate 2; the deflection x against the radius r around 180 Hz

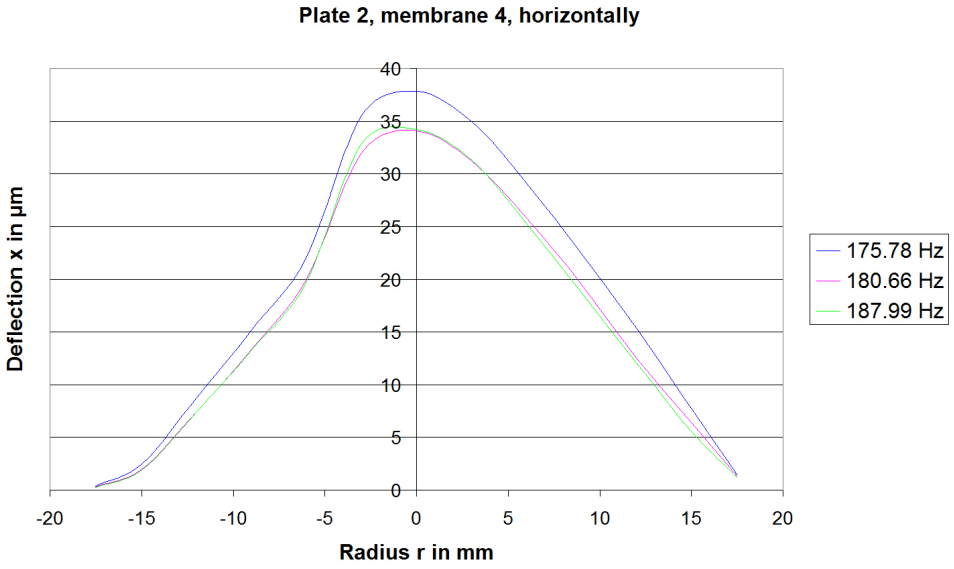


Figure 5.112 Horizontal measurement points of membrane m4 of plate 2; the deflection x against the radius r around 180 Hz

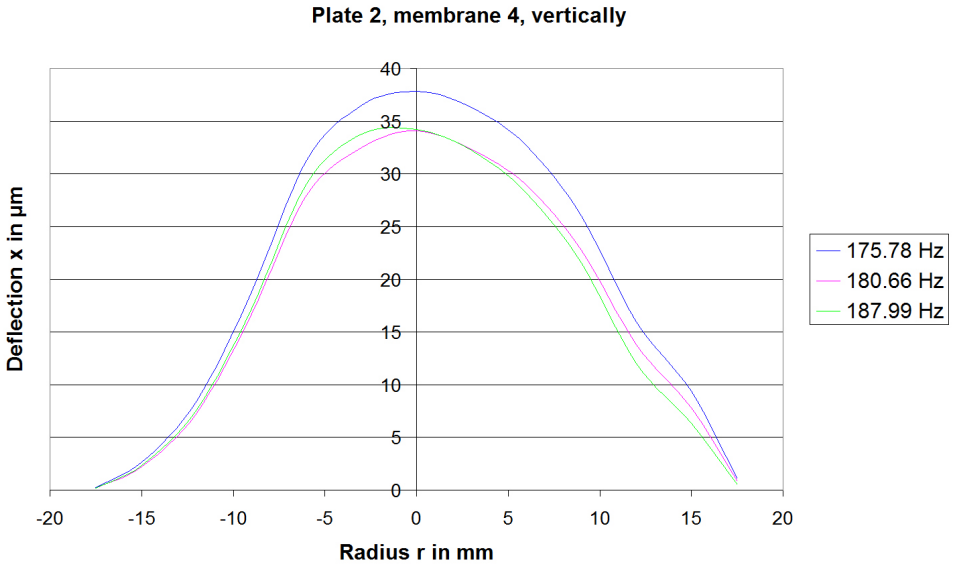


Figure 5.113 Vertical measurement points of membrane m4 of plate 2; the deflection x against the radius r around 180 Hz

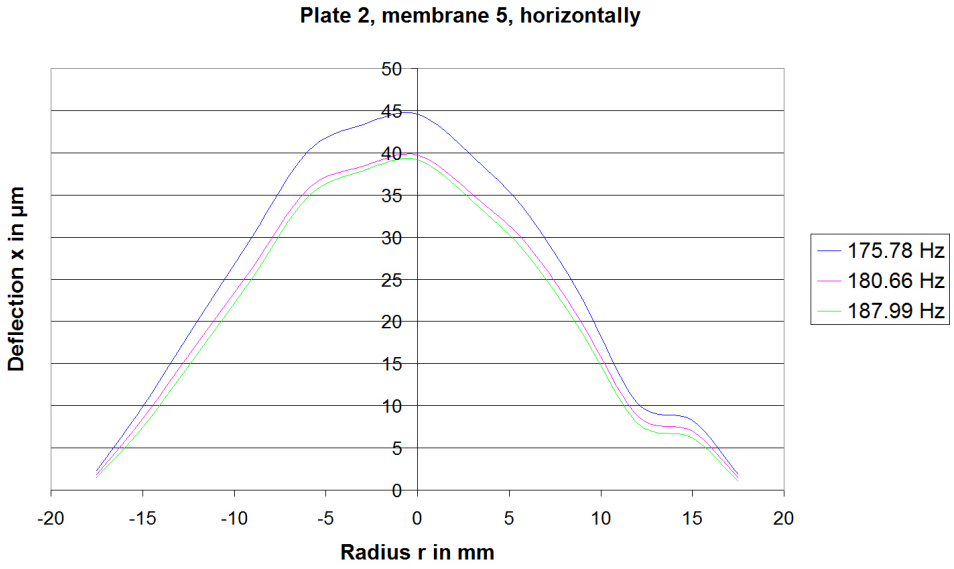


Figure 5.114 Horizontal measurement points of membrane m5 of plate 2; the deflection x against the radius r around 180 Hz

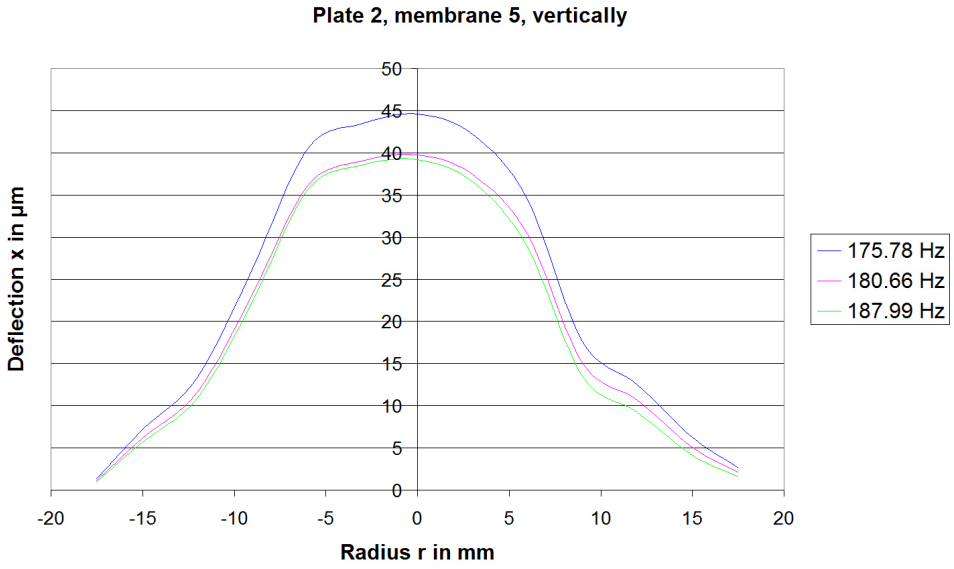


Figure 5.115 Vertical measurement points of membrane m5 of plate 2; the deflection x against the radius r around 180 Hz

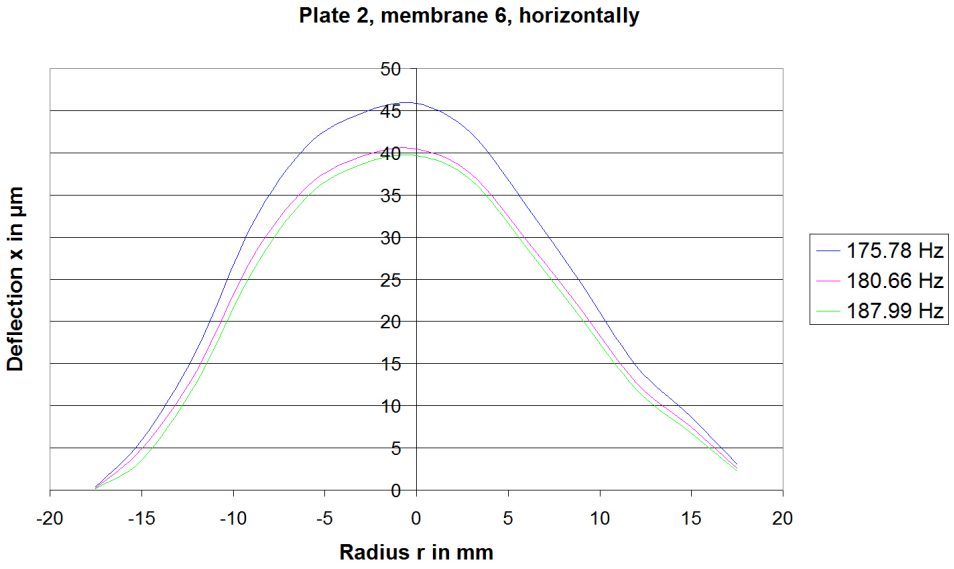


Figure 5.116 Horizontal measurement points of membrane m6 of plate 2; the deflection x against the radius r around 180 Hz

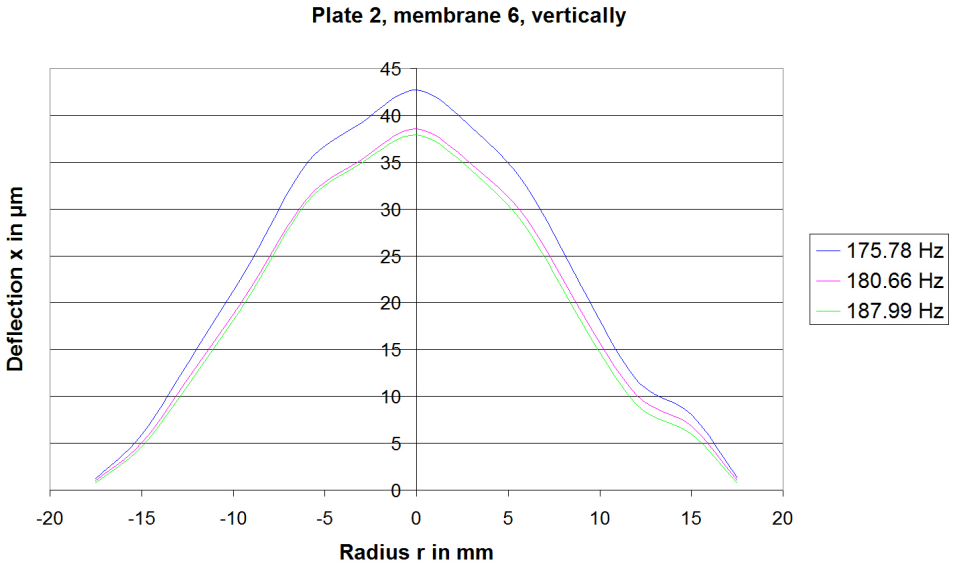


Figure 5.117 Vertical measurement points of membrane m6 of plate 2; the deflection x against the radius r around 180 Hz

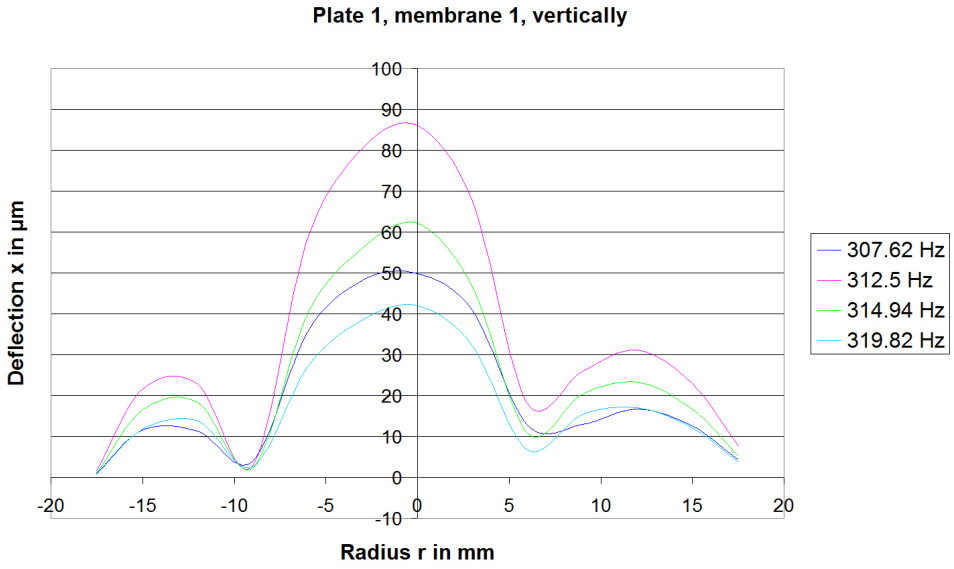


Figure 5.118 Vertical measurement points of membrane m1 of plate 1; the deflection x against the radius r around 310 Hz

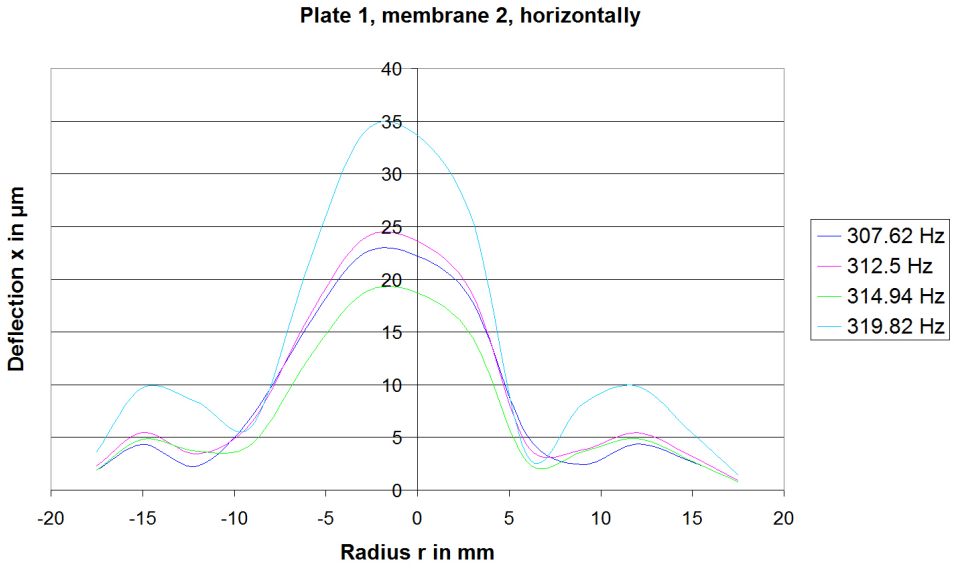


Figure 5.119 Horizontal measurement points of membrane m1 of plate 2; the deflection x against the radius r around 310 Hz

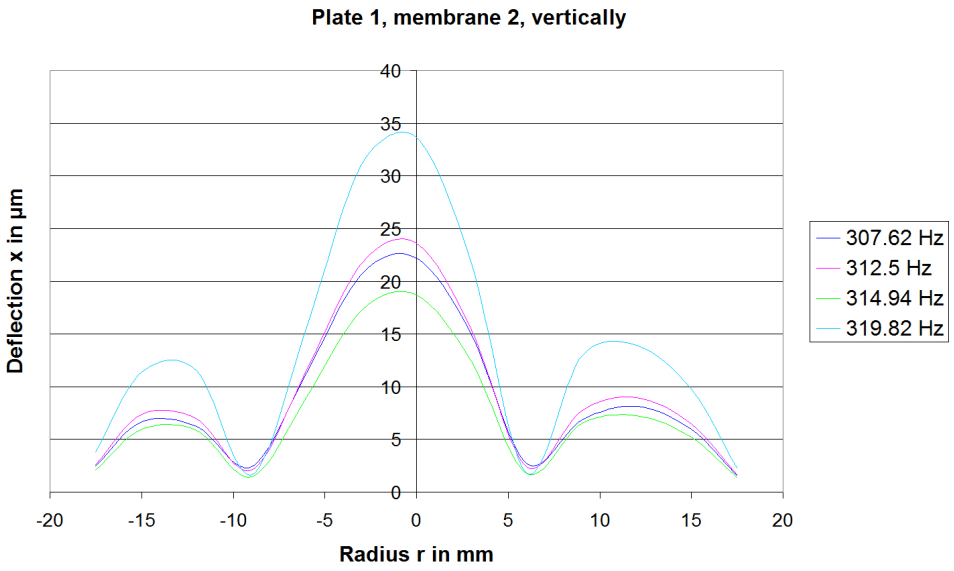


Figure 5.120 Vertical measurement points of membrane m2 of plate 1; the deflection x against the radius r around 310 Hz

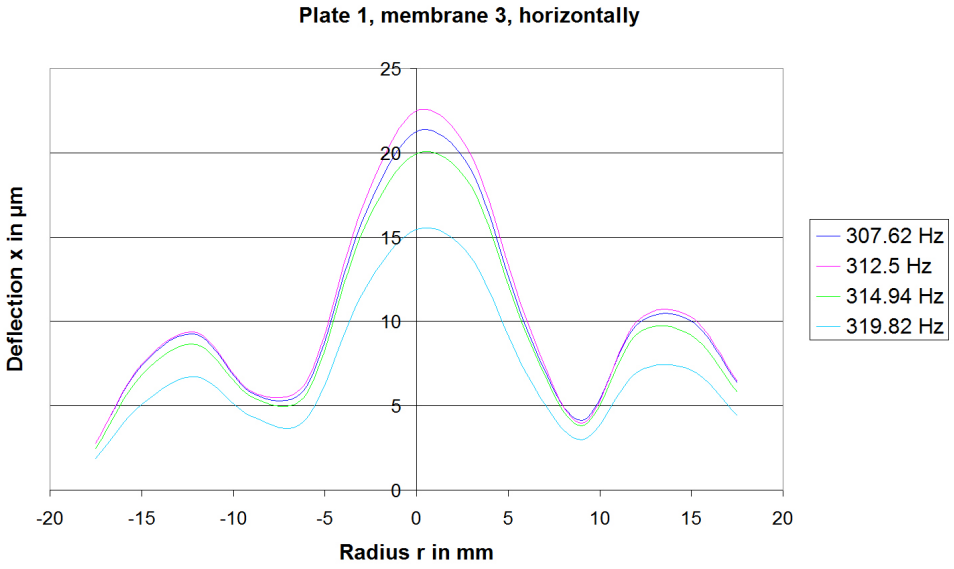


Figure 5.121 Horizontal measurement points of membrane m3 of plate 1; the deflection x against the radius r around 310 Hz

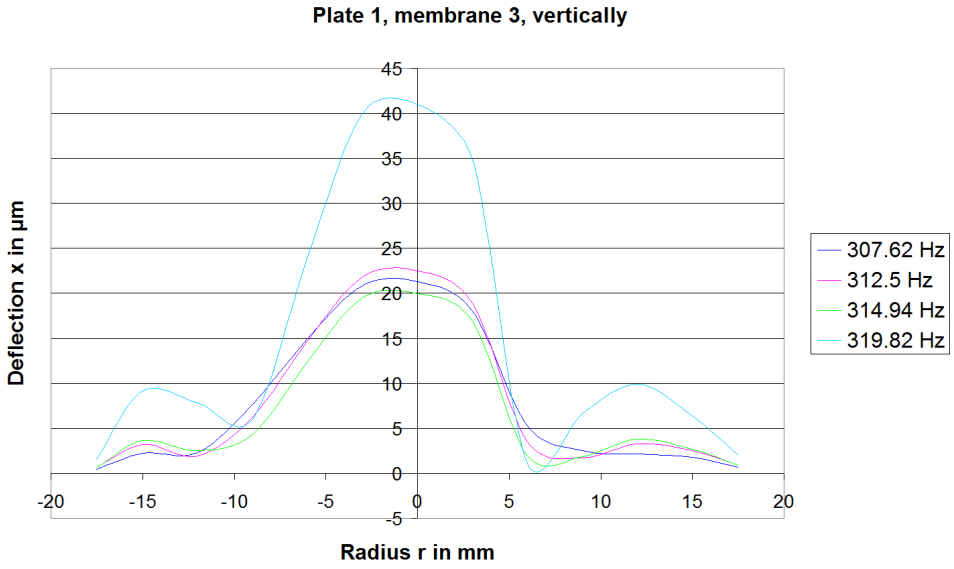


Figure 5.122 Vertical measurement points of membrane m3 of plate 1; the deflection x against the radius r around 310 Hz

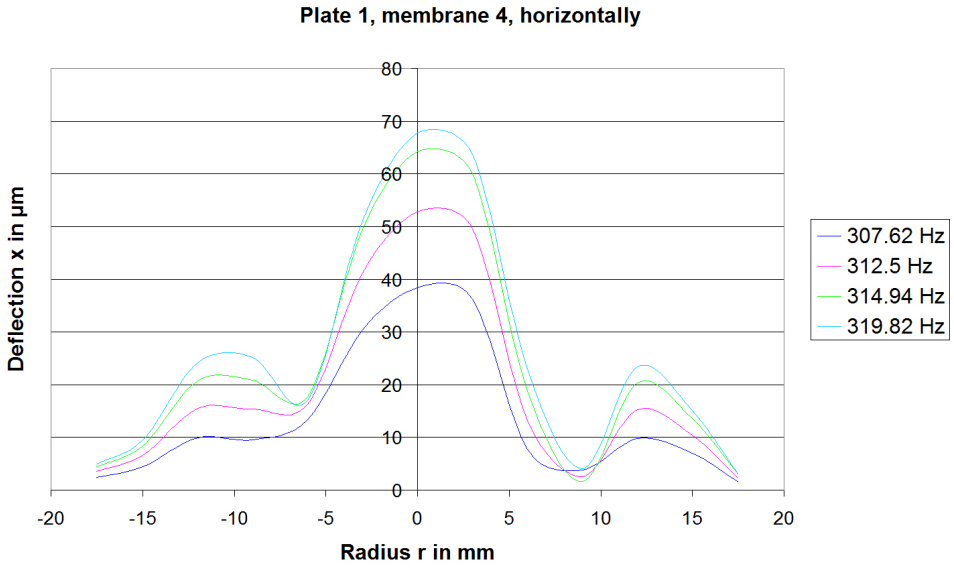


Figure 5.123 Horizontal measurement points of membrane m4 of plate 1; the deflection x against the radius r around 310 Hz

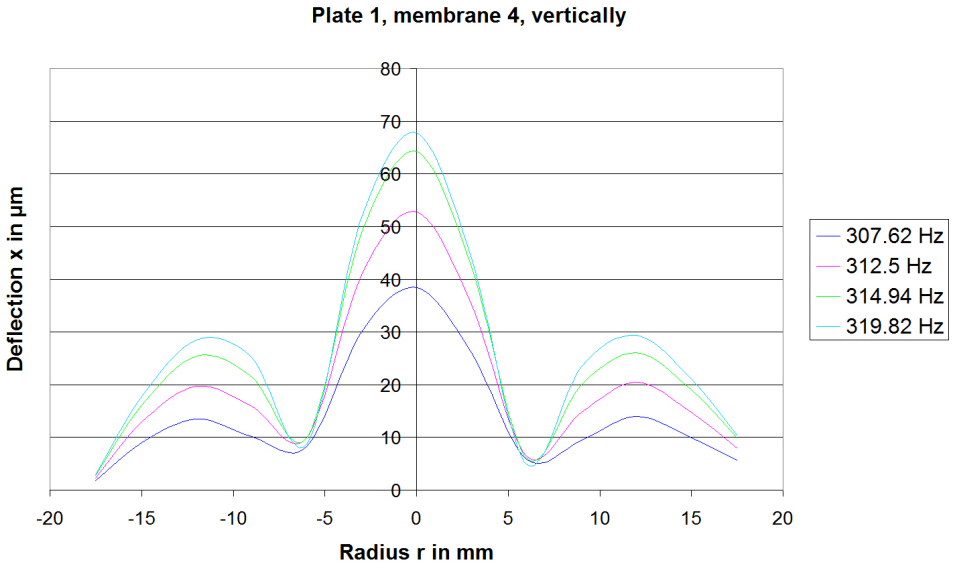


Figure 5.124 Vertical measurement points of membrane m4 of plate 1; the deflection x against the radius r around 310 Hz

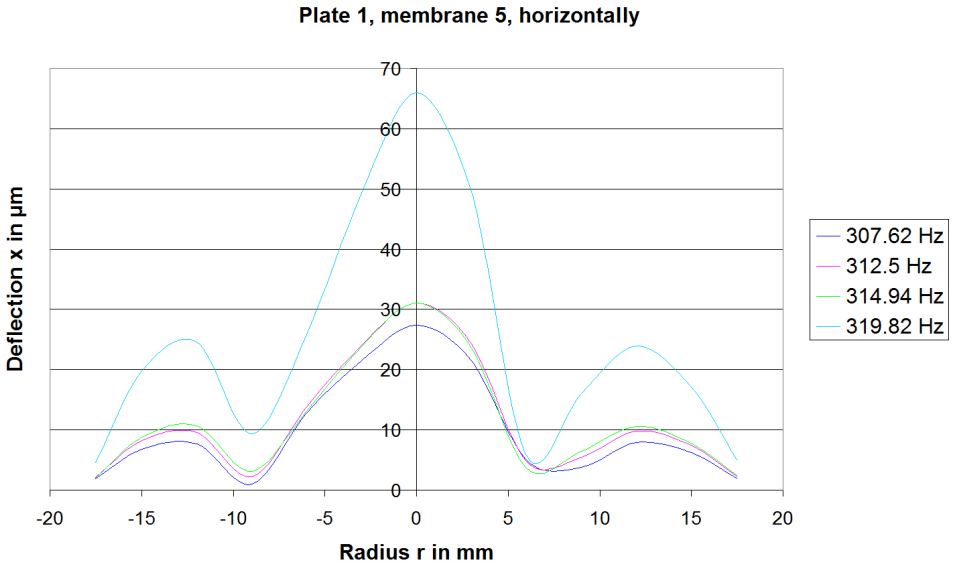


Figure 5.125 Horizontal measurement points of membrane m5 of plate 1; the deflection x against the radius r around 310 Hz

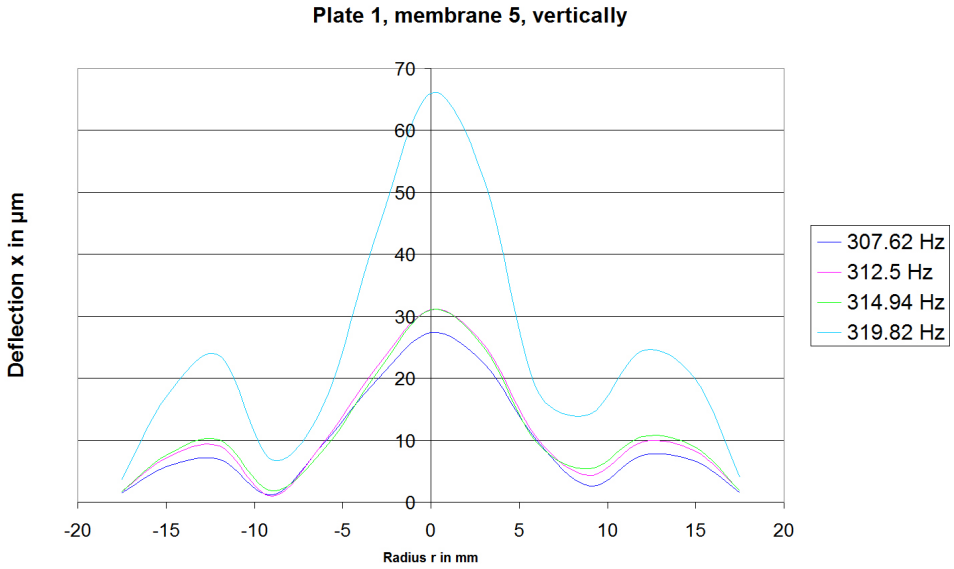


Figure 5.126 Vertical measurement points of membrane m5 of plate 1; the deflection x against the radius r around 310 Hz

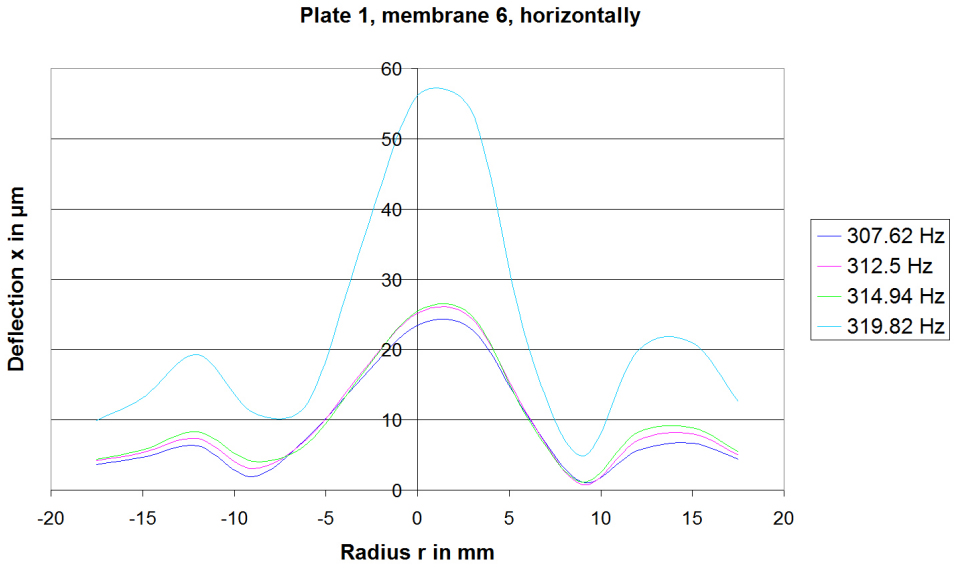


Figure 5.127 Horizontal measurement points of membrane m6 of plate 1; the deflection x against the radius r around 310 Hz

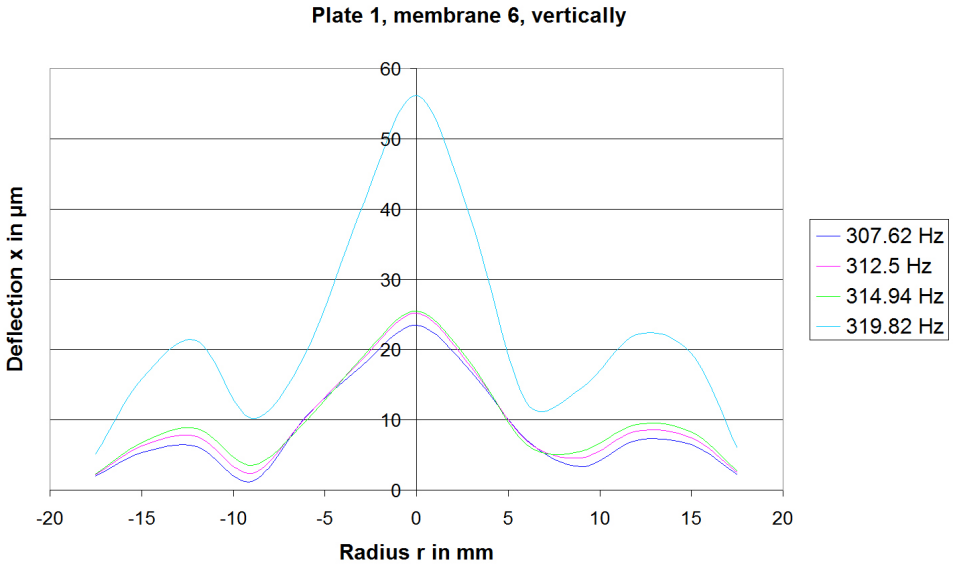


Figure 5.128 Vertical measurement points of membrane m6 of plate 1; the deflection x against the radius r around 310 Hz

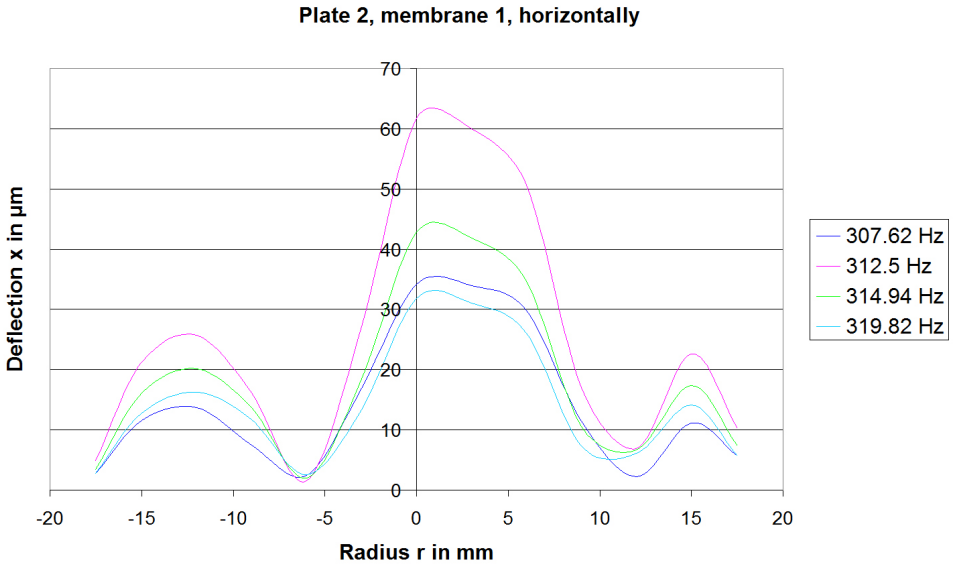


Figure 5.129 Horizontal measurement points of membrane m1 of plate 2; the deflection x against the radius r around 310 Hz

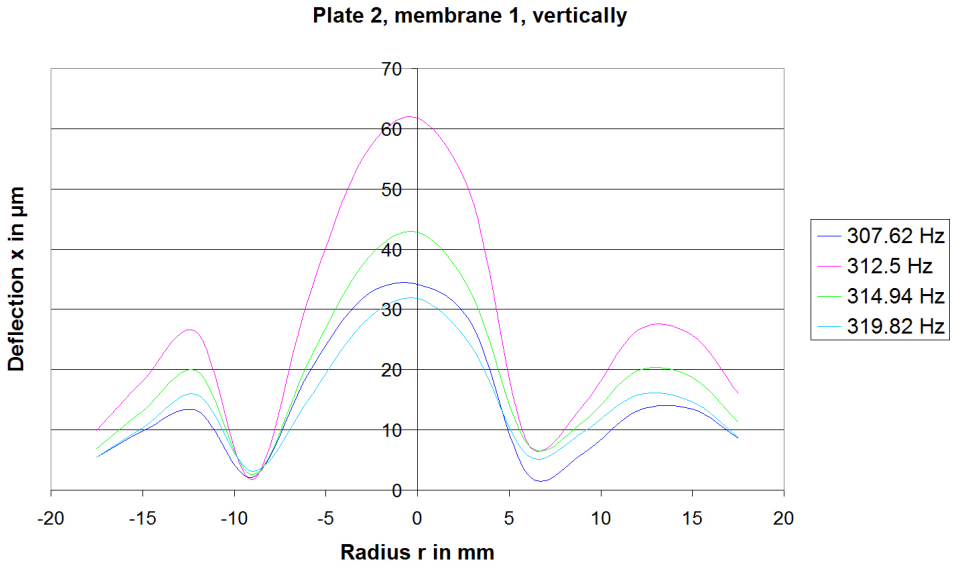


Figure 5.130 Vertical measurement points of membrane m1 of plate 2; the deflection x against the radius r around 310 Hz

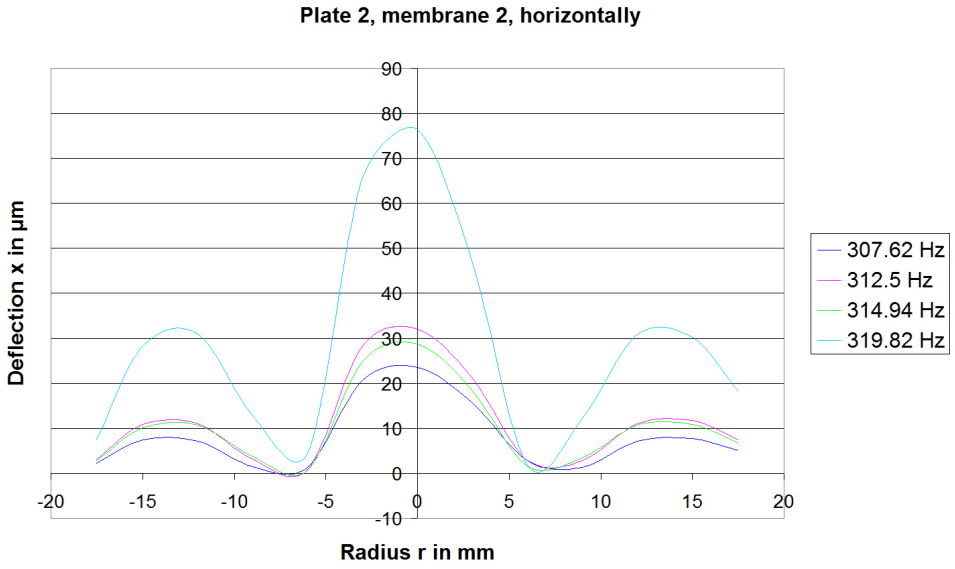


Figure 5.131 Horizontal measurement points of membrane m2 of plate 2; the deflection x against the radius r around 310 Hz

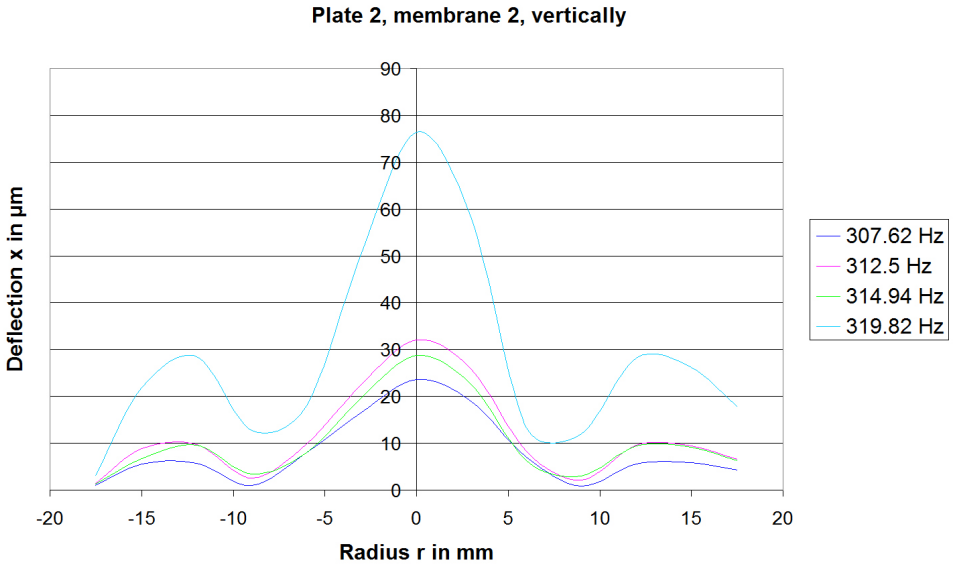


Figure 5.132 Vertical measurement points of membrane m2 of plate 2; the deflection x against the radius r around 310 Hz

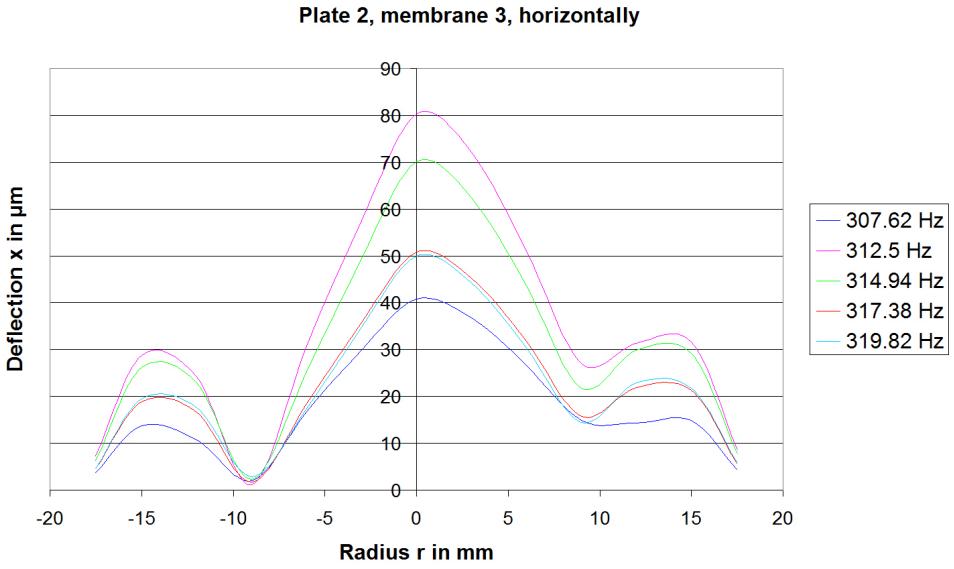


Figure 5.133 Horizontal measurement points of membrane m3 of plate 2; the deflection x against the radius r around 310 Hz

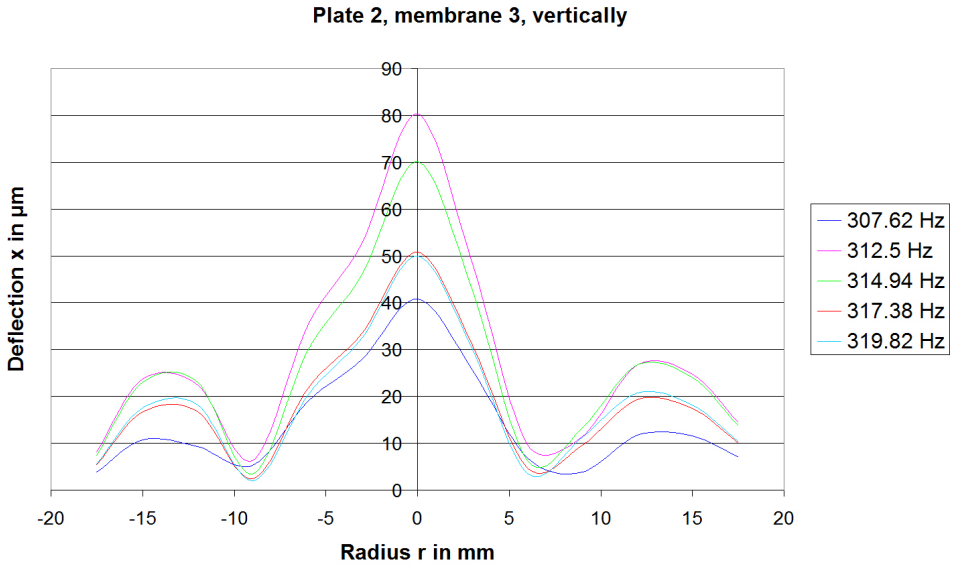


Figure 5.134 Vertical measurement points of membrane m3 of plate 2; the deflection x against the radius r around 310 Hz

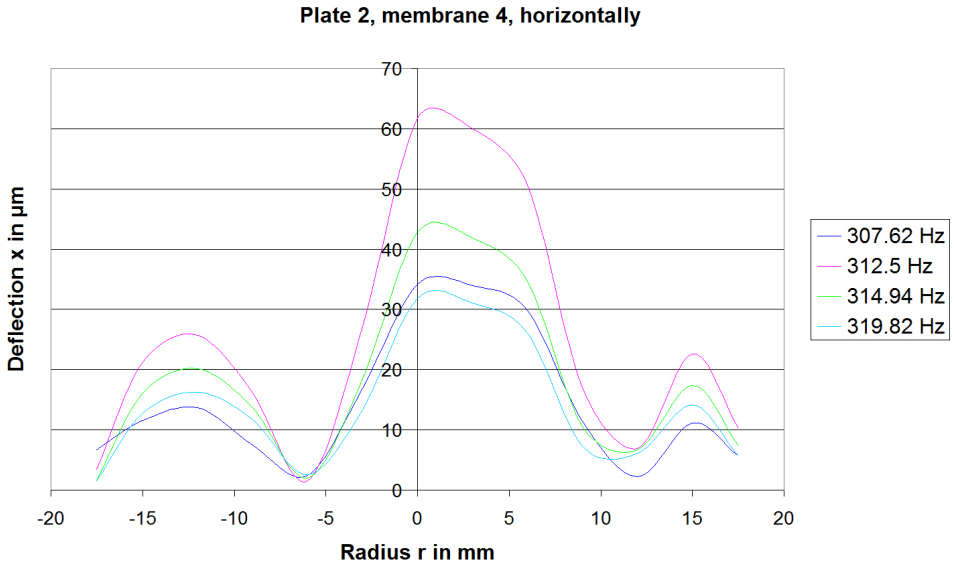


Figure 5.135 Horizontal measurement points of membrane m4 of plate 2; the deflection x against the radius r around 310 Hz

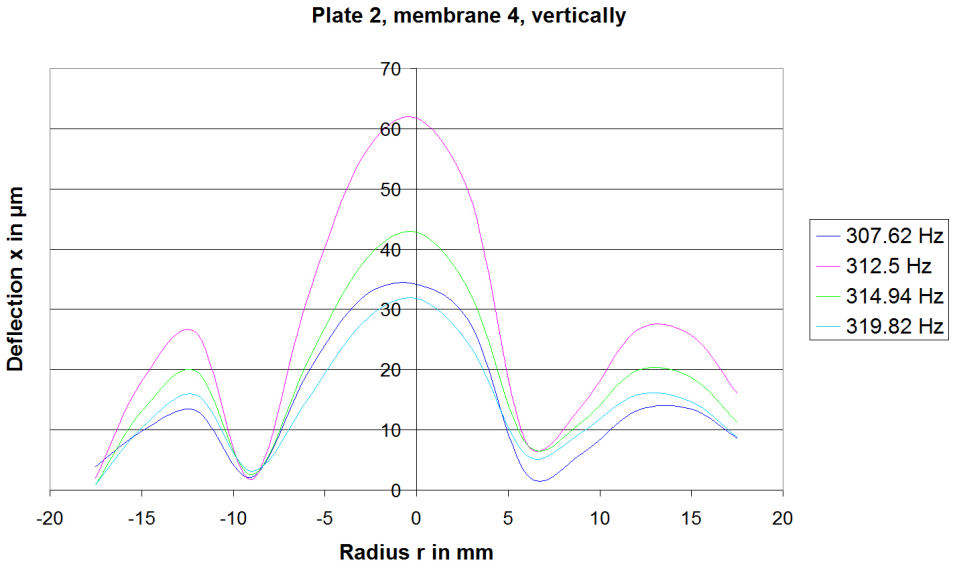


Figure 5.136 Vertical measurement points of membrane m4 of plate 2; the deflection x against the radius r around 310 Hz

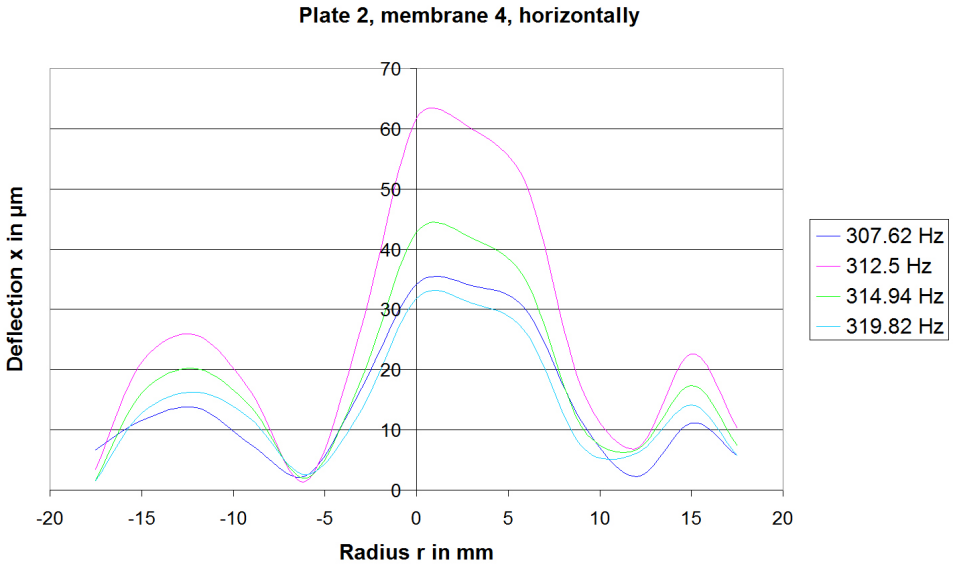


Figure 5.137 Horizontal measurement points of membrane m4 of plate 2; the deflection x against the radius r around 310 Hz

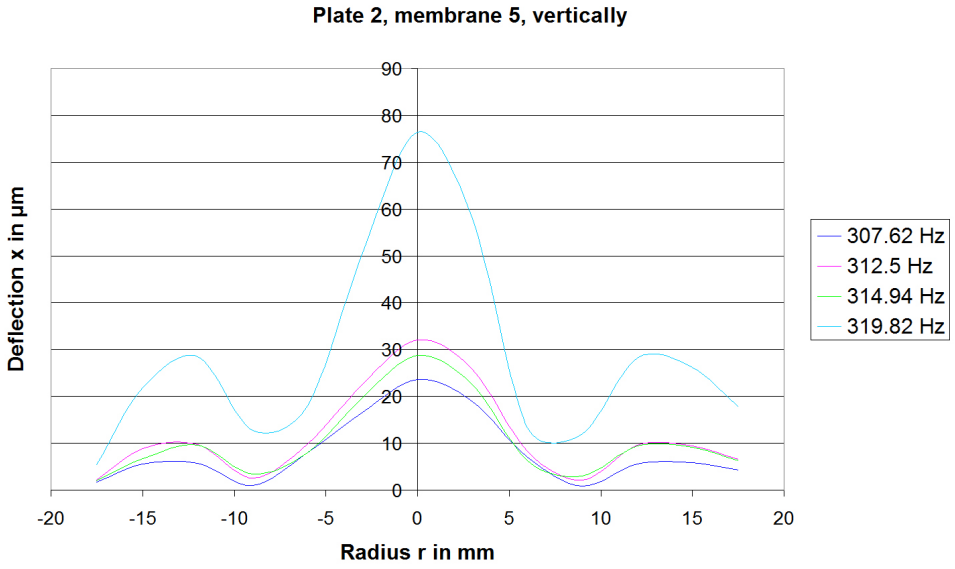


Figure 5.138 Vertical measurement points of membrane m5 of plate 2; the deflection x against the radius r around 310 Hz

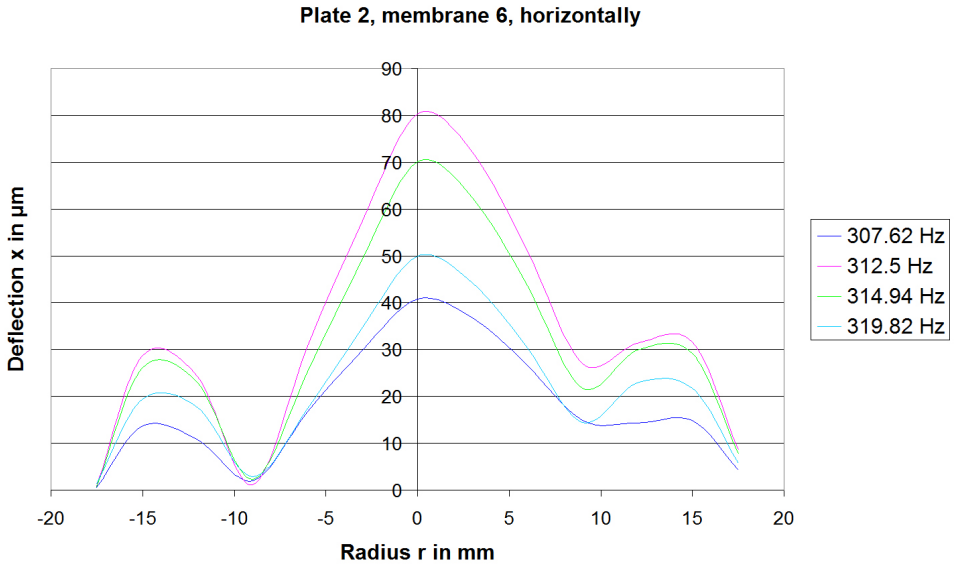


Figure 5.139 Horizontal measurement points of membrane m6 of plate 2; the deflection x against the radius r around 310 Hz

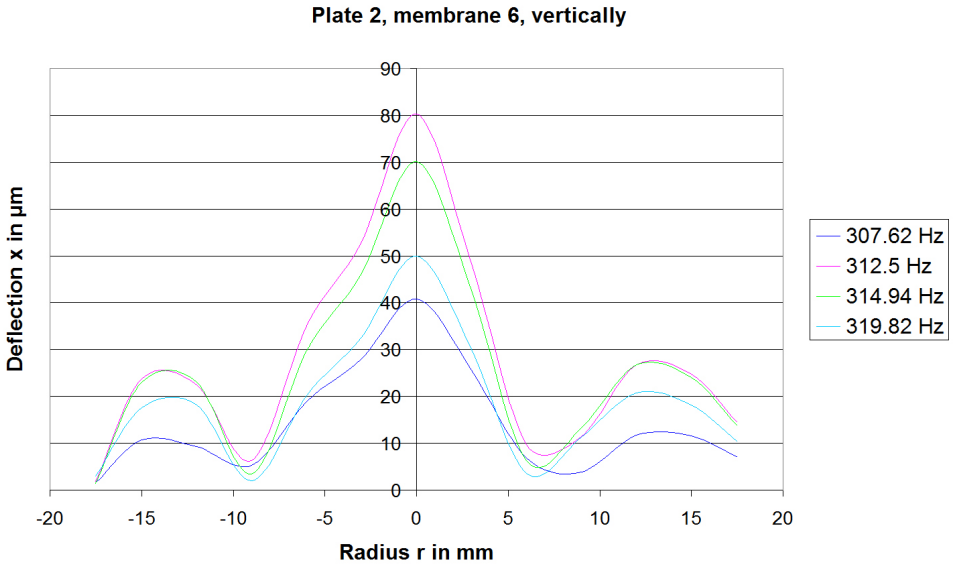


Figure 5.140 Vertical measurement points of membrane m6 of plate 2; the deflection x against the radius r around 310 Hz

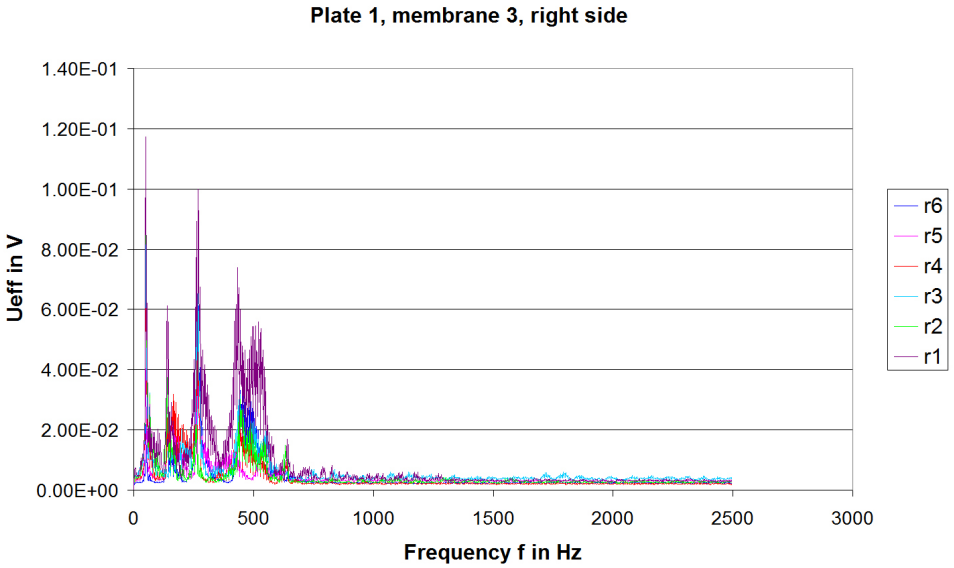


Figure 5.141 All data points (1024) from the right side of membrane m3 of plate 1; the FFT of the laser vibrometer signal U_{eff} against the frequency; the well was filled with 2.5 ml of water; a chirp signal was applied.

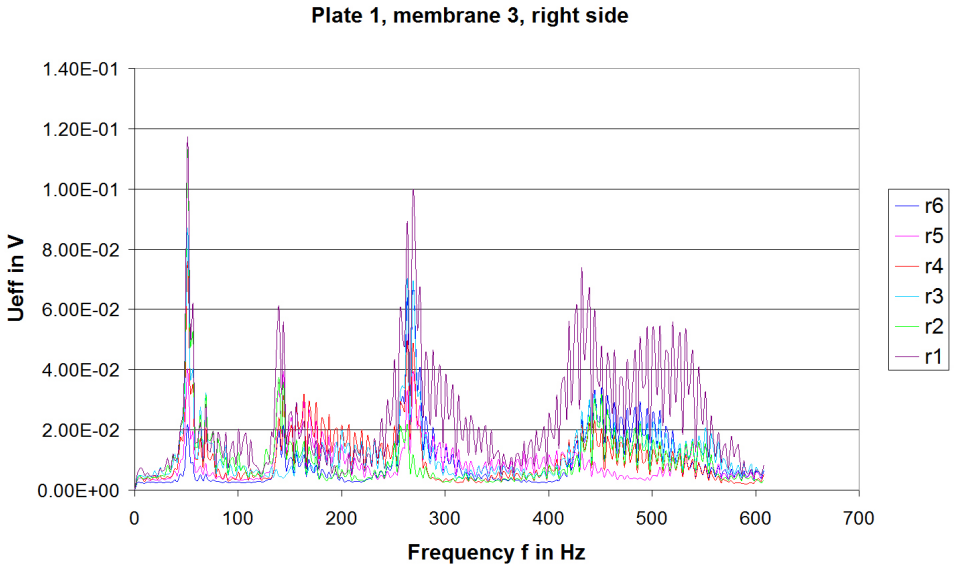


Figure 5.142 First 250 data points from the right side of membrane m3 of plate 1; the FFT of the laser vibrometer signal U_{eff} against the frequency; the well was filled with 2.5 ml of water; a chirp signal was applied.

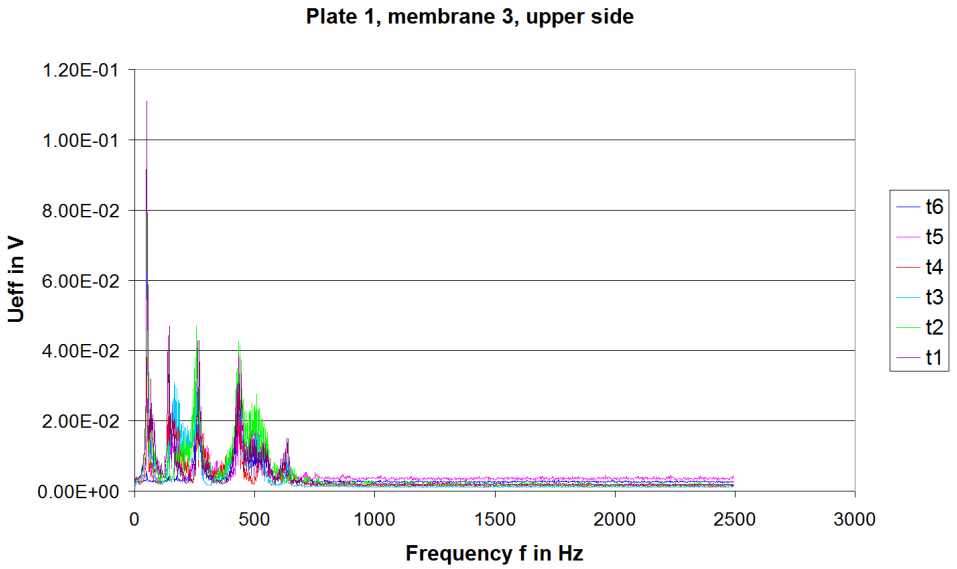


Figure 5.143 All data points (1024) from the upper side of membrane m3 of plate 1; the FFT of the laser vibrometer signal U_{eff} against the frequency; the well was filled with 2.5 ml of water; a chirp signal was applied.

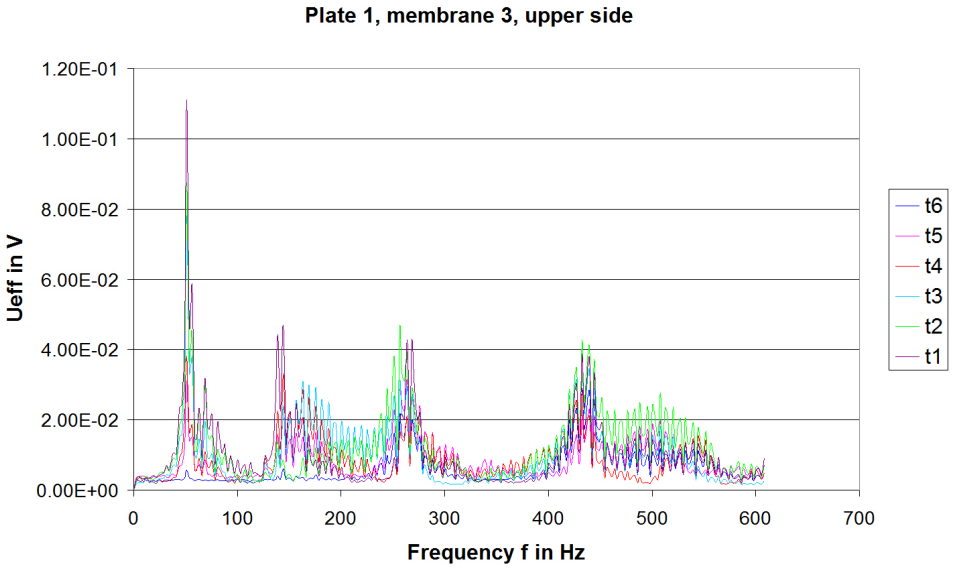


Figure 5.144 First 250 data points from the upper side of membrane m3 of plate 1; the FFT of the laser vibrometer signal U_{eff} against the frequency; the well was filled with 2.5 ml of water; a chirp signal was applied.

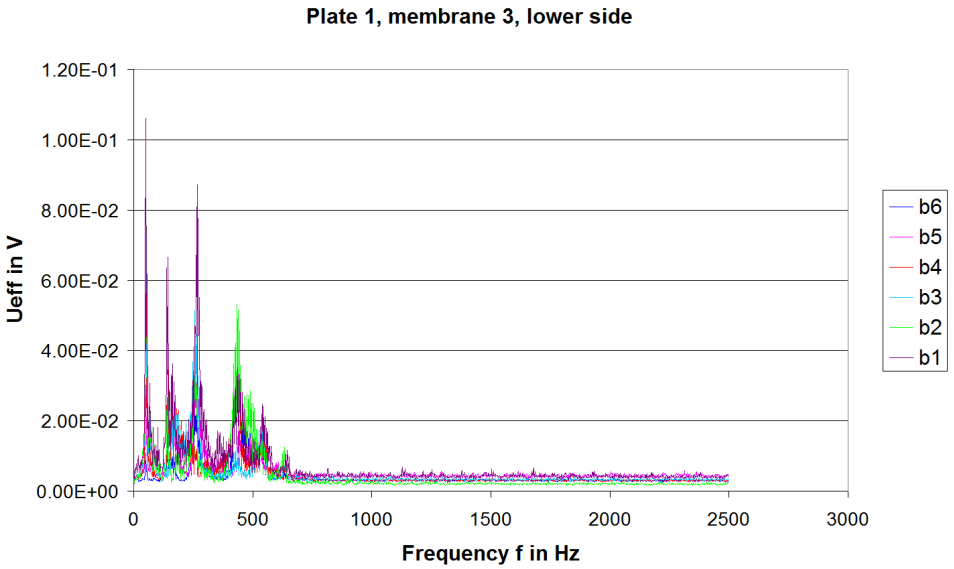


Figure 5.145 All data points (1024) from the lower side of membrane m3 of plate 1; the FFT of the laser vibrometer signal U_{eff} against the frequency; the well was filled with 2.5 ml of water; a chirp signal was applied.

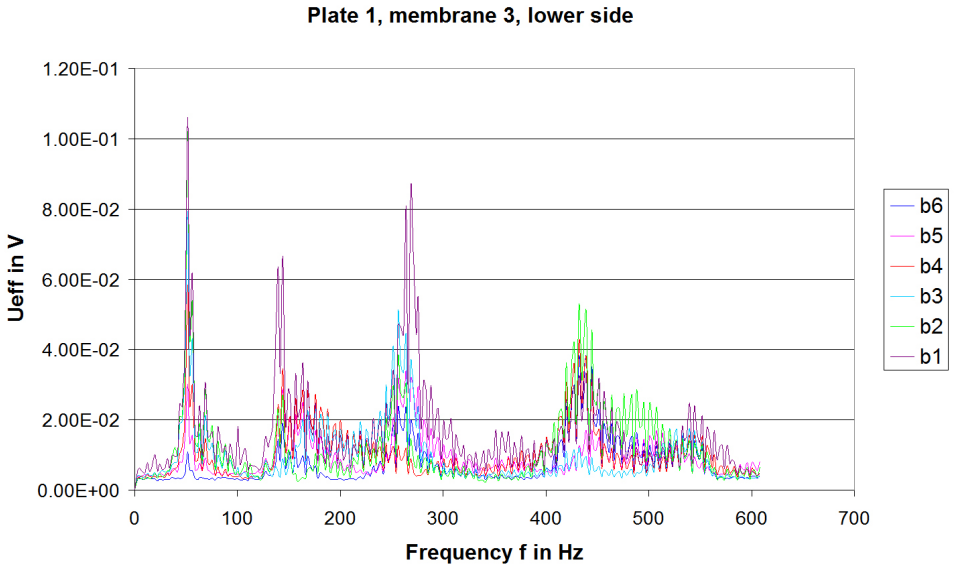


Figure 5.146 First 250 data points from the lower side of membrane m3 of plate 1; the FFT of the laser vibrometer signal U_{eff} against the frequency; the well was filled with 2.5 ml of water; a chirp signal was applied.

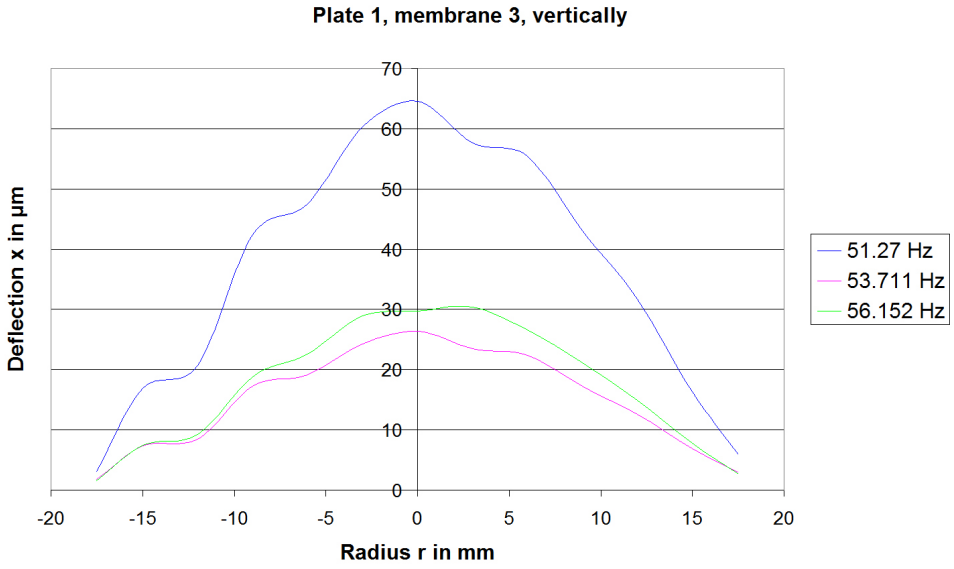


Figure 5.147 Vertical measurement points of membrane m1 of plate 1; the deflection x against the radius r around 55 Hz; the well was filled with 2.5 ml of water;

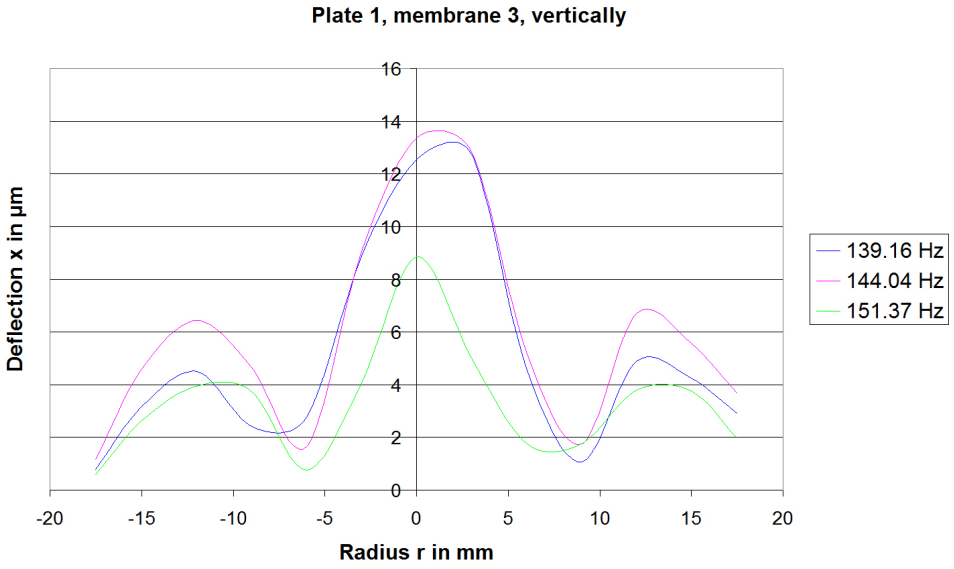


Figure 5.148 Vertical measurement points of membrane m1 of plate 1; the deflection x against the radius r around 140 Hz; the well was filled with 2.5 ml of water;

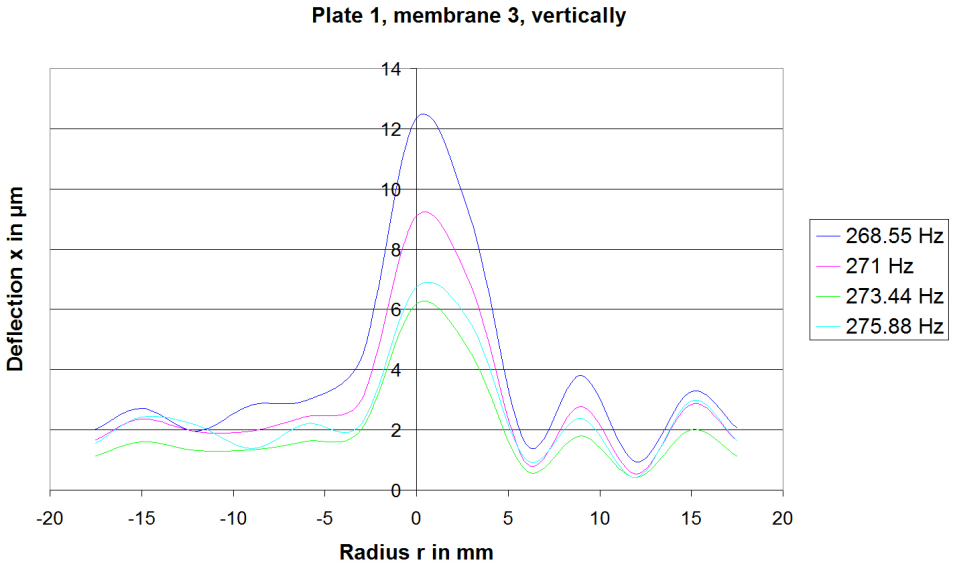


Figure 5.149 Vertical measurement points of membrane m1 of plate 1; the deflection x against the radius r around 270 Hz; the well was filled with 2.5 ml of water;

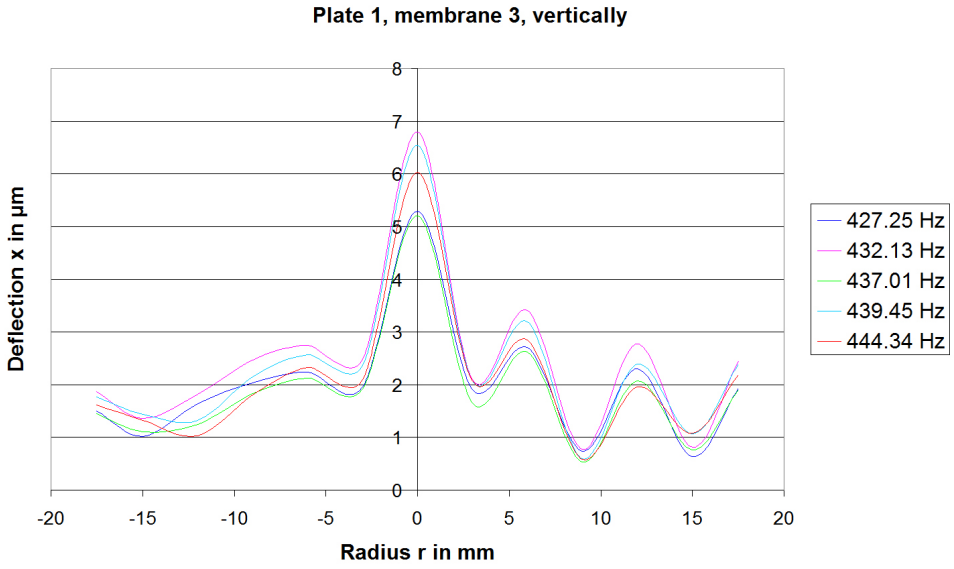


Figure 5.150 Vertical measurement points of membrane m1 of plate 1; the deflection x against the radius r around 440 Hz; the well was filled with 2.5 ml of water;

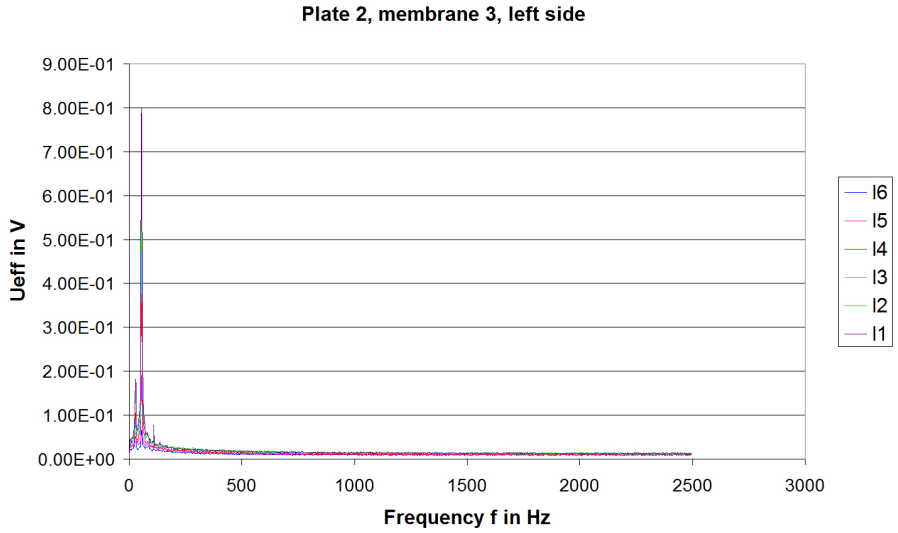


Figure 5.151 All data points (1024) from the left side of membrane m3 of plate 2; the FFT of the laser vibrometer signal U_{eff} against the frequency; the well was filled with 2.5 ml of water; a sinusoidal signal with 55 Hz was applied

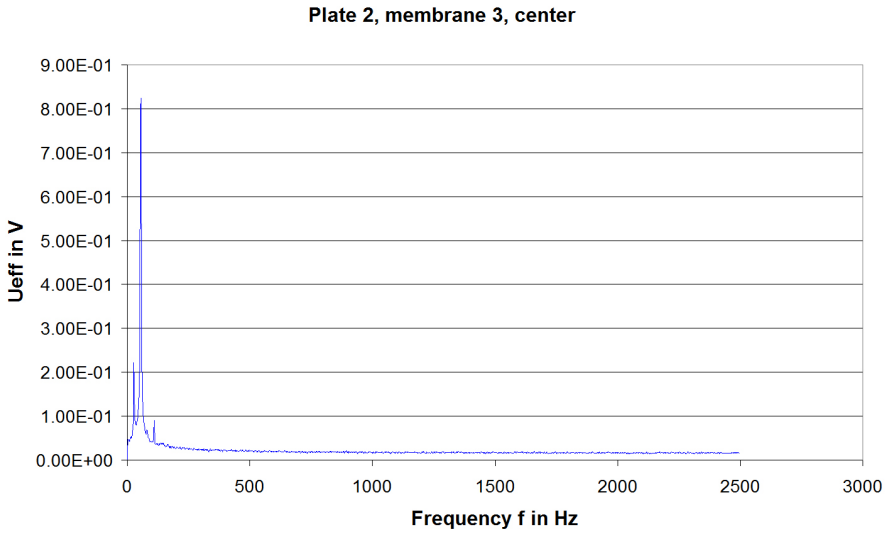


Figure 5.152 All data points (1024) from the center of membrane m3 of plate 2; the FFT of the laser vibrometer signal U_{eff} against the frequency; the well was filled with 2.5 ml of water; a sinusoidal signal with 55 Hz was applied

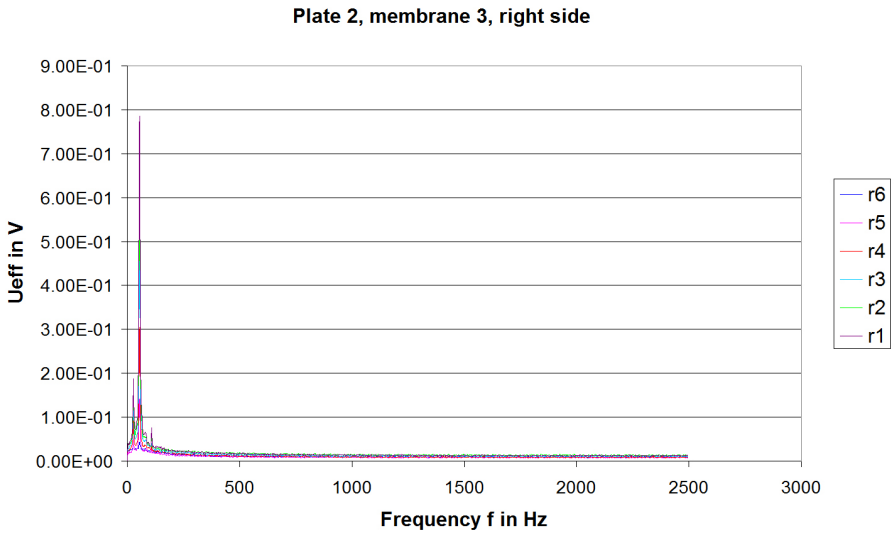


Figure 5.153 All data points (1024) from the right side of membrane m3 of plate 2; the FFT of the laser vibrometer signal U_{eff} against the frequency; the well was filled with 2.5 ml of water; a sinusoidal signal with 55 Hz was applied

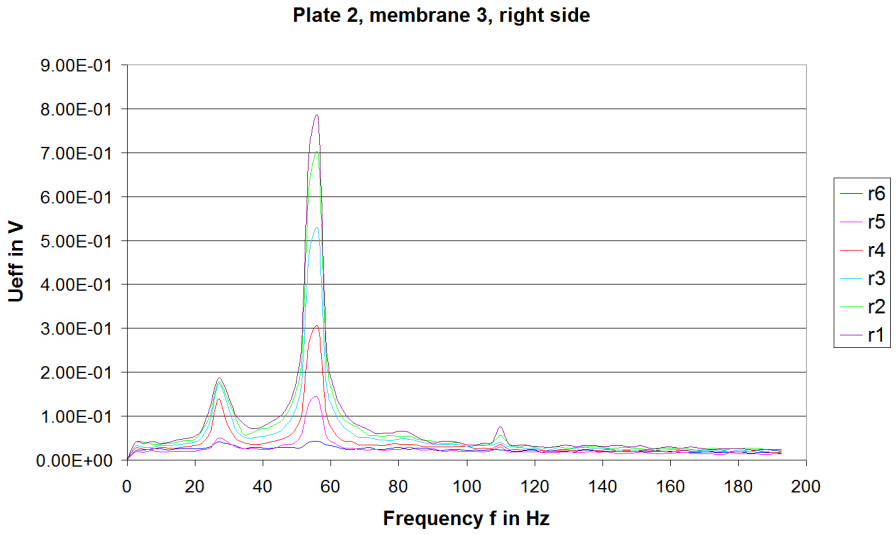


Figure 5.154 First 80 data points (until a frequency of 192.87 Hz) from the right side of membrane m3 of plate 2; the FFT of the laser vibrometer signal U_{eff} against the frequency; the well was filled with 2.5 ml of water; a sinusoidal signal with 55 Hz was applied

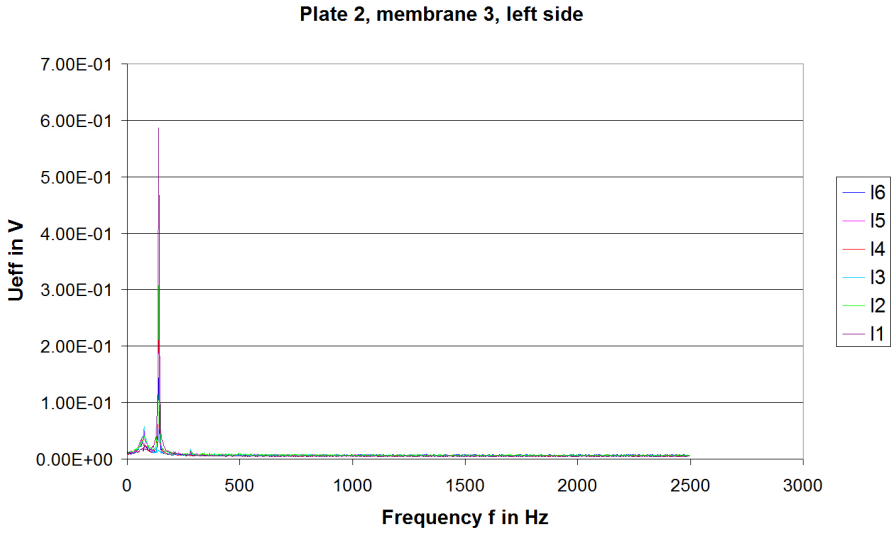


Figure 5.155 All data points (1024) from the left side of membrane m3 of plate 2; the FFT of the laser vibrometer signal U_{eff} against the frequency; the well was filled with 2.5 ml of water; a sinusoidal signal with 140 Hz was applied

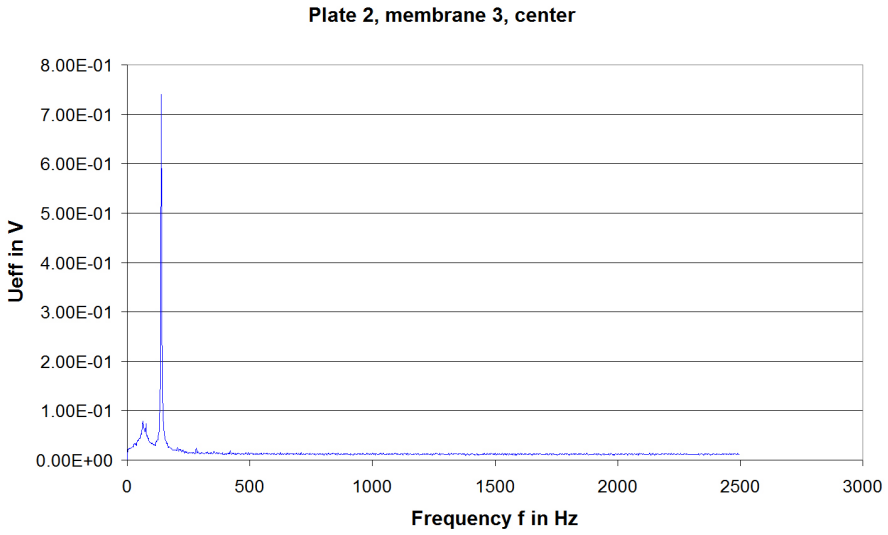


Figure 5.156 All data points (1024) from the center of membrane m3 of plate 2; the FFT of the laser vibrometer signal U_{eff} against the frequency; the well was filled with 2.5 ml of water; a sinusoidal signal with 140 Hz was applied

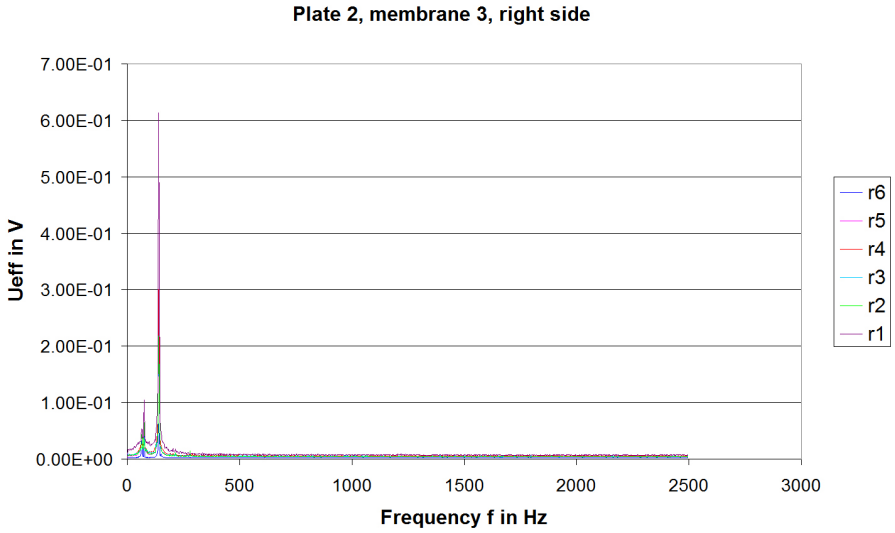


Figure 5.157 All data points (1024) from the right side of membrane m3 of plate 2; the FFT of the laser vibrometer signal U_{eff} against the frequency; the well was filled with 2.5 ml of water; a sinusoidal signal with 140 Hz was applied

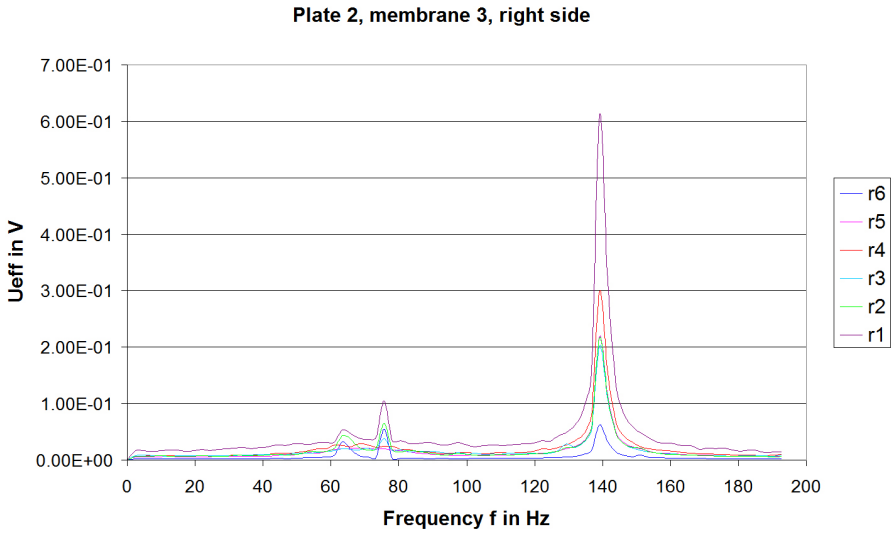


Figure 5.158 First 140 data points (until a frequency of 192.87 Hz) from the right side of membrane m3 of plate 2; the FFT of the laser vibrometer signal U_{eff} against the frequency; the well was filled with 2.5 ml of water; a sinusoidal signal with 140 Hz was applied

5

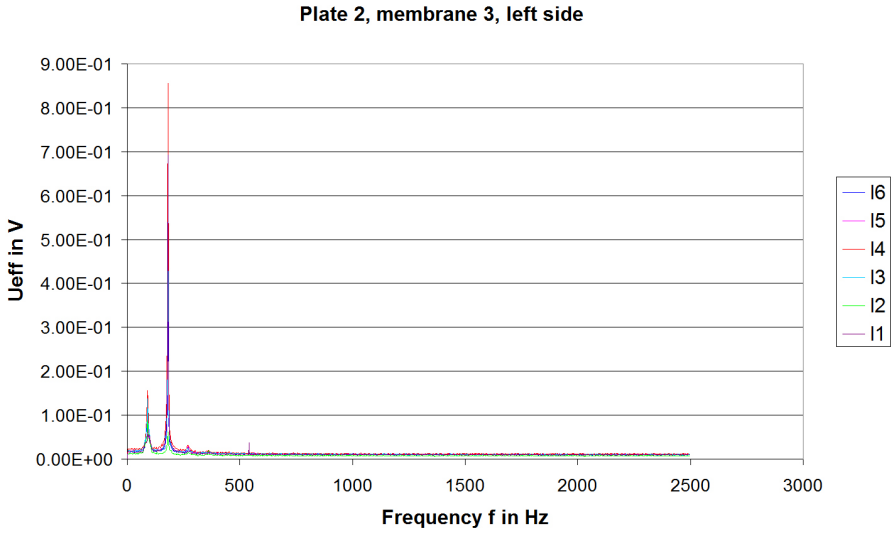


Figure 5.159 All data points (1024) from the left side of membrane m3 of plate 2; the FFT of the laser vibrometer signal U_{eff} against the frequency; the well was filled with 2.5 ml of water; a sinusoidal signal with 180 Hz was applied

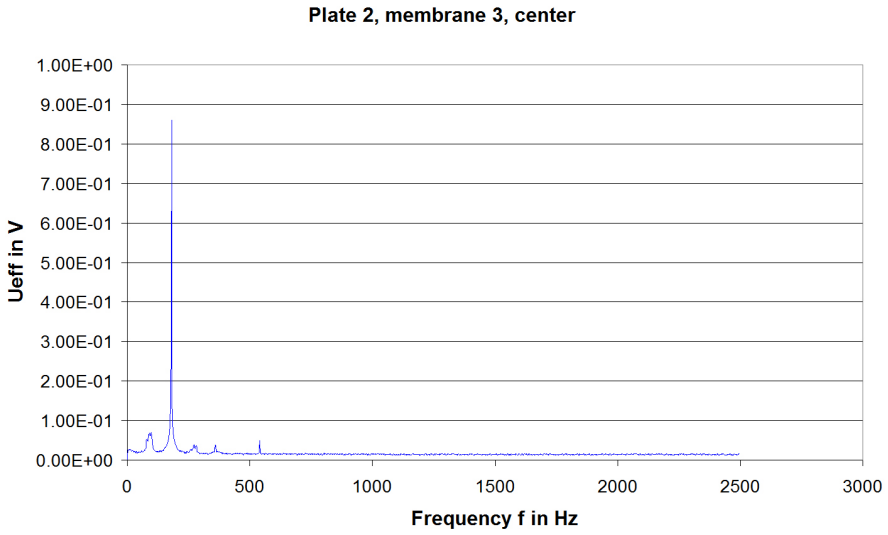


Figure 5.160 All data points (1024) from the center of membrane m3 of plate 2; the FFT of the laser vibrometer signal U_{eff} against the frequency; the well was filled with 2.5 ml of water; a sinusoidal signal with 180 Hz was applied

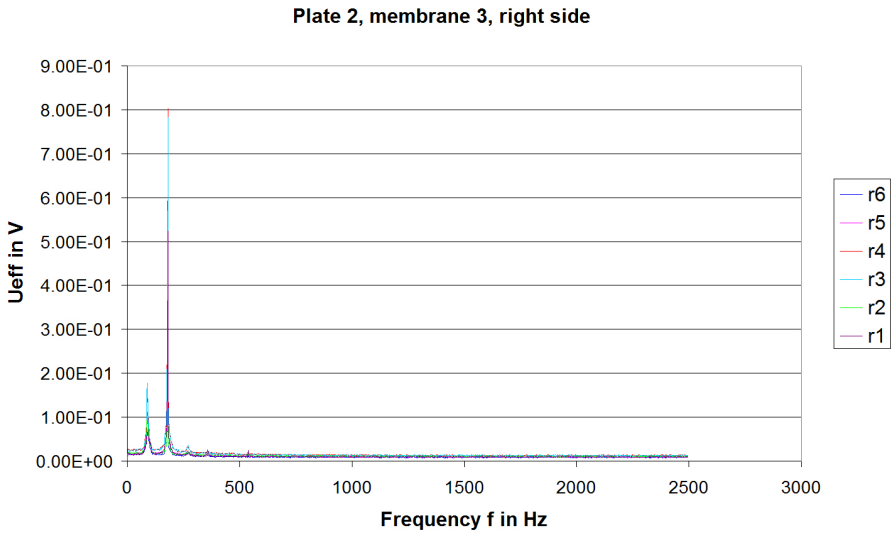


Figure 5.161 All data points (1024) from the right side of membrane m3 of plate 2; the FFT of the laser vibrometer signal U_{eff} against the frequency; the well was filled with 2.5 ml of water; a sinusoidal signal with 180 Hz was applied

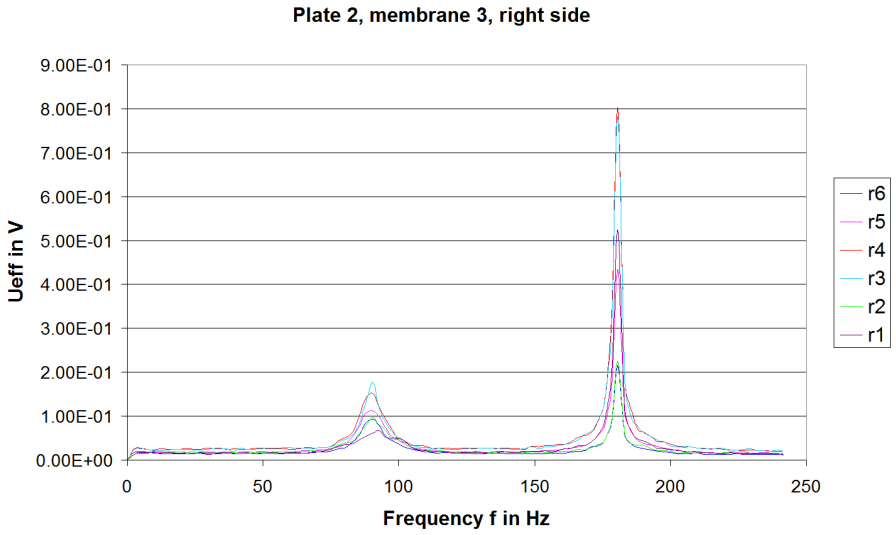


Figure 5.162 First 100 data points (until a frequency of 241.7 Hz) from the right side of membrane m3 of plate 2; the FFT of the laser vibrometer signal U_{eff} against the frequency; the well was filled with 2.5 ml of water; a sinusoidal signal with 180 Hz was applied

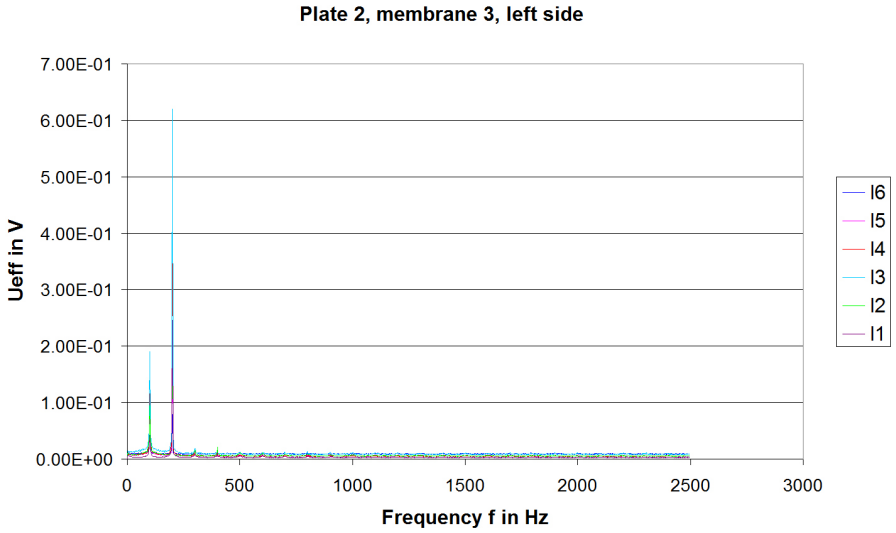


Figure 5.163 All data points (1024) from the left side of membrane m3 of plate 2; the FFT of the laser vibrometer signal U_{eff} against the frequency; the well was filled with 2.5 ml of water; a sinusoidal signal with 200 Hz was applied

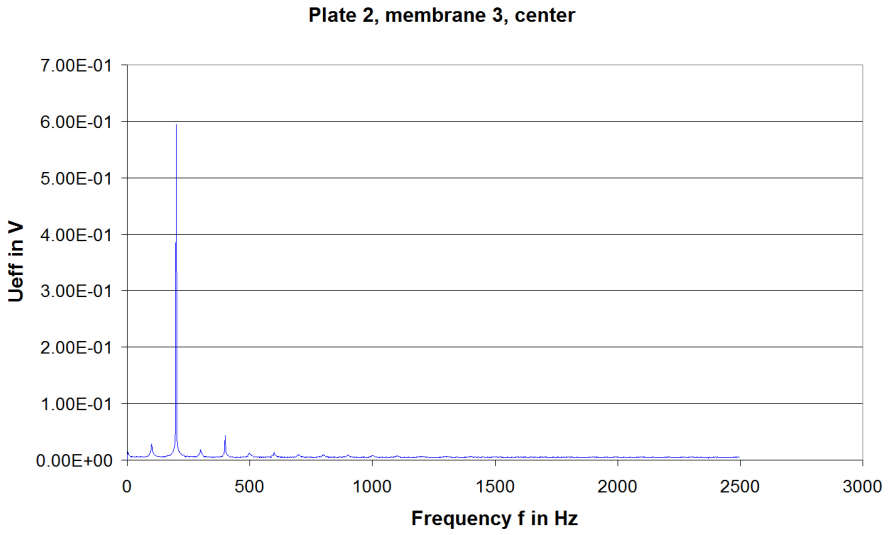


Figure 5.164 All data points (1024) from the center of membrane m3 of plate 2; the FFT of the laser vibrometer signal U_{eff} against the frequency; the well was filled with 2.5 ml of water; a sinusoidal signal with 200 Hz was applied

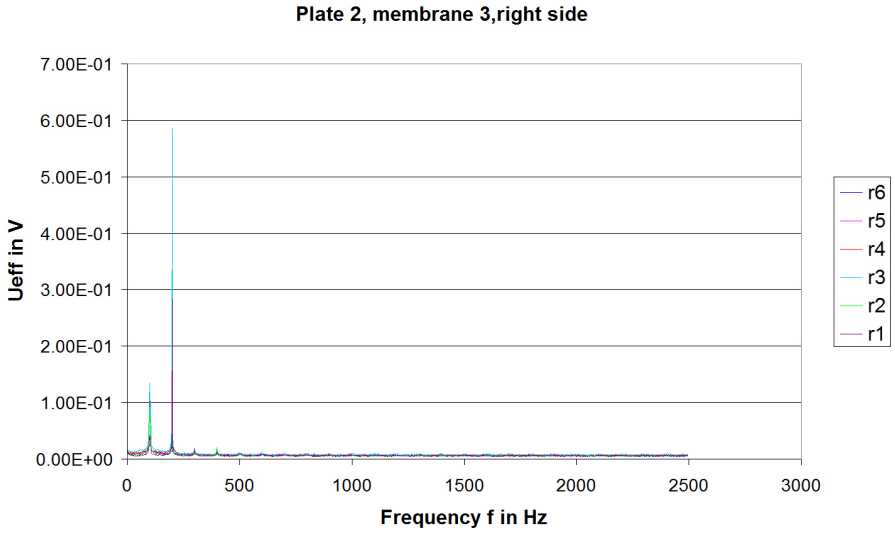


Figure 5.165 All data points (1024) from the right side of membrane m3 of plate 2; the FFT of the laser vibrometer signal U_{eff} against the frequency; the well was filled with 2.5 ml of water; a sinusoidal signal with 200 Hz was applied

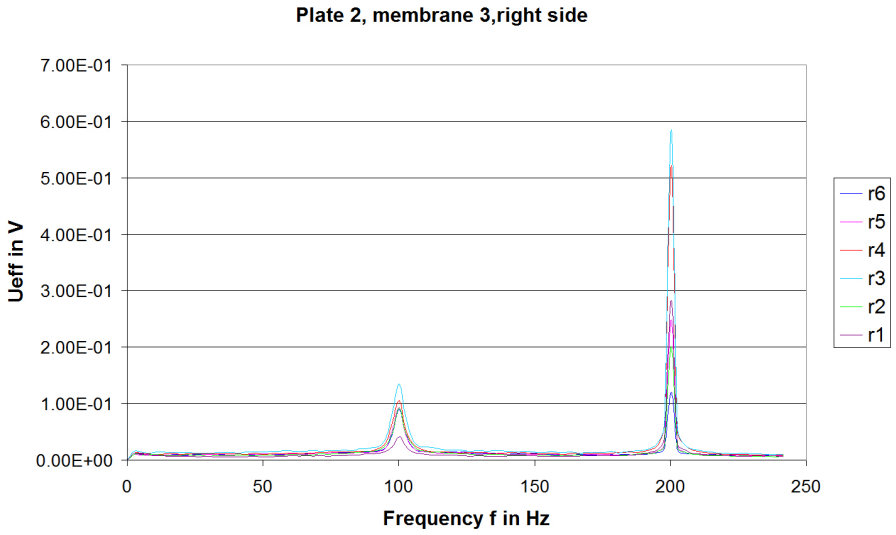


Figure 5.166 First 100 data points (until a frequency of 241.7 Hz) from the right side of membrane m3 of plate 2; the FFT of the laser vibrometer signal U_{eff} against the frequency; the well was filled with 2.5 ml of water; a sinusoidal signal with 200 Hz was applied

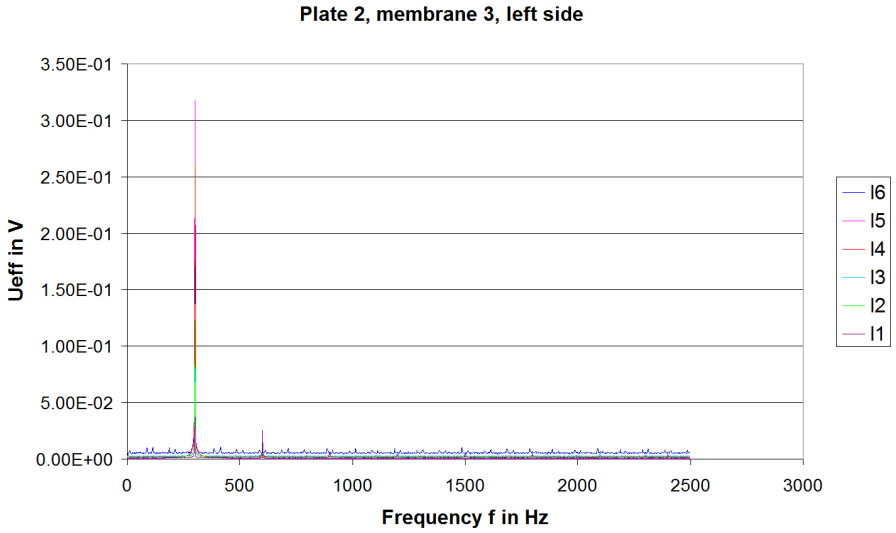


Figure 5.167 All data points (1024) from the left side of membrane m3 of plate 2; the FFT of the laser vibrometer signal U_{eff} against the frequency; the well was filled with 2.5 ml of water; a sinusoidal signal with 300 Hz was applied

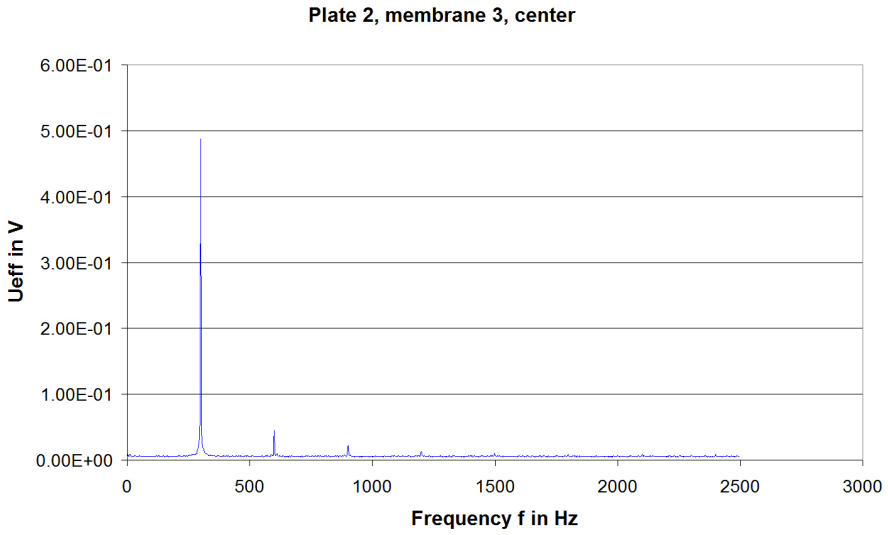


Figure 5.168 All data points (1024) from the center of membrane m3 of plate 2; the FFT of the laser vibrometer signal U_{eff} against the frequency; the well was filled with 2.5 ml of water; a sinusoidal signal with 300 Hz was applied

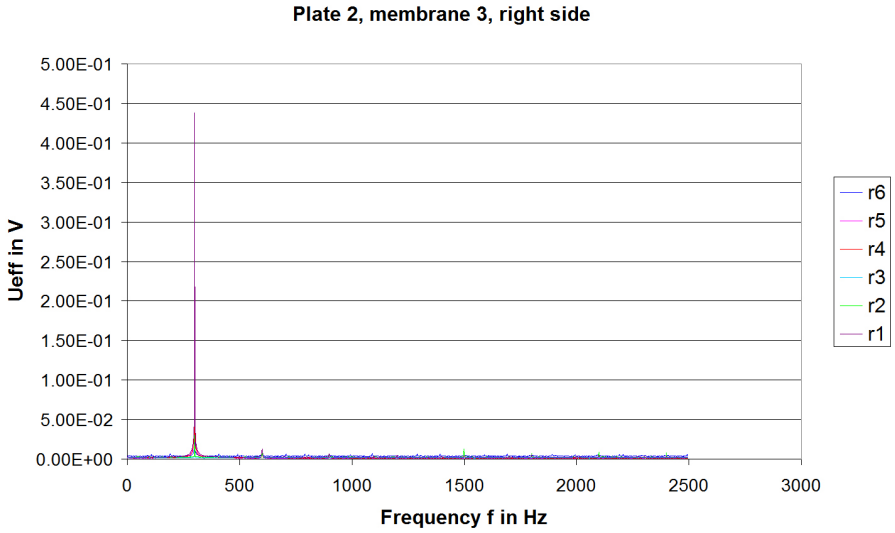


Figure 5.169 All data points (1024) from the right side of membrane m3 of plate 2; the FFT of the laser vibrometer signal U_{eff} against the frequency; the well was filled with 2.5 ml of water; a sinusoidal signal with 300 Hz was applied

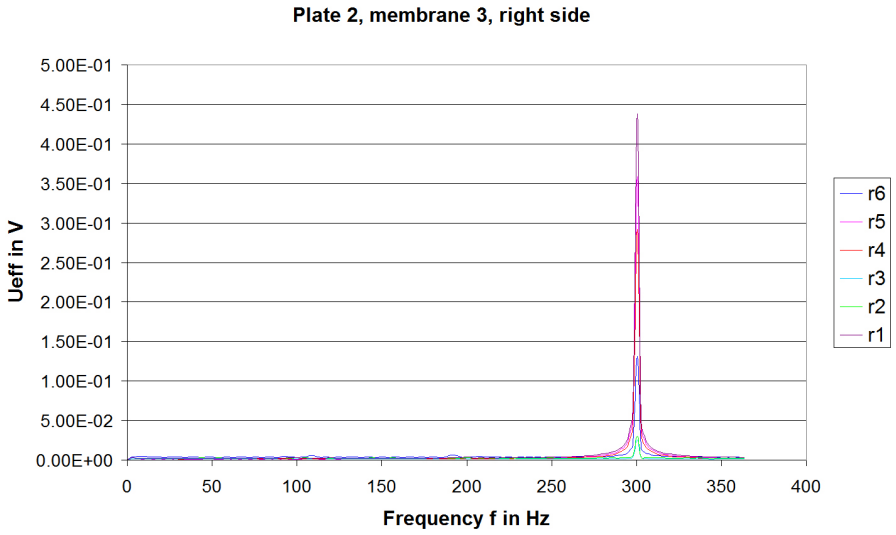


Figure 5.170 First 150 data points (until a frequency of 363.77 Hz) from the right side of membrane m3 of plate 2; the FFT of the laser vibrometer signal U_{eff} against the frequency; the well was filled with 2.5 ml of water; a sinusoidal signal with 300 Hz was applied

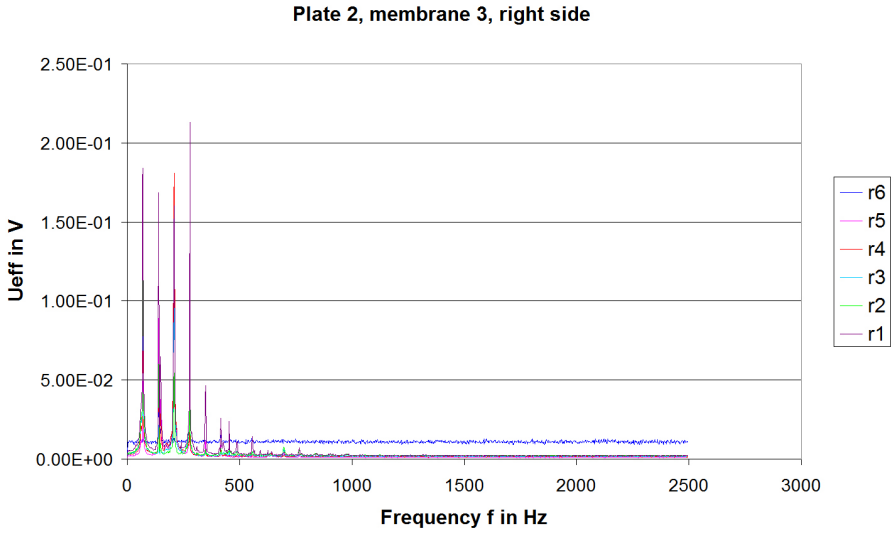


Figure 5.171 All data points (1024) from the right side of membrane m3 of plate 2; the FFT of the laser vibrometer signal U_{eff} against the frequency; the well was filled with 2.5 ml of water; a artificial larynx signal was applied.

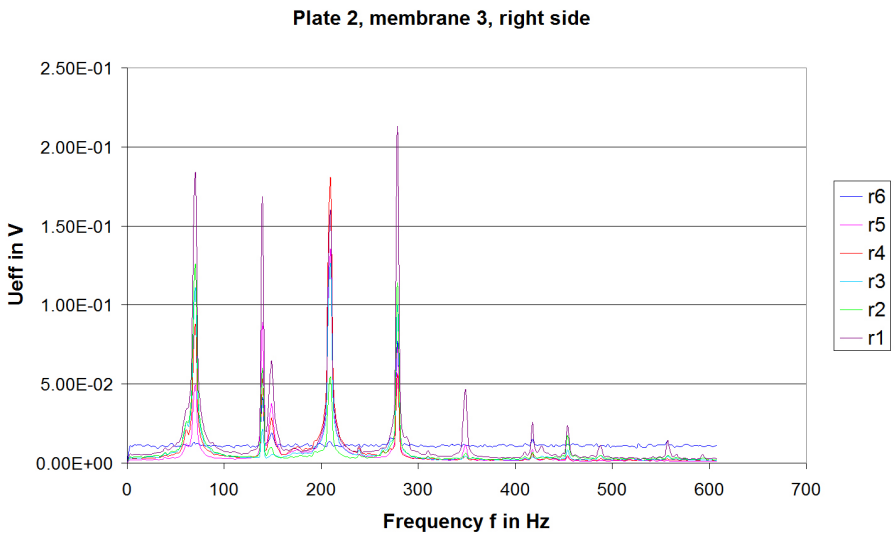


Figure 5.172 First 250 data points from the right side of membrane m3 of plate 2; the FFT of the laser vibrometer signal U_{eff} against the frequency; the well was filled with 2.5 ml of water; a artificial larynx signal was applied.

6 Appendix B

To examine the correlations between the signals gathered from the center of the membranes of the two plates the pearson correlation coefficient was calculated. The result for the correlation of the membranes for each plate is shown in Table 6.1 and Table 6.2. The result of the examination of the correlation between the membranes of the two plates is provided in Table 6.3.

Table 6.1 The rounded pearson coefficients to describe the correlation between the membranes of plate 1.

x		y		Pearson
plate	membrane	plate	membrane	
1	m1	1	m2	0.784
1	m1	1	m3	0.779
1	m1	1	m4	0.960
1	m1	1	m5	0.857
1	m1	1	m6	0.818
1	m2	1	m3	0.980
1	m2	1	m4	0.847
1	m2	1	m5	0.944
1	m2	1	m6	0.951
1	m3	1	m4	0.858
1	m3	1	m5	0.949
1	m3	1	m6	0.981
1	m4	1	m5	0.931
1	m4	1	m6	0.901
1	m5	1	m6	0.982

Table 6.2 The rounded pearson coefficients to describe the correlation between the membranes of plate 2.

x		y		Pearson
plate	membrane	plate	membrane	
2	m1	2	m2	0.890
2	m1	2	m3	0.984
2	m1	2	m4	0.856
2	m1	2	m5	0.865
2	m1	2	m6	0.811
2	m2	2	m3	0.890
2	m2	2	m4	0.720
2	m2	2	m5	0.986
2	m2	2	m6	0.913
2	m3	2	m4	0.795
2	m3	2	m5	0.861
2	m3	2	m6	0.794
2	m4	2	m5	0.700
2	m4	2	m6	0.652
2	m5	2	m6	0.891

Table 6.3 The rounded pearson coefficients to describe the correlation between the membranes of plate and the membranes of plate 2.

x		y		Pearson
plate	membrane	plate	membrane	
1	m1	2	m1	0.984
1	m1	2	m2	0.852
1	m1	2	m3	0.990
1	m1	2	m4	0.825
1	m1	2	m5	0.821
1	m1	2	m6	0.761
1	m2	2	m1	0.840
1	m2	2	m2	0.921
1	m2	2	m3	0.815
1	m2	2	m4	0.696
1	m2	2	m5	0.949
1	m2	2	m6	0.980
1	m3	2	m1	0.824
1	m3	2	m2	0.918
1	m3	2	m3	0.808
1	m3	2	m4	0.665
1	m3	2	m5	0.952
1	m3	2	m6	0.992
1	m4	2	m1	0.960
1	m4	2	m2	0.932
1	m4	2	m3	0.978
1	m4	2	m4	0.774
1	m4	2	m5	0.903
1	m4	2	m6	0.835
1	m5	2	m1	0.892
1	m5	2	m2	0.985
1	m5	2	m3	0.890
1	m5	2	m4	0.727
1	m5	2	m5	0.992
1	m5	2	m6	0.942
1	m6	2	m1	852
1	m6	2	m2	0.956
1	m6	2	m3	0.847
1	m6	2	m4	0.682
1	m6	2	m5	0.979
1	m6	2	m6	0.972

7 Appendix C

Below the pictures of the plates with the different coatings over 8 days are provided. Two pictures of each well were made. Day 1 represents the day of the cell seeding.

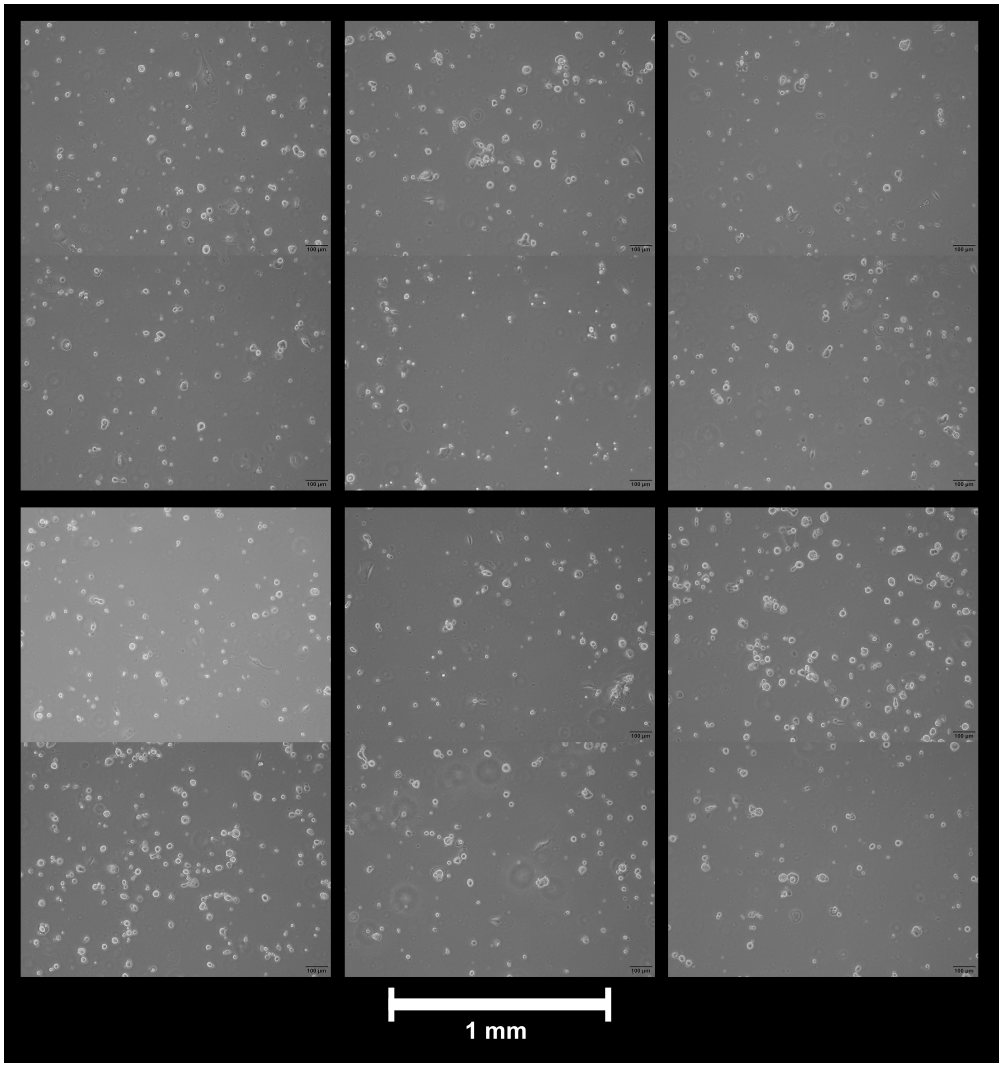


Figure 7.1 Cells in the plate with collagen type I coating on day 1, 4 hours after seeding

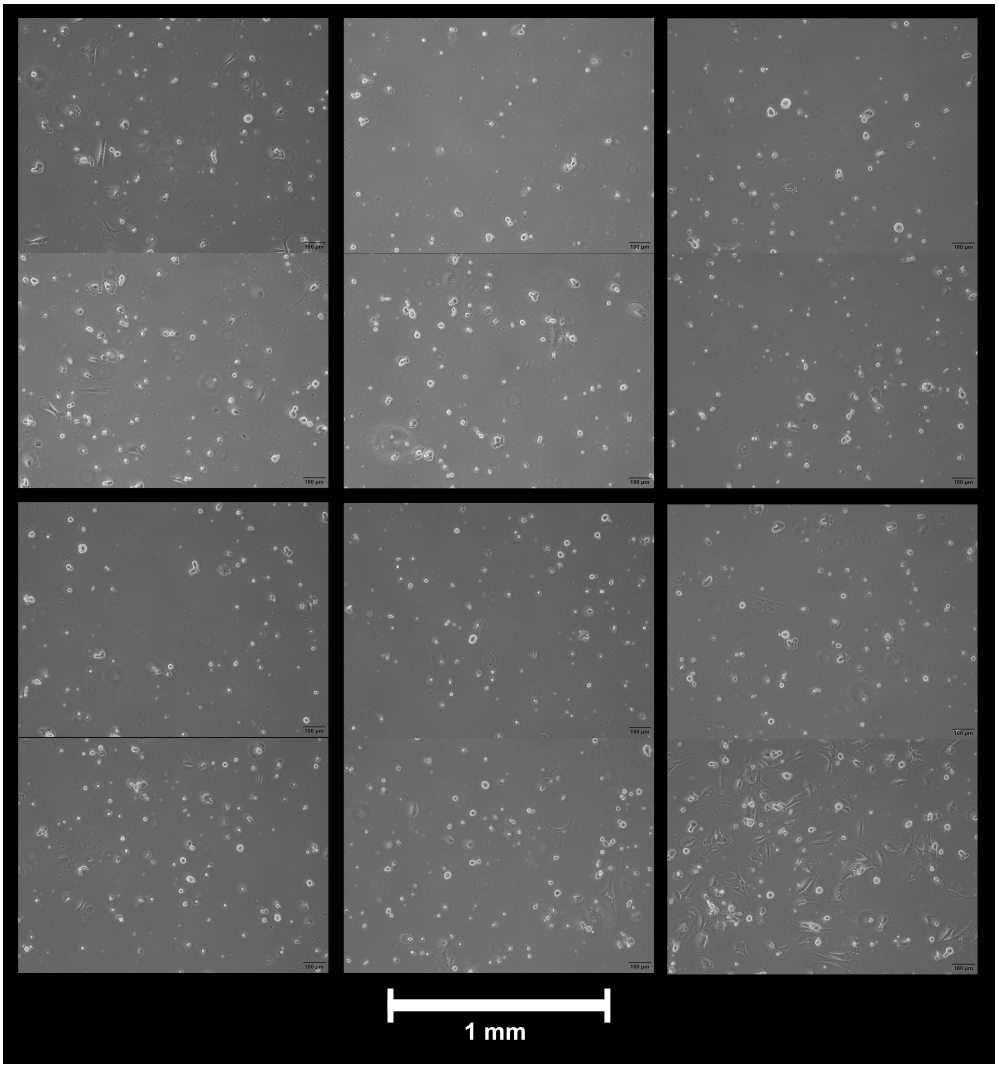


Figure 7.2 Cells in the plate with pronection coating on day 1, 4 hours after seeding

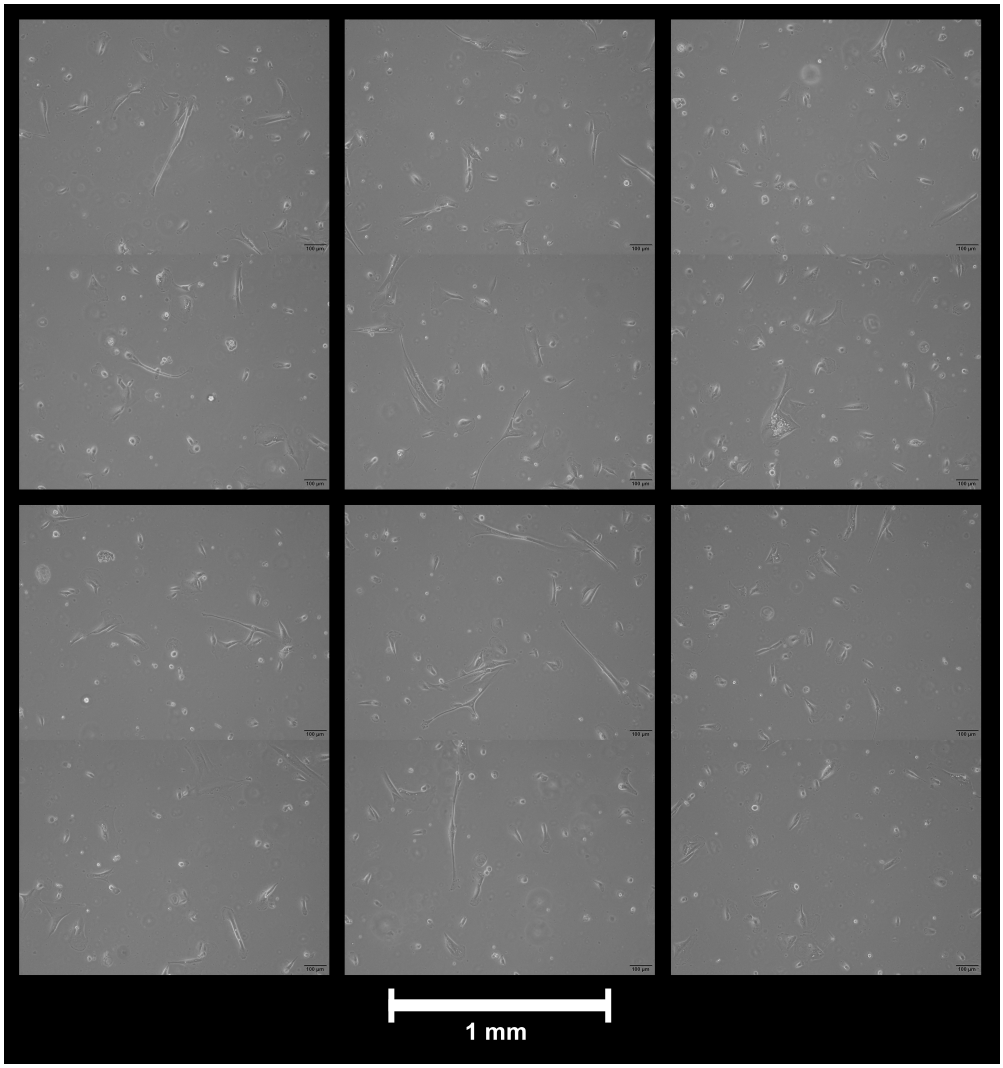


Figure 7.3 Cells in the plate with collagen type I coating on day 1, 4 hours after seeding

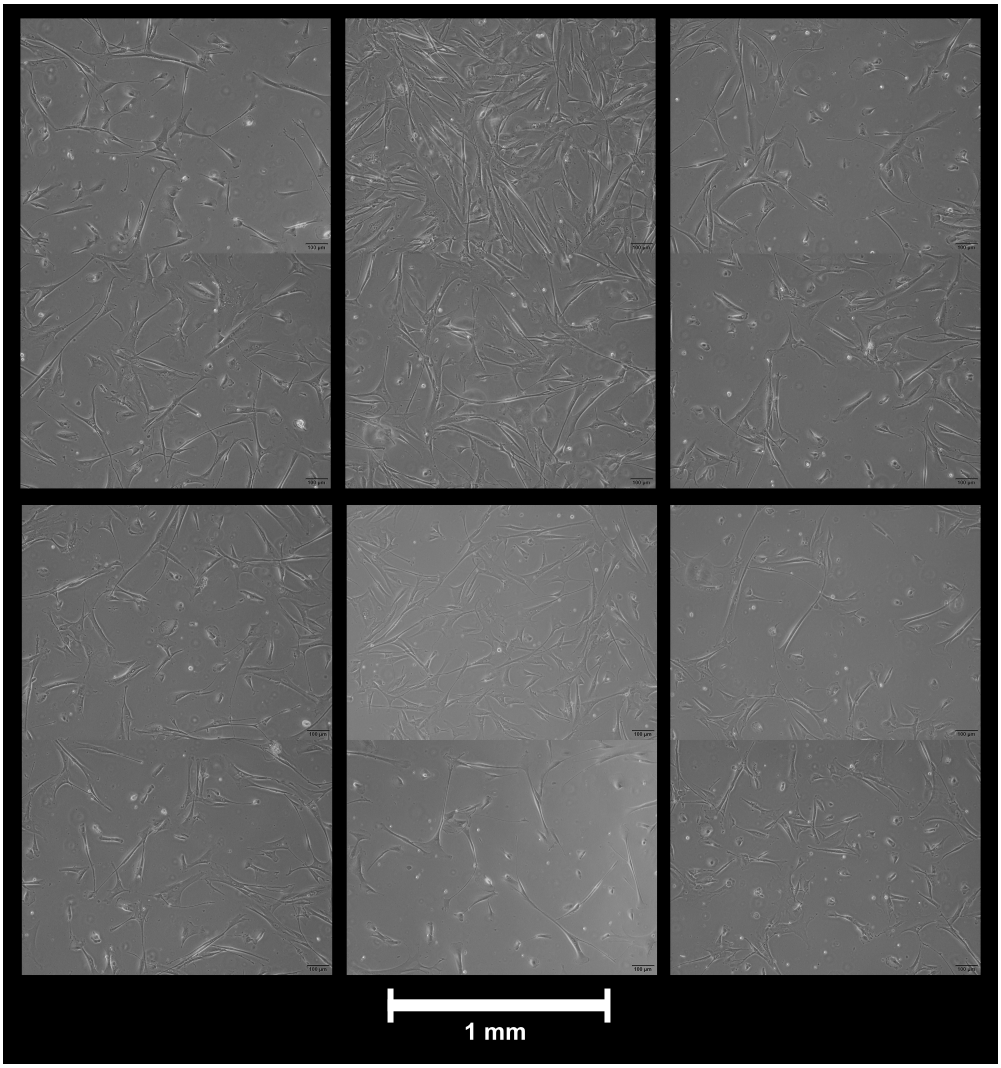


Figure 7.4 Cells in the plate with pronection coating on day 1, 4 hours after seeding

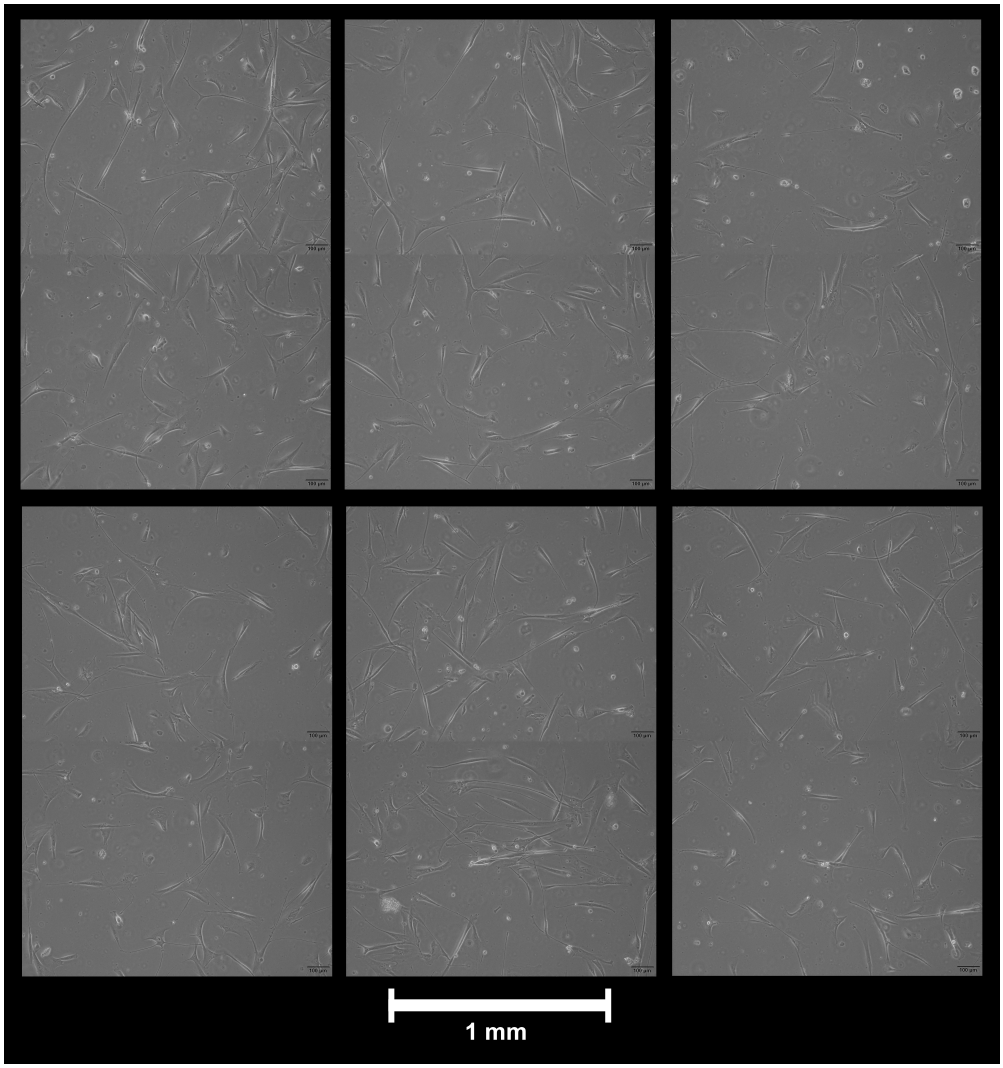


Figure 7.5 Cells in the plate with collagen type I coating on day 1, 4 hours after seeding

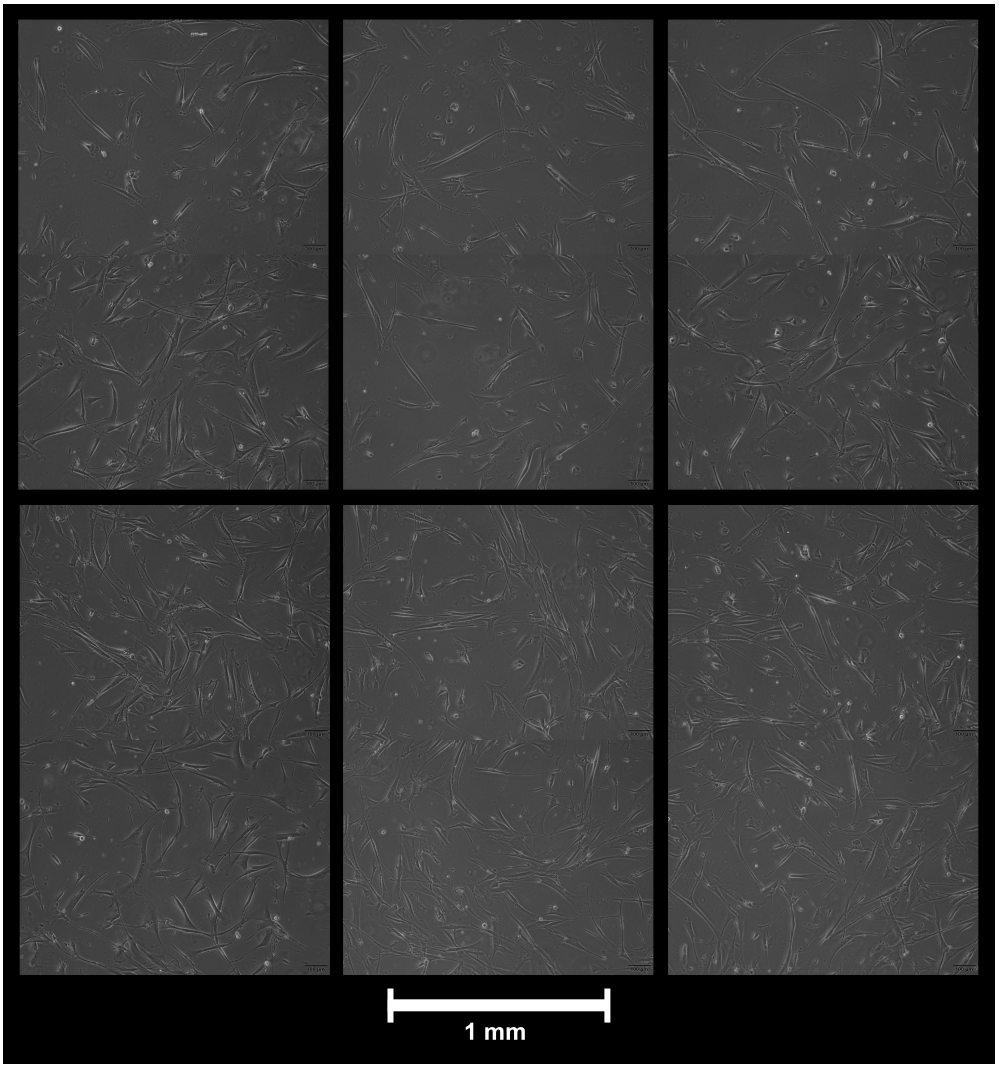


Figure 7.6 Cells in the plate with pronection coating on day 1, 4 hours after seeding

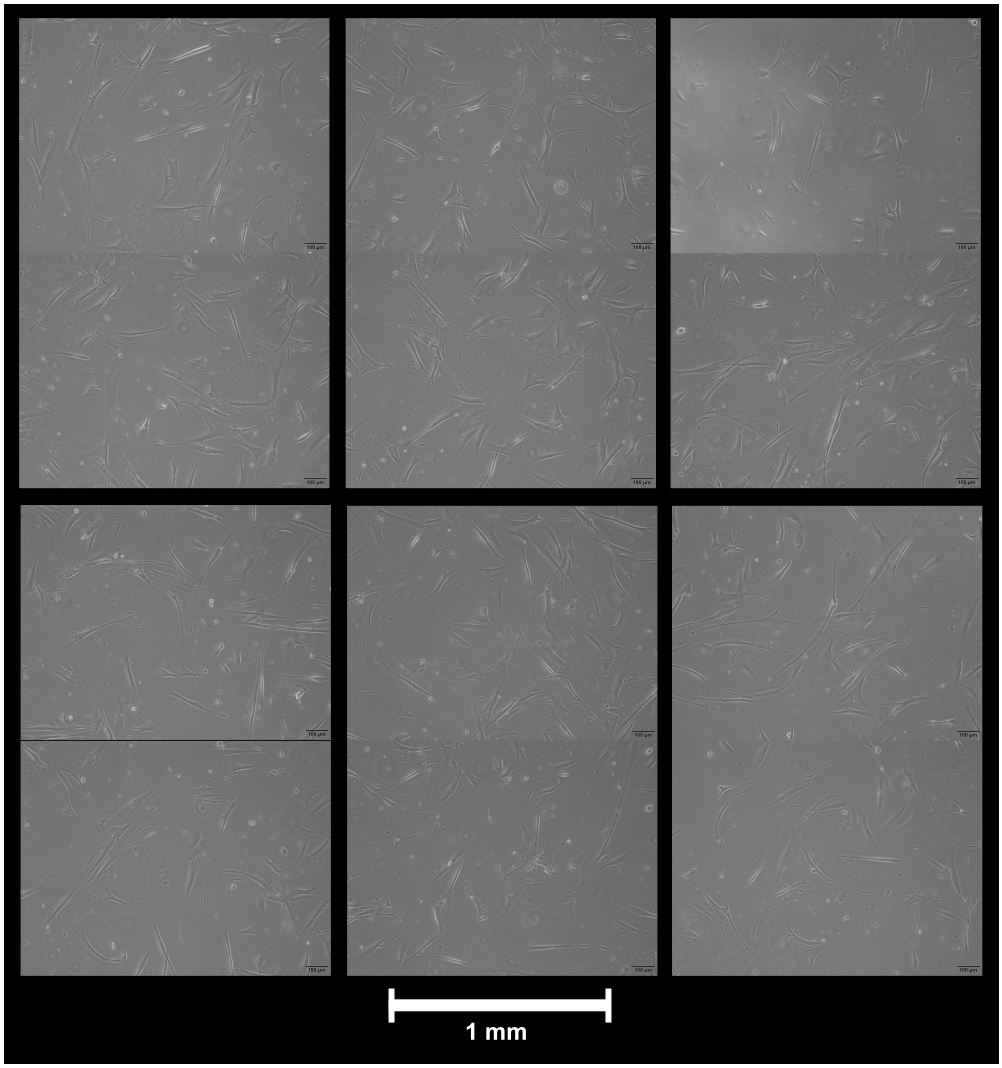


Figure 7.7 Cells in the plate with collagen type I coating on day 1, 4 hours after seeding

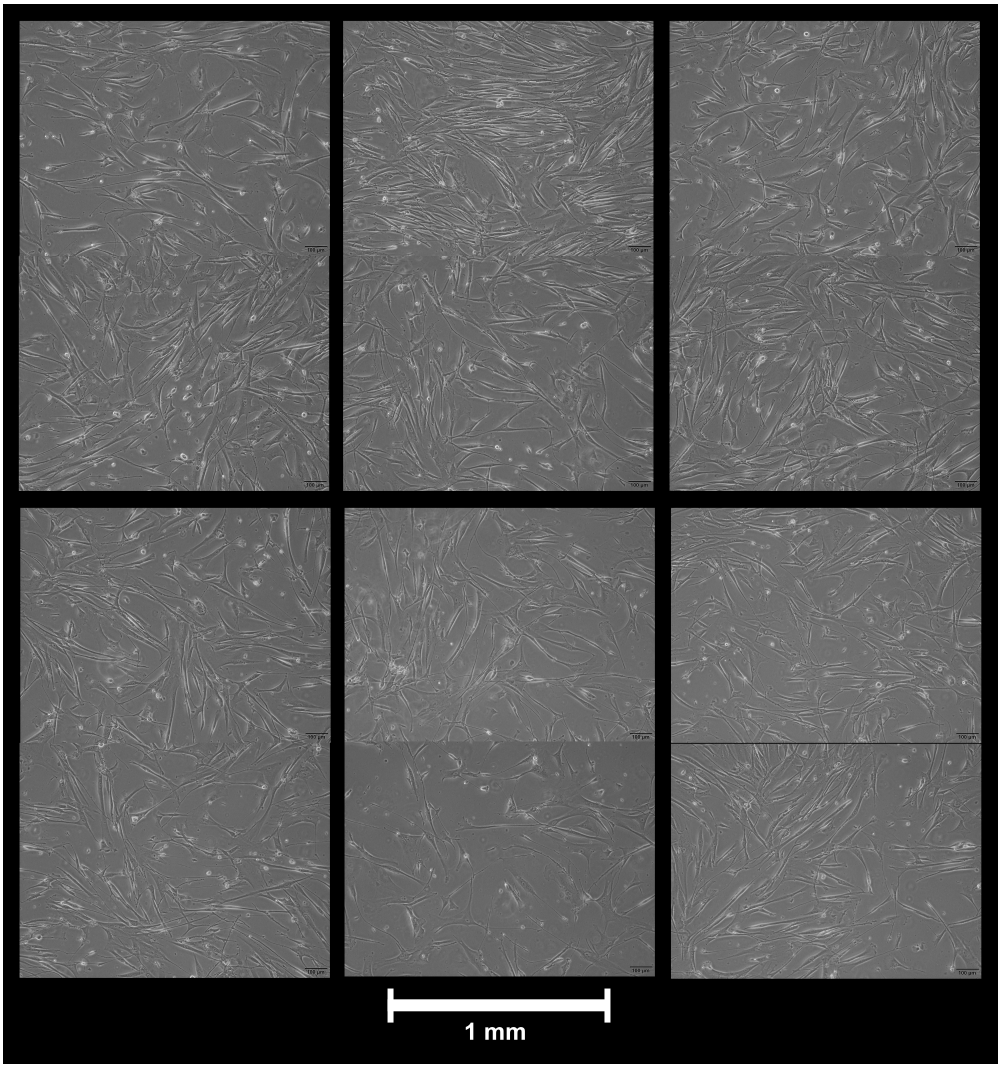


Figure 7.8 Cells in the plate with pronection coating on day 1, 4 hours after seeding

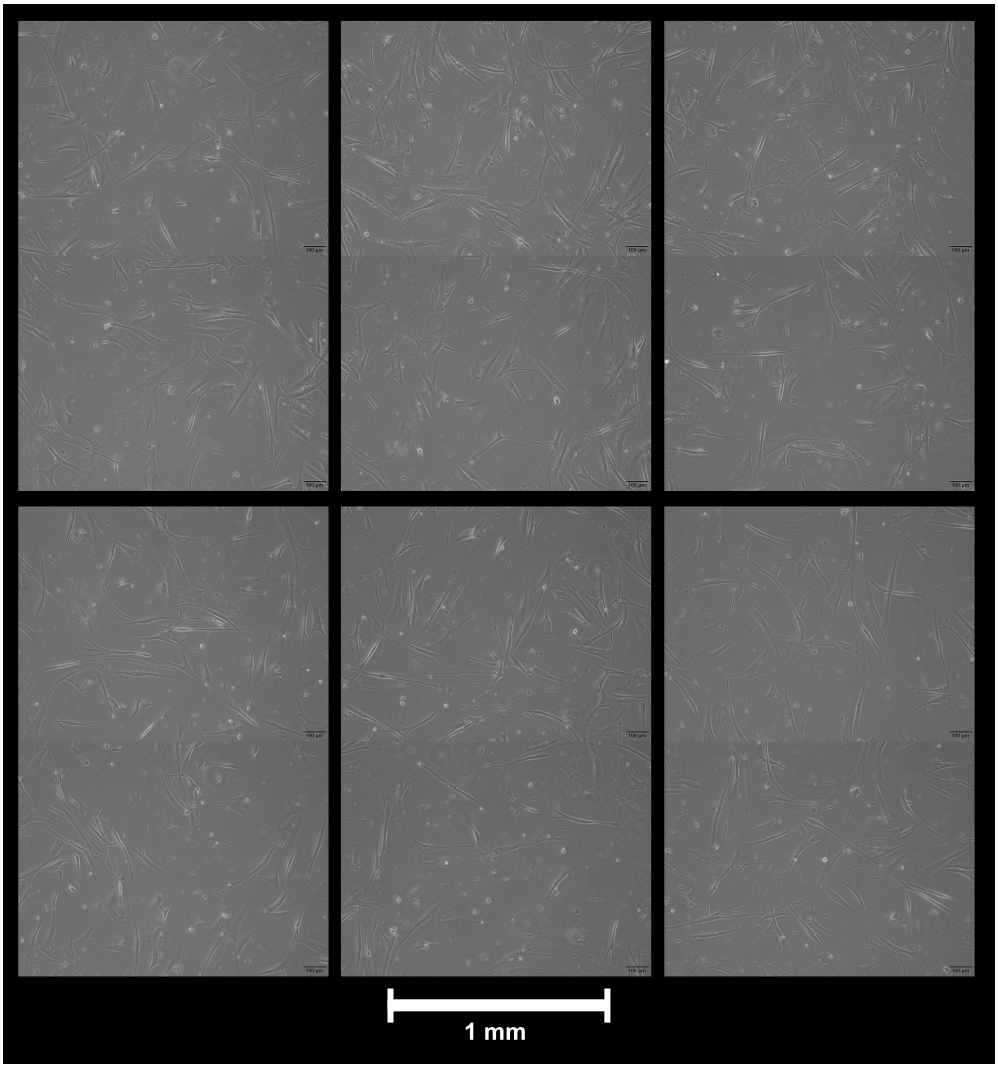


Figure 7.9 Cells in the plate with collagen type I coating on day 1, 4 hours after seeding

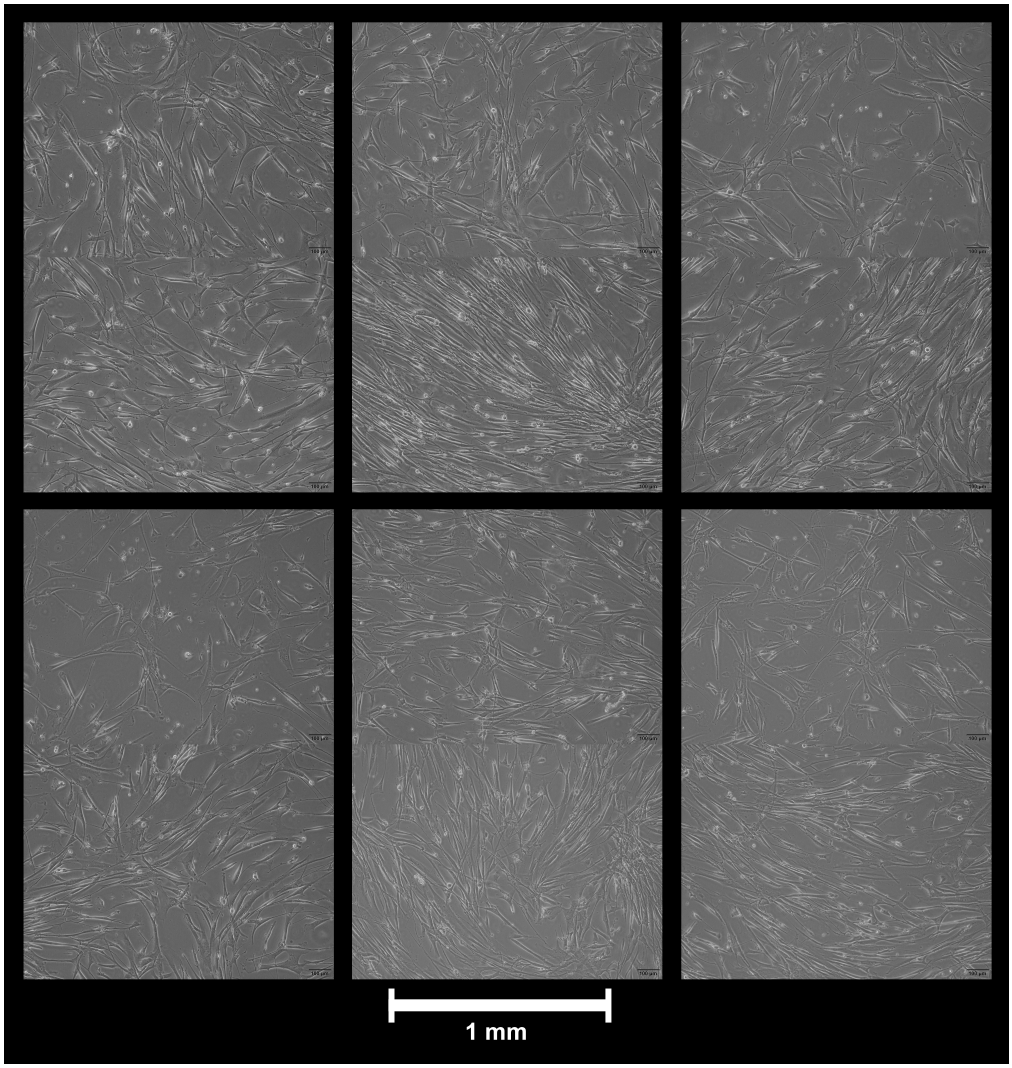


Figure 7.10 Cells in the plate with pronection coating on day 1, 4 hours after seeding

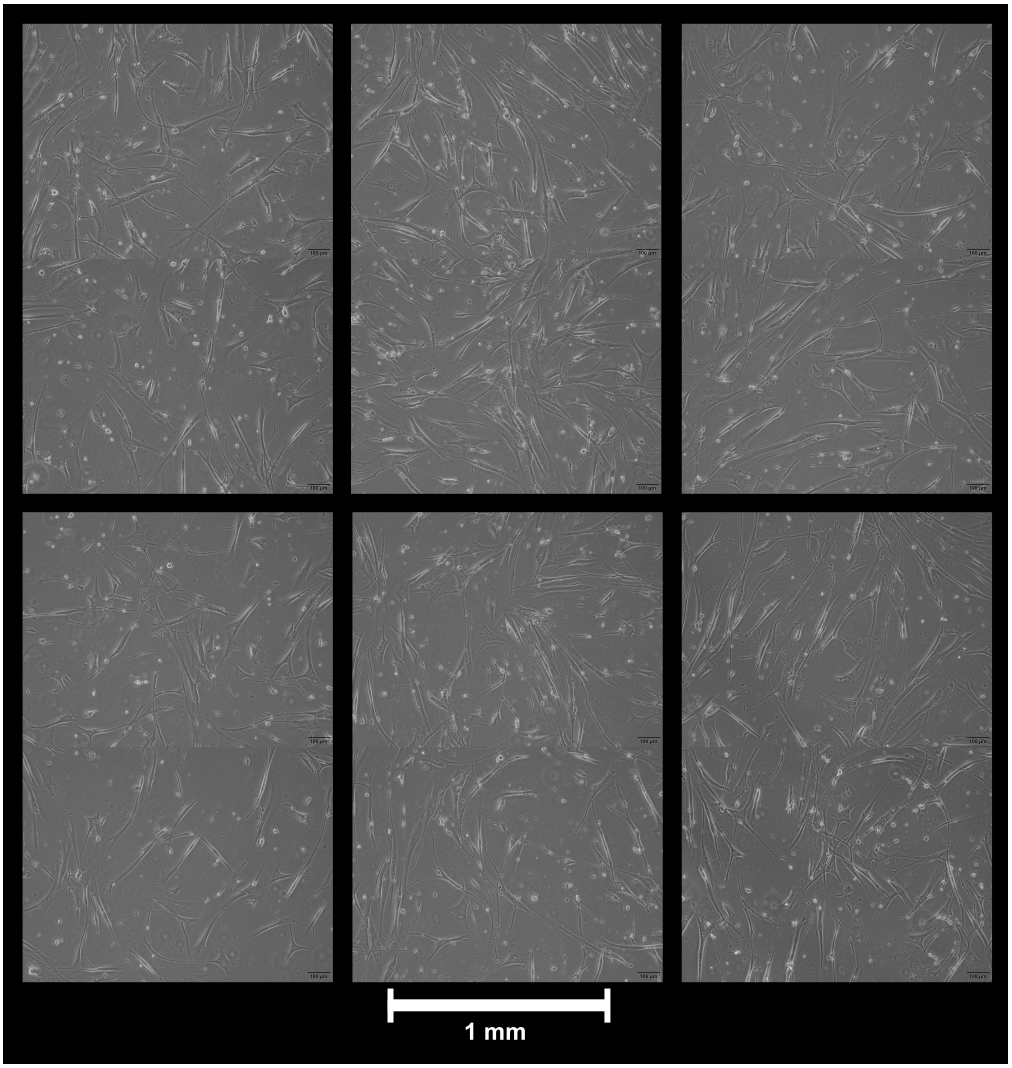


Figure 7.11 Cells in the plate with collagen type I coating on day 1, 4 hours after seeding

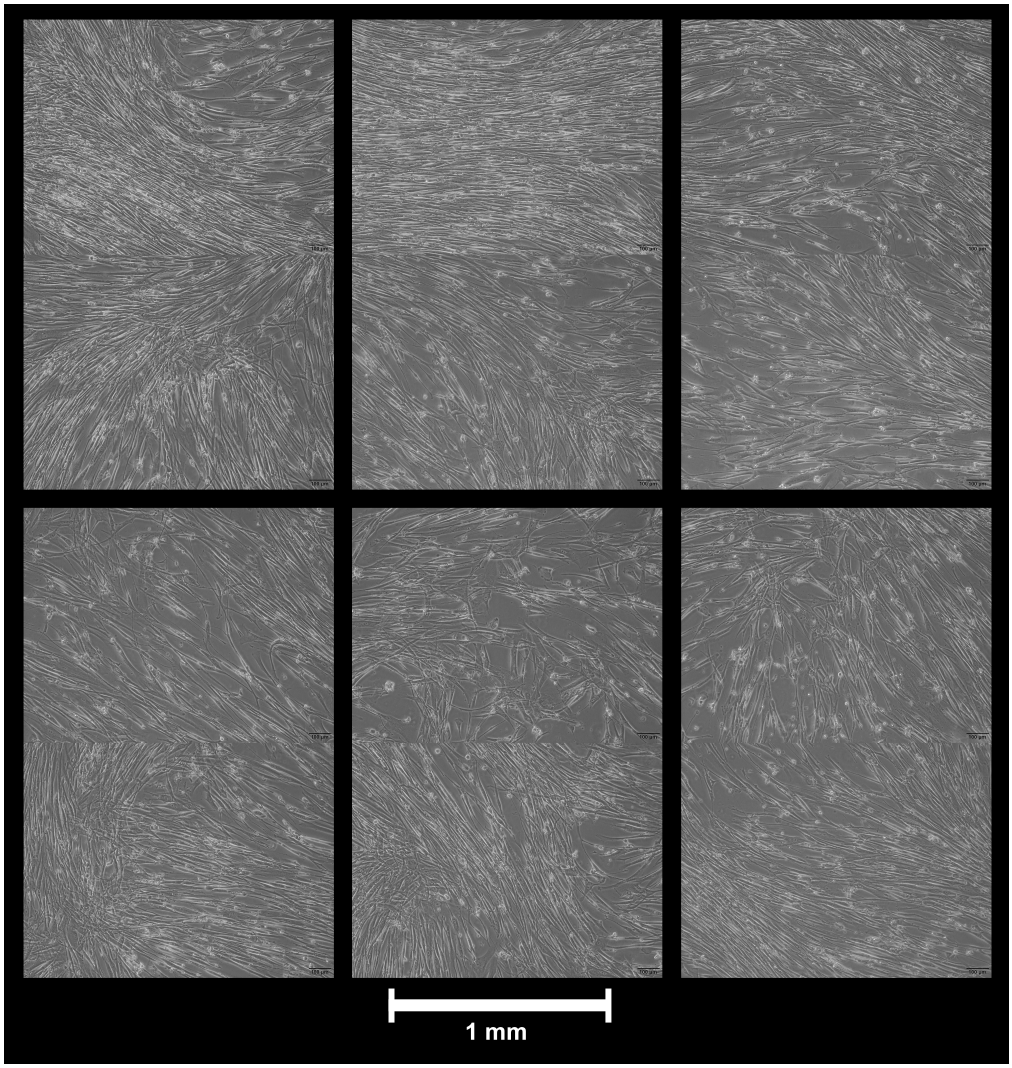


Figure 7.12 Cells in the plate with pronection coating on day 1, 4 hours after seeding

8 Appendix D

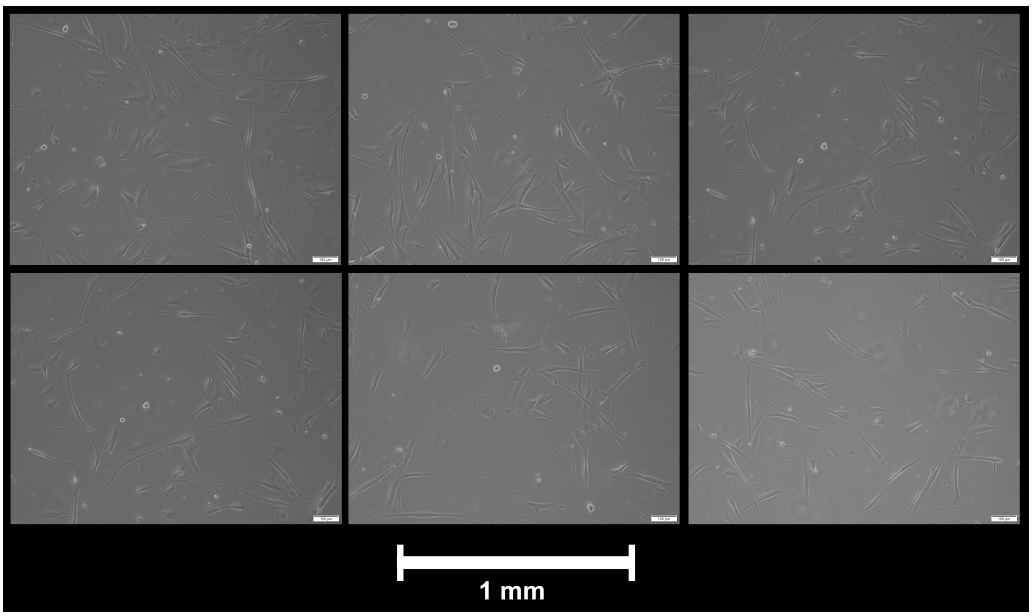


Figure 8.1 Images of the six wells of the static culture of experiment #2, after the vibration period.

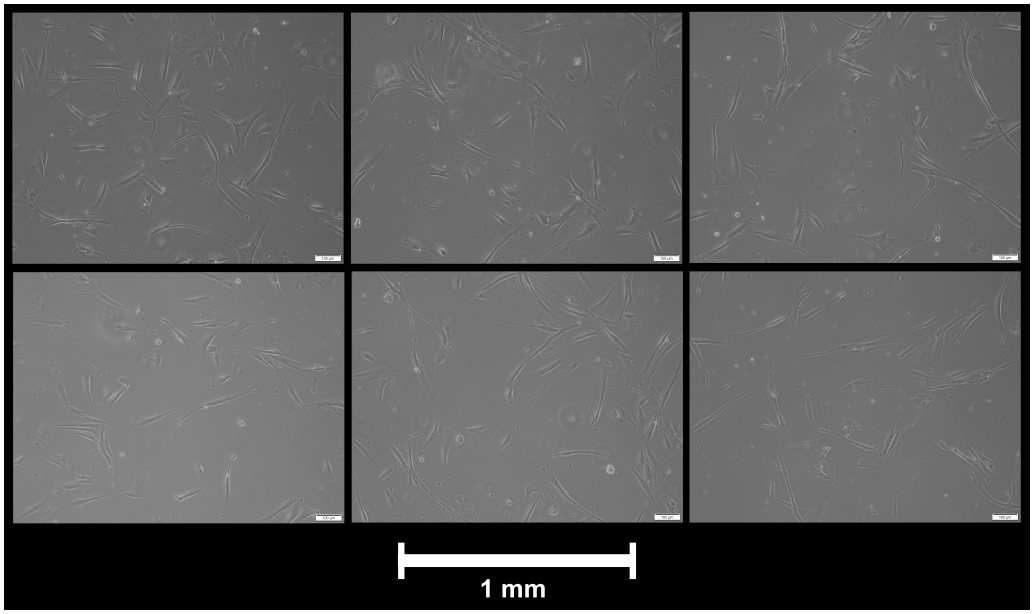


Figure 8.2 Images of the six wells of the vibrated culture plate of experiment #2, after the vibration period.

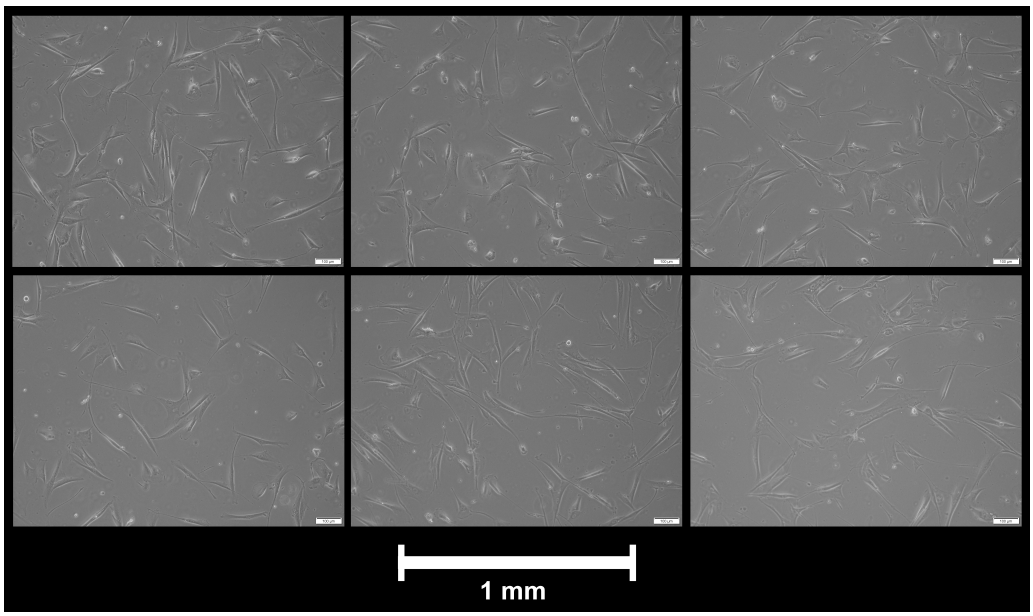


Figure 8.3 Images of the six wells of the static culture of experiment #3, after the vibration period.

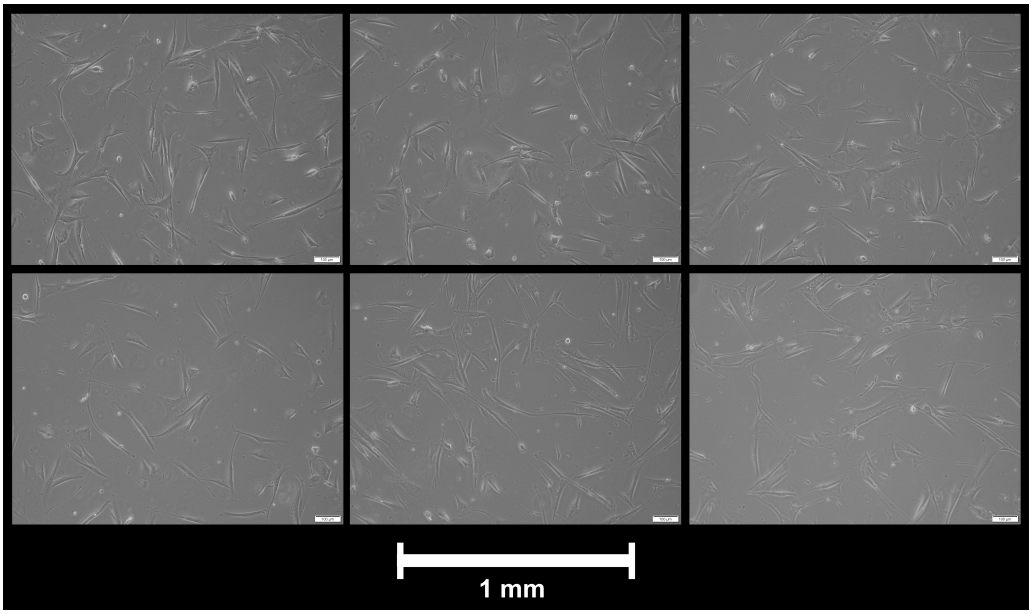


Figure 8.4 Images of the six wells of the vibrated culture plate of experiment #3, after the vibration period.

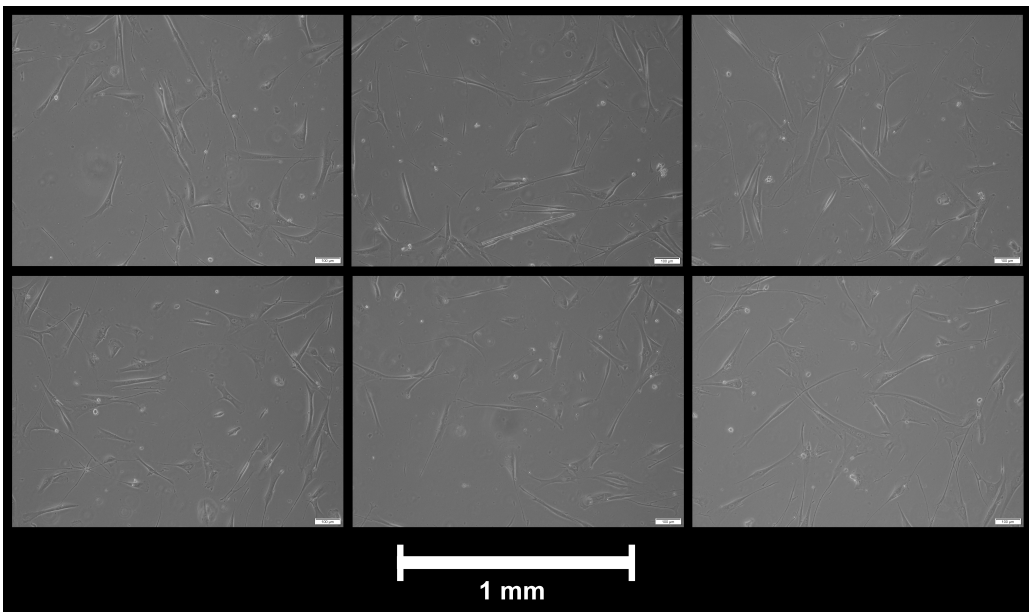


Figure 8.5 Images of the six wells of the static culture of experiment #4, before the vibration period.

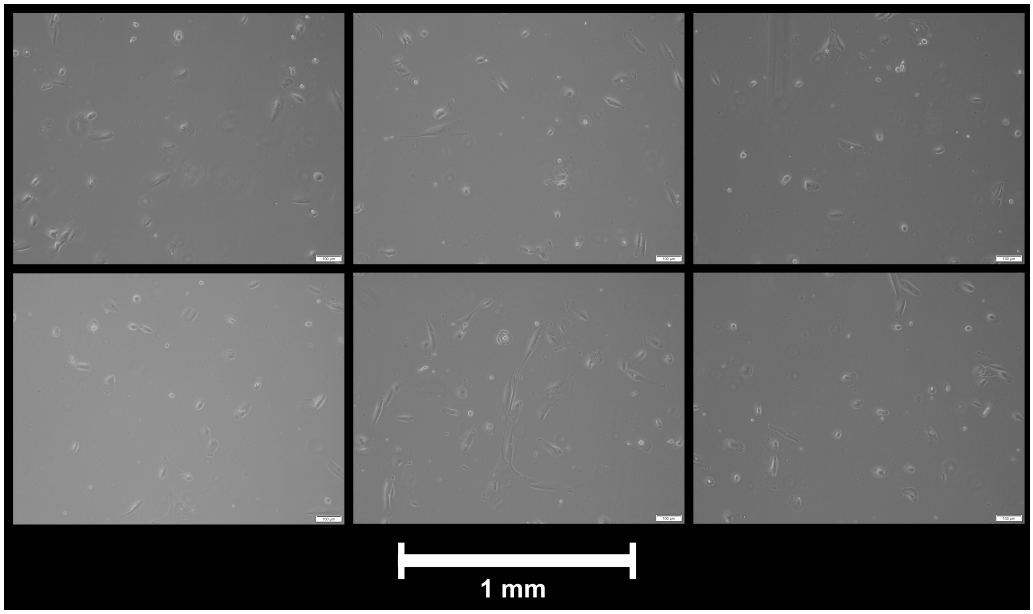


Figure 8.6 Images of the six wells of the vibrated culture plate of experiment #4, before the vibration period.

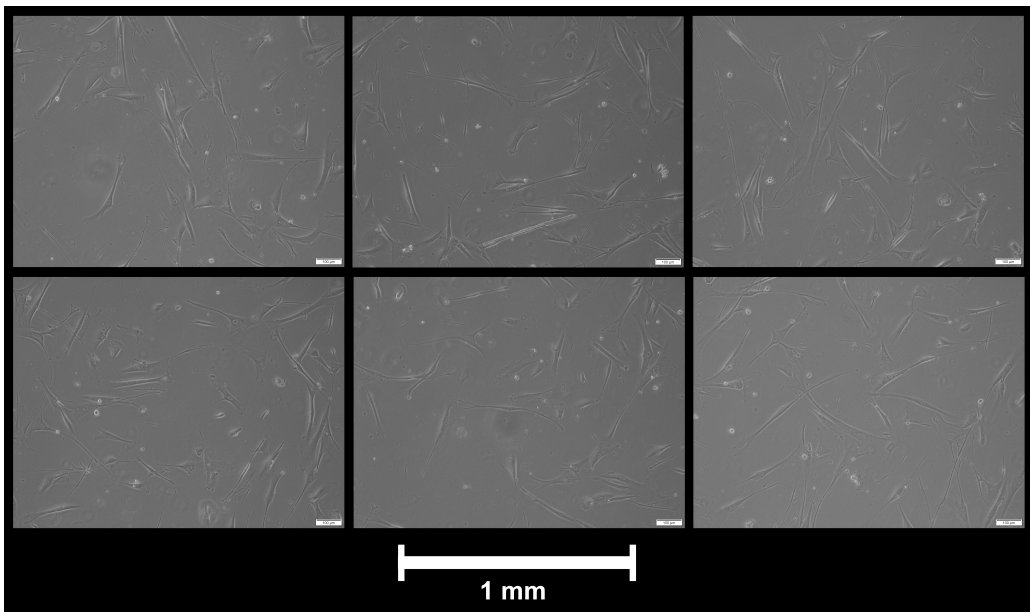


Figure 8.7 Images of the six wells of the static culture of experiment #4, after the vibration period.

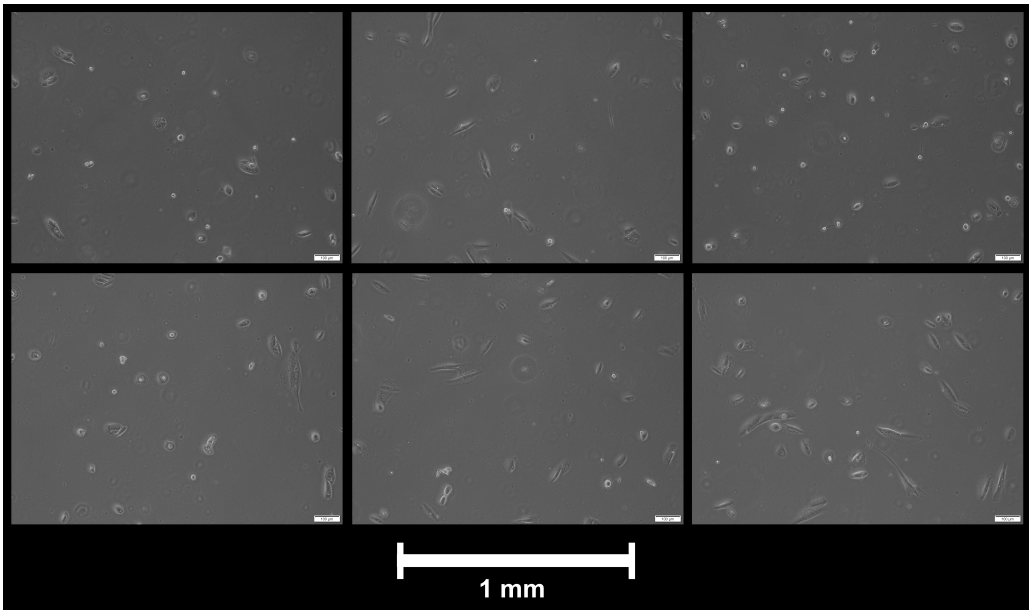


Figure 8.8 Images of the six wells of the vibrated culture plate of experiment #4, after the vibration period.

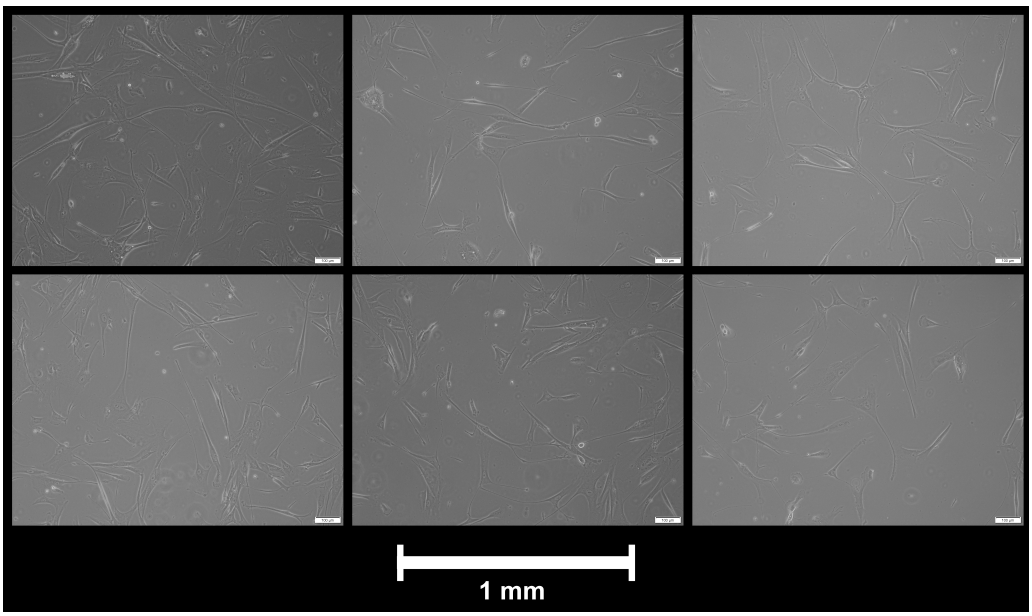


Figure 8.9 Images of the six wells of the static culture of experiment #5, before the vibration period.

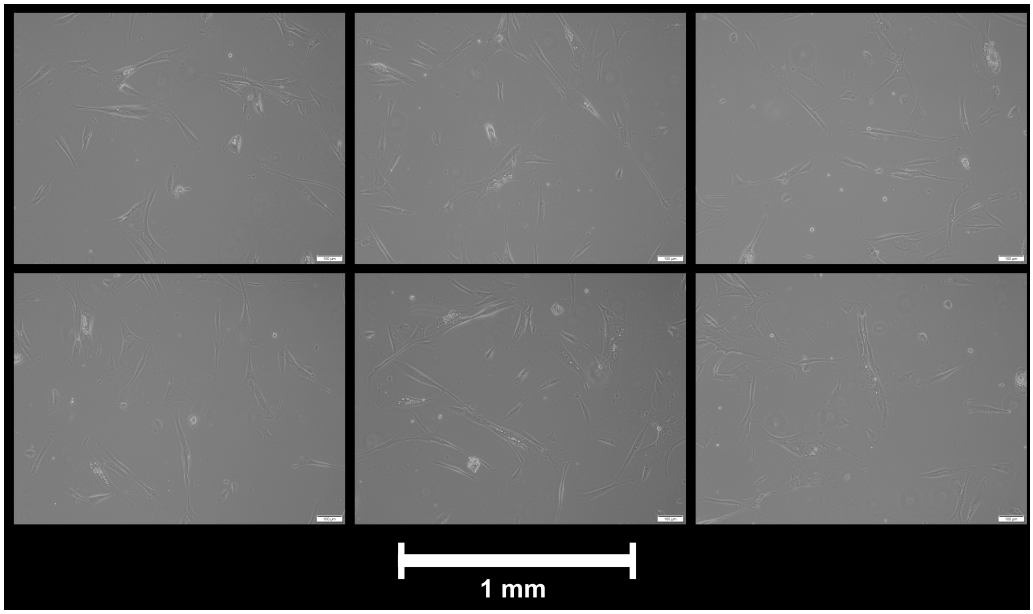


Figure 8.10 Images of the six wells of the vibrated culture plate of experiment #5, before the vibration period.

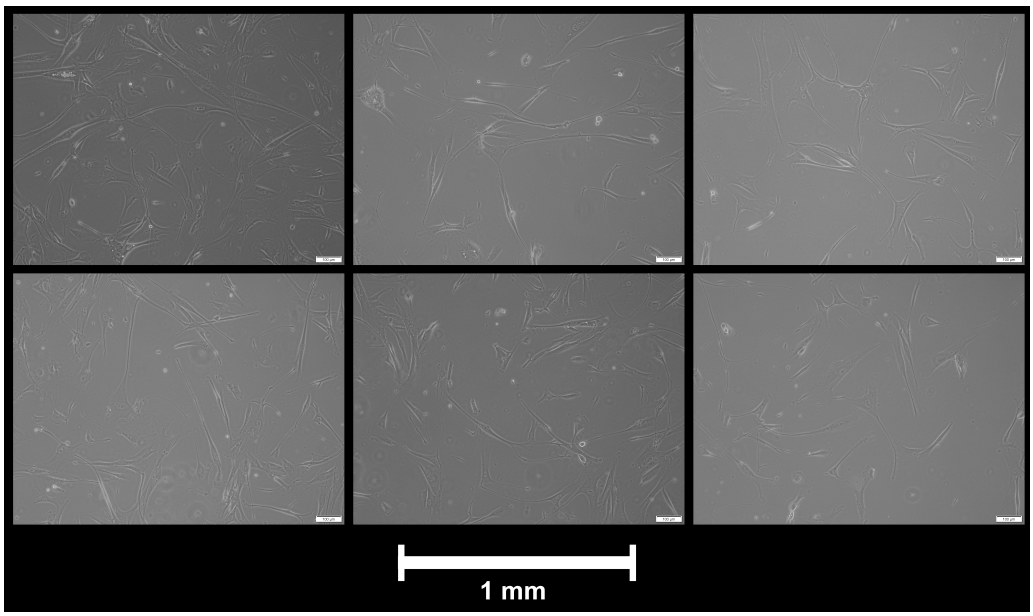


Figure 8.11 Images of the six wells of the static culture of experiment #5, after the vibration period.

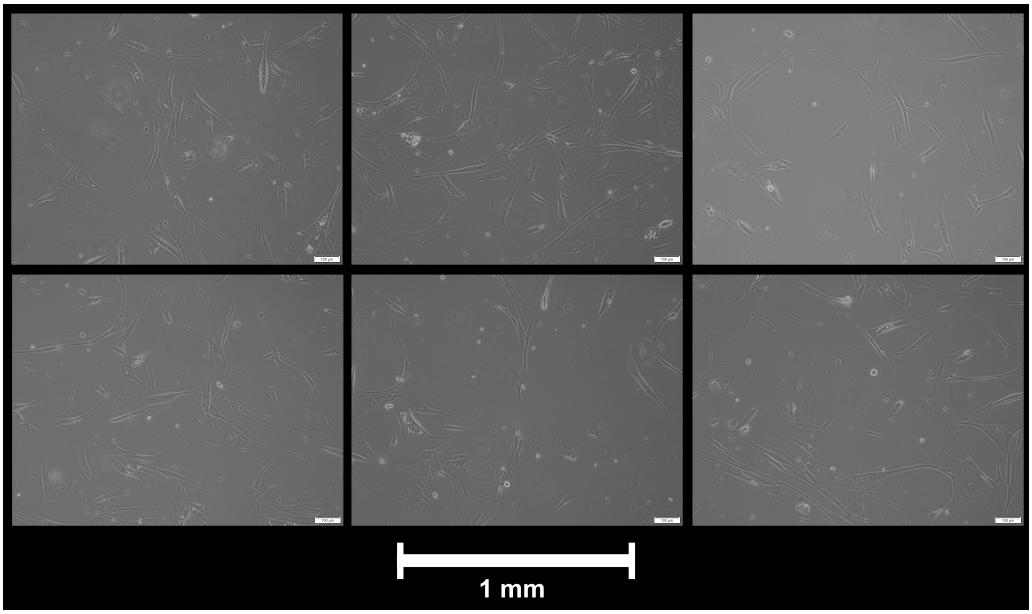


Figure 8.12 Images of the six wells of the vibrated culture plate of experiment #5, after the vibration period.

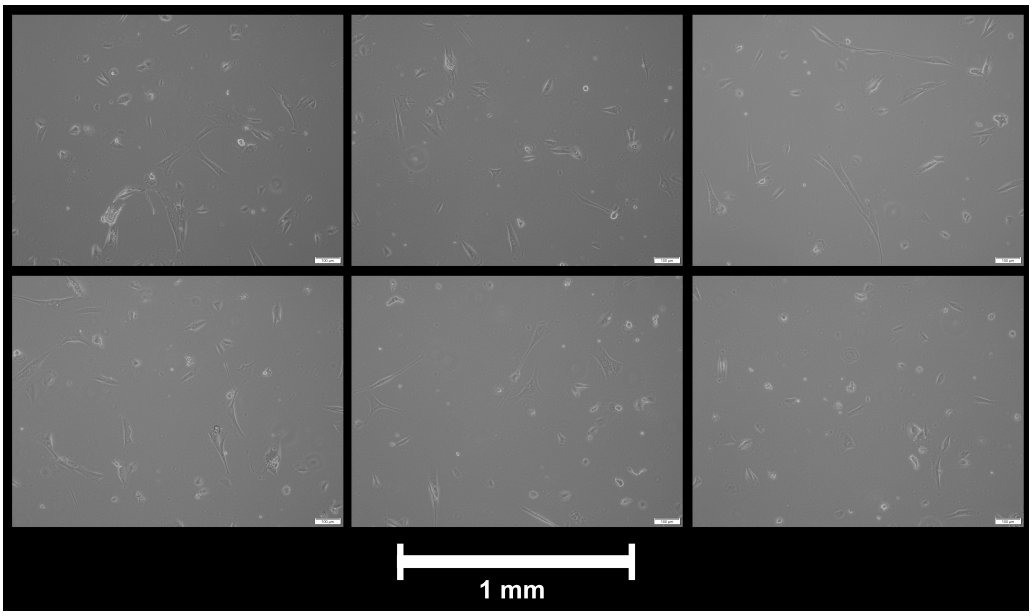


Figure 8.13 Images of the six wells of the static culture of experiment #6, before the vibration period. There was a contamination visible after the vibration period, so the experiment was restarted.

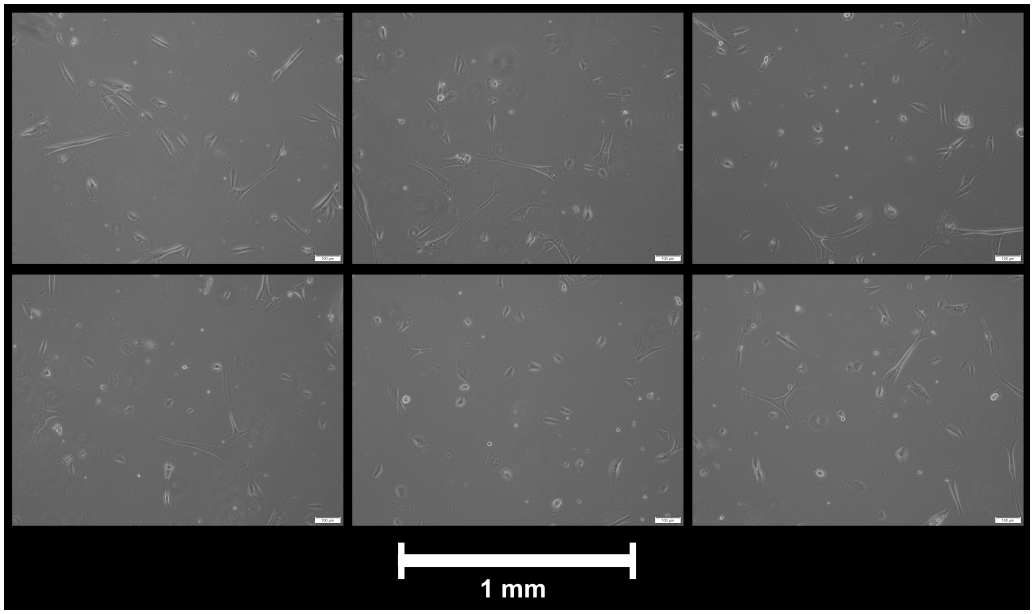


Figure 8.14 Images of the six wells of the vibrated culture plate of experiment #6, before the vibration period. There was a contamination visible after the vibration period, so the experiment was restarted.

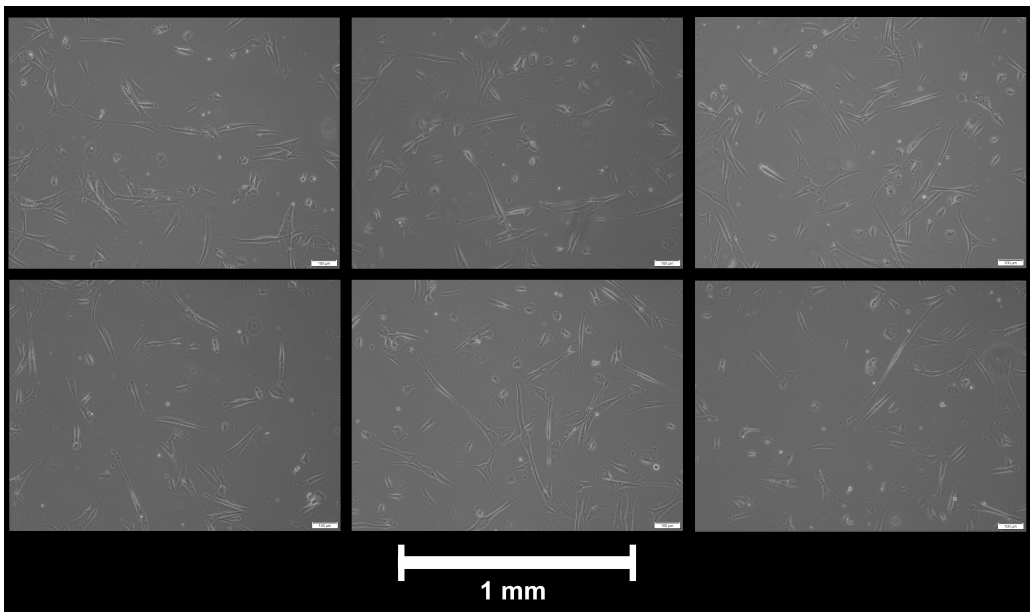


Figure 8.15 Images of the six wells of the static culture of experiment #6, before the vibration period.

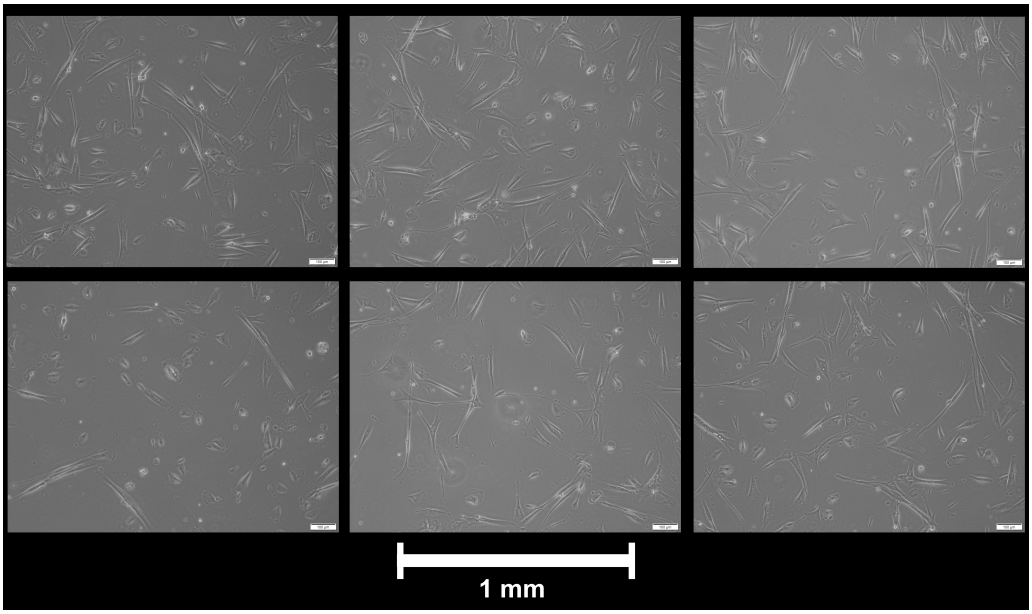


Figure 8.16 Images of the six wells of the vibrated culture plate of experiment #6, before the vibration period.

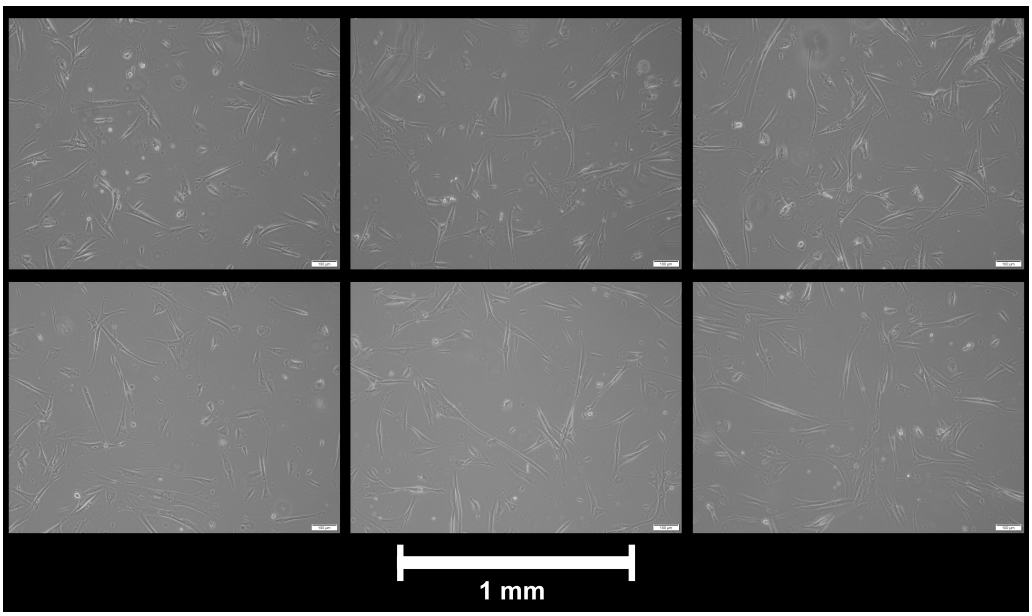


Figure 8.17 Images of the six wells of the static culture of experiment #6, after the vibration period.

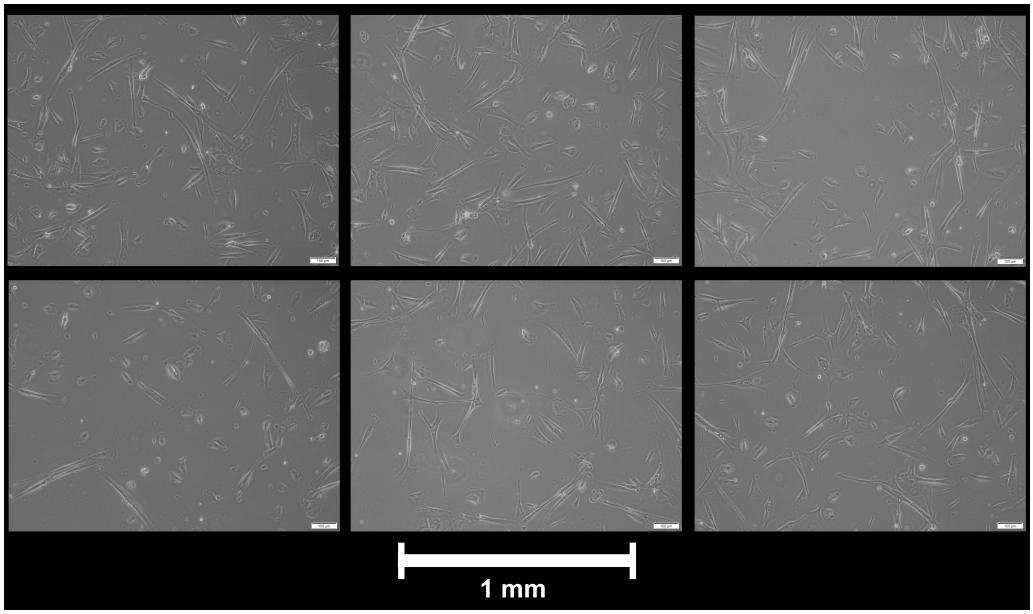
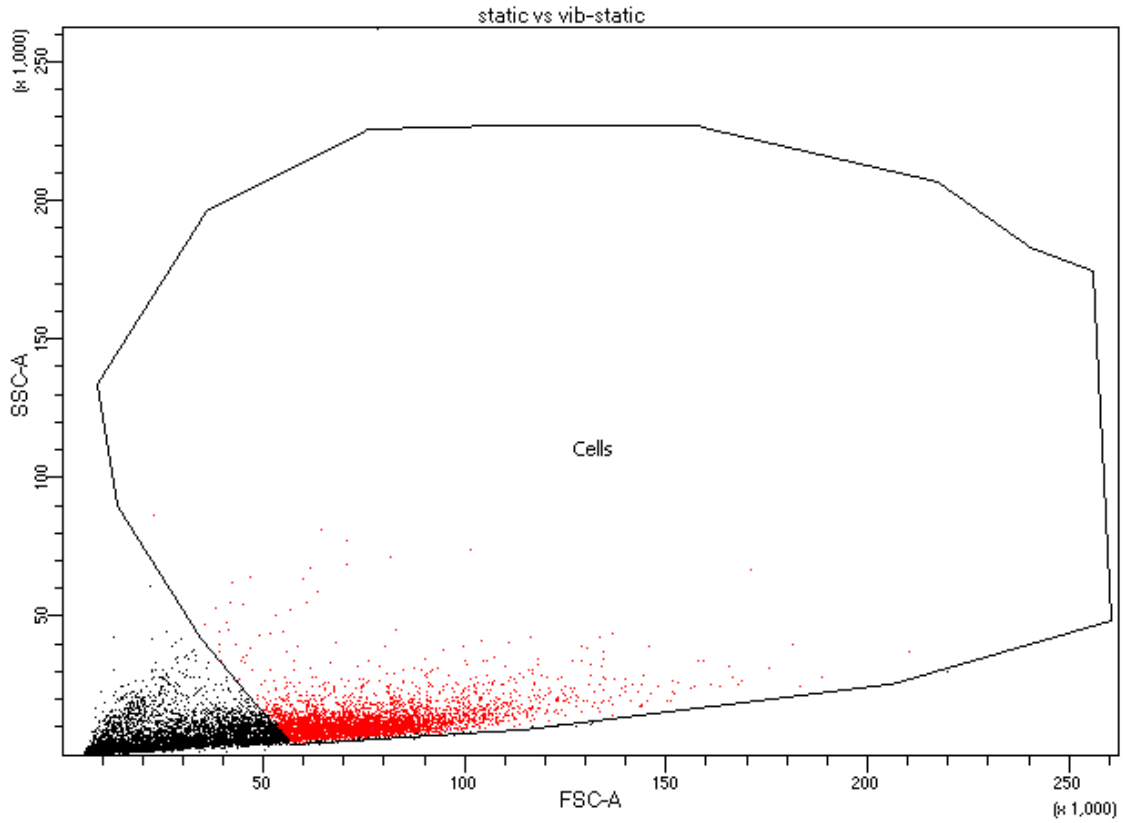
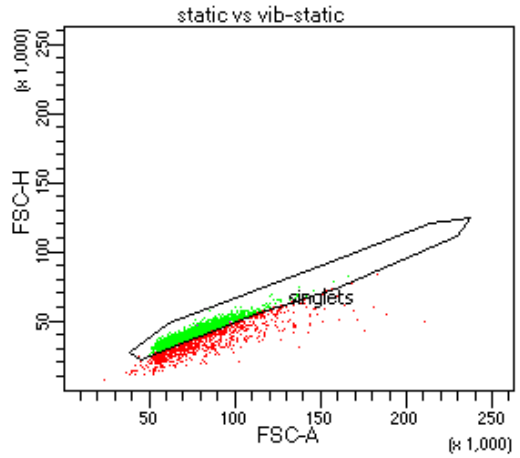
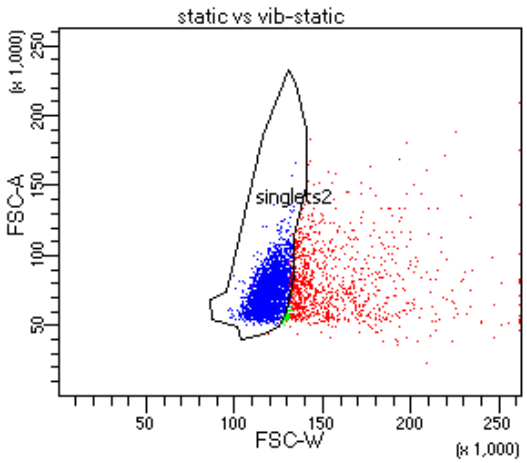


Figure 8.18 Images of the six wells of the vibrated culture plate of experiment #6, after the vibration period.

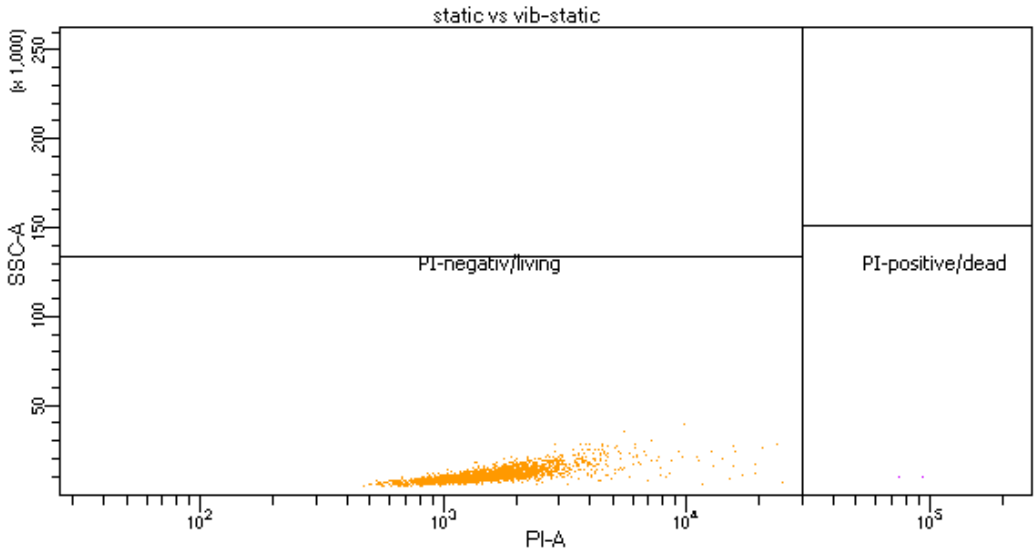
Experiment #1 static stained

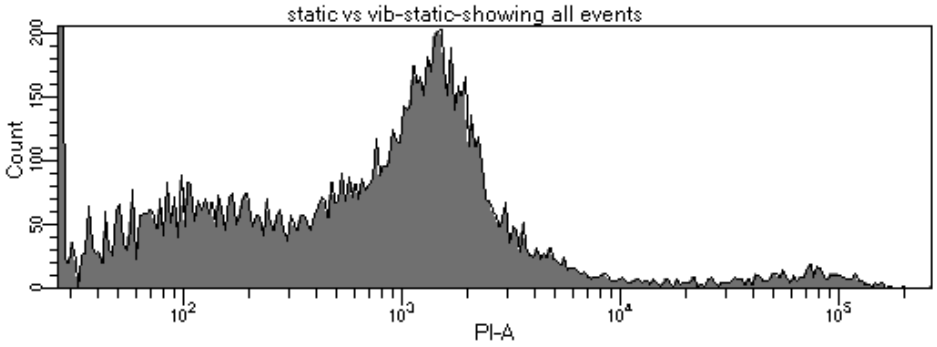


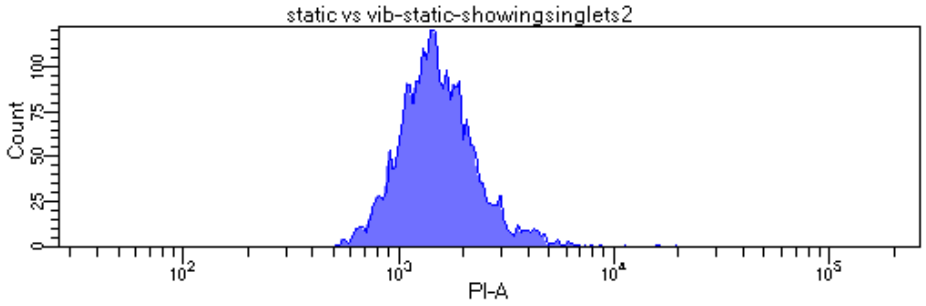




Experiment #1 static stained



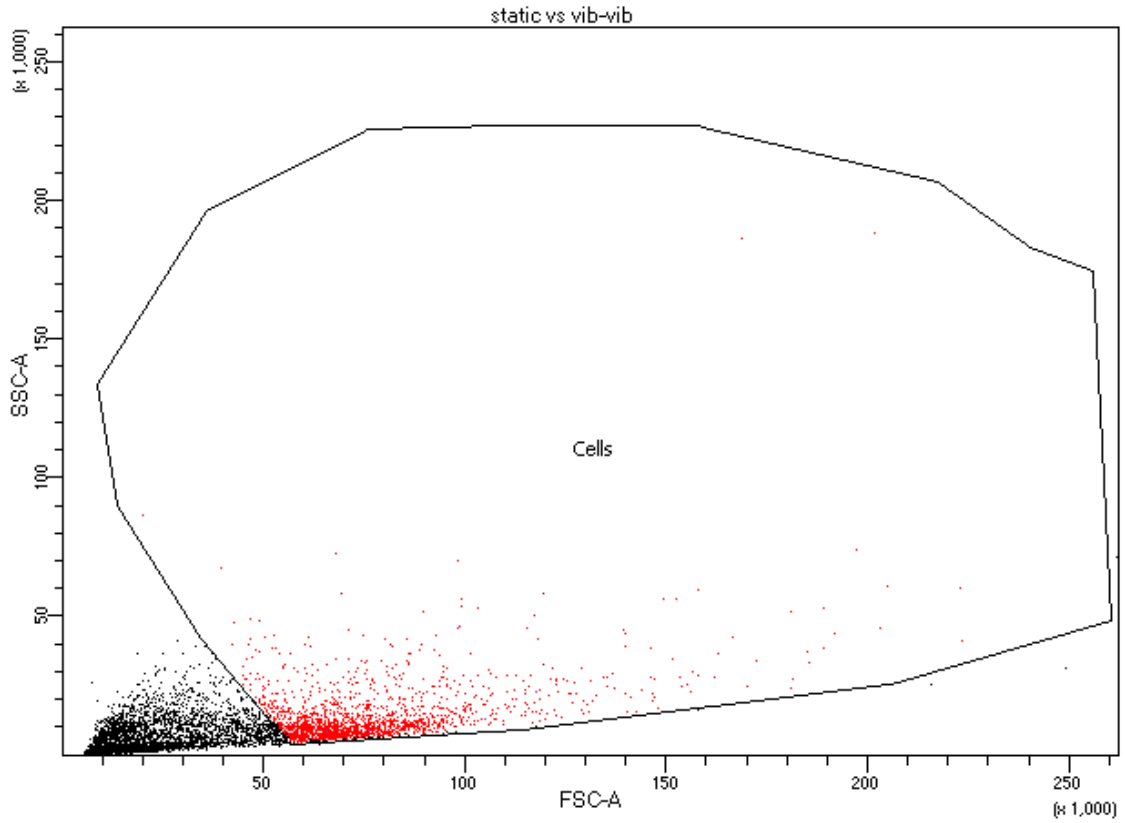


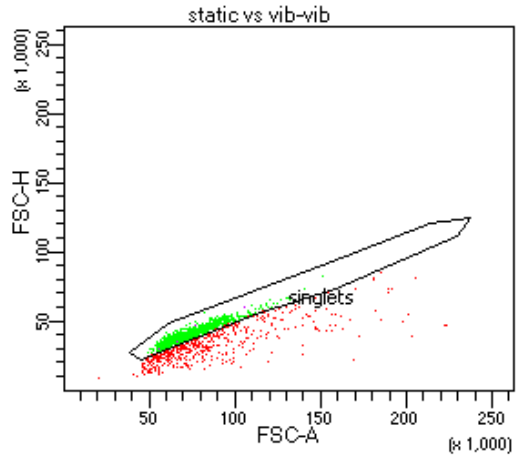


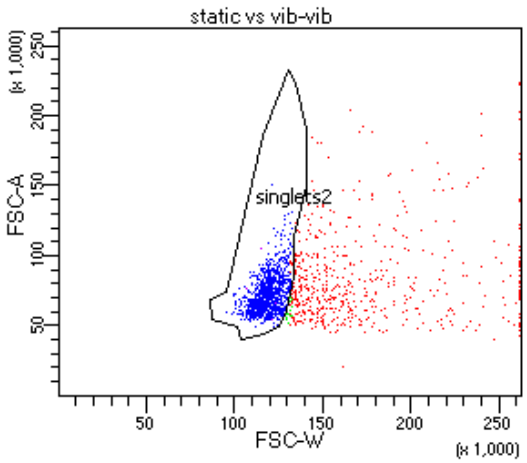
Tube: static

Population	#Events	%Parent	%Total
All Events	12,538	####	100.0
Cells	3,898	31.1	31.1
singlets	2,898	74.3	23.1
singlets2	2,866	98.9	22.9
PI-negativ/living	2,864	99.9	22.8
PI-positive/dead	2	0.1	0.0

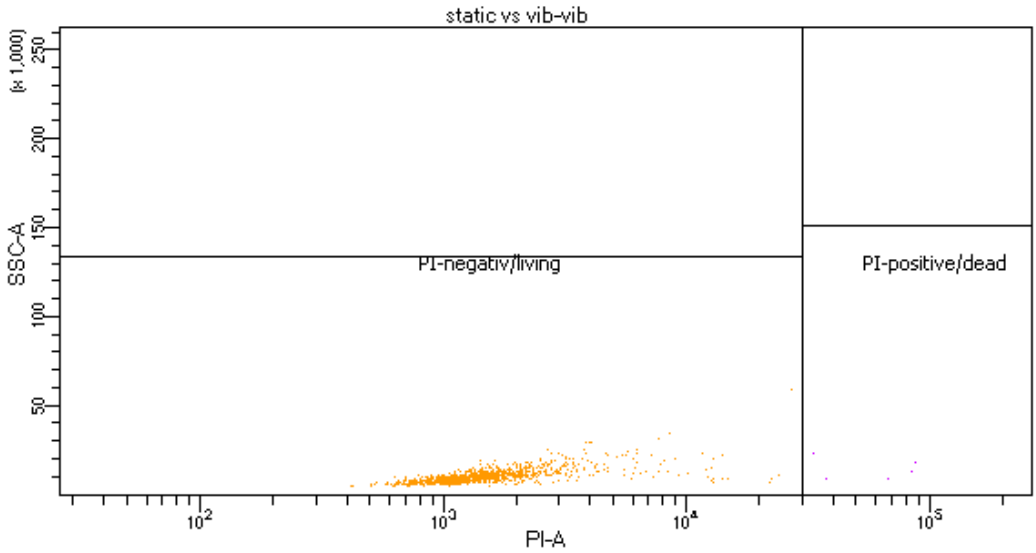
Experiment #1 vibrated stained

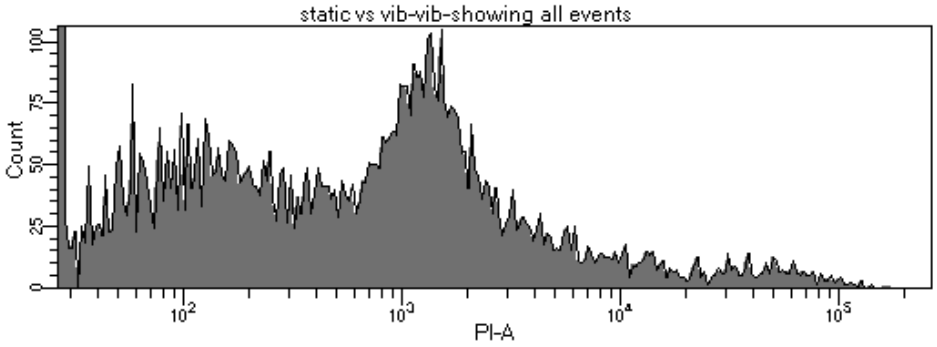


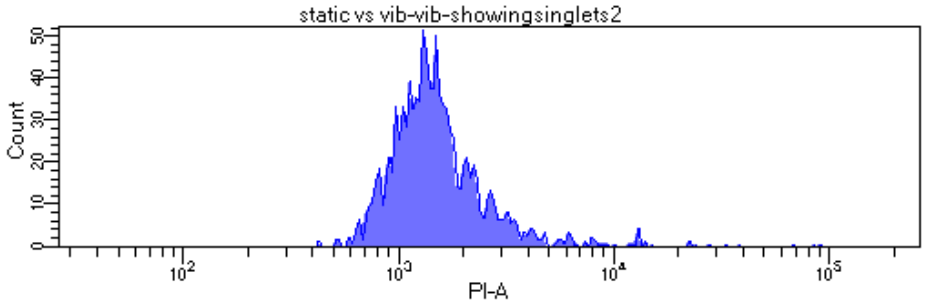




Experiment #1 vibrated stained



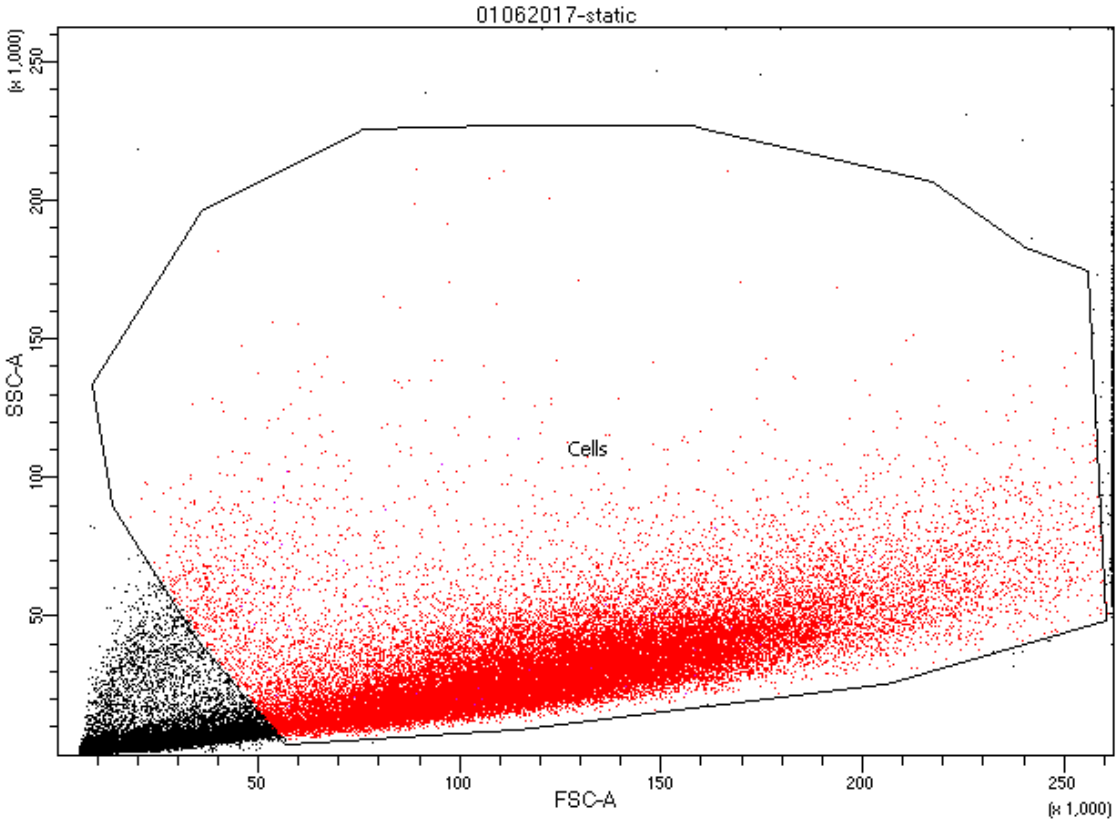


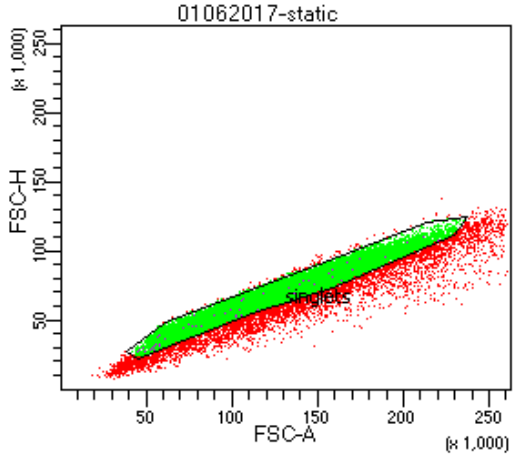


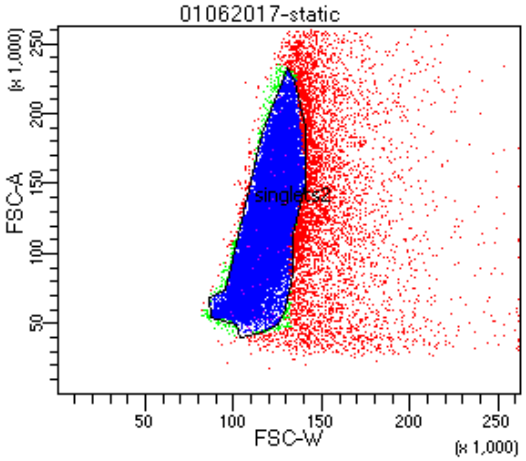
Tube: vib

Population	#Events	%Parent	%Total
All Events	8,228	####	100.0
Cells	1,671	20.3	20.3
singlets	1,121	67.1	13.6
singlets2	1,102	98.3	13.4
PI-negativ/living	1,097	99.5	13.3
PI-positive/dead	5	0.5	0.1

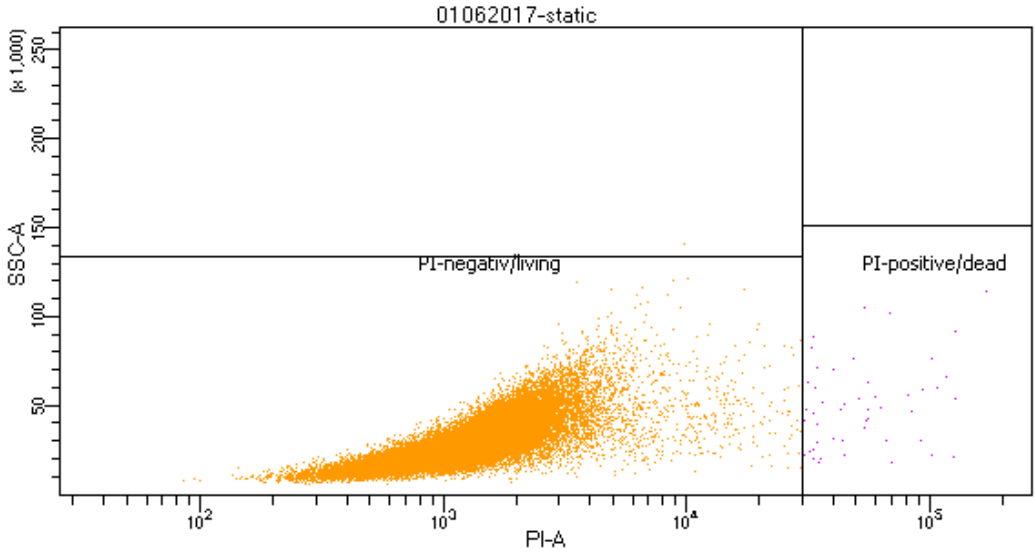
Experiment #2 static stained

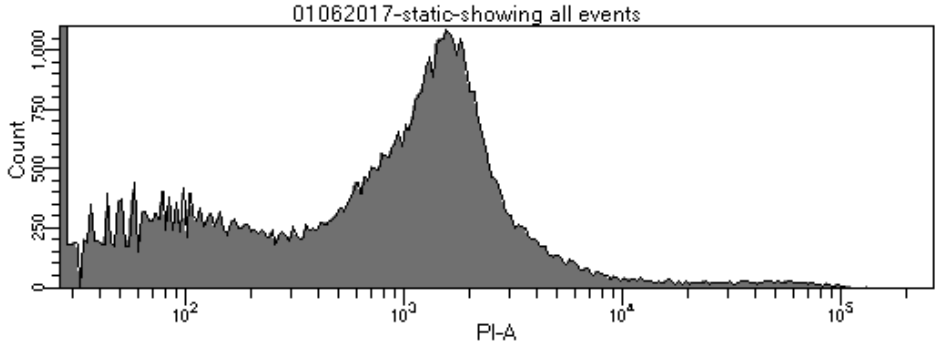


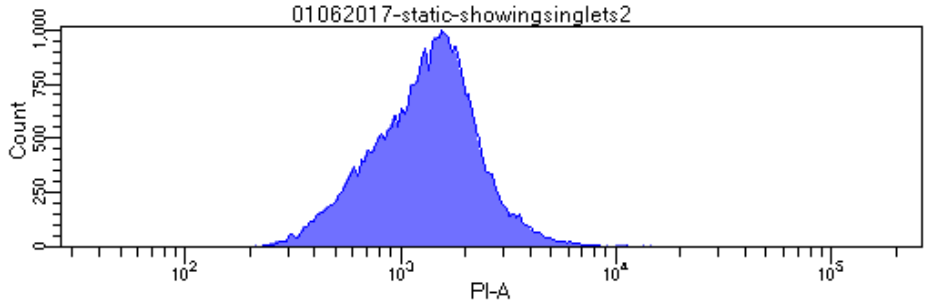




Experiment #2 static stained



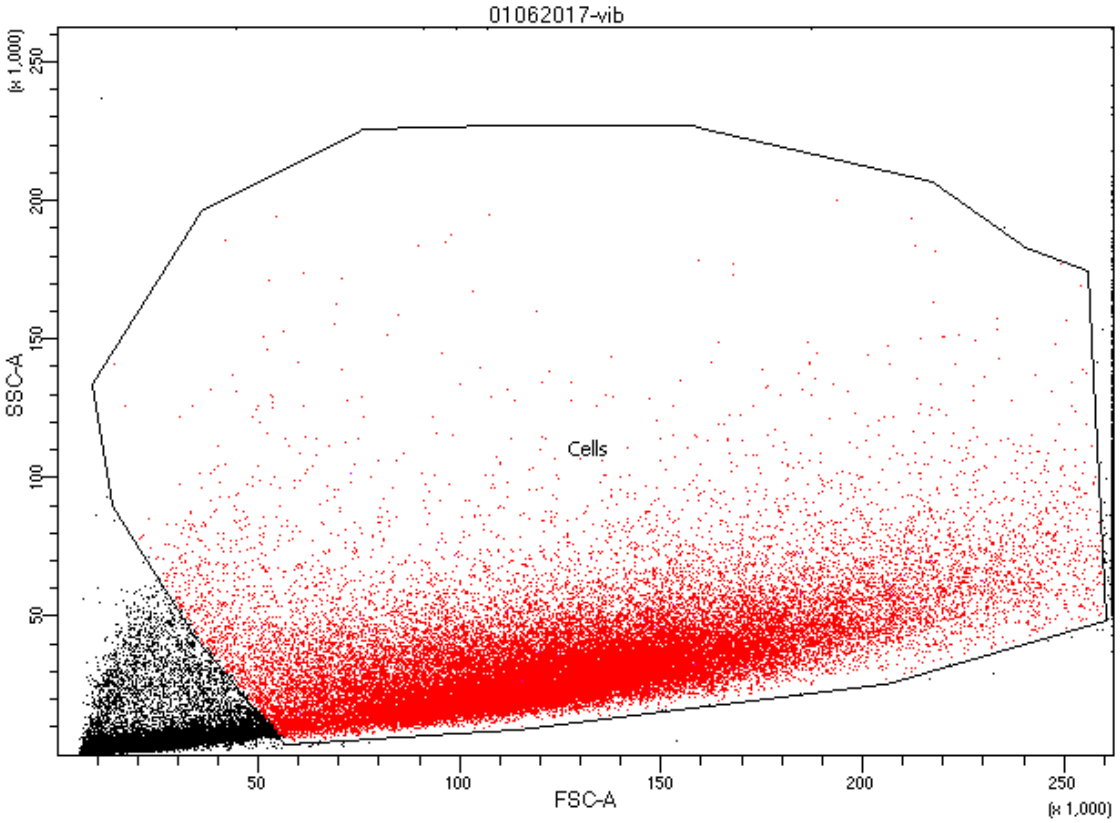


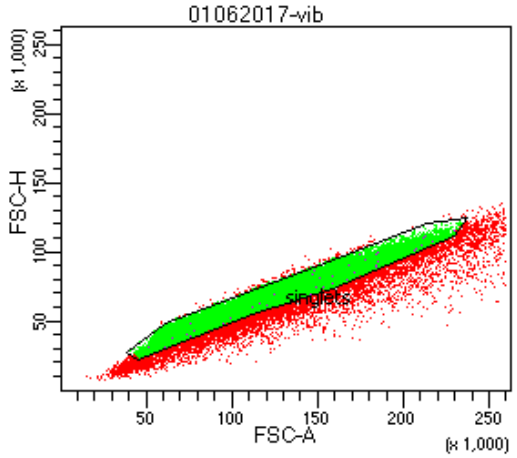


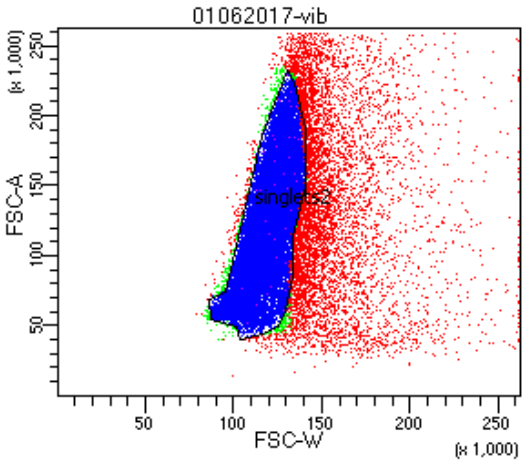
Tube: static

Population	#Events	%Parent	%Total
All Events	70,000	####	100.0
Cells	39,252	56.1	56.1
singlets	34,375	87.6	49.1
singlets2	34,031	99.0	48.6
PI-negativ/living	33,983	99.9	48.5
PI-positive/dead	48	0.1	0.1

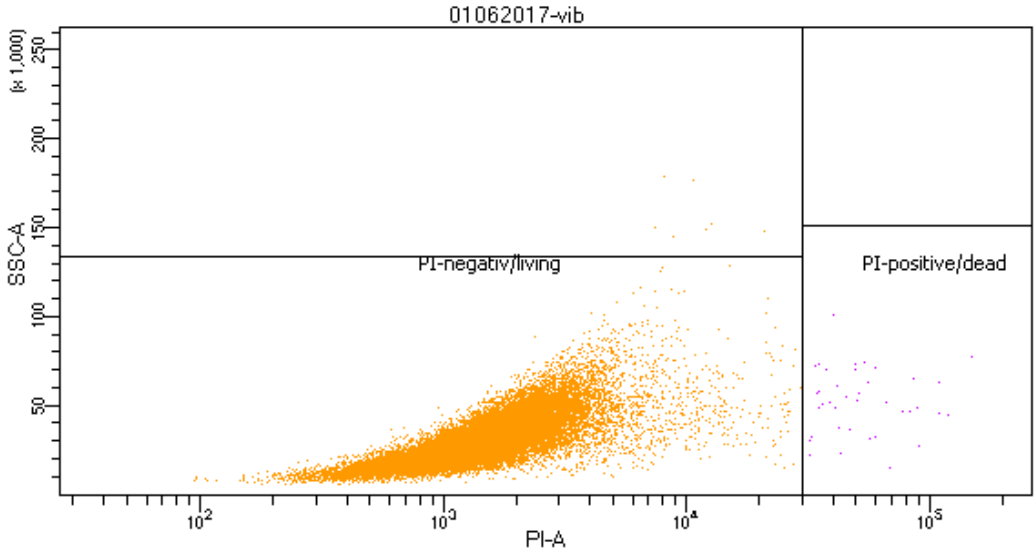
Experiment #2 vibrated stained

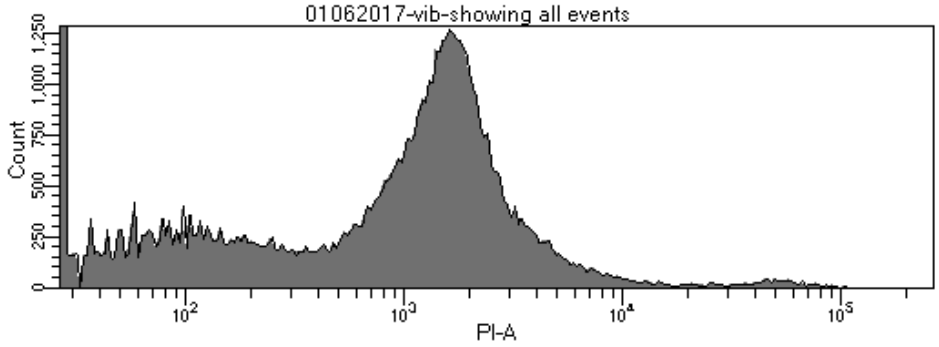


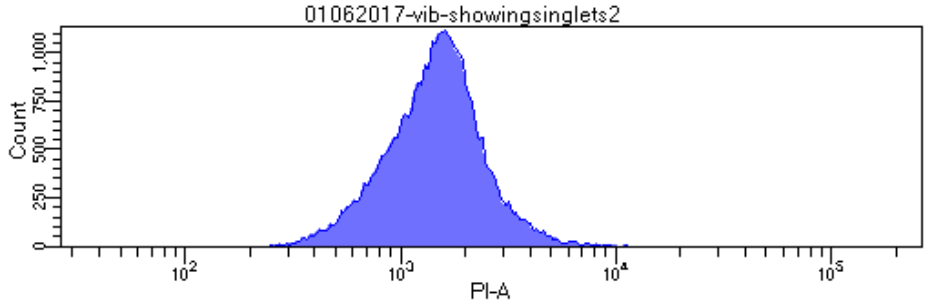




Experiment #2 vibrated stained



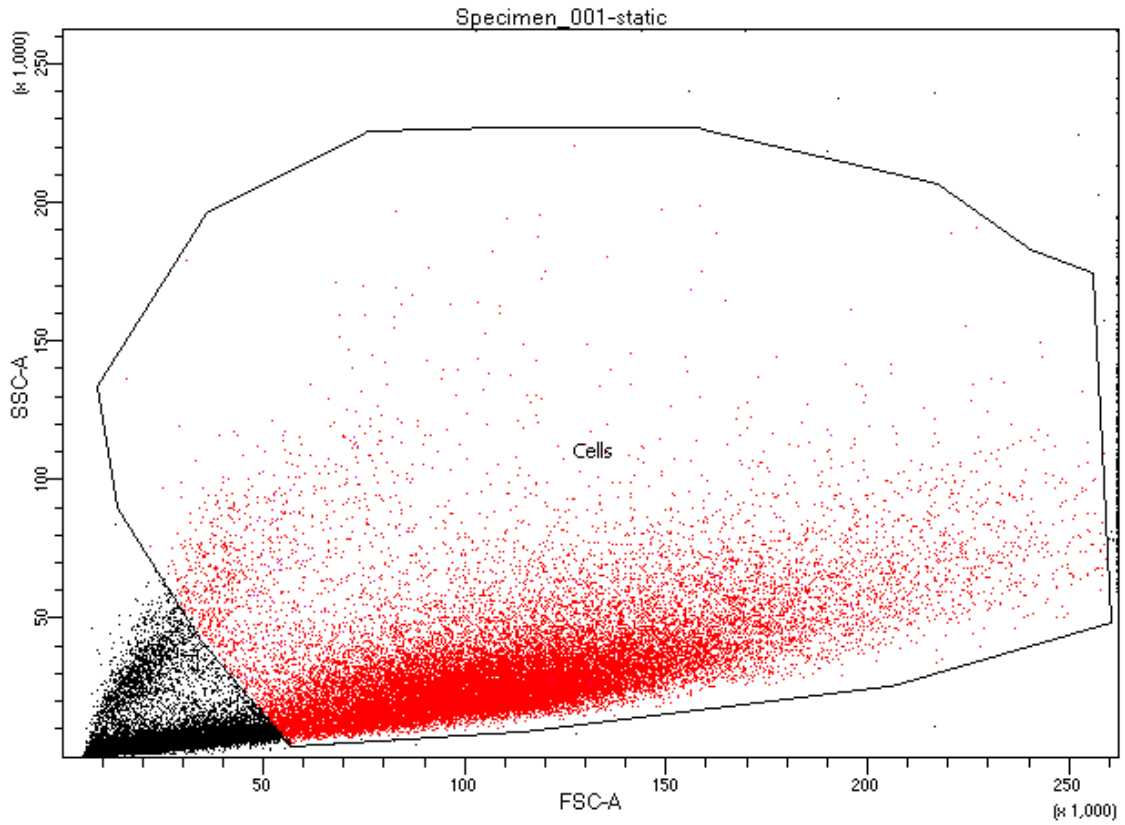


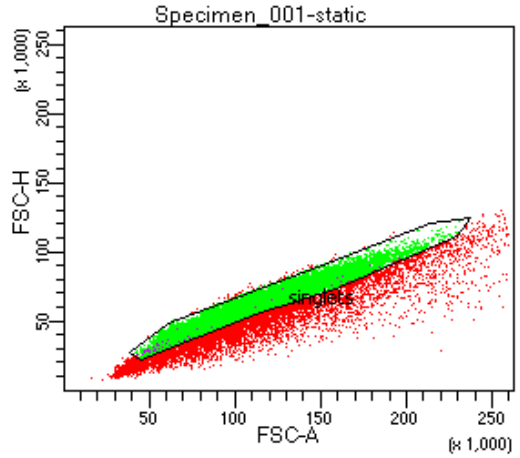


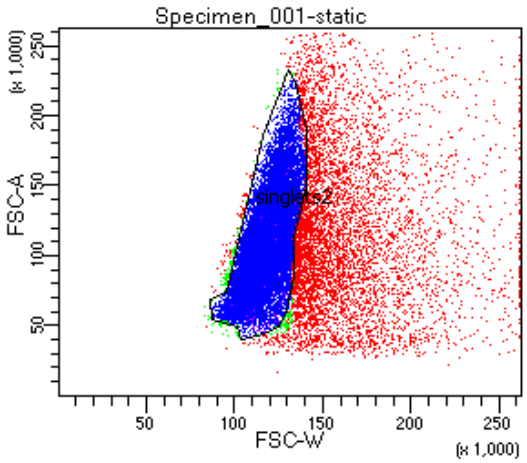
Tube: vib

Population	#Events	%Parent	%Total
All Events	70,000	####	100.0
Cells	41,912	59.9	59.9
singlets	35,226	84.0	50.3
singlets2	34,801	98.8	49.7
PI-negativ/living	34,762	99.9	49.7
PI-positive/dead	39	0.1	0.1

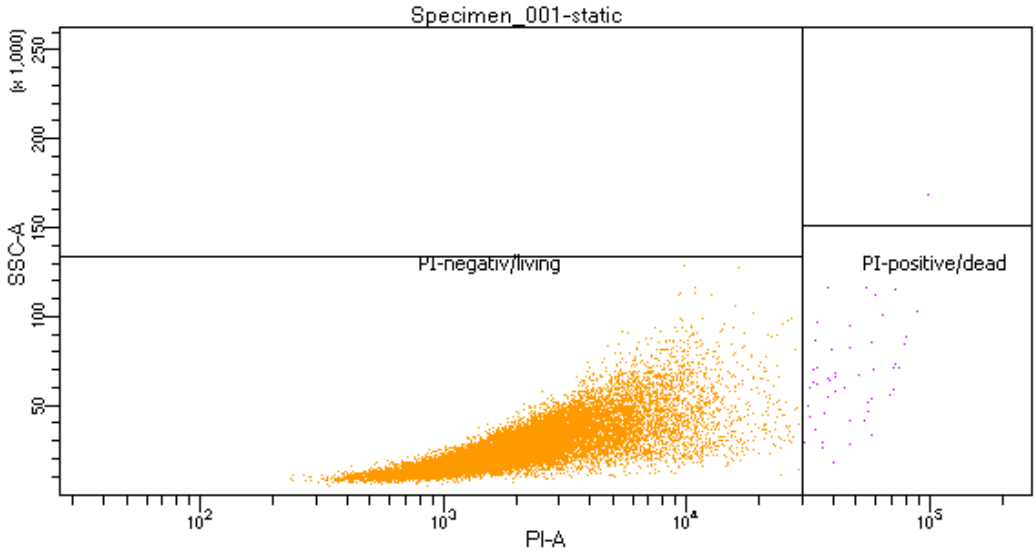
Experiment #3 static stained

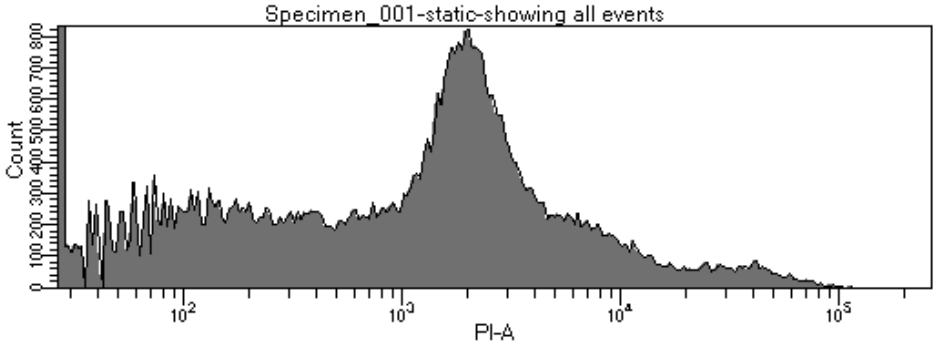


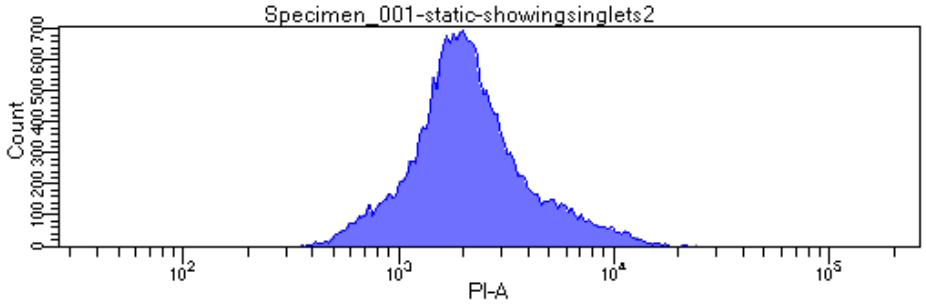




Experiment #3 static stained



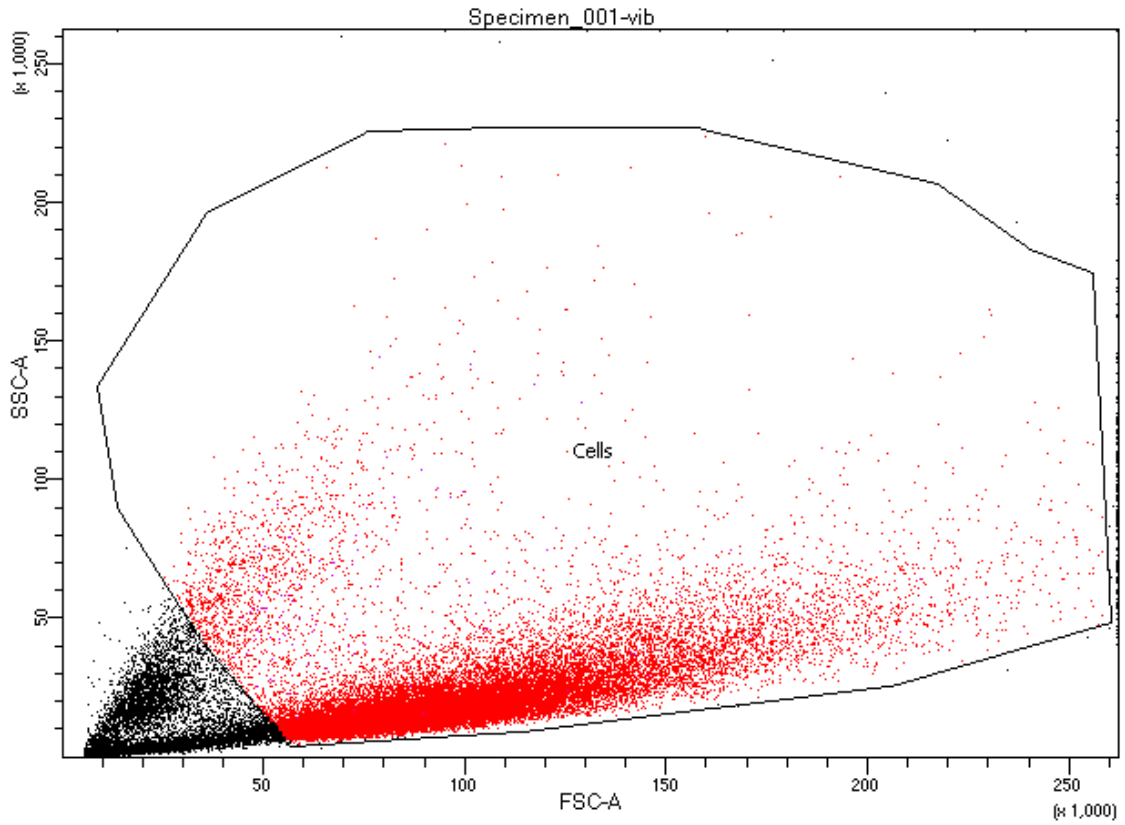


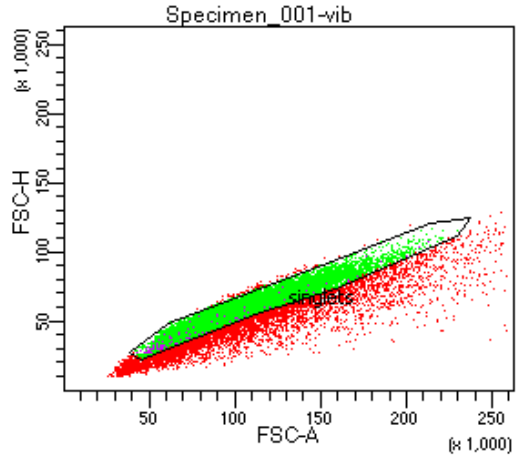


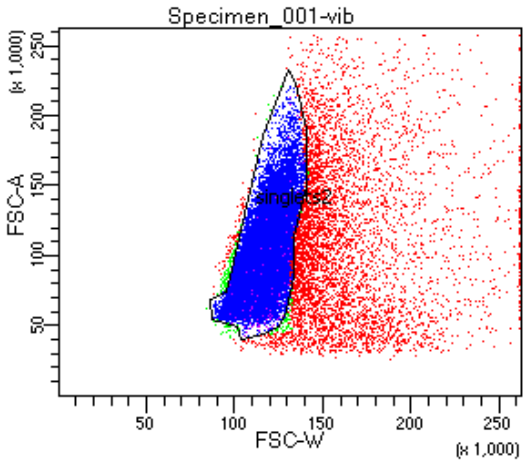
Tube: static

Population	#Events	%Parent	%Total
All Events	58,358	####	100.0
Cells	30,060	51.5	51.5
singlets	23,721	78.9	40.6
singlets2	23,497	99.1	40.3
PI-negativ/living	23,447	99.8	40.2
PI-positive/dead	50	0.2	0.1

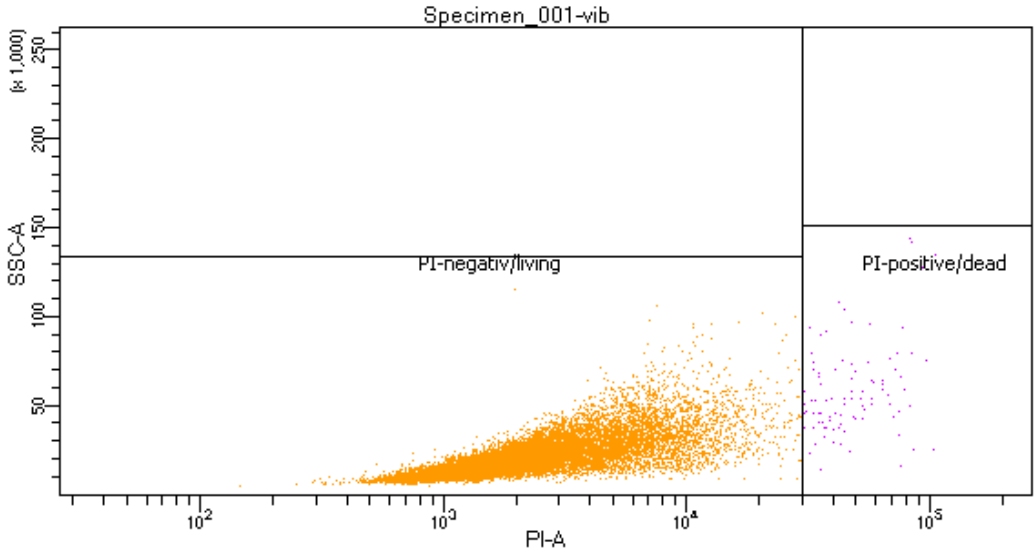
Experiment #3 vibrated stained

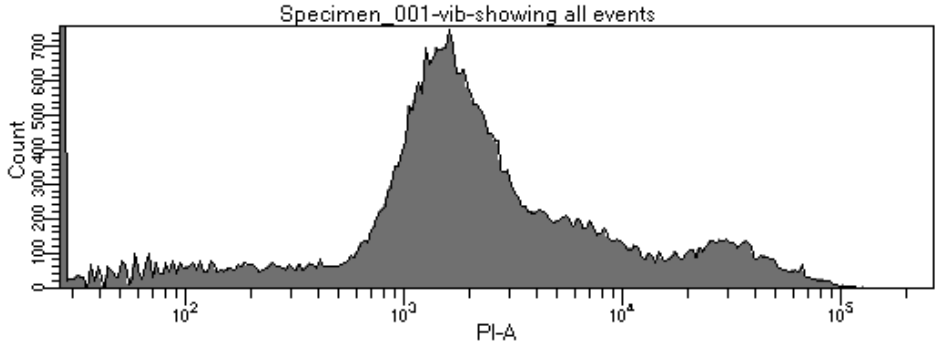


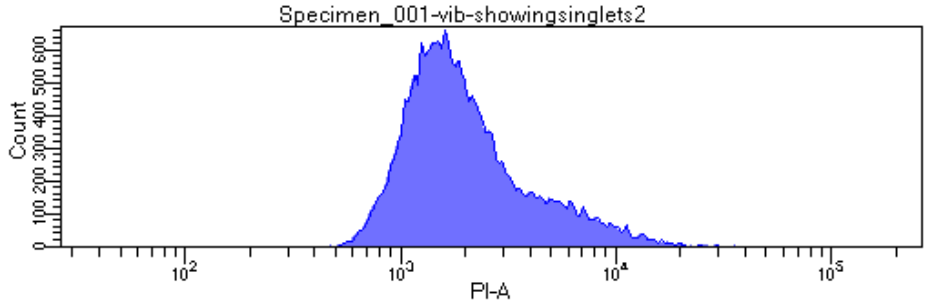




Experiment #3 vibrated stained



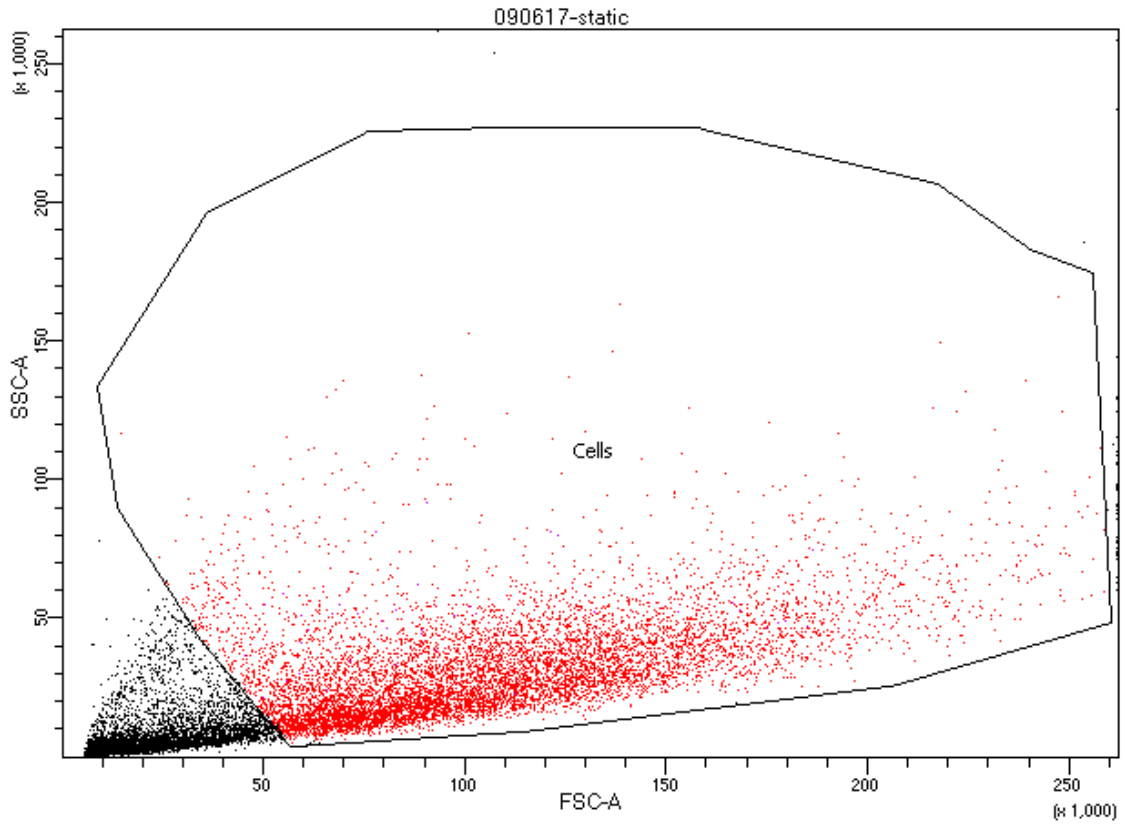


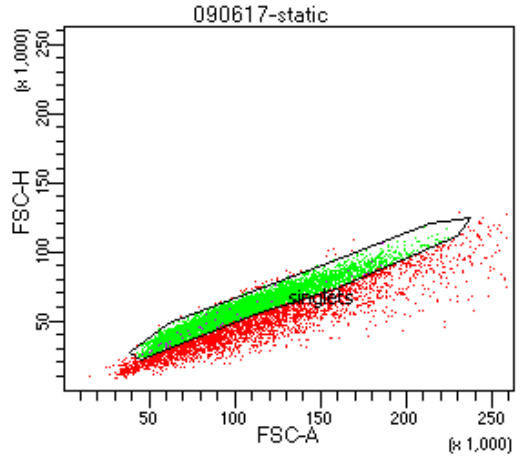


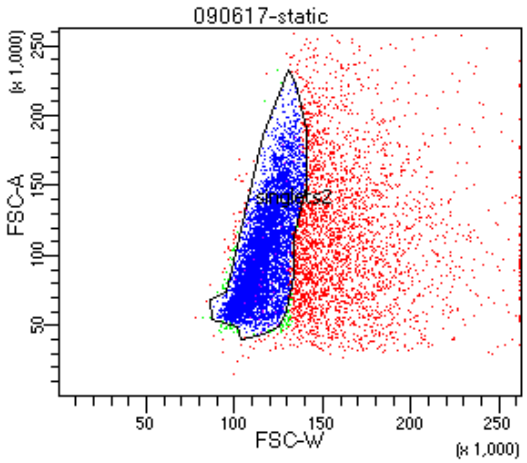
Tube: vib

Population	#Events	%Parent	%Total
All Events	40,000	####	100.0
Cells	28,150	70.4	70.4
singlets	22,956	81.5	57.4
singlets2	22,736	99.0	56.8
PI-negativ/living	22,642	99.6	56.6
PI-positive/dead	94	0.4	0.2

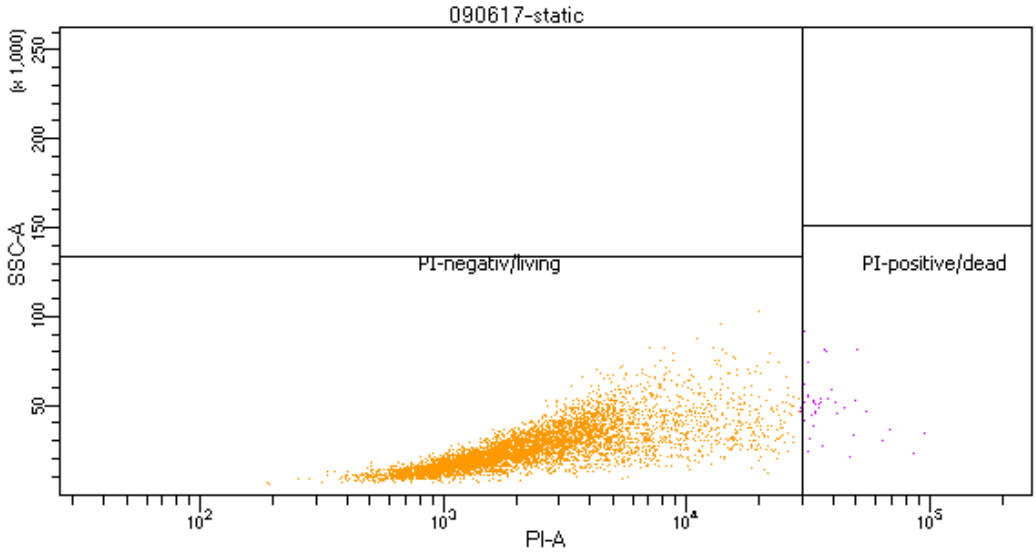
Experiment #4 static stained

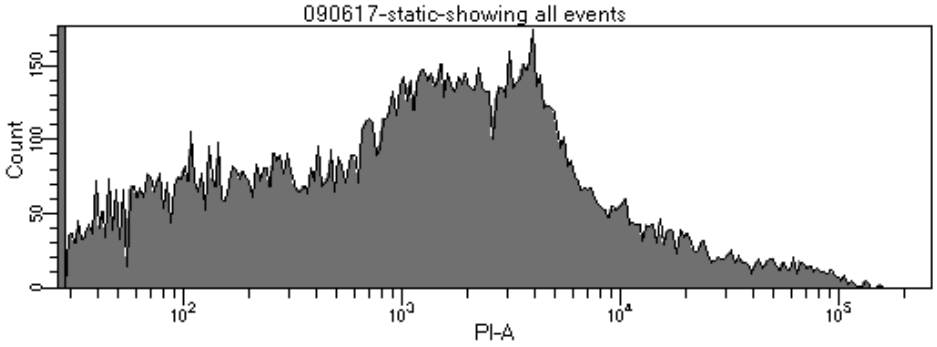


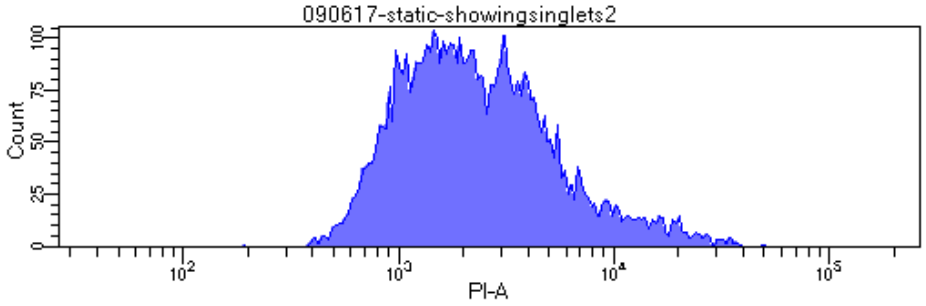




Experiment #4 static stained



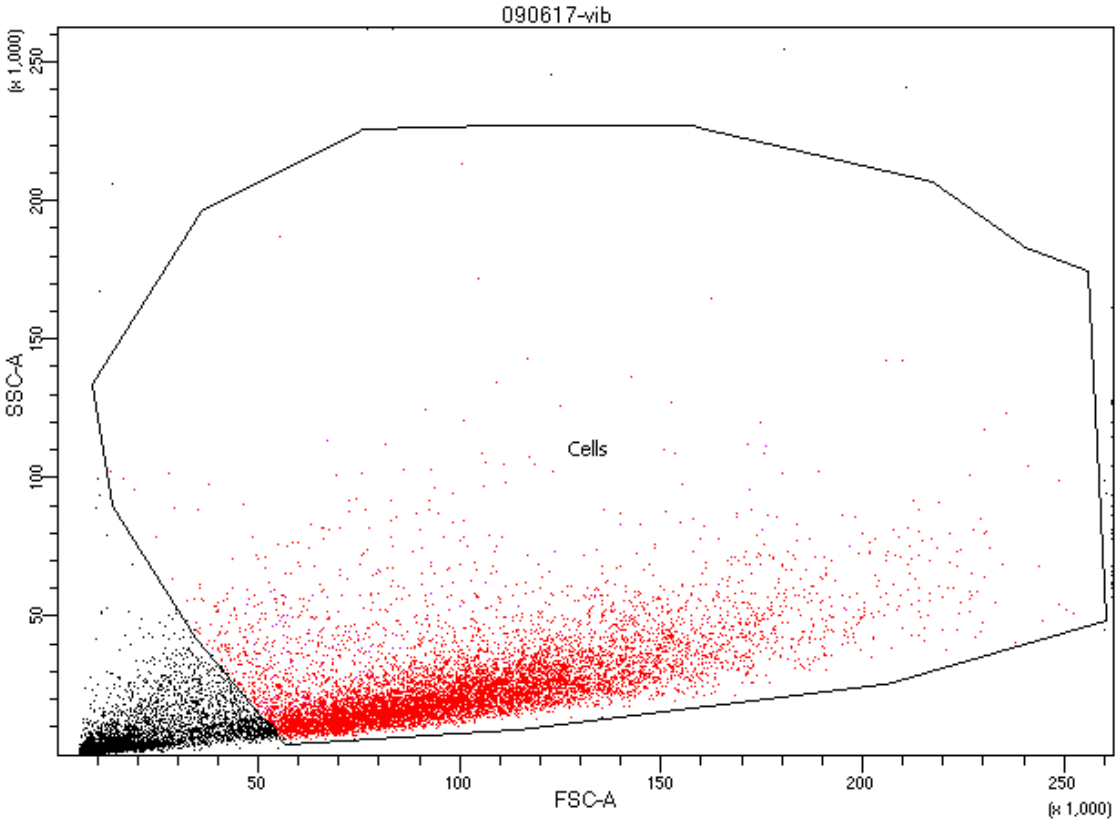


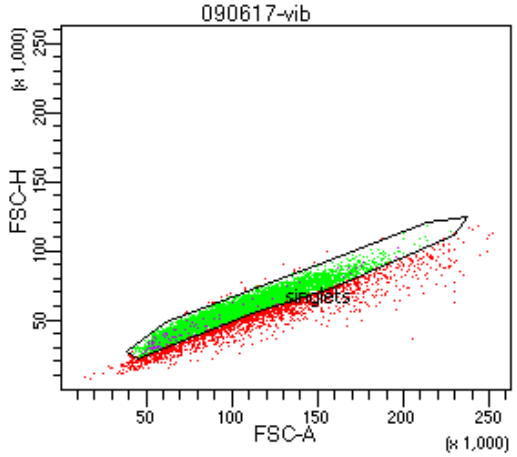


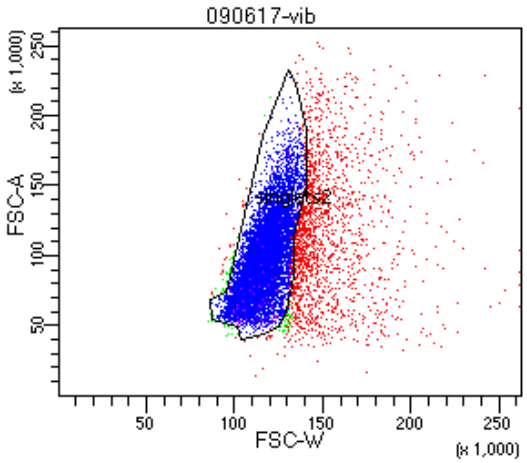
Tube: static

Population	#Events	%Parent	%Total
All Events	17,857	####	100.0
Cells	8,577	48.0	48.0
singlets	5,704	66.5	31.9
singlets2	5,577	97.8	31.2
PI-negativ/living	5,537	99.3	31.0
PI-positive/dead	40	0.7	0.2

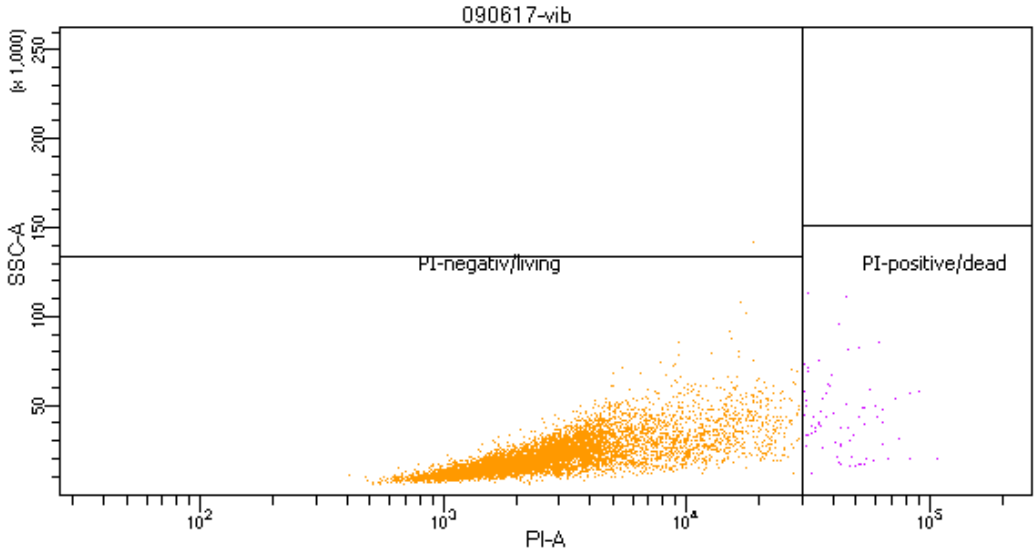
Experiment #4 vibrated stained

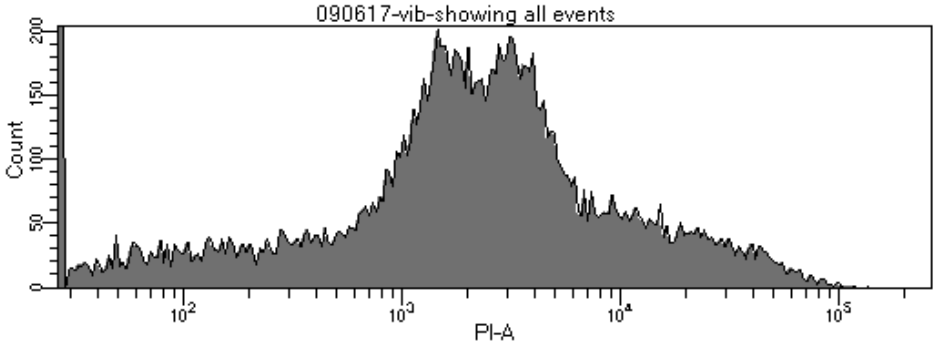


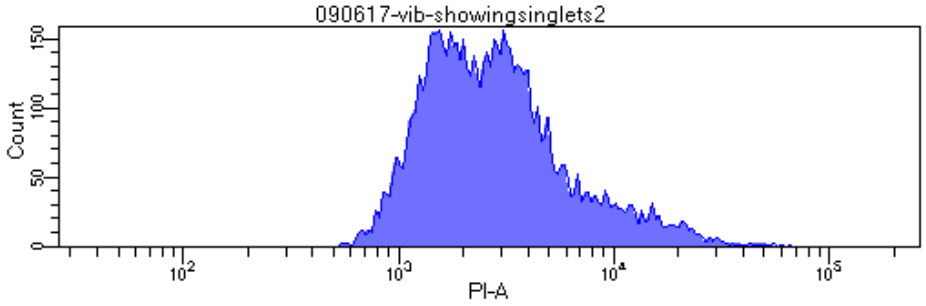




Experiment #4 vibrated stained



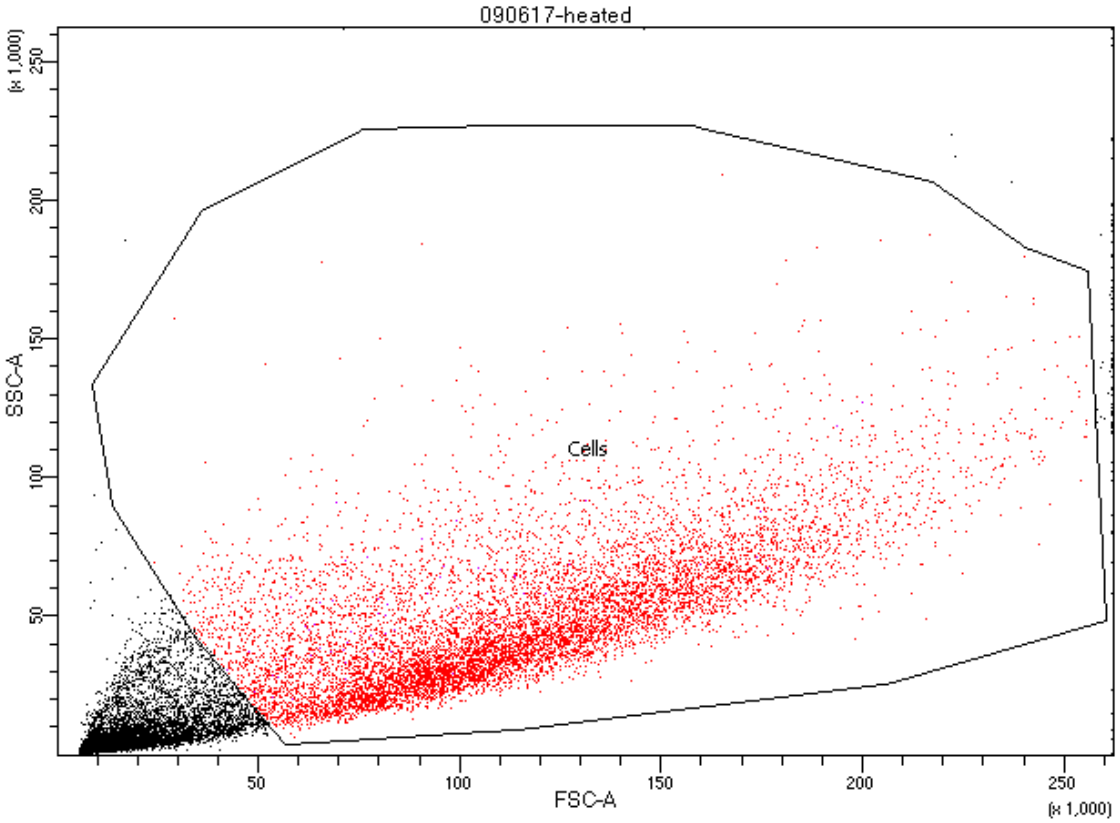


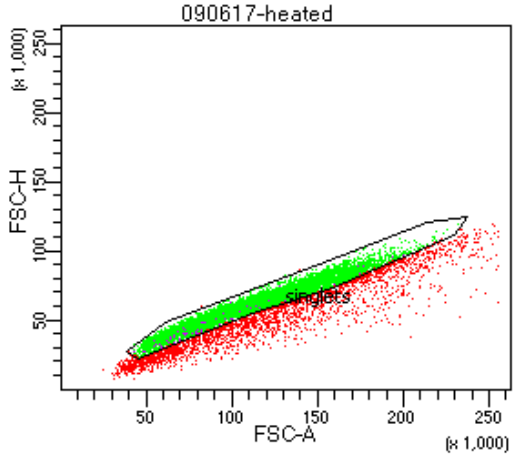


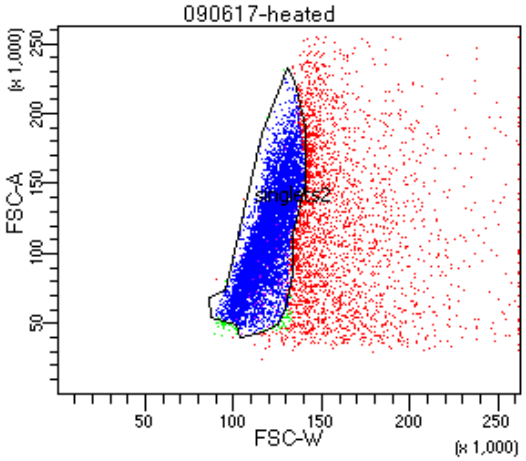
Tube: vib

Population	#Events	%Parent	%Total
All Events	14,999	####	100.0
Cells	9,414	62.8	62.8
singlets	7,617	80.9	50.8
singlets2	7,521	98.7	50.1
PI-negativ/living	7,442	98.9	49.6
PI-positive/dead	79	1.1	0.5

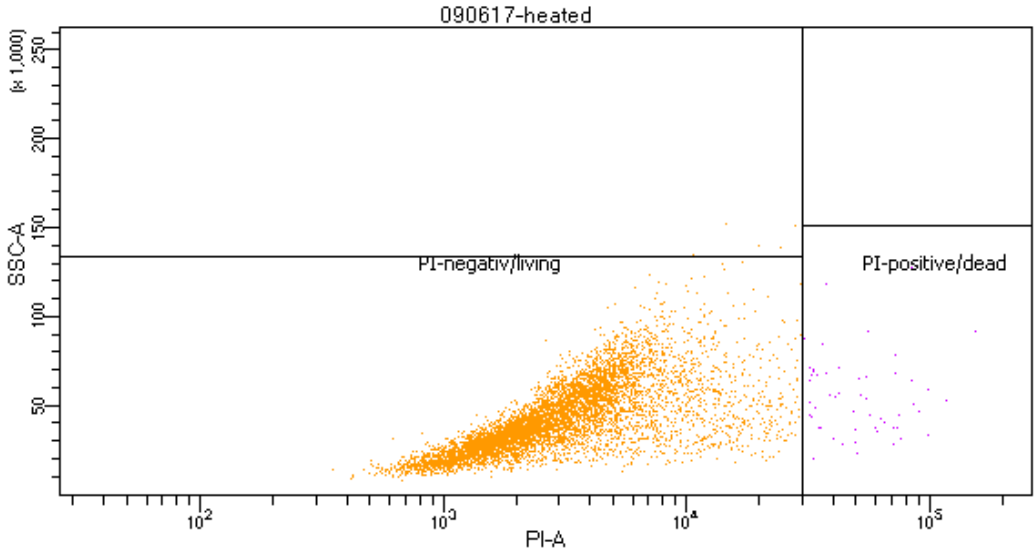
Experiment #4 heated stained

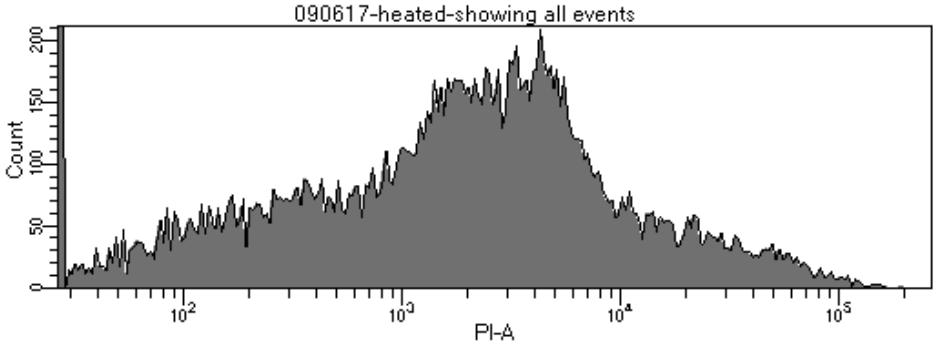


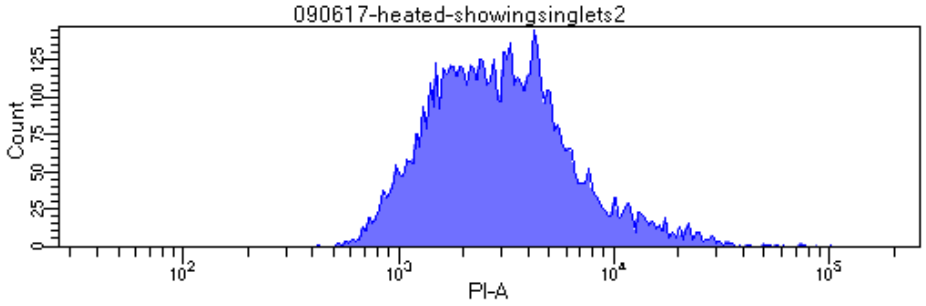




Experiment #4 heated stained



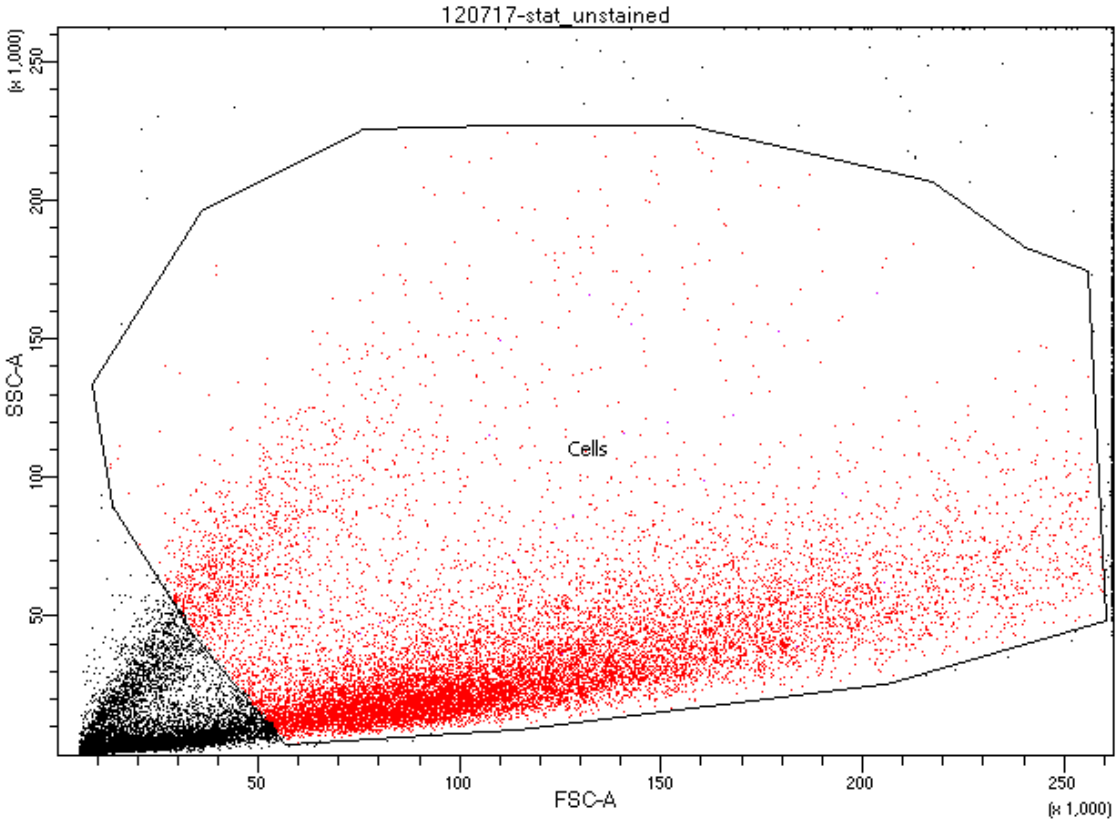


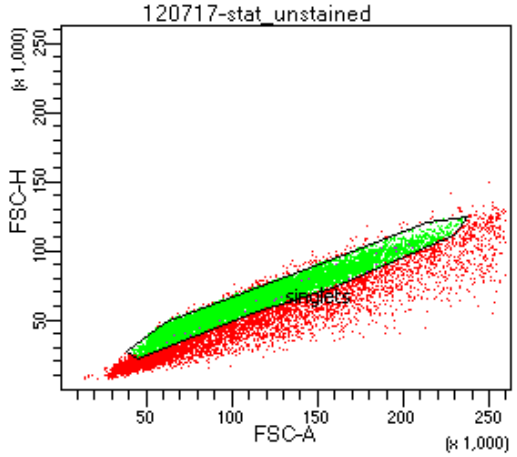


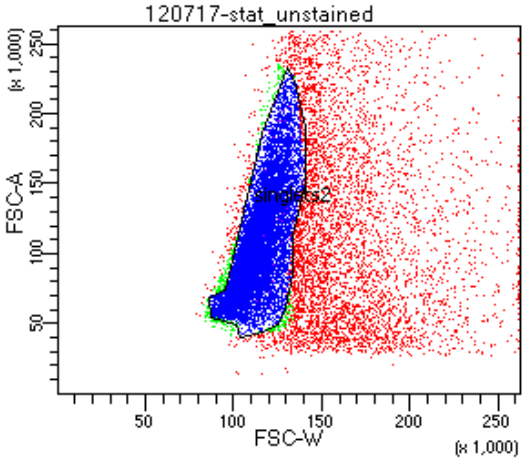
Tube: heated

Population	#Events	%Parent	%Total
All Events	17,984	####	100.0
Cells	9,343	52.0	52.0
singlets	6,779	72.6	37.7
singlets2	6,689	98.7	37.2
PI-negativ/living	6,632	99.1	36.9
PI-positive/dead	57	0.9	0.3

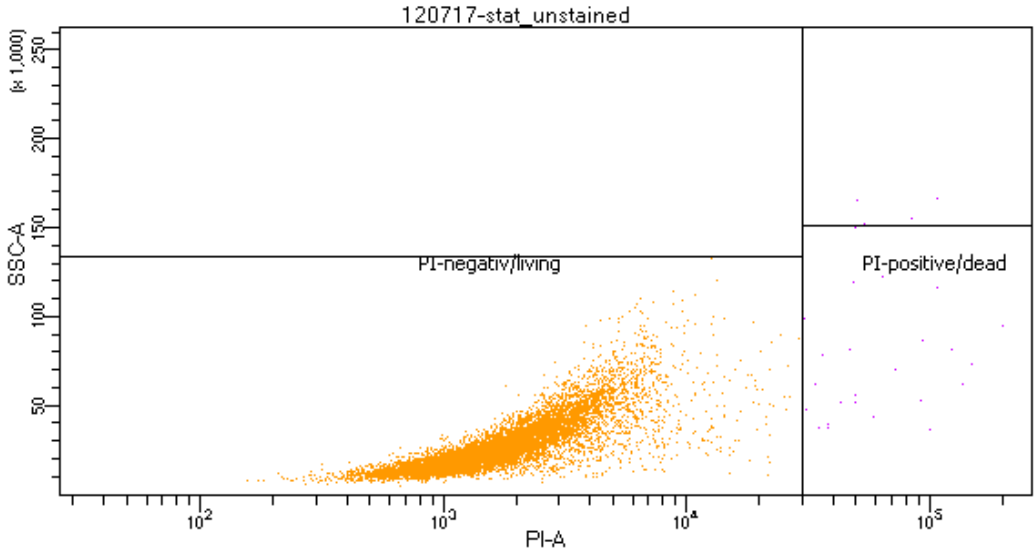
Experiment #5 static unstained

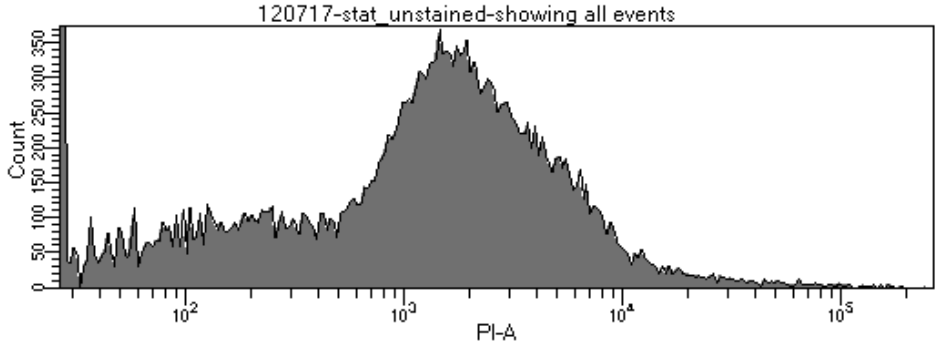


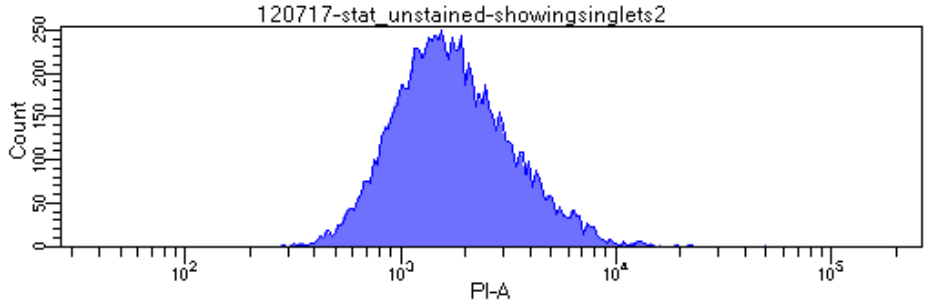




Experiment #5 static unstained



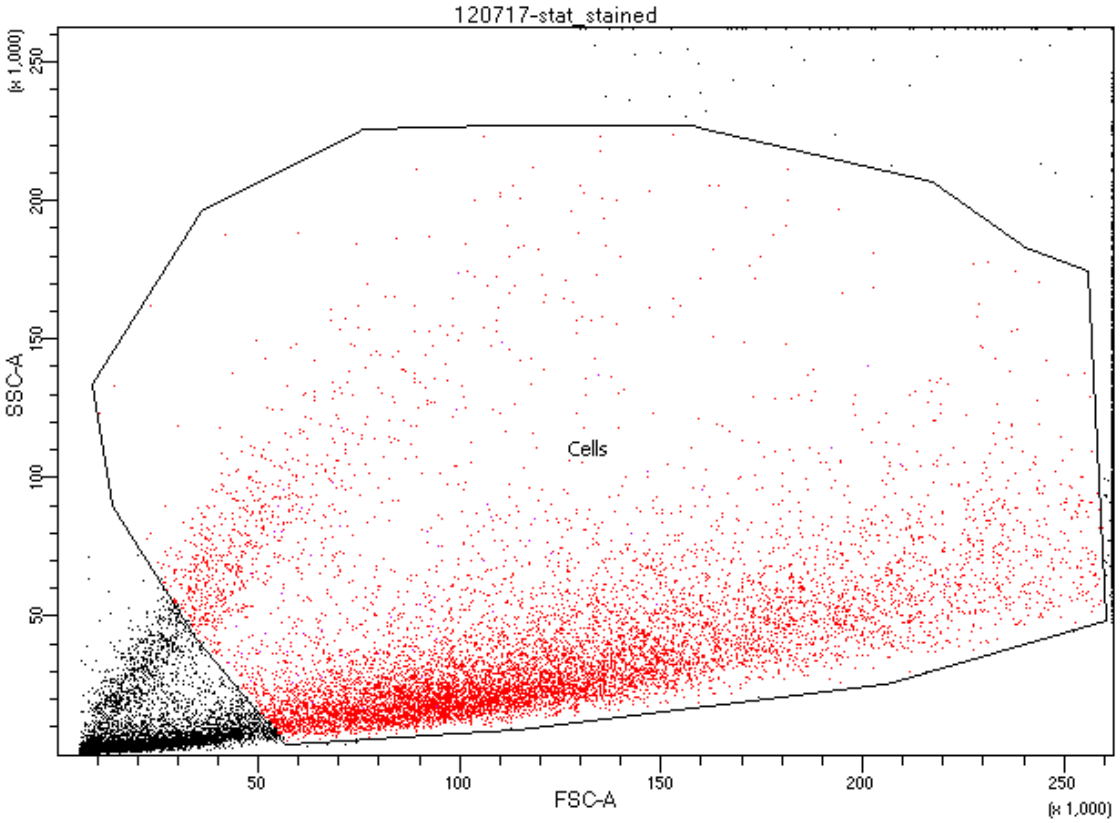


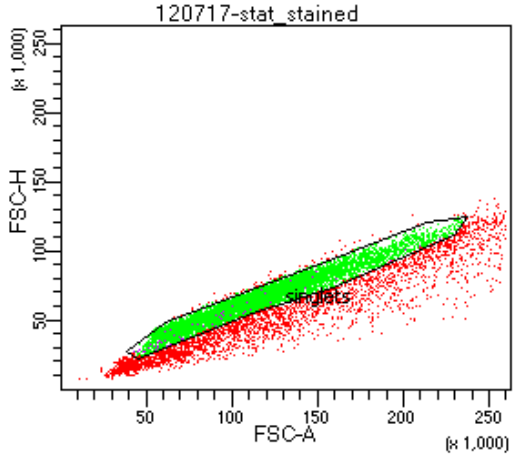


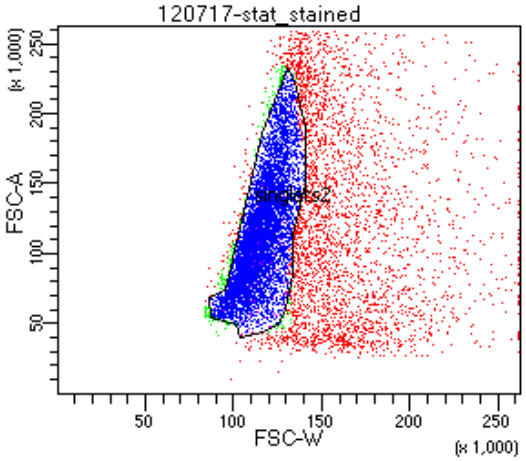
Tube: stat_unstained

Population	#Events	%Parent	%Total
All Events	27,444	####	100.0
Cells	15,254	55.6	55.6
singlets	10,518	69.0	38.3
singlets2	10,150	96.5	37.0
PI-negativ/living	10,121	99.7	36.9
PI-positive/dead	29	0.3	0.1

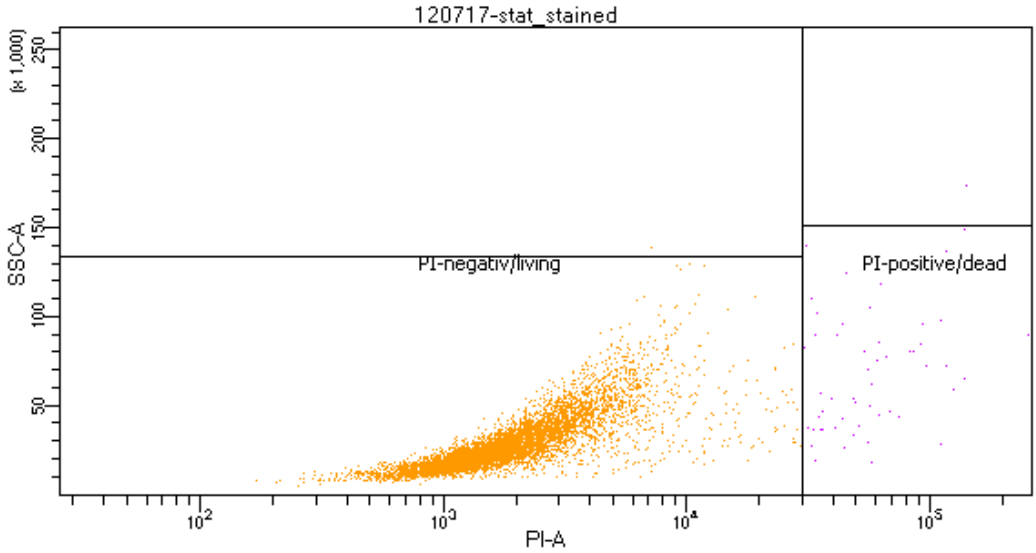
Experiment #5 static stained

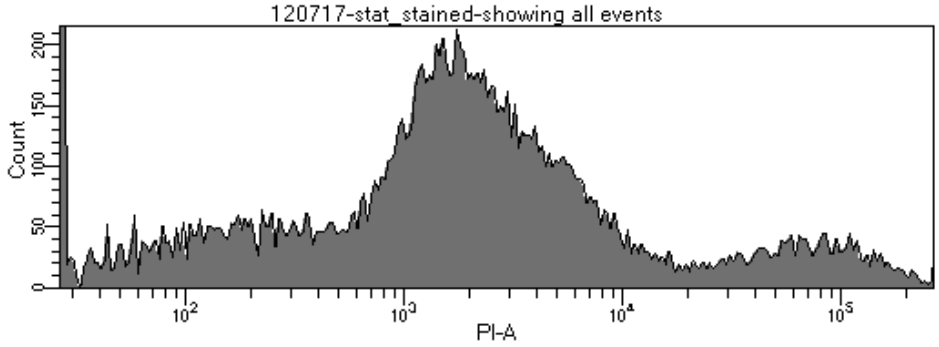


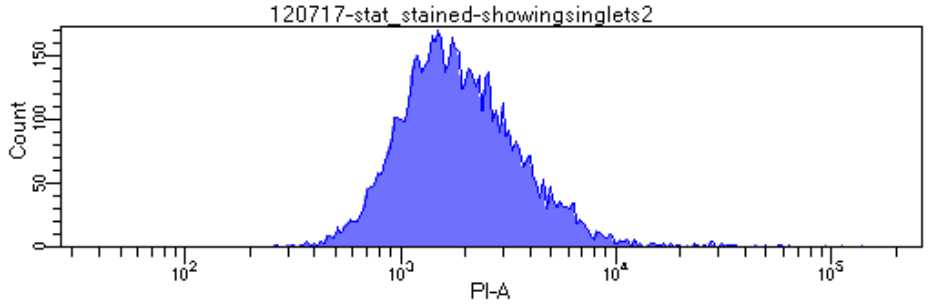




Experiment #5 static stained



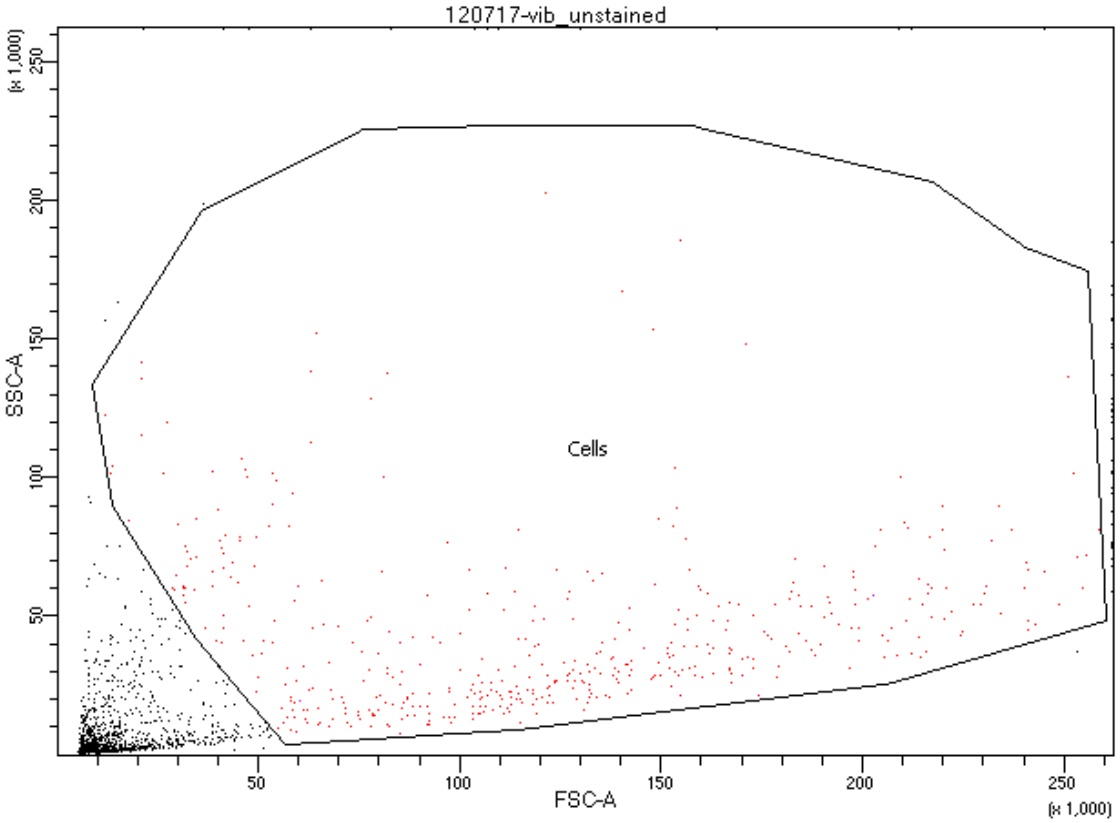


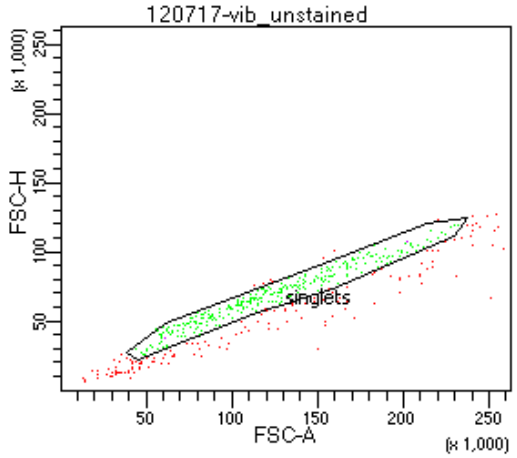


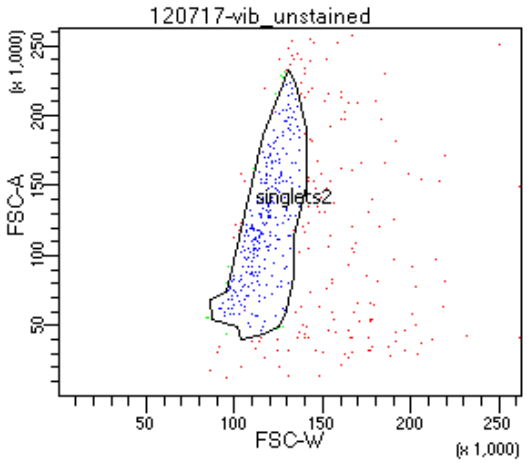
Tube: stat_stained

Population	#Events	%Parent	%Total
All Events	16,681	####	100.0
Cells	9,900	59.3	59.3
singlets	6,853	69.2	41.1
singlets2	6,642	96.9	39.8
PI-negativ/living	6,586	99.2	39.5
PI-positive/dead	56	0.8	0.3

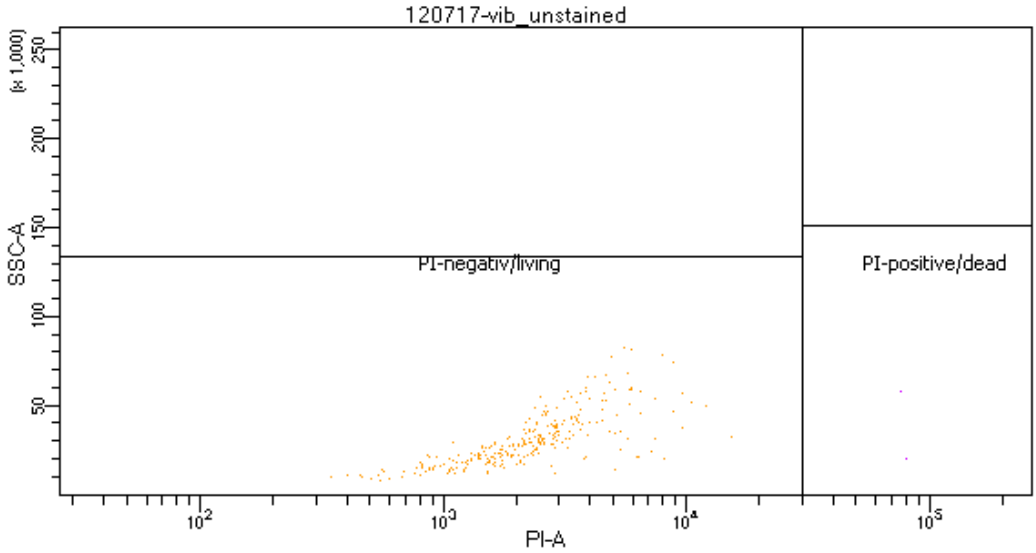
Experiment #5 vibrated unstained

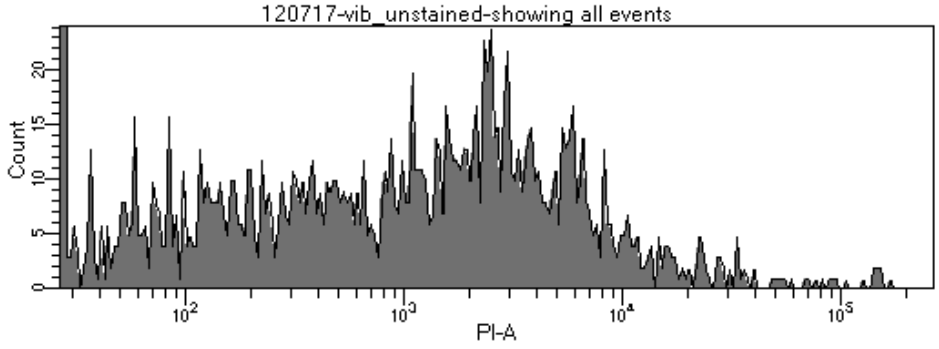


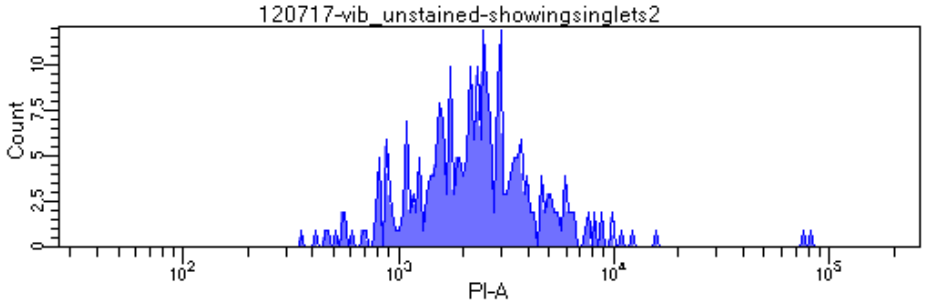




Experiment #5 vibrated unstained



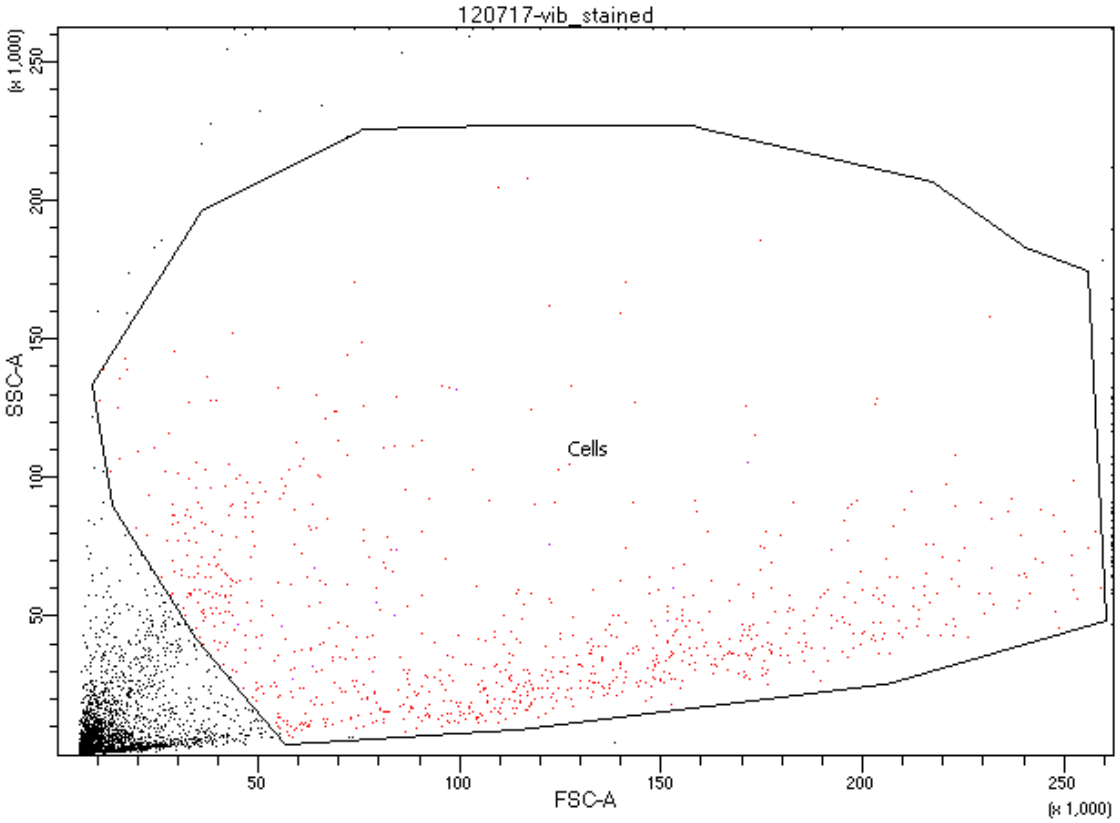


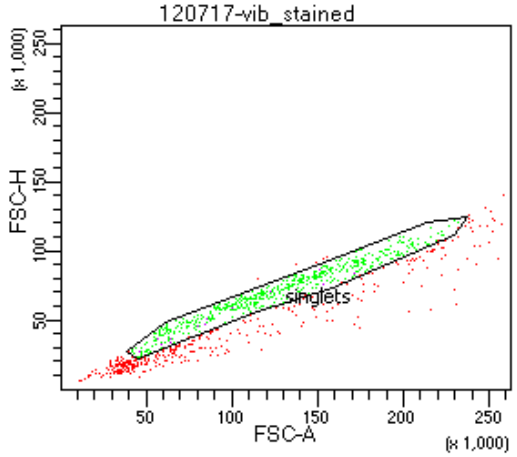


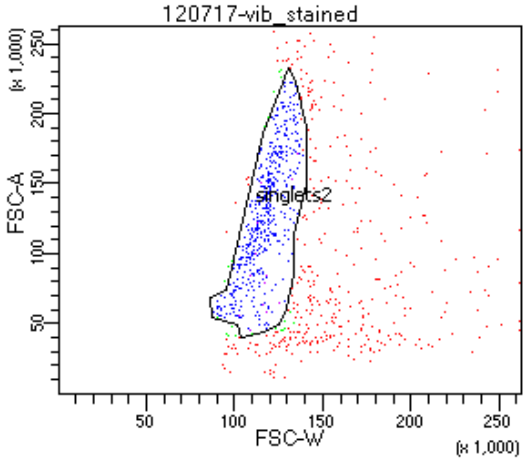
Tube: vib_unstained

Population	#Events	%Parent	%Total
All Events	1,666	####	100.0
Cells	462	27.7	27.7
singlets	295	63.9	17.7
singlets2	281	95.3	16.9
PI-negativ/living	279	99.3	16.7
PI-positive/dead	2	0.7	0.1

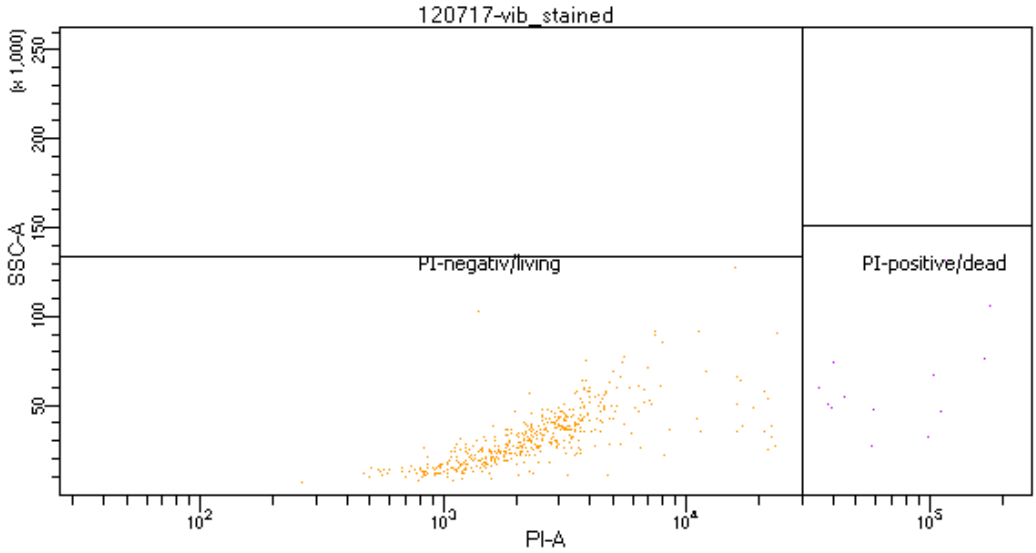
Experiment #5 vibrated stained

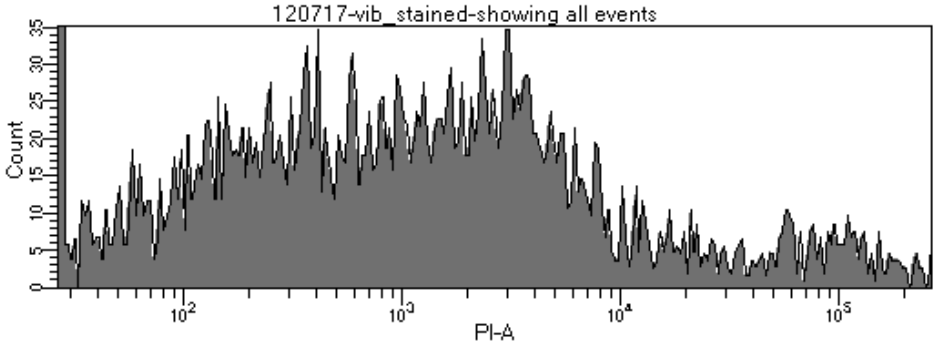


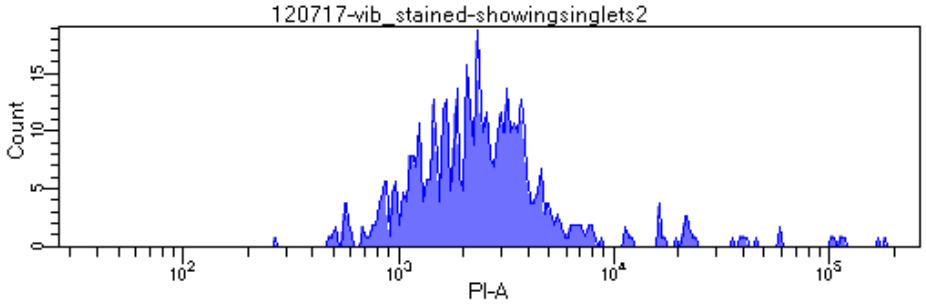




Experiment #5 vibrated stained



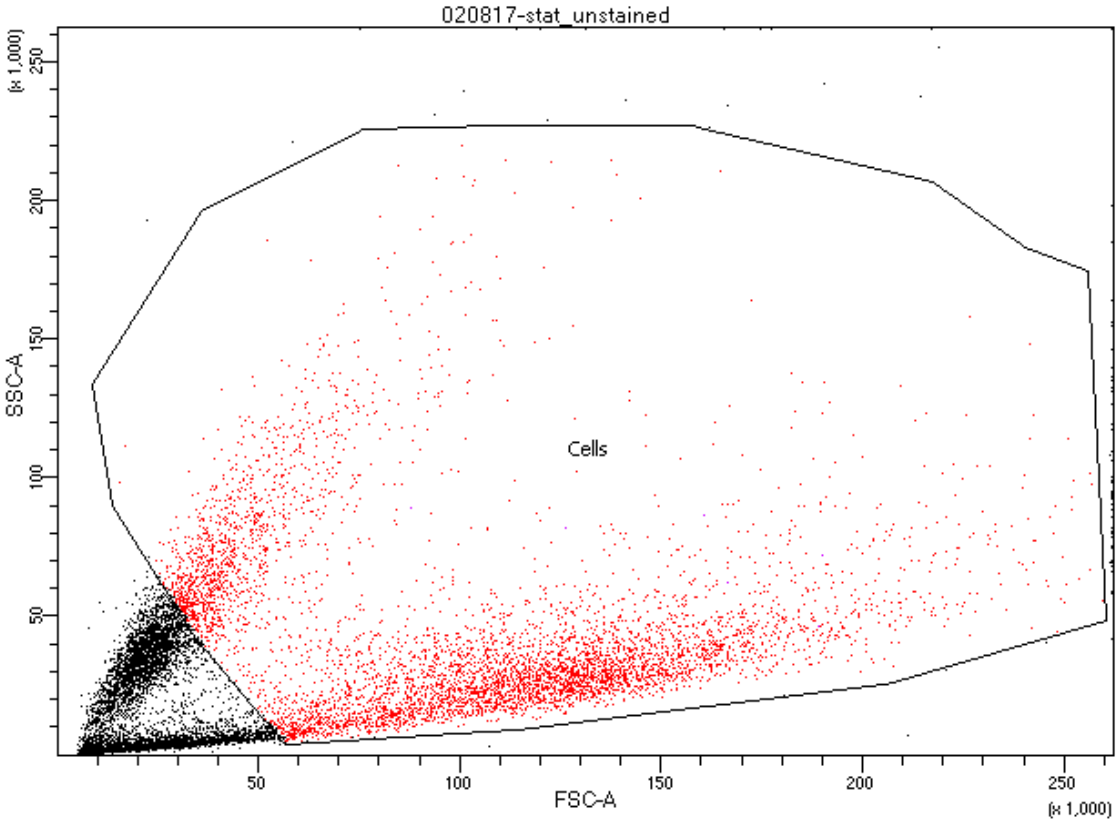


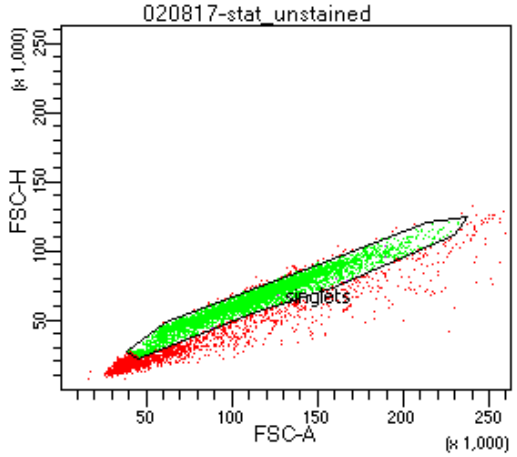


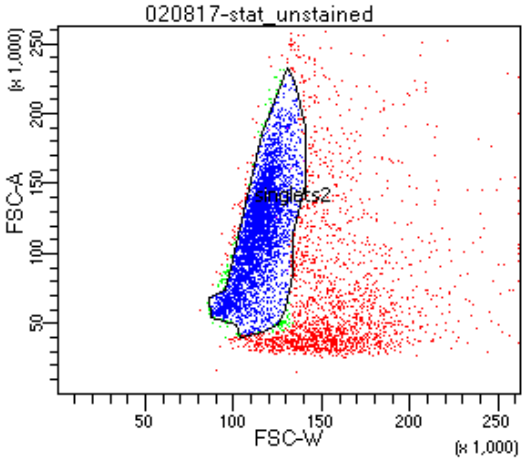
Tube: vib_stained

Population	#Events	%Parent	%Total
All Events	3,646	####	100.0
Cells	898	24.6	24.6
singlets	522	58.1	14.3
singlets2	495	94.8	13.6
PI-negativ/living	482	97.4	13.2
PI-positive/dead	13	2.6	0.4

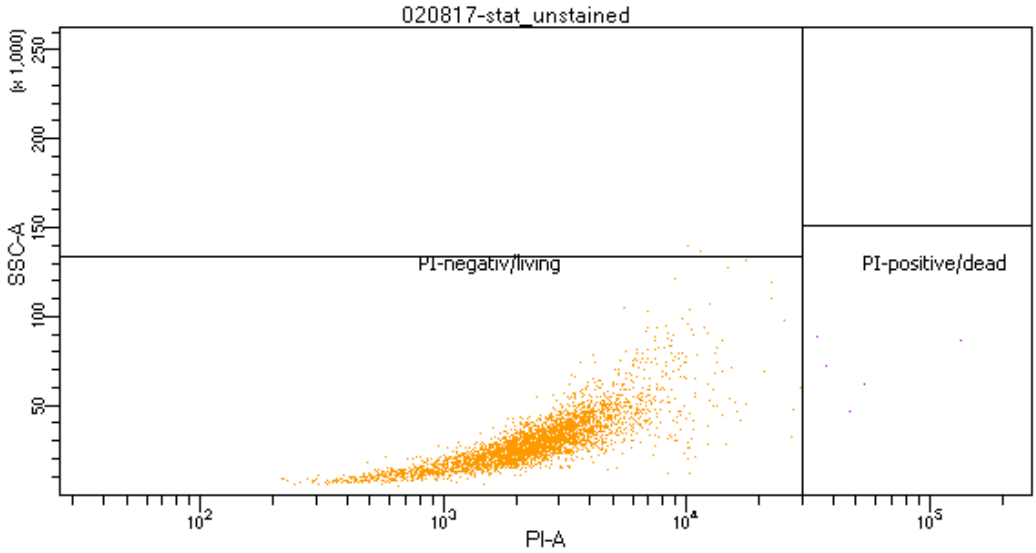
Experiment #6 static unstained

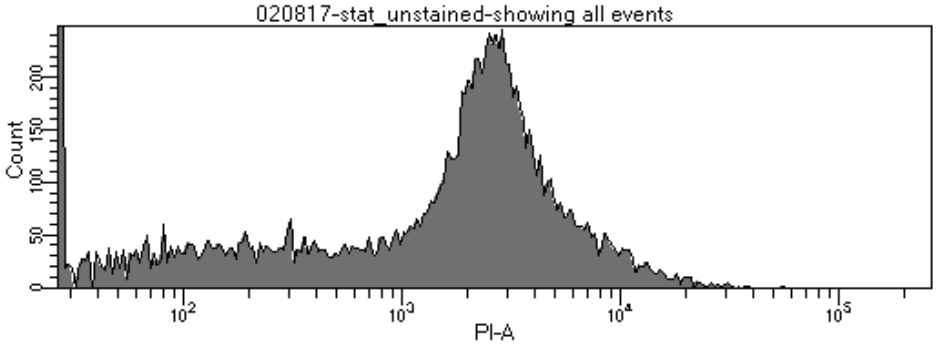


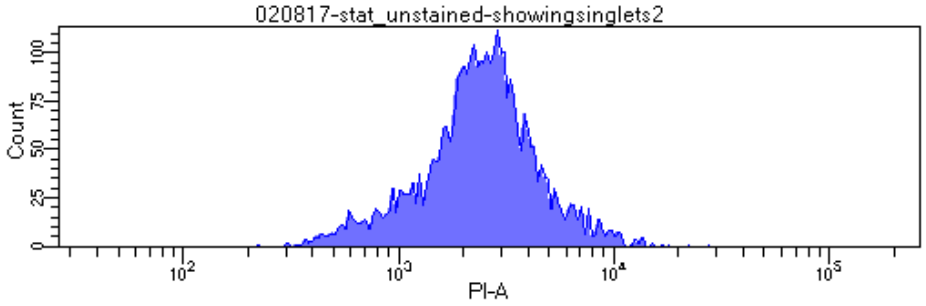




Experiment #6 static unstained



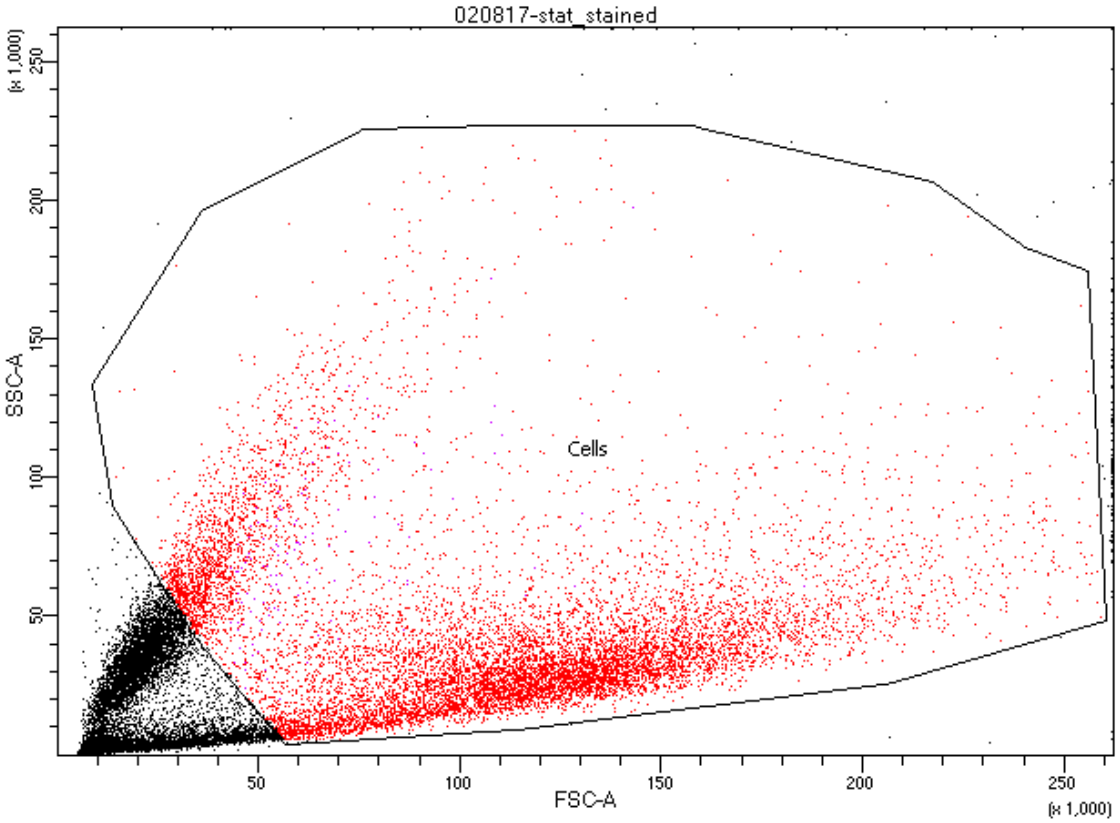


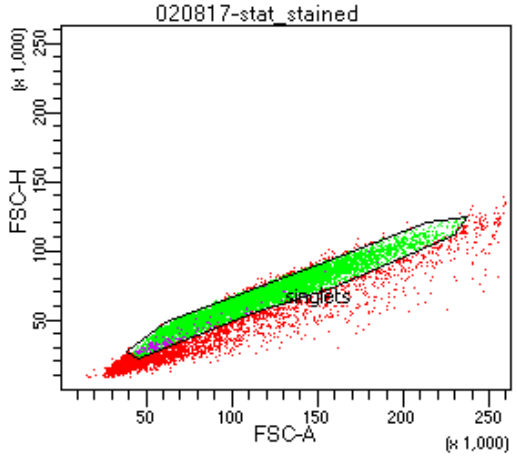


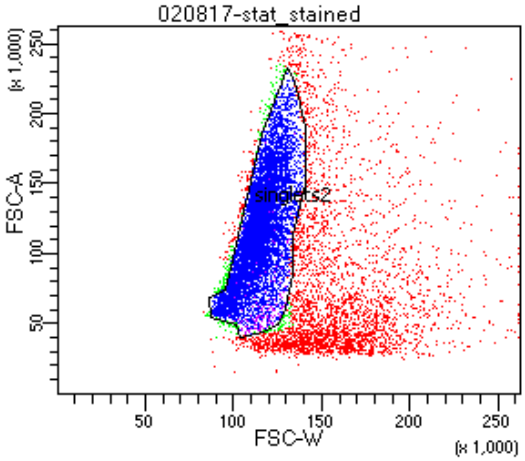
Tube: stat_unstained

Population	#Events	%Parent	%Total
All Events	12,449	####	100.0
Cells	5,636	45.3	45.3
singlets	3,795	67.3	30.5
singlets2	3,652	96.2	29.3
PI-negativ/living	3,646	99.8	29.3
PI-positive/dead	6	0.2	0.0

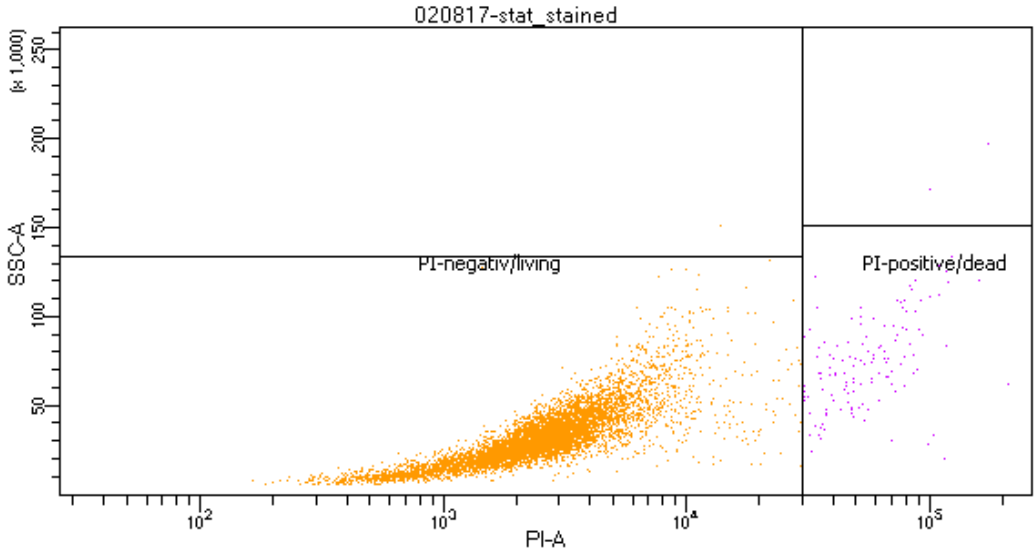
Experiment #6 static stained

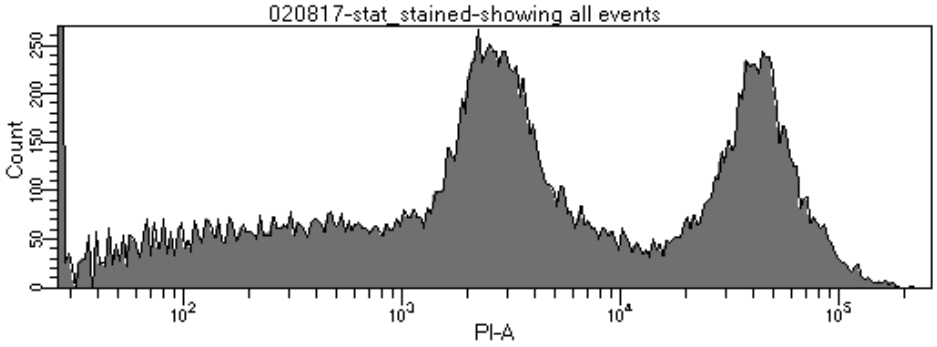


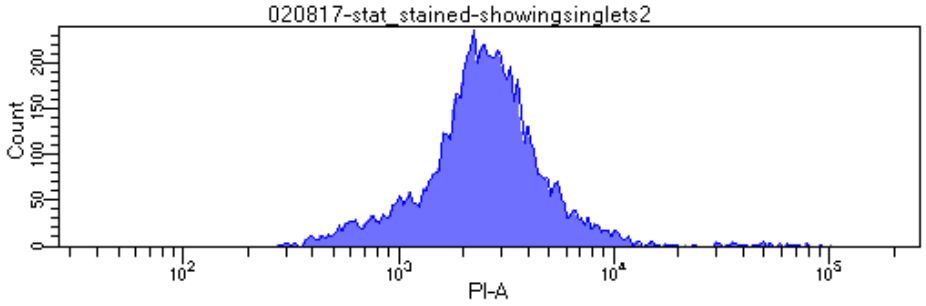




Experiment #6 static stained



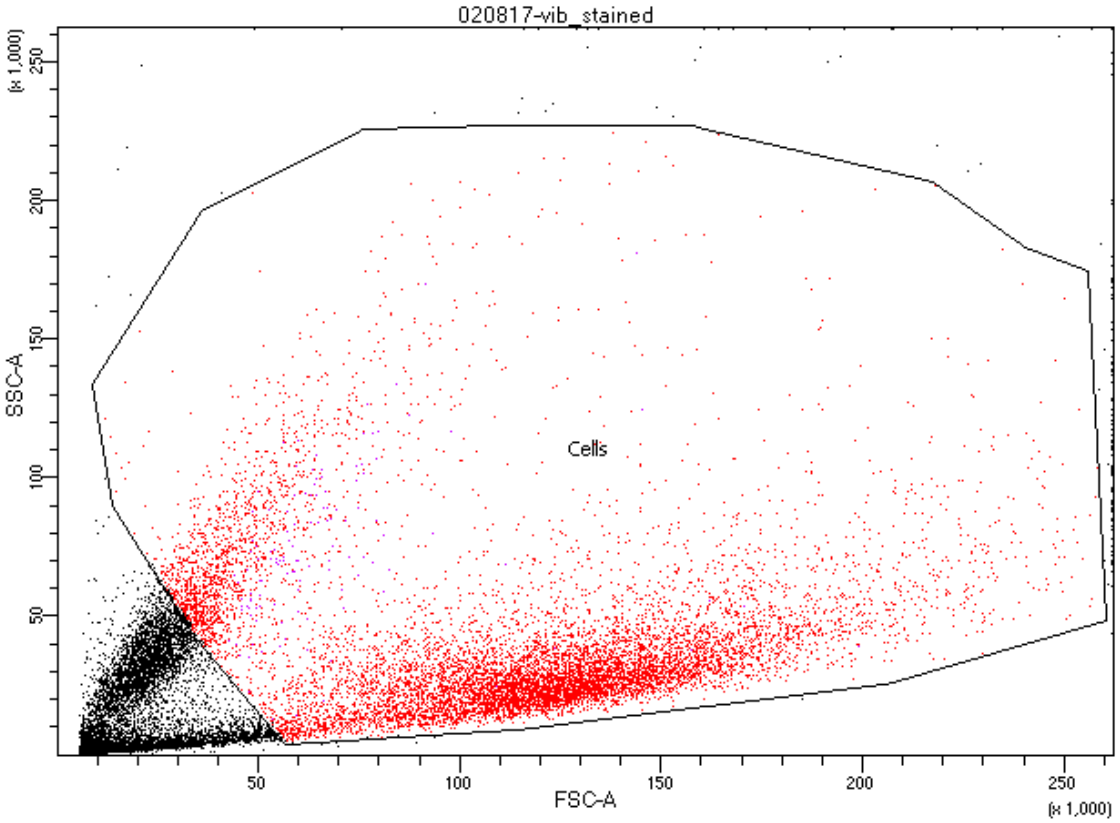


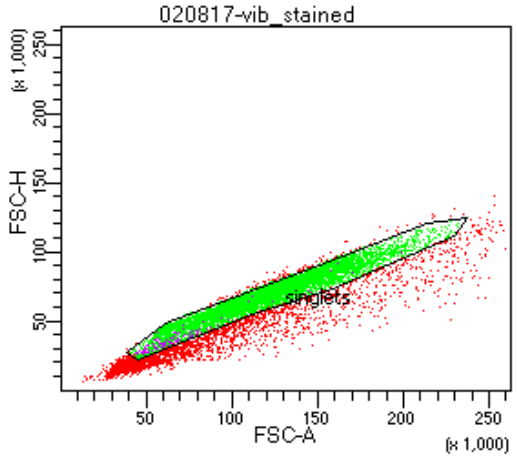


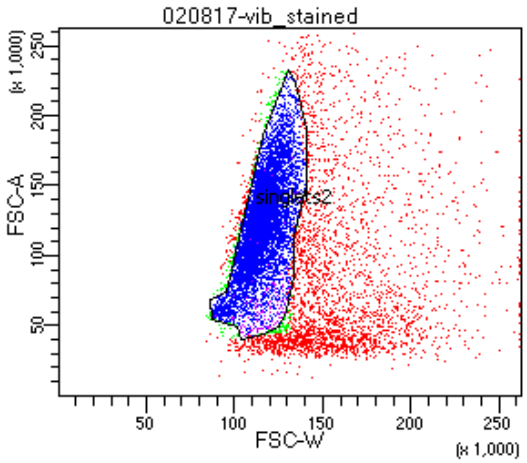
Tube: stat_stained

Population	#Events	%Parent	%Total
All Events	22,332	####	100.0
Cells	11,262	50.4	50.4
singlets	8,043	71.4	36.0
singlets2	7,793	96.9	34.9
PI-negativ/living	7,661	98.3	34.3
PI-positive/dead	132	1.7	0.6

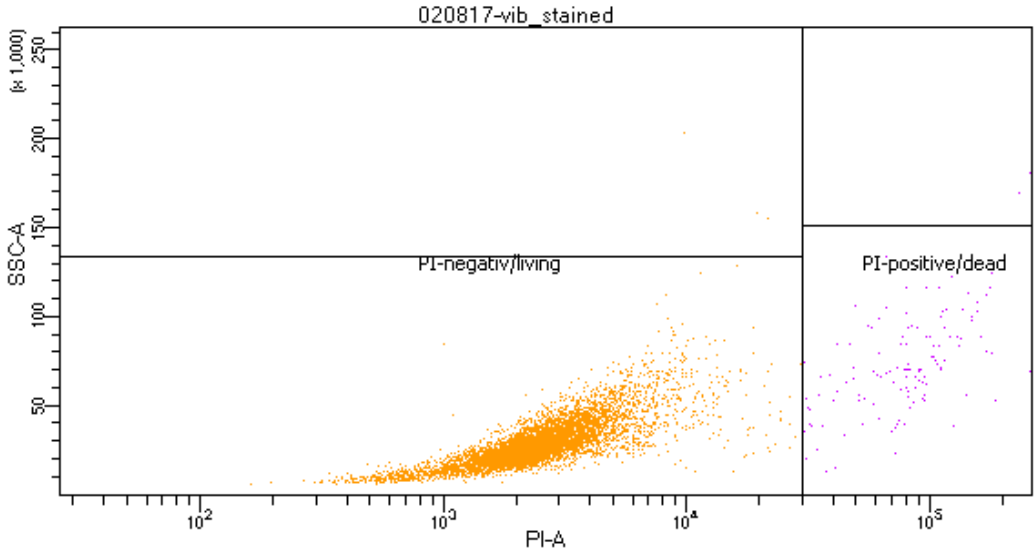
Experiment #6 vibrated unstained

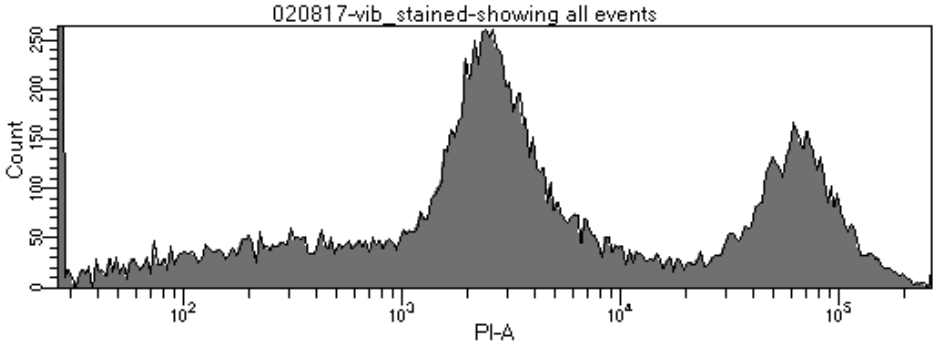


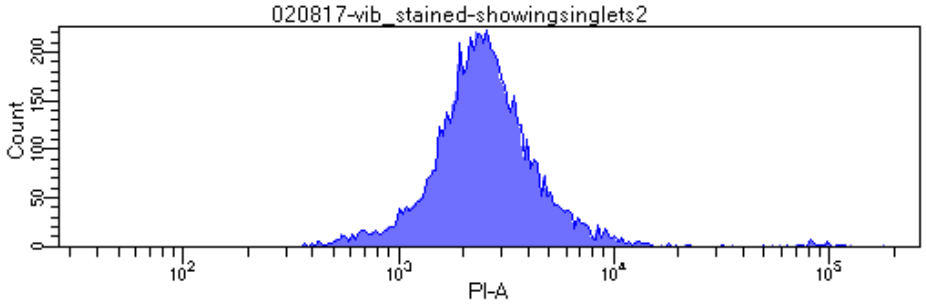




Experiment #6 vibrated unstained



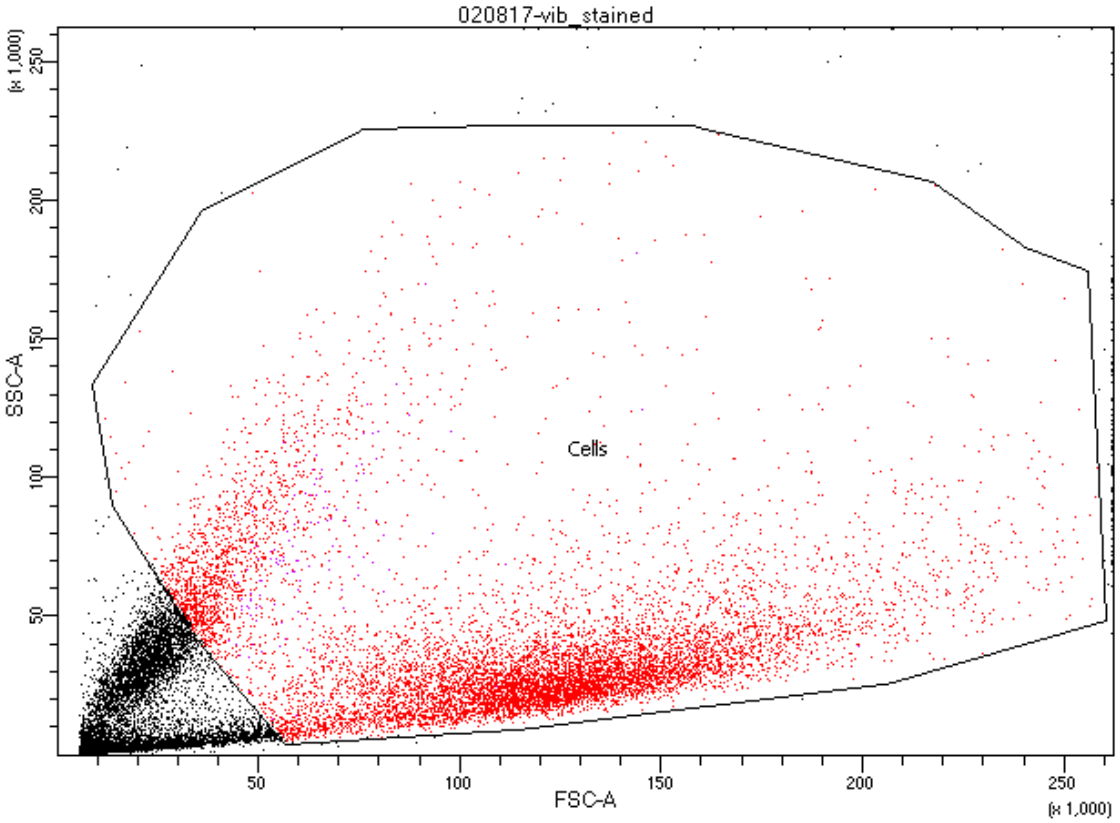


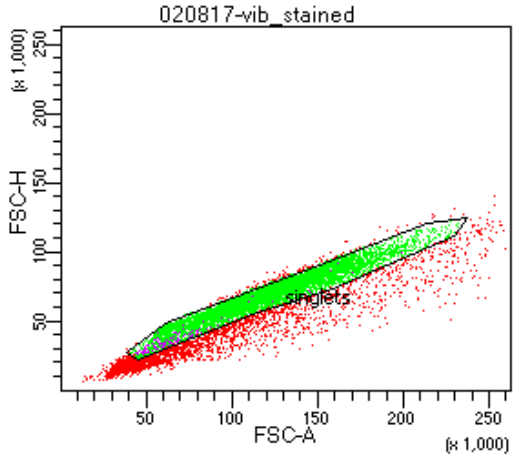


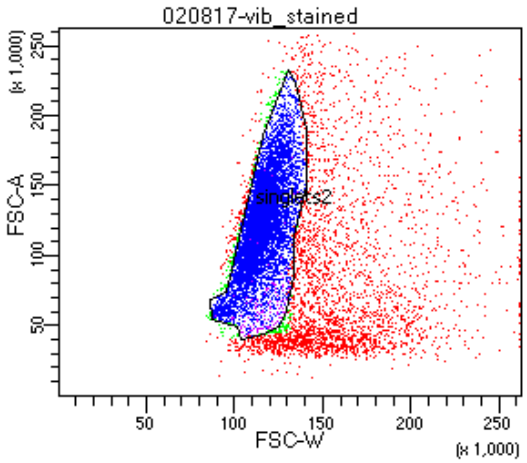
Tube: vib_stained

Population	#Events	%Parent	%Total
All Events	17,726	####	100.0
Cells	9,887	55.8	55.8
singlets	7,019	71.0	39.6
singlets2	6,778	96.6	38.2
PI-negativ/living	6,653	98.2	37.5
PI-positive/dead	125	1.8	0.7

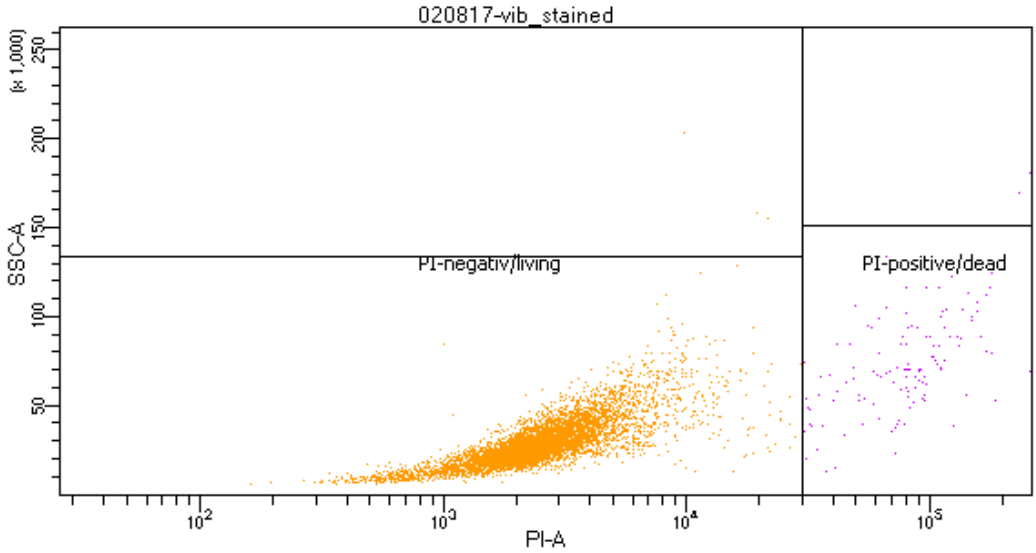
Experiment #6 vibrated stained

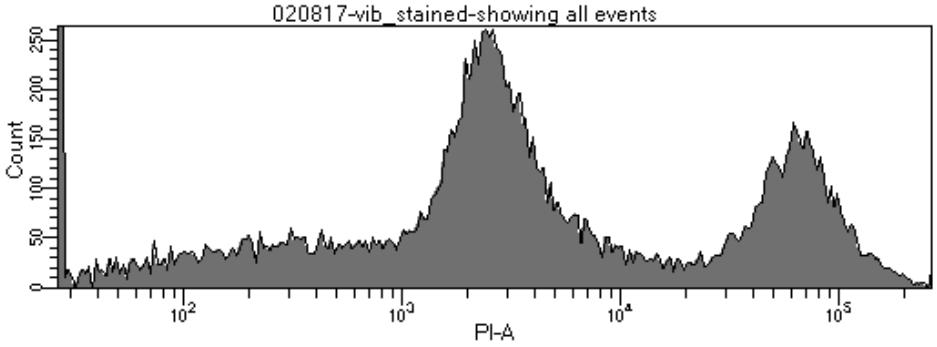


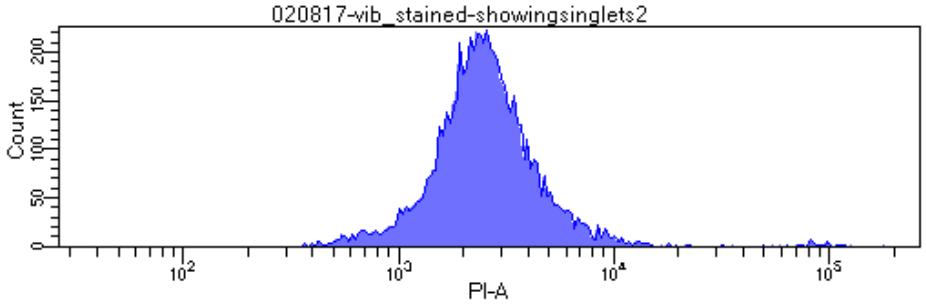




Experiment #6 vibrated stained



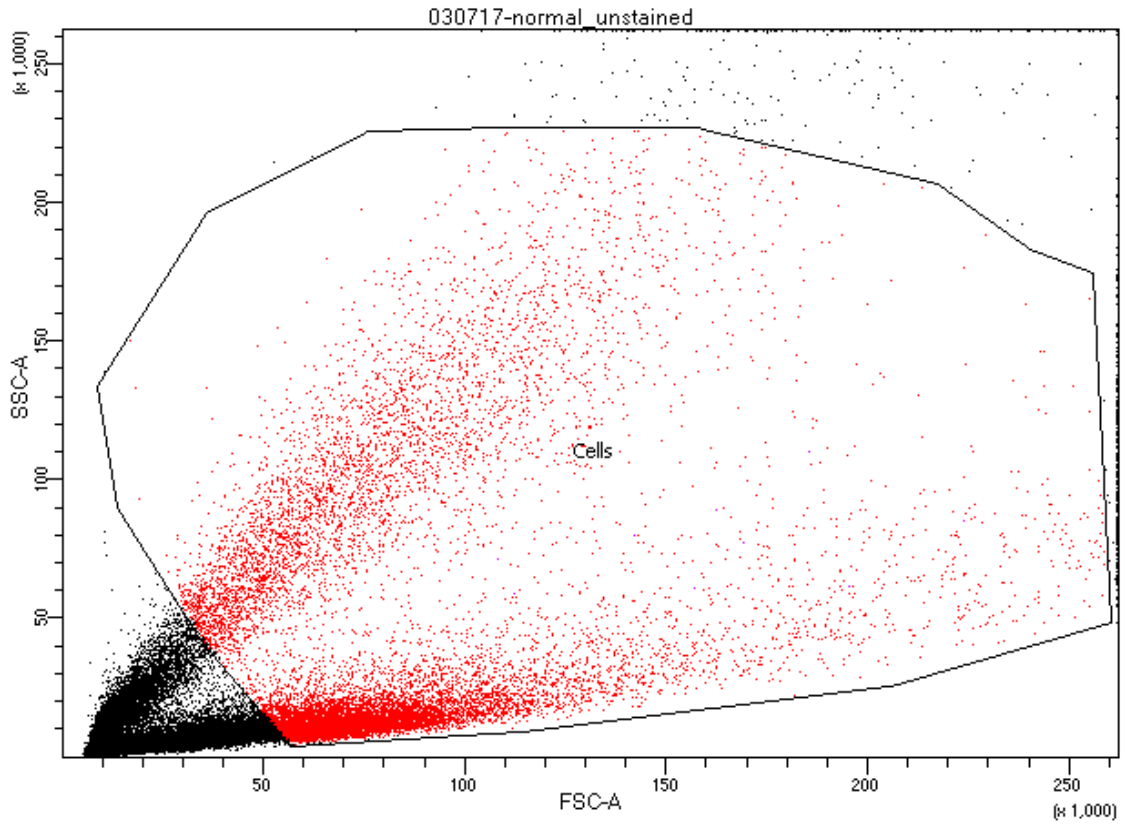


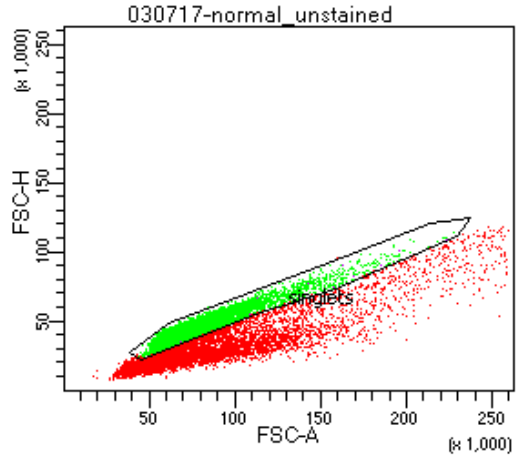


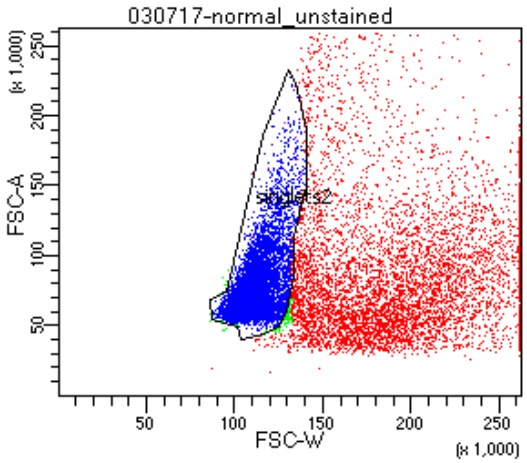
Tube: vib_stained

Population	#Events	%Parent	%Total
All Events	17,726	####	100.0
Cells	9,887	55.8	55.8
singlets	7,019	71.0	39.6
singlets2	6,778	96.6	38.2
PI-negativ/living	6,653	98.2	37.5
PI-positive/dead	125	1.8	0.7

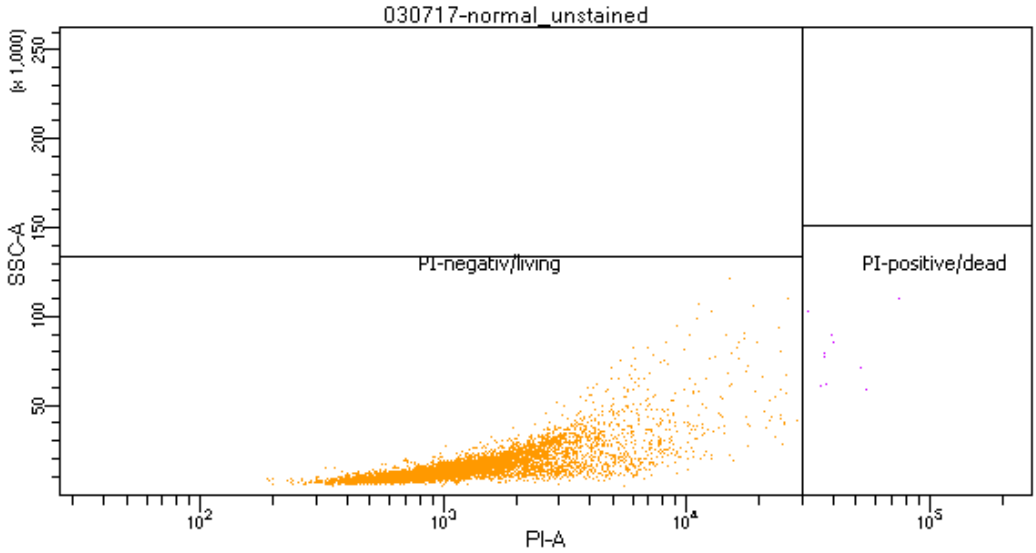
Heating Experiment between #4 and #5
normal unstained

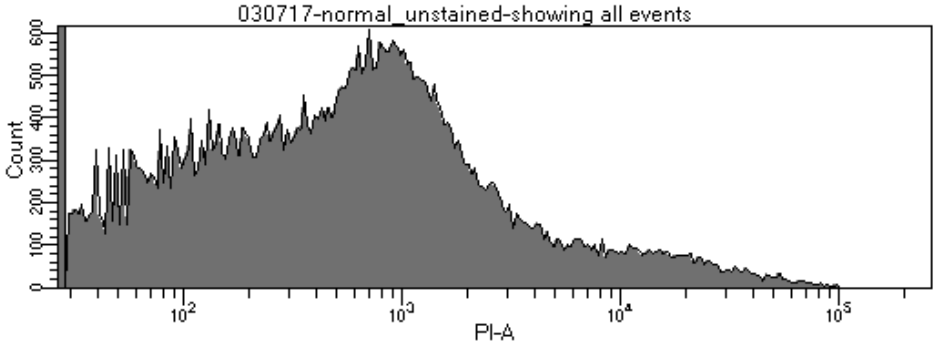


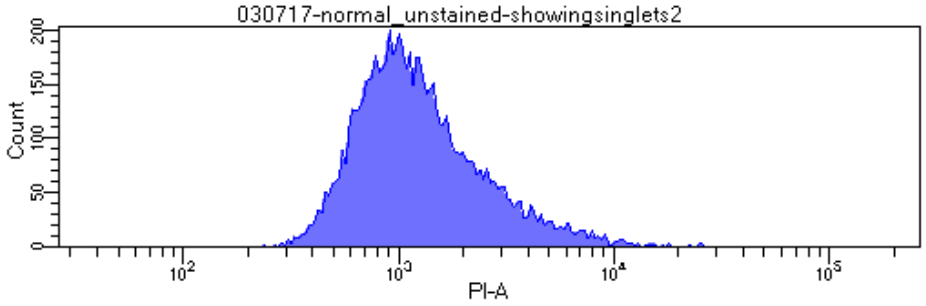




Heating Experiment between #4 and #5
normal unstained





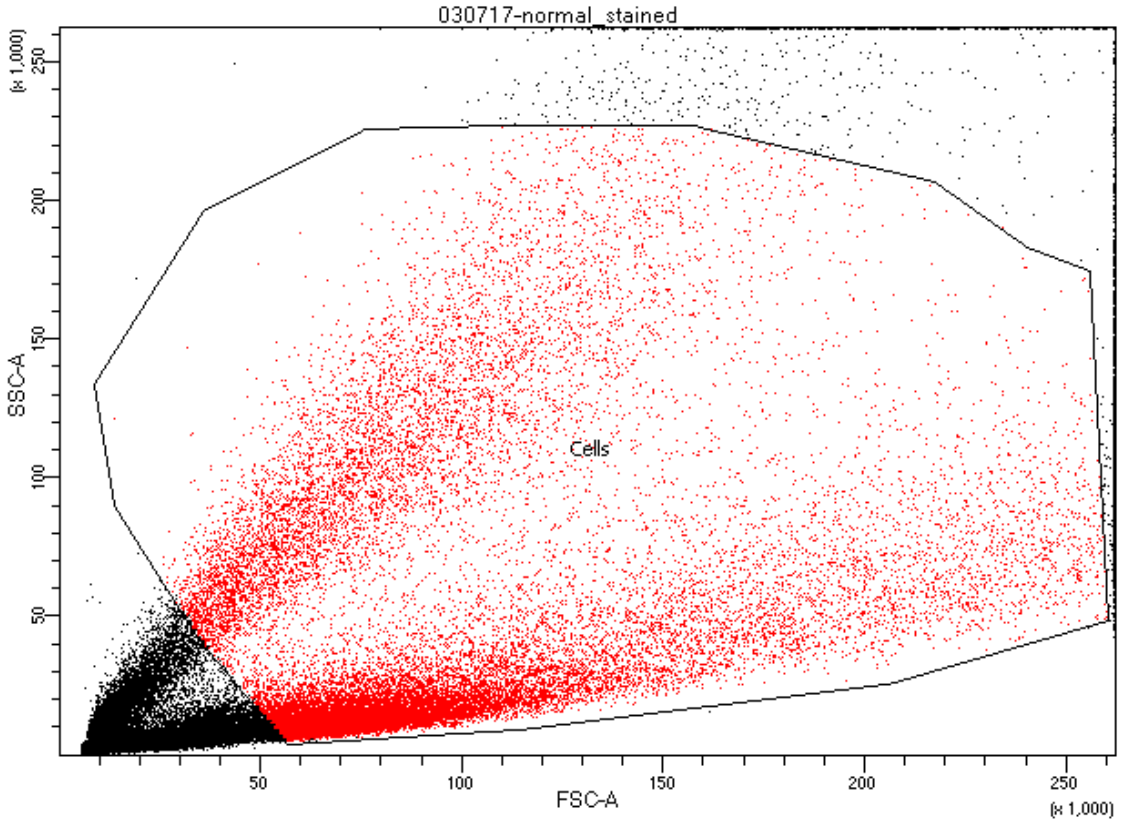


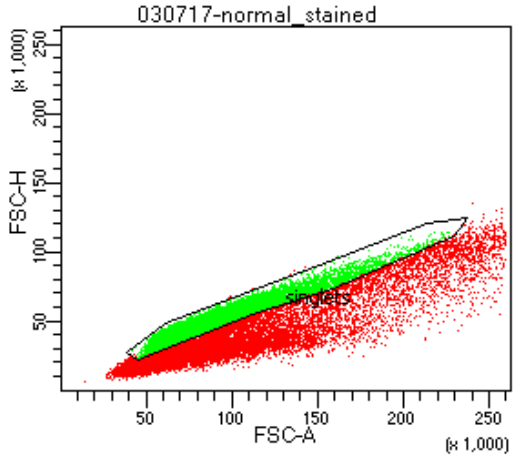
Tube: normal_unstained

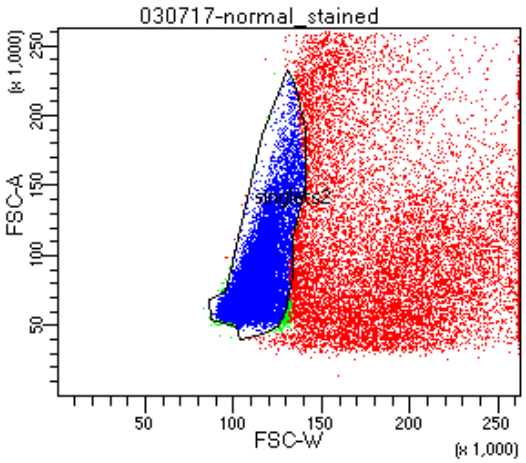
Population	#Events	%Parent	%Total
All Events	60,000	####	100.0
Cells	13,800	23.0	23.0
singlets	7,614	55.2	12.7
singlets2	7,497	98.5	12.5
PI-negativ/living	7,487	99.9	12.5
PI-positive/dead	10	0.1	0.0

Heating Experiment between #4 and #5

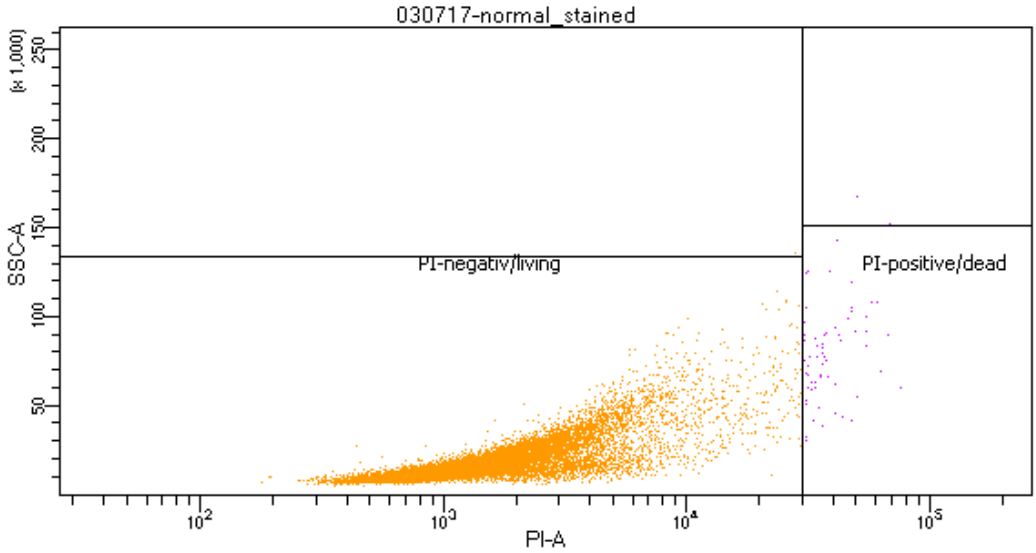
normal stained

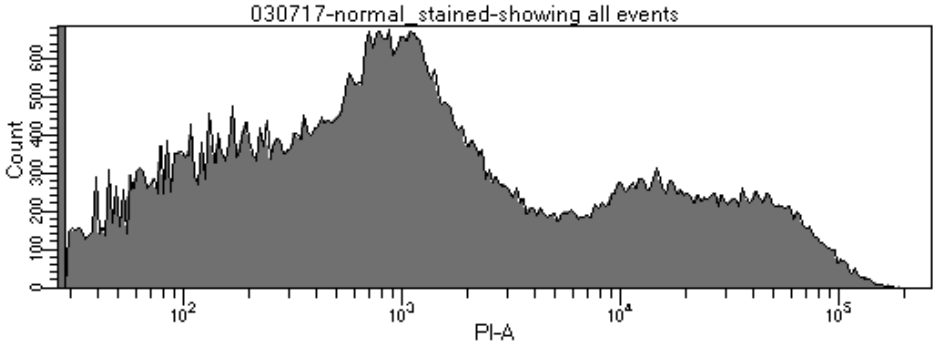


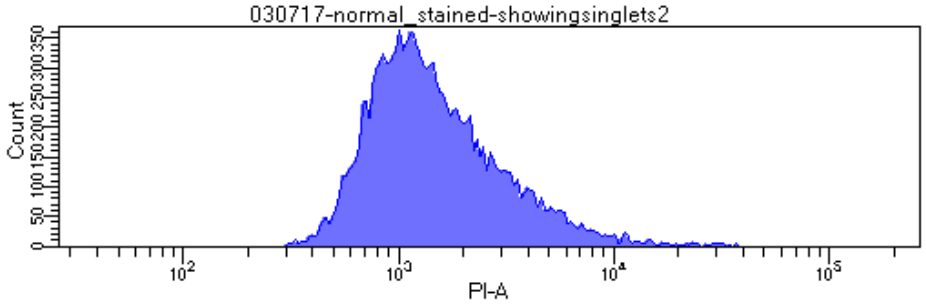




Heating Experiment between #4 and #5
normal stained





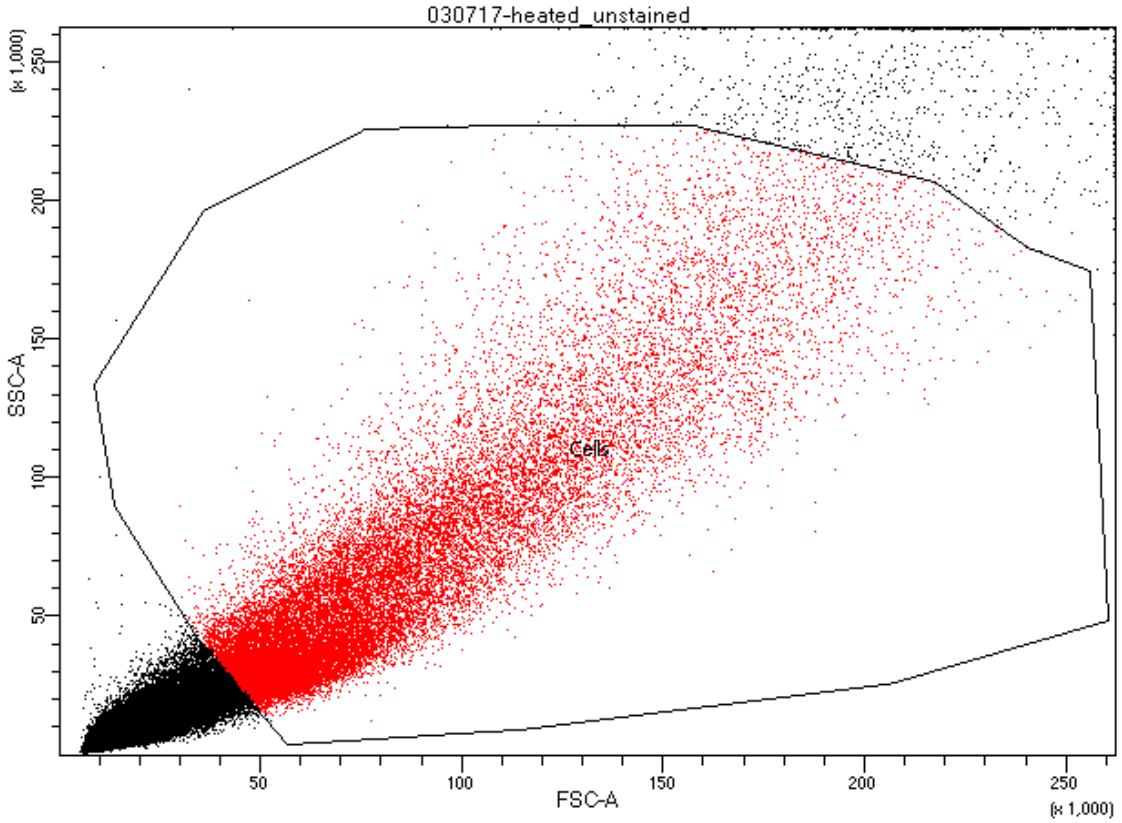


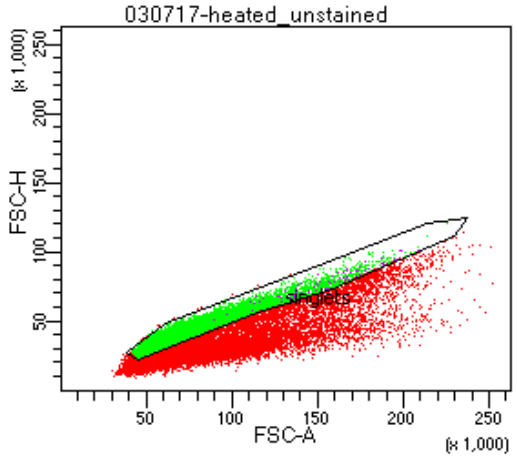
Tube: normal_stained

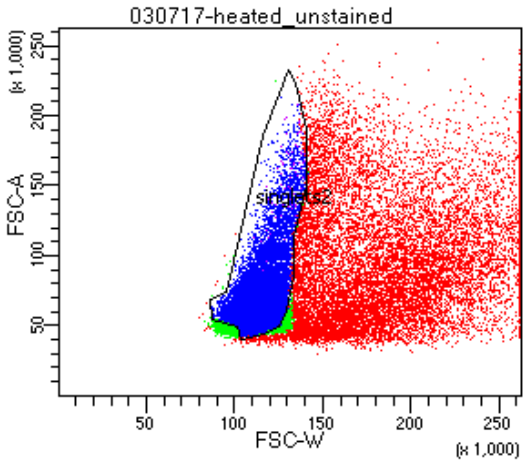
Population	#Events	%Parent	%Total
All Events	80,000	####	100.0
Cells	27,203	34.0	34.0
singlets	14,935	54.9	18.7
singlets2	14,763	98.8	18.5
PI-negativ/living	14,696	99.5	18.4
PI-positive/dead	67	0.5	0.1

Heating Experiment between #4 and #5

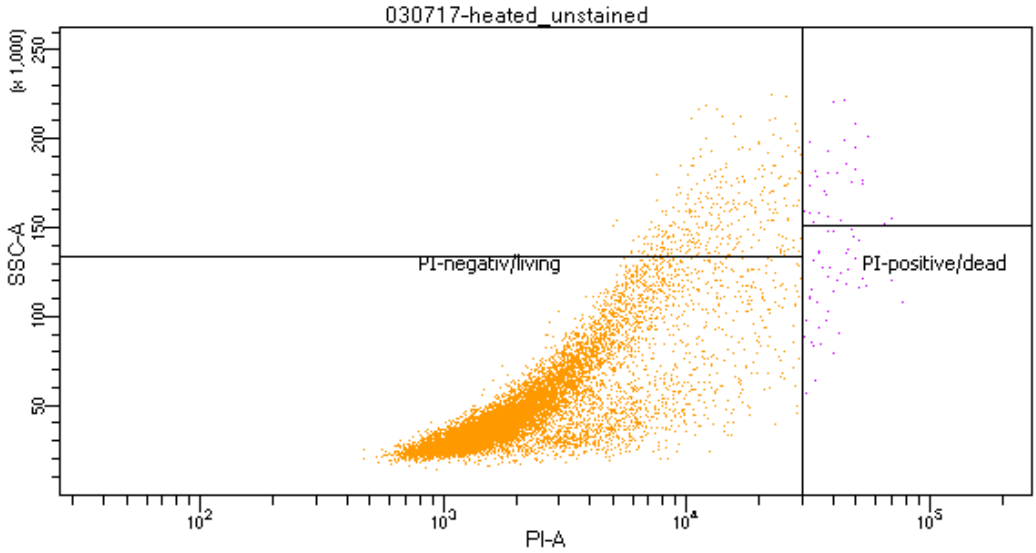
heated unstained

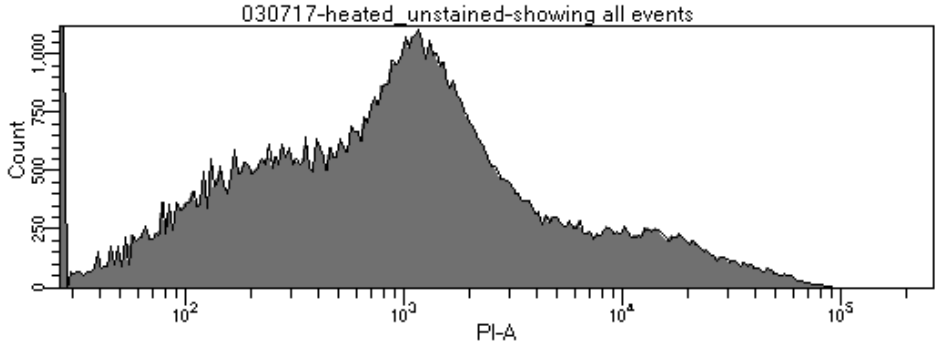


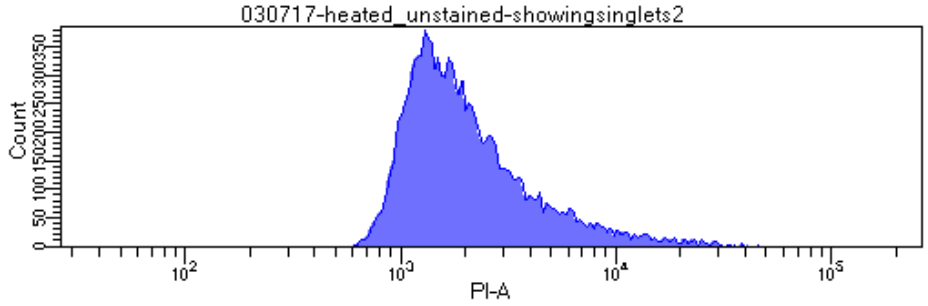




Heating Experiment between #4 and #5
heated unstained





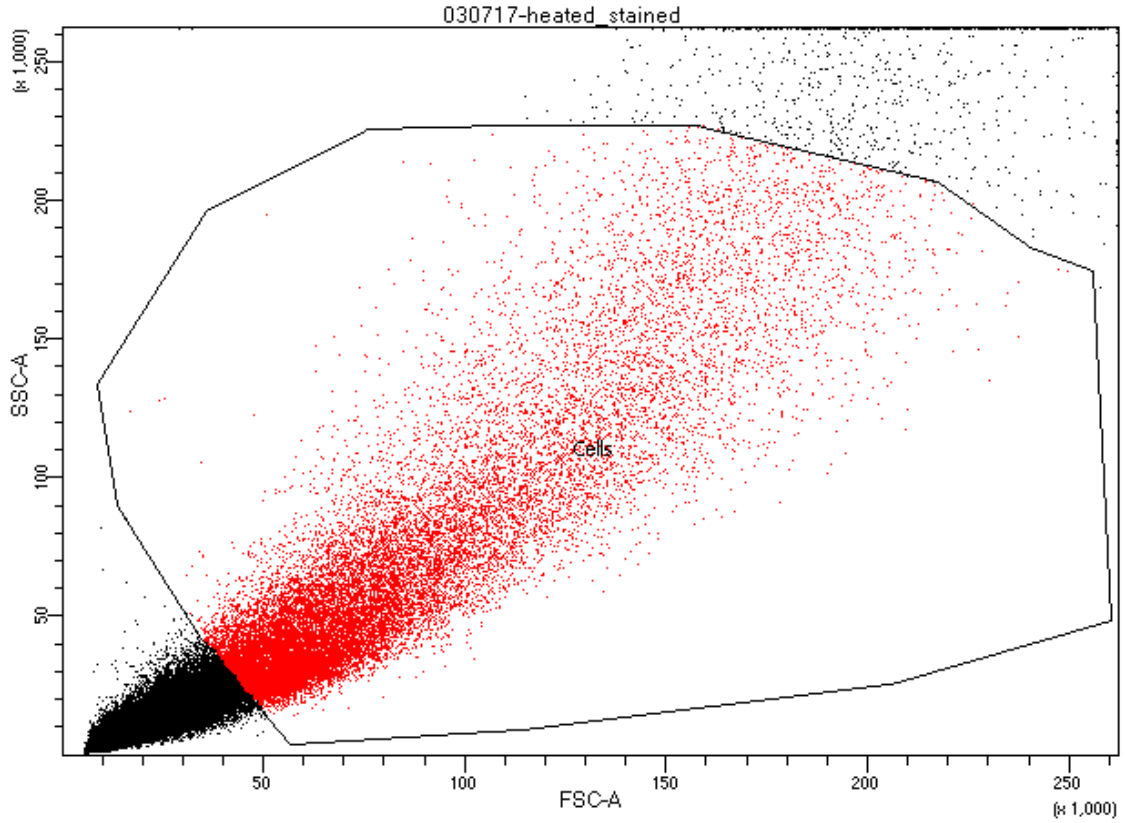


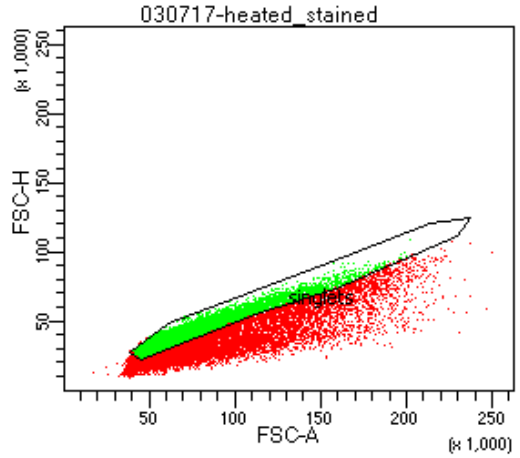
Tube: heated_unstained

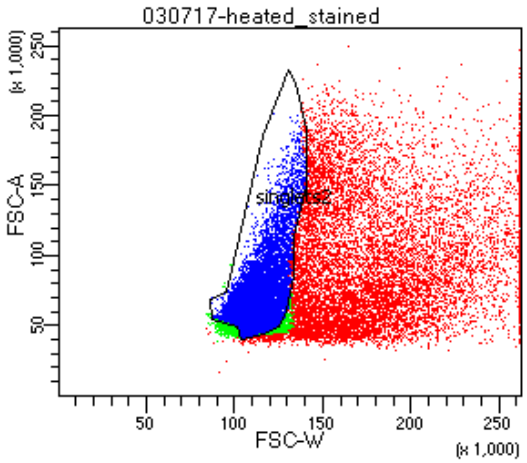
Population	#Events	%Parent	%Total
All Events	90,000	####	100.0
Cells	27,413	30.5	30.5
singlets	13,791	50.3	15.3
singlets2	12,341	89.5	13.7
PI-negativ/living	12,268	99.4	13.6
PI-positive/dead	73	0.6	0.1

Heating Experiment between #4 and #5

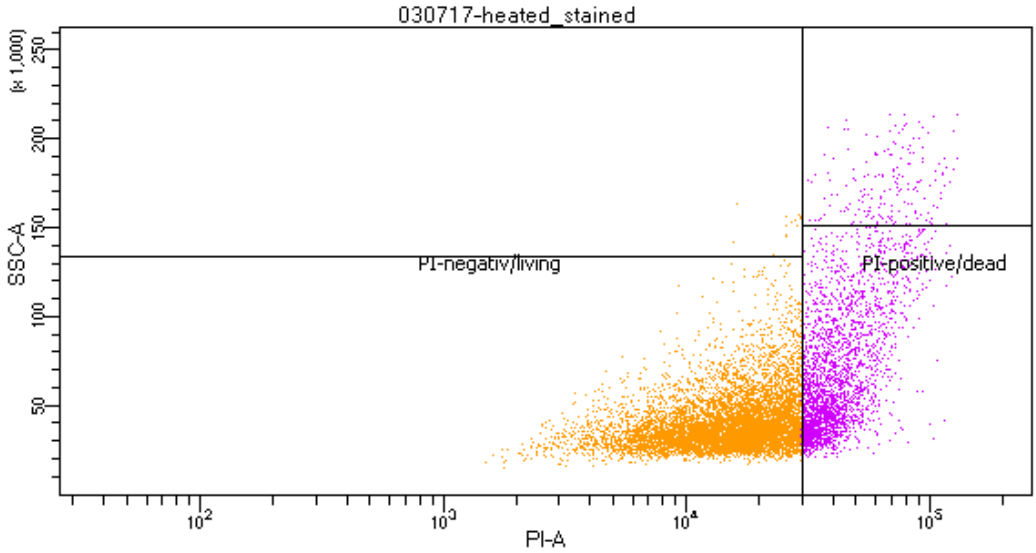
heated stained

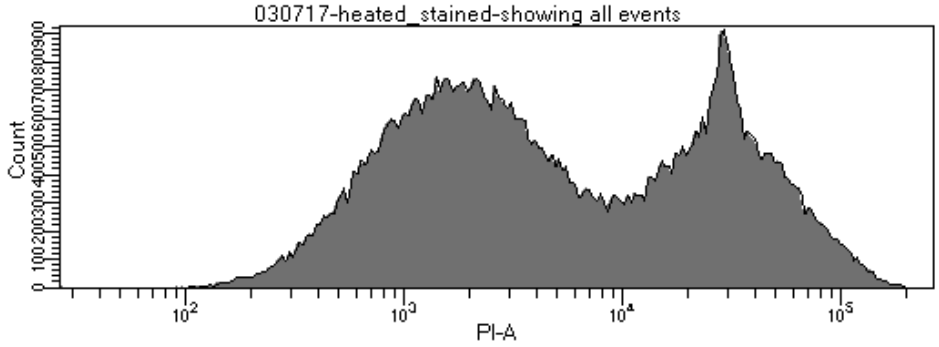


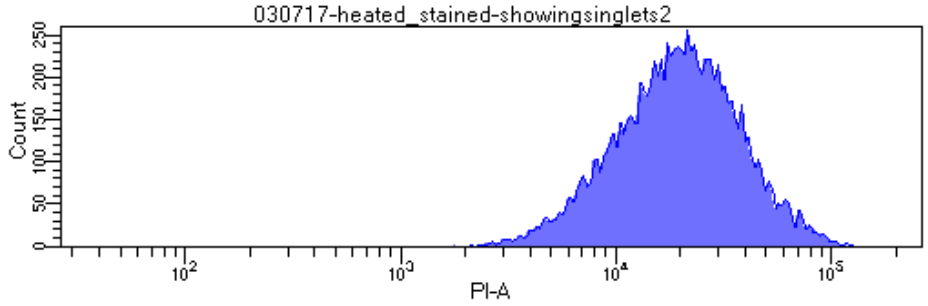




Heating Experiment between #4 and #5
heated stained







Tube: heated_stained

Population	#Events	%Parent	%Total
All Events	80,000	####	100.0
Cells	22,514	28.1	28.1
singlets	12,219	54.3	15.3
singlets2	10,807	88.4	13.5
PI-negativ/living	8,091	74.9	10.1
PI-positive/dead	2,716	25.1	3.4

Bibliography

F. Alipour, S. Jaiswal and S. Vigmostad. Vocal Fold Elasticity in the Pig, Sheep, and Cow Larynges. *Journal of Voice*, 25: 130-136, 2011.

F. Alipour and S. Vigmostad. Measurement of Vocal Folds Elastic Properties for Continuum Modeling. *Journal of Voice*, 26: 816.e21-816.e29, 2012.

W. Arnold and U. Ganzer. Kapitel 2.16 Kehlkopf: Eckdaten zur klinischen Physiologie *Checkliste Hals-Nasen-Ohren-Heilkunde*, pp. 58-59, 2011. Thieme Verlag.

H. G. Boenninghaus and T. Lenarz. Kapitel 12: Larynx und Trachea: Anatomie und Physiologie *HNO*, pp. 246-249, 2007. Springer Verlag.

H. G. Boenninghaus and T. Lenarz. Kapitel 24: Stimm-, Sprech- und Sprachstörungen: Sprach- und Stimmbildung *HNO*, pp. 348-349, 2007. Springer Verlag.

M. Brown and C. Wittwer. Flow Cytometry: Principls and Clinical Applications in Hematology. *Clinical Chemistry*, 46: 1221-1229, 2000.

R. W. Chan, S. D. Gray and I. R. Titze. The importance of hyaluronic acid in vocal fold biomechanics. *Otolaryngology - Head and Neck Surgery*, 124: 607-614, 2001.

R. W. Chan, M. Fu, L. Young ans N. Tirunagari. Relative Contributions of Collagen and Elastin to Elasticity of the Vocal Fold Under Tension. *Annals of Biomedical Engineering*, 35: 1471-1483, 2007.

X. Chen and S. L. Thibeault. Biocompatibility of a synthetic extracellular matrix on immortalized vocal fold fibroblasts in 3-D culture. *Acta Biomateriala*, 6: 2940-2948, 2010.

D. K. Chhetri, Z. Zhang and J. Neubauer. Measurement of Young's Modulus of Vocal Folds by Indentation. *Journal of Voice*, 25: 1-7, 2011.

Schemata of a Larynx; Copyright 2001 Benjamin Cummings, an imprint of Addison Wesley Longman, Inc.; retrieved from: URL {http://www.apsubiology.org/anatomy/2020/2020_Exam_Reviews/Exam_3/larynx$\%$20figure.jpg} on 12/06/2017.

S. H. Dailey, I. Tateya, D. Montequin, N. V. Welham and E. Goodyer. Viscoelastic Measurements of Vocal Folds Using the Linear Skin Rheometer. *Journal of Voice*, 23: 142-150, 2009.

H. W. Eichel. Kapitel 6: Kehlkopf und Luftröhre *HNO-Heilkunde, Phoniatrie und Pädaudiologie: für Sprachtherapeuten*, p. 143-153, 2014. Urban & Fischer Verlag.

H. W. Eichel. Kapitel 8: Stimmstörungen *HNO-Heilkunde, Phoniatrie und Pädaudiologie: für Sprachtherapeuten*, p. 197, 200-202, 237, 2014. Urban & Fischer Verlag.

H. W. Eichel. Kapitel 9: Sprach- und Sprechstörungen *HNO-Heilkunde, Phoniatrie und Pädaudiologie: für Sprachtherapeuten*, p. 239-243, 2014. Urban & Fischer Verlag.

A. Faller and M. Schünke. Kapitel 6.3.3 Kehlkopf (Larynx) *Der Körper des Menschen - Einführung in Bau und Funktion*, pp. 264-269, 2012. Thieme Verlag.

A. J. E. Farran, S. S. Teller, F. Jia, R. J. Clifton, R. L. Duncan and X. Jia. Design and characterization of a dynamic vibrational culture system. *Journal of Tissue Engineering and Regenerative Medicine*, 7: 213-225, 2013.

Scheme of the mode of operation of the FlexCell system; retrieved from: URL `{http://www.flexcellint.com/picts/equibiaxial.jpg}` on 01/08/2017.

G. Friedrich. Kapitel 1: Grundlagen I: Physiologie von Stimme und Sprechen In G. Friedrich, W. Biegenzahn, P. Zorowka *Phoniatrie und Pädaudiologie: Einführung in die medizinischen, psychologischen und linguistischen Grundlagen von Stimme, Sprache und Gehör*, pp. 36-67, 2013. Verlag Hans Huber.

J. Gaston, B. Q. Rios, R. Bartlett, C. Berchtold and S. L. Thibeault. The Response of Vocal Fold Fibroblasts and Mesenchymal Stromal Cells to Vibration *PLoS ONE*, 7: 1-9, 2012.

E. Goodyer, S. Hemmerich, F. Müller, J. B. Kobler and M. Hess. The shear modulus of the human vocal fold, preliminary results from 20 larynxes. *Eur Arch Otorhinolaryngol*, 264: 45-50, 2007.

E. Goodyer, N. V. Welham, S. H. Choi, M. Yamashita and S. H. Dailey. The Shear Modulus of the Human Vocal Fold in a Transverse Direction. *Journal of Voice*, 23: 151-155, 2009.

M. Graupp, S. Bachna-Rotter, C. Gerstenberger, G. Friedrich, E. Fröhlich-Sorger, K. Kiesler, M. Gugatschka. The unsolved chapter of vocal fold scars and how tissue engineering could help us solve the problem. *Eur Arch Otorhinolaryngol*, 273: 2279-2284, 2015.

S. D. Gray. Cellular Physiology of the vocal folds. *Otolaryngol Clin North Am.*, 33: 679-698, 2000.

S. D. Gray and I. R. Titze. Biomechanical and histological observations of vocal fold fibrous proteins. *Ann Otol Rhinol Laryngol*, 109: 77-85, 2000.

B. Hampel and J. Woisetschläger. Frequency- and space-resolved measurement of local density fluctuations in air by laser vibrometry. *Meas. Sci. Technol.*, 17: 2835-2842, 2006.

C. J. Hartnick, R. Rehbar, V. Prasad. Development and Maturation of the Pediatric Human Vocal Fold Lamina Propria. *Laryngoscope*, 115: 4-15, 2005.

H. Iro and F. Waldfahrer. Chapter 17: Larynx and Trachea In R. Probst, G. Grevers, H. Iro *Basic Otorhinolaryngology: A Step-by-Step Learning Guide*, pp. 338-341, 2005. Thieme Verlag.

R. R. Jahan-Tigh, C. Ryan, G. Obermoser and K. Schwarzenberger. Flow Cytometry. *Journal of Investigative Dermatology*, 132: 1-6, 2012.

M. E. Jetté and S. Thibeault. Chapter 3: Morphology of vocal fold mucosa: Histology to Genomics In R. H. Colton, J. K. Casper, R. Leonard *Understanding Voice Problems: A Physiological Perspective for Diagnosis and Treatment*, pp. 64-75, 2011. Lippincott Williams and Wilkins.

J. E. Kelleher, T. Siegmund, R. W. Chan and E. A. Henslee. Optical measurements of vocal fold tensile properties: Implications for phonatory mechanics. *Journal of Biomechanics*, 44: 1729-1734, 2011.

J. E. Kelleher, T. Siegmund, M. Du, E. Naseri and R. W. Chan. Empirical measurements of biomechanical anisotropy of the human vocal fold lamina propria. *Biomechanics and Modeling in Mechanobiology*, 12: 555-567, 2013.

S. Kiminori. Chapter 4: Functional Fine Structures of the Human Vocal Fold Mucosa. In J. S. Rubin, R. T. Sataloff, G. S. Korovin *Diagnosis and Treatment of Voice Disorders*, pp. 41-48, 2003. Thomson Delmar Learning.

A. L. Lalwani. Section VIII. Larynx and Hypopharynx *CURRENT Diagnosis & Treatment Otolaryngology: Head and Neck Surgery*, p. 436-444, 2011. Lange Current Series.

N. Latifi, H. K. Heris, S. Kazemirad and L. Mongeau. Development of a Self-Oscillating Mechanical Model to Investigate the Biological Response of Human Vocal Fold Fibroblasts to Phono-Mimetic Stimulation. *ASME 2014 International Mechanical Engineering Congress and Exposition*, 3: 1-7, 2014.

N. Latifi, H. K. Heris, S. L. Thomson, R. Taher, S. Kazemirad, S. Sheibani, N. Y. K. Li-Jessen, H. Vali and L. Mongeau. A Flow Perfusion Bioreactor System for Vocal Fold Tissue Engineering Applications. *Tissue Engineering Part C Methods*, 22: 823-838, 2016.

L. Li, J. M. Stiadle, H. K. Lau, A. B. Zerdoum, X. Jia, S. L. Thibeault and K. L. Kiick. Tissue engineering-based therapeutic strategies for vocal fold repair and regeneration. *Biomaterials*, 108: 91-110, 2016.

L. Oren, D. Dembinski, E. Gutmark and S. Khosla. Characterization of the Vocal Fold Vertical Stiffness in a Canine Model. *Journal of Voice*, 28: 297-304, 2014.

C. Piazza, J. C. Ribeiro, M. Bernal-Sprekelsen, A. Paiva and G. Peretti. Chapter 6.1: Anatomy and Physiology of the Larynx and Hypopharynx In M. Anniko, M. Bernal-Sprekelsen, V. Bonkowsky, P. Bradley and S. Iurato *Otorhinolaryngology, Head and Neck Surgery (European Manual of Medicine)*, pp. 461-471, 2008. Springer.

R. L. Ringel, J. C. Kahane, P. J. Hillsamer, A. S. Lee and S. F. Badylak. The Application of Tissue Engineering Procedures to Repair the Larynx. *Journal of Speech, Language, and Hearing Research*, 49: 194-208, 2006.

A. K. Rohlfs, E. Goodyer, T. Clauditz, M. Hess, M. Kob, S. Koops. K. Püschel, F. W. Roemer and F. Müller. The anisotropic nature of the human vocal fold: an ex vivo study. *Eur Arch Otorhinolaryngeol*, 270: 1885-1895, 2013.

F. Rosanowski and U. Eysholt. Chapter 18: Voice Disorders In R. Probst, G. Grevers, H. Iro *Basic Otorhinolaryngology: A Step-by-Step Learning Guide*, p. 386, 2005. Thieme Verlag.

C. T. Sasaki and Y.-H. Kim. Chapter 3: Anatomy of the Human Larynx. In J. S. Rubin, R. T. Sataloff, G. S. Korovin *Diagnosis and Treatment of Voice Disorders*, pp. 27-40, 2003. Thomson Delmar Learning.

R. C. Scherer. Chapter 7: Laryngeal Function During Phonation. In J. S. Rubin, R. T. Sataloff, G. S. Korovin *Diagnosis and Treatment of Voice Disorders*, pp. 87-106, 2003. Thomson Delmar Learning.

L. Sitnik, K. Pentós, M. Magdziak-Toklowicz and R. Wrobel. The Laser Doppler Vibrometry in mechatronics diagnostics. *Archives of Civil and Mechanical Engineering*, 15: 962-970, 2015.

E. J. Speckmann, J. Hescheler and R. Khling. Kapitel 4: Auditorisches System *Physiologie*, pp. 238-240, 2013. Urban & Fischer Verlag.

E. J. Speckmann, J. Hescheler and R. Khling. Kapitel 21: Altern und Tod *Physiologie*, p. 760, 2013. Urban & Fischer Verlag.

H. Sweet. Part I - The Organs of Speech *A Handbook of Phonetics - Including a Popular Exposition of the Principles of Spelling Reform*, pp. 1-2, 2013. Cambridge University Press.

I. R. Titze. Comments on the myoelastic - aerodynamic theory of phonation. *J Speech Hear Res.*, 23: 495-510, 1980.

I. R. Titze, R. W. Hitchcock, K. Broadhead, K. Webb, W. Li, S. D. Gray and P. A. Tresco. Design and validation of a bioreactor for engineering vocal fold tissues under combined tensile and vibrational stresses. *Journal of Biomechanics*, 37: 1521-1529, 2004.

Z. Tong, A. B. Zerdoum, R. L. Duncan, X. Jia. Dynamic Vibration Cooperates with Connective Tissue Growth Factor to Modulate Stem Cell Behaviors. *Tissue Engineering Part A*, 20: 1922-1934, 2014.

J. Van den Berg. Myoelastic-Aerodynamic Theory Of Voice Production. *J Speech Hear Res.*, 1: 227-44, 1958.

J. C. Wolchok, C. Brokopp, C. J. Underwood, P. A. Tresco. The effect of bioreactor induced vibrational stimulation on extracellular matrix production from human derived fibroblasts. *Biomaterials*, 30: 327-335, 2009.

A. B. Zerdoum, Z. Tong, B. Bachman and X. Jia. Construction and Characterization of a Novel Vocal Fold Bioreactor *Journal of Visualized Experiments*, 90: 1-16, 2014.

Statutory Declaration

I declare that I have authored this Thesis independently, that I have not used other than the declared sources/resources, and that I have explicitly marked all material, which has been quoted by the relevant reference.

date

signature